Pharmacological studies on the probable mechanism of action of Khamira Gaozaban Sada (KGS) in the management of Hypertension, involving Quality Control and formulation optimization studies for this age old Unani preparation

THESIS SUBMITTED BY

MD.ADIL SHAHARYAR

DOCTOR OF PHILOSOPHY (PHARMACY)

DEPARTMENT OF PHARMACEUTICAL TECHNOLOGY
FACULTY OF ENGINEERING & TECHNOLOGY (FET)
JADAVPUR UNIVERSITY
KOLKATA-700032
INDIA

2024

Dedicated

To

My Beloved

Ammi (Shahzadi Begum)

Abbu (Md. Mansoor Alam)

&

Wife (Aqsa Yamin Fatma)

JADAVPUR UNIVERSITY

KOLKATA-700032, INDIA

INDEX NO.: 286/Ph/19

Index No: 286/19/Ph

1. Title of the Thesis: Pharmacological studies on the probable mechanism of action of Khamira Gaozaban Sada (KGS) in the management of Hypertension, involving Quality Control and formulation optimization studies for this age old Unani preparation

2. Name, Designation & Institution of the Supervisor:

Prof. Sanmoy Karmakar
Professor of Pharmacology and Toxicology,
Dept. of Pharmaceutical Technology,
Jadavpur University, Kolkata 700032 India

3. List of Publications:

Research and Review articles:

- Anand K, Mandal P, Karmakar S, Bhowmik R, Shaharyar MA, Mandal A, Sarkar A, De A, Chakraborty S, Ray S, Bhowmik M. Evaluation of cilnidipine-loaded self-micro-emulsifying drug delivery system (SMEDDS) by quantification of comparative pharmacokinetic parameters using validated LC-ESI-MS/MS bioanalytical method and pharmacodynamic assessment. Annales Pharmaceutiques Françaises 2024, 82.1134-1149. Elsevier Masson. https://doi.org/10.1016/j.pharma.2024.07.007
- Bhowmik R, Shaharyar MA, Kanakal MM, Sarkar A, Farhana SA, Hussain SM, Khan A, Mandal P, Roshan S, Mitra A, Karmakar S. Ayurvedic herbal formulations Haridra Khanda and Manjisthadi Kwath (brihat) in the management of allergic rhinitis: A pharmacological study. Heliyon. 2024, 10.1016/j.heliyon.2024.e31937
- Bhowmik R, Shaharyar MA, Sarkar A, Mandal A, Anand K, Shabana H, Mitra A, Karmakar S. Immunopathogenesis of urticaria: a clinical perspective on histamine and cytokine involvement. Inflammation Research. 2024;73(5):877-96. https://doi.org/10.1007/s00011-024-01869-6
- Karmakar S, Mandal A, Bhowmik R, Shaharyar Ma, Anand K, Mandal P, Sarkar A. Natural hepatoprotectives earthworm extract protein & goat milk in-vitro model rat primary hepatocytes exposed to carbon tetrachloride revealed toxicity and oxidative stress. Journal of Research in Pharmacy. 2024 ;28(1) https://doi.org/0.29228/jrp.693
- Mandal P, Chakraborty S, Shaharyar MA, Bhowmik R, Sarkar A, Mandal A, Karmakar S, Pal tk. Evaluation of efficacy of teneligliptin by quantification with

active glucagon like peptide-1 (glp-1) from indian human plasma using novel bio-analytical method in lc-esi-ms/ms. https://doi.org/10.20959/wjpr202322-30536.

- Shaharyar MA, Bhowmik R, Al-Abbasi FA, AlGhamdi SA, Alghamdi AM, Sarkar A, Kazmi I, Karmakar S. Vaccine Formulation Strategies and Challenges Involved in RNA Delivery for Modulating Biomarkers of Cardiovascular Diseases: A Race from Laboratory to Market. Vaccines. 2023;11(2):241. **https://doi.org/10.3390/vaccines11020241**
- Bhowmik R, Shaharyar MA, Sarkar A, De A, Mandal A, Shabana H, Karmakar S, Karmakar S. Role of Natural Products in Inflammatory Pharmacology: Harnessing Nature's Potential Through Drug Delivery for Therapeutic Intervention. https://doi.org/10.53555/jchr.v13.i4s.759
- Sarkar A, Saha R, Saha S, Bhowmik R, Chatterjee A, Paul A, Maji A, Shaharyar MA, Karmakar S, Sarkar B, Maity TK. Transesterification, GC-MS profiling, and in vitro antimicrobial potential of oil obtained from seeds of Citrus maxima (Burm.) Merr. Industrial Crops and Products. 2022.189:115764.https://doi.org/10.1016/j.indcrop.2022.115764
- Shaharyar MA, Bhowmik R, Afzal O, Altamimi AS, Alzarea SI, Almalki WH, Ali SZ, Mandal P, Mandal A, Ayoob M, Kazmi I. Anti-Hypertensive Activity of Some Selected Unani Formulations: An Evidence-Based Approach for Verification of Traditional Unani Claims Using LC-MS/MS for the Evaluation of Clinically Relevant Blood Parameters in Laboratory Rats. Journal of Clinical Medicine. 2022 11,628. **https://doi.org/10.3390/jcm11154628**
- Rahman M, Almalki WH, Alrobaian M, Iqbal J, Alghamdi S, Alharbi KS, Alruwaili NK, Hafeez A, Shaharyar MA, Singh T, Waris M. Nanocarriers-loaded with natural actives as newer therapeutic interventions for treatment of hepatocellular carcinoma. Expert Opinion on Drug Delivery. 2021 3;18(4):489-513. https://doi.org/10.1080/17425247.2021.1854223
- Anand K, Karmakar S, Mandal P, Shaharyar MA, Bhowmik R, Mondal A, Ray S, Karmakar S. Formulation Development, Optimization, and Characterization of Cilnidipine-Loaded Self-microemulsifying Drug Delivery System.; https://doi.org/10.21276/apjhs.2021.9.1.05
- Sengupta M, Shaharyar MA, Rahman M, Anand K, Kundu A. Vitamin C loaded chemically modified nano carrier for human health care application. Current Biochemical Engineering. 2020 1;6(1):34-40. https://doi.org/10.2174/2212711906666190903113903
- Guha A, Shaharyar MA, Ali KA, Roy SK, Kuotsu K. Smart and intelligent stimuli responsive materials: an innovative step in drug delivery system. Current Biochemical Engineering. 2020 1;6(1):41-52. https://doi.org/10.2174/2212711906666190723142057
- Anand K, Ray S, Rahman M, Shaharyar A, Bhowmik R, Bera R, Karmakar S. Nano-emulgel: emerging as a smarter topical lipidic emulsion-based nanocarrier for skin healthcare applications. Recent patents on anti-infective drug discovery. 2019 ,1;14(1):16-35. https://doi.org/10.2174/1574891X14666190717111531
- Saleem S, Shaharyar MA, Khusroo MJ, Ahmad P, Rahman RU, Ahmad K, Alam MJ, Al-Harbi NO, Iqbal M, Imam F. Anticancer potential of rhamnocitrin 4′-β-d-galactopyranoside against N-diethylnitrosamine-induced hepatocellular carcinoma

in rats. Molecular and cellular biochemistry. 2013; 384:147-53. https://doi.org/10.1007/s11010-013-1792-6

- Kazmi I, Rahman M, Afzal M, Gupta G, Saleem S, Afzal O, Shaharyar MA, Nautiyal U, Ahmed S, Anwar F. Anti-diabetic potential of ursolic acid stearoyl glucoside: A new triterpenic gycosidic ester from Lantana camara. Fitoterapia. 2012 1;83(1):142-6. https://doi.org/10.1016/j.fitote.2011.10.004
- Mandal A, Bhowmik R, Anand MA, Mandal P, Akhtar J, Karmakar S, Karmakar S. The protective action of earthworm protein powder/mwco 50 kda fraction on experimental hepatic damage: an invivo/invitro approach involving inflammatory tnf-α and il-6.2023. https://doi.10.31838/ecb/2023.12.si5.0114

Book Chapters:

- Das A, Paul P, Raj M, Sarkar A, De A, Banerjee T, Bhowmik R, Shaharyar MA, Anand K, Biswas E, Ghosh N. Chemiluminescence-based biosensor: From principle to its applications. Fundamentals of Biosensors in Healthcare 2025, 315-336. Academic Press. https://doi.org/10.1016/B978-0-443-21658-9.00012-7
- Reza KH, Das PP, Hossain CM, Shaharyar MA, Pal S, Ali SZ, Kazmi I. Mechanism of action of cholinergic drugs. InHow Synthetic Drugs Work 2023. 27-46. Academic Press. https://doi.org/10.1016/B978-0-323-99855-0.00002-6
- Jana S, Gayen S, Kumari R, Patra S, Haldar PK, Bhowmik R, Shaharyar MA, Mandal A, Mazumdar H, Karmakar S. Mechanism of action of antifungal agents. How Synthetic Drugs Work 2023. 431-445. Academic Press. https://doi.org/10.1016/B978-0-323-99855-0.00019-1
- Bhowmik R, Shaharyar MA, Anand K, Mazumdar H, Mandal A, Mandal P, Chakraborty S, Panday P, Karmakar S. Mechanism of action of drugs used in hypertension. How Synthetic Drugs Work 2023. 349-367. Academic Press. https://doi.org/10.1016/B978-0-323-99855-0.00015-4
- Patra S, Gupta P, Kumari R, Jana S, Haldar PK, Bhowmik R, Mandal A, Shaharyar MA, Mazumdar H, Anand K, Karmakar S. Insights into the mode of action of antianginal and vasodilating agents. How Synthetic Drugs Work 2023. 329-348. Academic Press. https://doi.org/10.1016/B978-0-323-99855-0.00014-2
- Kumari R, Jana S, Patra S, Haldar PK, Bhowmik R, Mandal A, Anand K, Mazumdar H, Shaharyar MA, Karmakar S. Insights into the mechanism of action of antiviral drugs. How Synthetic Drugs Work 2023, 447-475. Academic Press. https://doi.org/10.1016/B978-0-323-99855-0.00020-8
- Mandal A, Das P, Bhowmik R, Mazumdar H, Shaharyar MA, Kumari R, Jana S, Patra S, Haldar PK, Karmakar S. An insight into the agents used for immunomodulation and their mechanism of action. How synthetic drugs work 2023. 503-528. Academic Press. https://doi.org/10.1016/B978-0-323-99855-0.00022-1
- Chakraborty M, Das PP, Chandra S, Shaharyar MA, Sarkar N, Mukherjee S, Paul S, Bhowmik R, Haldar PK, Karmakar S, Chakraborty J. Toxicology of nanoformulations and materials in tissue engineering. Nanostructured Materials for Tissue Engineering 2023. 281-316 Elsevier. https://doi.org/10.1016/B978-0-323-95134-0.00006-7
- Mazumdar H, Bhowmik R, Shaharyar MA, Mandal A, Anand K, Patra S, Kumari R, Jana S, Haldar PK, Karmakar S. Mechanism of action of antiarrhythmic drugs. How

Synthetic Drugs Work 2023. 289-327. Academic Press. https://doi.org/10.1016/B978-0-323-99855-0.00013-0

- Ali KA, Maity A, Roy SD, Pramanik SD, Das PP, Shaharyar MA. Insight into the mechanism of steroidal and non-steroidal anti-inflammatory drugs. InHow Synthetic Drugs Work 2023 Jan. 61-94. Academic Press. https://doi.org/10.1016/B978-0-323-99855-0.00004-X
- Gupta MS, Shaharyar MA, Rahman M, Anand K, Kazmi I, Afzal M, Karmakar S. Ursolic Acid: A Pentacyclic Triterpene from Plants in Nanomedicine. InBiomarkers as Targeted Herbal Drug Discovery 2021, 65-100) Apple Academic Press. https://doi.org/10.1201/9781003045526
- Shaharyar MA, Rahman M, Anand K, Hossain CM, Kazmi I, Karmakar S. Rosmarinic Acid: A Boon in the Management of Cardiovascular Disease. Biomarkers as Targeted Herbal Drug Discovery 2021, 229-248). Apple Academic Press. https://doi.org/10.1201/9781003045526
- Anand K, Ray S, Shaharyar MA, Rahman M, Bhowmik R, Karmakar S, Gupta MS. Delivery of Herbal Cardiovascular Drugs in the Scenario of Nanotechnology: An Insight. Biomarkers as Targeted Herbal Drug Discovery. 2021 :133-54. https://doi.org/10.1201/9781003045526
- Shaharyar MA, Rahman M, Alam K, Beg S, Anand K, Hossain CM, Guha A, Afzal M, Kazmi I, Rub RA, Karmakar S. Nanomedicines for the Treatment of Gastric and Colonic Diseases. Nanomedicine for the Treatment of Disease 2019 ; 239-270. Apple Academic Press. https://doi.org/10.1201/9780429425714
- Rahman M, Alam K, Shaharyar MA, Beg S, Hafeez A, Kumar V. Conventional to Novel Targeted Approaches for Brain Tumors: The Role of Nanomedicines for Effective Treatment. Nanomedicine for the Treatment of Disease 2019; 329-354. Apple Academic Press. https://doi.org/10.1201/9780429425714
- Rahman M, Alam K, Shaharyar MA, Beg S, Hafeez A, Rub RA, Kumar V. Liposomal Nanomedicines as State-of-the-Art in the Treatment of Skin Disorders. InNanomedicine for the Treatment of Disease 2019; 305-328. Apple Academic Press. https://doi.org/10.1201/9780429425714
- Rahman M, Zaki Ahmad M, Kazmi I, Akhter S, Beg S, Gupta G, Afzal M, Saleem S, Ahmad I, Adil Shaharyar M, Jalees Ahmed F. Insight into the biomarkers as the novel anti-psoriatic drug discovery tool: a contemporary viewpoint. Current drug discovery technologies. 2012 1;9(1):48-62. https://doi.org/10.2174/157016312799304516

List of Patents: None

List of presentation in national / international Conferences:

- Participated in "National Workshop on Good Clinical Practice" (NWGCP-2024), held on 27th July, 2024, organized by ABS Clinical Solution in collaboration with Bioequivalence Study Centre, Jadavpur University, Kolkata.
- Participated in "National Seminar on Pharmacovigilance and its importance in Unani Medicine" held on 3rd February 2024 at Dr. K.P. Basu Hall, Jadavpur University, Kolkata.
- Participated in 3rd International Conference and Buyers Sellers Meet For Medicinal Plants used in Lifestyle Products on 6th December, 2023, held at Dr. Triguna Sen Auditorium, Jadavpur University, Kolkata, Theme: "Streaming of Supply Chain and Decentralized Value Addition of Medicinal Plants," organized by Jadavpur University and sponsored by National Medicinal Plants Board (NMPB), Ministry of AYUSH, Govt. of India.
- Participated in "National Workshop on GCP and Clinical Trial Conduct" held on 24th June, 2023, at Dr. K.P. Basu Memorial Hall, Jadavpur University, Kolkata.
- Participated in Workshop on "PreCon-2K23, Pre-Conference Workshop on BA/BE Studies" of the 30th Annual Conference of Indian Pharmacological Society and Eastern Zonal Colloquium, held on 3rd March, 2023, at Dr. K.P. Basu Memorial Hall, Jadavpur University, Kolkata.
- Participated in Unani Day 2023-Pre-activities conducted by Regional Research Institute of Unani Medicine (Govt. of India), Kolkata in collaboration with RCFC (NMPB, Ministry of AYUSH), Jadavpur University, Kolkata & Peripheral Pharmacovigilance Centre (Unani), Kolkata on "Seminar/Awareness Programme on Pharmacovigilance in AYUSH" held on 7th February 2023, Jadavpur University, Kolkata.
- Poster Presentation titled "Khamira Gaozaban Sada, whether anti-hypertensive or else - a critical analysis involving dissonance between plasma biomarker and blood pressure in rats" at the 9th International Congress of Society for Ethnopharmacology, at JSS Academy of Higher Education and Research, Mysuru, Karnataka, India, 22nd April–24th April, 2022.
- Poster Presentation titled "Pharmacological Studies on the Mechanism of Action of Khamira Gaozaban Sada in the Management of Hypertension involving Quality Control and Formulation Optimization Studies for this Age-old Unani Preparation" at the 7th International Congress of Society for Ethnopharmacology, at Jamia Hamdard, New Delhi, India, 15th Feb–17th Feb, 2020.
- Participated in the National Seminar on "Clinical Research: Present Scenario in Pharmacovigilance and Clinical Trials" held in the Department of Pharmaceutical Technology, Jadavpur University, 2018.
- Participated in the "Continuing Education Programme for Pharmacy Teachers" sponsored by the Pharmacy Council of India, organized by the Department of Pharmaceutical Technology, Jadavpur University, in 2018.

STATEMENT OF ORIGINALITY

I, Md. Adil Shaharyar registered on 20/06/2019 do hereby declare that this thesis entitled **"Pharmacological studies on the probable mechanism of action of Khamira Gaozaban Sada (KGS) in the management of Hypertension, involving Quality Control and formulation optimization studies for this age old Unani preparation"** contains literature survey and original research work done by the undersigned candidate as part of Doctoral studies.

All information in this thesis have been obtained and presented in accordance with existing academic rules and ethical conduct. I declare that, as required by these rules and conduct, I have fully cited and referred all materials and results that are not original to this work.

I also declare that I have checked this thesis as per the "Policy on Anti Plagiarism, Jadavpur University, 2019", and the level of similarity as checked by iThenticate software is 9 %.

Signature of the Candidate: Md. Adil Shaharyar

Date: 07/07/2025

Certified by Supervisor: 07/07/2025

(Signature with date, seal)

Sanmoy Karmakar, M.Pharm, PhD
Professor & Former Head
In-charge Bioequivalence Study Center
Dept. of Pharmaceutical Technology
JADAVPUR UNIVERSITY, KOL - 32,INDIA

CERTIFICATE FROM THE SUPERVISOR

This is to certify that the thesis entitled "**Pharmacological studies on the probable mechanism of action of Khamira Gaozaban Sada (KGS) in the management of Hypertension, involving Quality Control and formulation optimization studies for this age old Unani preparation**" submitted by Shri. Md.Adil Shaharyar, who got his name registered on 20/06/2019 [Registration No:1021913011 (Ref. no. D-7/E/472/19)] for the award of Ph.D (Engg./Pharmacy) degree Jadavpur University is absolutely based upon his own work under the supervision of Prof. Sanmoy Karmakar and that neither his thesis nor any part of the thesis has been submitted for any degree/diploma or any other academic award anywhere before.

Sanmoy Karmakar

07/07/2025

Sanmoy Karmakar, M.Pharm, PhD
Professor & Former Head
In-charge Bioequivalence Study Center
Dept. of Pharmaceutical Technology
JADAVPUR UNIVERSITY, KOL - 32,INDIA

Prof. Sanmoy Karmakar (Supervisor)
Professor of Pharmacology and Toxicology,
Dept. of Pharmaceutical Technology,
Jadavpur University,
Kolkata 700032.
India

ACKNOWLEDGEMENT

First and foremost, I express my heartfelt gratitude to the Almighty Allah for granting me steadfastness throughout this challenging journey and for helping me from sources beyond my comprehension. The completion of my thesis represents the culmination of a long and arduous journey, during which I have been privileged to receive immense support and encouragement from many individuals and institutions. It is both an honour and a privilege to extend my gratitude to each one of them through this acknowledgement.

I extend my most profound appreciation to my supervisor, Prof. Sanmoy Karmakar, for his invaluable guidance, expertise, and unwavering support. His mentorship has not only shaped the direction of my research but also significantly enriched my intellectual growth. His few minutes of advice and suggestions are worth hours of contemplation and have often provided clarity and direction in moments of uncertainty, greatly enriching the quality of my work. This milestone in my academic journey would have been unattainable without his encouragement and insightful advice.

I am deeply thankful to Prof. Amalesh Samanta, Head of the Department at Jadavpur University, and the esteemed faculty members of the department for their valuable advice and continuous cooperation throughout this research.

My heartfelt gratitude goes to the CCRUM, Ministry of AYUSH, Government of India, for providing me with financial support in the form of a fellowship and contingency, which facilitated the successful completion of my project.

I sincerely thank my fellow research scholars for their camaraderie, kindness, and unyielding support, especially Rudranil Bhowmik, Avishek Mandal, Kumar Anand, Arnab Sarkar, Akash De, Avik Majhi, Tanmoy Banerjee and other juniors whose assistance, stimulating discussions, and shared moments in the laboratory have greatly enriched this journey. I would also like to extend my gratitude to Mr. Asit Mukherjee, whose dedicated efforts in supplying chemicals at the right time to our laboratory have been invaluable. Additionally, I am thankful to The Calcutta Unani Medical College and Hospital, as well as Ballygunge Science College (C.U), for their indispensable support.

To my parents, I owe my deepest gratitude for their kindness, moral support, and unwavering encouragement. Their faith in my abilities has been a constant source of motivation. I am equally indebted to my family for their understanding, love and sacrifices throughout this demanding journey. My heartfelt thanks go to my beloved wife, Aqsa Yamin

Fatma, for her patience, unwavering support, and endless encouragement. Their belief in me has been my strongest pillar of strength.

Lastly, I wish to express my sincere appreciation to the animals involved in this research. Their contributions, though not conventionally recognized, have been indispensable in advancing scientific knowledge. I am deeply committed to advocating for the ethical treatment of animals in research and ensuring that their sacrifices contribute meaningfully to societal progress.

Kolkata, 07/07/2025

Md. Adil Shaharyar

Md. Adil Shaharyar

PREFACE

This research work is carried out in partial fulfillment of Doctor of Philosophy (Pharmacy). The current research work entitled **"Pharmacological studies on the probable mechanism of action of Khamira Gaozaban Sada (KGS) in the management of Hypertension, involving Quality Control and formulation optimization studies for this age old Unani preparation"** showed its cardioprotective effect.

Unani practitioners/physicians in Indian Unani hospitals have long been clinically using KGS for patients with symptoms of “weak heart” (as per their terminologies). After much discussion with these unani physicians, we infer that by the term “weak heart” they indicated cardiac failure. Therefore, the current studies are designed to confirm these therapeutic claims of KGS, a low-cost medication used as an antihypertensive and cardioprotective preparation, as mentioned in ancient Unani literature.

The present study aims to investigate the anti-hypertensive activity of some selected unani formulations using L-NAME model. Group I or hypertensive control group: L-NAME administered for 7 days and left for the next 7 days; Group II or KASgroup: L-NAME administered (i.p) for 7 days and L-NAME + KAS (1000 mg/kg b.w) for the next 7 days; Group III or DMM group: L-NAME administered (i.p) for 7 days and L-NAME + DMM (2000 mg/kg b.w) for the next 7 days; Group IV or MSR group: L-NAME administered (i.p) for 7 days and L-NAME + MSR (300 mg/kg b.w) for the next 7 days; Group V or HJ group: L-NAME administered (i.p) for 7 days and L-NAME + HJ (113 mg/kg b.w) for the next 7 days; Group VI or KGS group: L-NAME administered (i.p) for 7 days and L-NAME +KGS (2000 mg/kg b.w) for the next 7 days. Non-invasive systolic blood pressure and RR-interval (ECG) was measured. Plasma was investigated for sodium, potassium, nitrite, ANP, adrenaline, noradrenaline and aldosterone on day 0, 7 and 14 using LC-MS/MS. Treatment showed a non-significant low reduction in SBP (systolic blood pressure) of KAS, MSR and HJ while that of DMM was quite significant ($p < 0.05$), but in the case of KGS, SBP increased. DMM on day 14 significantly ($p < 0.05$) reduced plasma nitrite while no significant plasma Na+ was noted. In the case of both DMM and KGS, potassium increased significantly ($p < 0.05$) on day 14. No significant changes in plasma ANP and aldosterone was observed against DMM and KGS while blood levels of adrenaline and noradrenaline significantly ($p < 0.05$) changed. No significant change in b.w. was found. L-NAME KAS, MSR and HJ showed no change in SBP while DMM showed a significant reduction in SBP with decreased plasma nitrite. Probably, DMM may have anti-hypertensive activity mediated through NO inhibition while KGS may involve central sympathomimetic action.

Another study explored the effects of two doses of KGS against Doxorubicin (DOX)-induced cardiac hypertrophy in male Wistar rats. For the first time, metabolite profiling of the methanolic extract of KGS and quantification of two specific metabolites in it were performed. Animals were divided into five groups (n=6): Control, DOX (15 mg/kg cumulative dose, i.p.), DOX + KGS Low Dose (1000 mg/kg, oral), DOX + KGS High Dose (2000 mg/kg, oral), and DOX + Captopril. KGS or Captopril was administered for two weeks alone and then combined with DOX for the last two weeks. Plasma noradrenaline, ANP (atrial natriuretic peptide), aldosterone were evaluated using LC-MS/MS and while Ang-II (angiotensin II) and ACE (angiotensin converting enzyme) using ELISA. In vivo parameters such as SBP (systolic blood pressure), QTc, HW/TL ratio, cardiac MDA, histopathology, mitochondrial proteins, and metabolite profiling (LC-qTOF-MS) were analyzed. Quantification of Rosmarinic acid (RA) and Trehalose (Tre) in KGS and molecular docking of tentatively detected bioactive metabolites with ACE were also conducted. KGS mitigated DOX-induced altered b.w., SBP, QTc, HW/TL ratio, cardiac MDA, histopathology, and plasma biomarkers (Ang-II, ACE, aldosterone, noradrenaline, ANP). The methanolic fraction exhibited the highest yield (5.8 ± 0.81%) and total phenolic content (TPC) (147.68 ± 2.05 mg GAE/g). RA and Tre were quantified at 0.110 ± 0.017 mg/g and 0.077 ± 0.005 mg/g, respectively. Among 30 detected tentative bioactive metabolites in negative mode, Tiliroside showed the strongest ACE binding in molecular docking studies, along with Ros, Cosmosiin, Aromadendrin 4'-glucoside, and Rhoifolin. KGS likely reduces DOX-induced cardiac hypertrophy by attenuating oxidative stress, improving histopathology and other parameters mainly through ACE modulating Ang-II and Noradrenaline levels. Elevated SBP in the DOX + KGS high group may involve ACE-independent pathways. KGS High dose exhibits anti-cardiac hypertrophic effects by ACE inhibition and Ang-II modulation. Additional metabolites, apart from RA and Tre, may also contribute to its cardioprotective effects of the polyherbal KGS.

Cardiac hypertrophy, a maladaptive response to sustained cardiac workload, often leads to heart failure and increased mortality. This study investigates the cardioprotective effects of KGS in two doses of 1000 and 2000 mg /kg b.w. against L-NAME-induced hypertension and isoproterenol (ISO)-induced cardiac hypertrophy models, i.e. increased cardiac workload. In the L-NAME model, KGS at a high dose decreased systolic blood pressure (SBP) and RR intervals, enhancing eNOS expression (IHC) and ultimately alleviating L-NAME-induced cardiac workload. At high dose KGS significantly mitigated ISO-induced prolonged QTc, decreased SBP, elevated myocardial malondialdehyde (MDA) levels,

plasma Noradrenaline, Ang-II, Aldosterone and ANP, histopathological changes, including fibrosis and myocyte disarray. Echocardiographic parameters, such as left ventricular mass and Anterior and posterior wall thickness, were decreased with KGS high-dose treatment, reflecting improved cardiac remodeling. Moreover, in vitro studies showed KGS protective effect against ISO-induced cytotoxicity and calcium overload in H9C2 cells, with significant restoration of cell viability at 200 µg/ml. KGS exhibited minimal CYP enzyme inhibition with IC50 >5 µg/ml, suggesting a low potential for drug-drug interactions and, subsequently, its application in combination drug administration. These findings highlight the potential of KGS, particularly at high doses, in reducing cardiac workload and preventing pathological cardiac remodeling, as well as its therapeutic potential for hypertension and hypertrophic cardiac conditions. Metabolite profiling of KGS revealed 19 tentatively detected metabolites which were Docked against eNOS and β1 adrenergic receptor. Tiliroside and Trehalose showed the best docking score against eNOS and β1 adrenergic receptor respectively KGS probably mitigates ISO-induced cardiac hypertrophy by reducing plasma Ang-II (in vivo) and intracellular calcium (in vivo), as observed in the in vitro study of H9C2 cells.

KGS shows potential as a cardioprotective agent by reducing hypertension (L-NAME), cardiac hypertrophy (DOX and ISO), and oxidative stress. Its effects are mediated through ACE inhibition, eNOS activation, Ang-II modulation and modulation of intracellular calcium (invitro) through bioactive metabolites like Rosmarinic acid (RA) and Trehalose (TR). With minimal CYP enzyme inhibition, KGS offers a promising and safe therapeutic option for cardiovascular conditions. It may act through RAAS offering significant cardio-protection.

KGS, a traditional Unani polyherbal formulation, contains RA and TRE, which are prone to instability and require a controlled release in the management of cardiovascular disorders. Conventional drug carriers like sodium alginate and chitosan improve the stability and release profiles of bioactive compounds. This study aims to develop KLCAB for the colonic delivery of RA and TRE. The objective was to formulate and optimize KLCAB using a Box-Behnken design. The study evaluated the encapsulation efficiency (%EE), drug loading content (LC), and release behaviour of the beads under different pH conditions.

Additionally, structural, thermal, and surface properties were characterized using Fourier-transform infrared spectroscopy (FTIR), thermogravimetric analysis (TGA), and scanning electron microscopy(SEM). Among the 16 formulations, F13 (5% sodium alginate, 10% $CaCl_2$, and 0.75% chitosan) demonstrated the highest %EE for RA (63.3%) and TRE

(25.1%) and the experimental data agreed with the Design expert-13 suggestions. FTIR confirmed successful encapsulation and ionic interactions between alginate and chitosan, while TGA revealed improved thermal stability of the KGS-loaded chitosan-coated pH-sensitive alginate beads. SEM analysis indicated that the chitosan coating reduced surface irregularities and enhanced bead uniformity. Swelling studies exhibited significant pH-dependent behaviour, with minimum swelling at pH 1.2 due to the compact polyelectrolyte complex (PEC) layer and pronounced swelling at pH 7.4 due to ion exchange and matrix erosion. Release profiles revealed a controlled, prolonged release of RA and TRE. F5 demonstrated the most favourable release characteristics, with Korsmeyer-Peppas and Higuchi's models fitting the release data under neutral and acidic conditions, respectively. This suggests a diffusion-controlled release mechanism influenced by matrix swelling and structural integrity.

The results indicate that increasing sodium alginate and $CaCl_2$ concentrations positively impacts encapsulation efficiency, while higher chitosan levels reduce it. The compact PEC layer formed by ionic interactions improved bead stability and modulated release. The beads exhibited enhanced performance at pH 7.4, making them suitable for colon-targeted drug delivery. The successful validation of the linear model highlights the reliability of the optimization process. KGS loaded Chitosan-coated pH sensitive alginate beads were effectively optimized for the delivery of RA and TRE, achieving stability, pH sensitivity, and controlled release. The findings underscore the potential of integrating traditional formulations like KGS into modern drug delivery systems, paving the way for improved therapeutic outcomes in chronic disease management.

KGS, a low-cost unani preparation, shows significant cardio-protection and anti-hypertensive activity, which confirms its traditional claims with relevant scientific evidence.

Kolkata, 07/07/2025

Md. Adil Shaharyar

Md. Adil Shaharyar

CONTENTS

LIST OF TABLES

LIST OF FIGURES

LIST OF ABBREVIATIONS

Short Form	Full Form
USM	Unani System of Medicine
KAS	Khamira Abresham Sada
KAHAW	Khamira Abresham Hakim Arshad Wala
KGS	Khamira Gaozaban Sada
Kilth-e-Balgam	Phlegmatic Humour
BMAE	Bombyx mori Aqueous Extract
DOX	Doxorubicin
SBP	Systolic Blood Pressure
TNF-α	Tumor Necrosis Factor-alpha
CVD	Cardiovascular Disease
WHO	World Health Organization
L-NAME	Nω-nitro-L-arginine methyl ester
i.p.	Intraperitoneal
DMM	Dawaul Misk Motadil
MSR	Mufarreh Shaikhur Rais
HS	Habb-e-Jadwar
ECG	Electrocardiogram
ANP	Atrial Natriuretic Peptide
NCD	Non-Communicable Disease
LC	Liquid Chromatography
QTRAP	Quadrupole Ion Trap
ESI	Electrospray Ionization
IS	Internal Standard
MRM	Multiple Reaction Monitoring
tpr	Total Peripheral Resistance
NOS	Nitric Oxide Synthase
NO	Nitric Oxide
CNS	Central Nervous System
SNS	Sympathetic Nervous System
RAAS	Renin-Angiotensin-Aldosterone System
Ang-II	Angiotensin-II
cGMP	Guanosine-3′,5′-Cyclic Monophosphate
CHD	Coronary Heart Disease
HF	Heart Failure

Short Form	Full Form
HR	Heart Rate
GFR	Glomerular Filtration Rate
NA	Noradrenaline
Mfg	Manufacturing
Lic	Licence
ACE	Angiotensin-Converting Enzyme
ACEI	Angiotensin-Converting Enzyme Inhibitors
ANG II	Angiotensin II
BSA	Bovine Serum Albumin
CHF	Congestive Heart Failure
ELISA	Enzyme-Linked Immunosorbent Assay
FSSAI	Food Safety and Standards Authority of India
GS1/GS2	Gas Supply 1/Gas Supply 2
H&E	Hematoxylin and Eosin
HW/TL	Heart Weight/Tail Length
IAEC	Institutional Animal Ethics Committee
LC-MS/MS	Liquid Chromatography-Mass Spectrometry/Mass Spectrometry
LV	Left Ventricular
MDA	Malondialdehyde
NIBP	Non-Invasive Blood Pressure
TBA	Thiobarbituric Acid
TCA	Trichloroacetic Acid
TMP	Total Mitochondrial Protein
Tris	Tris(hydroxymethyl)aminomethane
QTc	Corrected QT Interval
b.w.	Body Weight
LVEF	Left Ventricular Ejection Fraction
ROS	Reactive Oxygen Species
TPC	Total Phenolic Content
IL-6	Interleukin-6
CK-MB	Creatine Kinase-MB
LDH	Lactate Dehydrogenase
CSE	Cocoon Silk Extract
ECSE	Ethanolic Cocoon Silk Extract
ISO	Isoproterenol
VLDL	Very-Low-Density Lipoprotein

Short Form	Full Form
LDL	Low-Density Lipoprotein
HDL	High-Density Lipoprotein
OPA1	Ocular Atrophy 1
ACAT1	Acetyl-CoA Acetyltransferase 1
NDUFS1	NADH-ubiquinone Oxidoreductase 75 kDa Subunit
GLA	Gamma-Linolenic Acid
DGLA	Dihomogamma-Linolenic Acid
AA	Arachidonic Acid
PPARγ	Peroxisome Proliferator-Activated Receptor Gamma
C/EBPα	CCAAT/Enhancer-Binding Protein Alpha
SREBP-1c	Sterol Regulatory Element-Binding Protein 1c
WKY	Wistar Kyoto
SHR	Spontaneously Hypertensive Rats
SOPE	Saccharum Officinarum Peel Extract
DBP	Diastolic Blood Pressure
TXA2	Thromboxane A2
PGI2	Prostacyclin
6-keto-PGF1α	6-Ketoprostaglandin F1 Alpha
TXB2	Thromboxane B2
D-003	Sugarcane Wax Derivative
ERK	Extracellular Signal-Regulated Kinase
JNK	c-Jun N-terminal Kinase
NF-κB	Nuclear Factor Kappa B
ABCA1	ATP-Binding Cassette Transporter A1
ABCG1	ATP-Binding Cassette Transporter G1
CD36	Cluster of Differentiation 36
ACE2	Angiotensin-Converting Enzyme 2
AT1R	Angiotensin II Type 1 Receptor
MasR	Mas Receptor
gp91phox	Glycoprotein 91-Phagocyte Oxidase
APD	Action Potential Duration
Vmax	Maximum Depolarization Velocity
ICa.L	L-Type Calcium Current
INa.L	Late Sodium Current
INa.P	Peak Sodium Current
IK	Delayed Rectifier Potassium Current

Short Form	Full Form
Ito	Transient Outward Potassium Current
EAD	Early Afterdepolarization
DAD	Delayed Afterdepolarization
ATX II	Anemonia sulcata Toxin II
ΔMAP	Change in Mean Arterial Pressure
ΔSBP	Change in Systolic Blood Pressure
RAS	Renin-Angiotensin System
MABP	Mean Arterial Blood Pressure
IP	Intraperitoneal
ERK1/2	Extracellular Signal-Regulated Kinase ½
BASMCs	Bovine Aortic Vascular Smooth Muscle Cells
WTAAE	Whole-Tree Agarwood-Inducing Technique Alcohol Extract
Nrf2-ARE	Nuclear Factor Erythroid 2-Related Factor 2 - Antioxidant Response Element
HMG-CoA	3-Hydroxy-3-Methylglutaryl-Coenzyme A
PAF	Platelet-Activating Factor
C-14	Carbon-14
VEGF	Vascular Endothelial Growth Factor
ADP	Adenosine Diphosphate
AgNPs	Silver Nanoparticles
$AgNO_3$	Silver Nitrate
Akt	Protein Kinase B
ANPs	Atrial Natriuretic Peptides
APG7	Autophagy-Related Protein 7
AuNPs	Gold Nanoparticles
Bcl-2	B-cell Lymphoma 2
Bax	Bcl-2-Associated X Protein
BP	Blood Pressure
CAMs	Cell Adhesion Molecules
$CaCO_3$	Calcium Carbonate
Ca^{2+}	Calcium Ions
COX	Cyclooxygenase
CT	Cinnamomum Tamala
ECs	Endothelial Cells
eNOS	Endothelial Nitric Oxide Synthase
H_2O_2	Hydrogen Peroxide

Short Form	Full Form
HIF-1α	Hypoxia-Inducible Factor 1-alpha
HUVECs	Human Umbilical Vein Endothelial Cells
I/R	Ischemia-Reperfusion
IL-1β	Interleukin-1 Beta
LOX	Lipoxygenase
MAL	Mytilus Margaritiferus
MI	Myocardial Infarction
MMP	Mitochondrial Membrane Potential
Mo'tadil	Moderate Temperament (Unani term)
Muqawwi Qalb	Cardioprotective (Unani term)
Mufarrih	Exhilarant (Unani term)
Muharrik Hararat Gharizia	Heat Stimulating (Unani term)
NLRP3	NOD-, LRR-, and Pyrin Domain-Containing Protein 3
PGC-1α	Peroxisome Proliferator-Activated Receptor Gamma Coactivator 1-alpha
ppm	Parts Per Million
ROS	Reactive Oxygen Species
SAL	Santalum Album L.
Sr	Strontium
TGF-β1	Transforming Growth Factor Beta 1
VEGFA	Vascular Endothelial Growth Factor A
YAP	Yes-Associated Protein
Zoaf-e-Qalb	Cardiac Insufficiencies (Unani term)
MS	Malus sylvestris (scientific name of a plant)
OGD/Re	Oxygen-Glucose Deprivation/Re-Oxygen

CHAPTER- I

INTRODUCTION

1. Introduction

Unani medicine, originating from ancient Greek practices, expanded from Asia Minor to Persia, Arabia, and India. Its name, derived from the Turkish word "Yunan," meaning "Greek," reflects these roots. Introduced to India by Arab scholars who sought refuge following the Mongol invasions, Unani medicine gained prominence as Indian rulers welcomed these practitioners, integrating them into their courts and governments [1] Khusro Malik, the last king of Ghazni, ruled Lahore from 1160 to 1168 and was a notable supporter of Unani medicine. During his reign, physician Diya al-Din 'Abd al-Rafe, with the king's assistance, established the first Unani medicine centre in India, located in Lahore[2].

In 1976, the World Health Organization (WHO) recognized the USM as a globally practised form of alternative medicine, leading to its promotion in India and other countries [3].

In the USM, the balance of Akhlat (humors) is key to maintaining homeostasis in the body. The internal environment, known as Ratubat-al-Tajawif or Ratubat-ul-Uruq, has a specific Mizaj (temperament) that fluctuates within a certain range. Preserving the proper quality and quantity of Ratubat-al-Tajawif is essential for an individual's health [4]

The allopathic system is known for its advanced research and specialized technology; however, it is often associated with adverse effects. In contrast, the USM is considered safer, with fewer side effects and reduced iatrogenicity. Its growing global appeal is due to its effectiveness in managing psychosomatic and chronic diseases [5]. The USM employs various formulations, including solid forms like Habb, Qurs, Shyaf, and Sanoon; semi-solid forms such as Majoon, Itrifal, Jawarish, and Khamira; liquid forms like Maul jubn and Maul-asl; and gaseous treatments like Bakhoor.In the USM, the term "Khamira" refers to a fermented confection that Hakeem initially formulated during the Mogul period. Khamira is a semi-solid formulation known as Majoon. It is manufactured by combining a decoction of herbal remedies or powdered drugs with a base (Qiwam) consisting of sugar or sugar mixed with honey. In addition to herbal ingredients, medications of animal and mineral origin are also combined, either by dissolving them in water or as a finely powdered form. When the decoction turns, white and fermented, scented medications like saffron and musk are combined. Cardiac medications are formulated to have high bioavailability and rapid onset of action. The Khamiras are named according to the ingredients utilized in their manufacture, such as Khamira Aabresham, Khamira Gaozaban Sada, Khamira Marwareed, Khamira Sandal, and others. Khamiras typically function as a cardio-tonic and also as a

tonic for essential organs like the brain, liver, and stomach. It is also used to treat many conditions such as palpitations, heart weakness, weakness of significant organs, cough, cold, catarrh, and respiratory and neurological disorders[6].

A 2023 report based on data from the National Health and Nutrition Examination Survey (NHANES) from 2017 to 2020 highlights that cardiovascular disease (CVD), including coronary heart disease (CHD), stroke, heart failure (HF), and hypertension, affected 48.6% of U.S. adults aged 20 and older, approximately 127.9 million people in 2020. CVD prevalence increases with age for both genders. Excluding hypertension, 9.9% of adults—around 28.6 million—were affected by CVD (CHD, HF, and stroke) in 2020[7] . Over the past 60 years, the incidence of Coronary Heart Disease (CHD) in India has significantly increased. In urban populations, the rate has risen from 1% to 9%–10%, while in rural areas it has increased from 1% to 4%–6%. Using strict criteria based on clinical Q waves, the prevalence of CHD is estimated at 1%–2% in rural areas and 2%–4% in urban populations [8]

Large cohort studies have shown that high blood pressure is a significant risk factor for heart failure, atrial fibrillation, chronic kidney disease, heart valve diseases, aortic syndromes, and dementia, as well as coronary heart disease and stroke. [9]

Given the global rise in the prevalence of cardiovascular disorders, as mentioned above, it is crucial to conduct a comprehensive assessment of the traditional practice of using Khamira for treating heart diseases in USM. This review article aims to evaluate the traditional and scientific perspectives on three selected Khamira formulations, namely KAS, KAHAW and KGS in the management of cardiovascular diseases. By exploring the principles of the USM, detailing the preparation methods, and justifying the inclusion of sugar in Khamira, this review seeks to integrate traditional knowledge with contemporary scientific evidence. Further, the review will analyze *in vitro* and *in vivo* studies on the plant components present in the selected Khamira's and their primary phytoconstituents, assessing their pharmacological activity and therapeutic potential in cardiovascular disorders.

The Aim and Objective of the study are:

1. Pharmacological investigation of Khamira Gaozaban Sada (a low-cost traditional Unani preparation) with particular application of this Unani preparation in the management of hypertension involving cardiac function.
2. Development of Quality control standards and formulation optimization studies for Khamira Gaozaban Sada, particularly in terms of present conventional dosage forms.

Search methodolgy

Relevant research and review articles were gathered from various online databases, including PubMed, ScienceDirect, Scopus, Google, and Web of Science. The articles were chosen from various databases by using important keywords like “unani”, “Unani system of medicine”, “Khamira” , “Khamira Abreesham Sada, Khamira Abreesham Hakim Arshad Wala, and Khamira Gaozaban Sada”, “cardiac hypertrophy” “hypertension” “cardiovascular disorders” arrhythmia” “various plants names present in the particular Khamira and various phytoconstituents present in that particular plant for possible cardiovascular activity, etc. These collected research and review articles were inspected thoroughly.

USM in a nutshell

The USM is based on essential factors important for optimal human life and are as follows (i) Material cause: Arkan (Primordial Essence), Akhlat (Humours), Aza (Organs), Arwaah (Pneuma), (ii) Formal cause: Mizaj (temperament), Quwa (faculties), Tarkeeb (Structure), (iii) Efficient cause: Six essential factors (Hawe-Muheet, Makool Wa Mashroob, Harkat badni, Harkat Nafsani, Naum wa Yaqza and Istifragh wa Ehtebas), and non-essential factors, and (iv) Final cause: Afa’al (Functions) (Figure 1). Therefore, the intended result is the Afa'al (functions), so the malfunction of a specific organ reveals the disorder of that organ. The proper structure and function of organs are essential for maintaining health, and any structural or nutritional defects—originating from the imbalance in humours—can disrupt functions. This imbalance, whether caused by qualitative disruptions in the organ (Kaifiyat) or the regulatory force (Tabiyat), leads to disease. Arkan are the fundamental building blocks in Unani medicine, and their proper arrangement results in the optimal functioning of organs. The unique combination of Arkan forms the distinctive Mizaj (temperament) of each organ, which determines its specific functions. Disease arises when there are abnormalities in either structure or function, which Unani medicine categorizes as Su-e-

Mizaj (abnormal temperament). The treatment approach, Ilaj Biz-Zid (heteropathy), aims to restore balance by addressing the abnormal Mizaj. Mizaj is at the core of diagnosis and treatment in USM, with its characteristics—like moisture (Rutubat), dryness (Yubusat), heat (Hararat), and coldness (Burudat), which are easily analysed through observation and sensory evaluation. An individual's health depends on maintaining the right balance of Mizaj, and any imbalance, often reflected in disturbed humours, indicates disease. The equilibrium of humour and the balance of Mizaj are essential for diagnosing and treating diseases, ensuring both the health of organs and the overall body in Unani medicine [10,11].

Figure 1: The USM emphasizes harmony and balance within the body. The system is based on important concepts such as Arkan (elements), Mizaj (temperament), Akhlat (humors), Aaza (organs), Arwah (vital spirit), Quwa (faculties), and Afaal (functions). Each component plays a vital role in maintaining overall health and treating diseases.

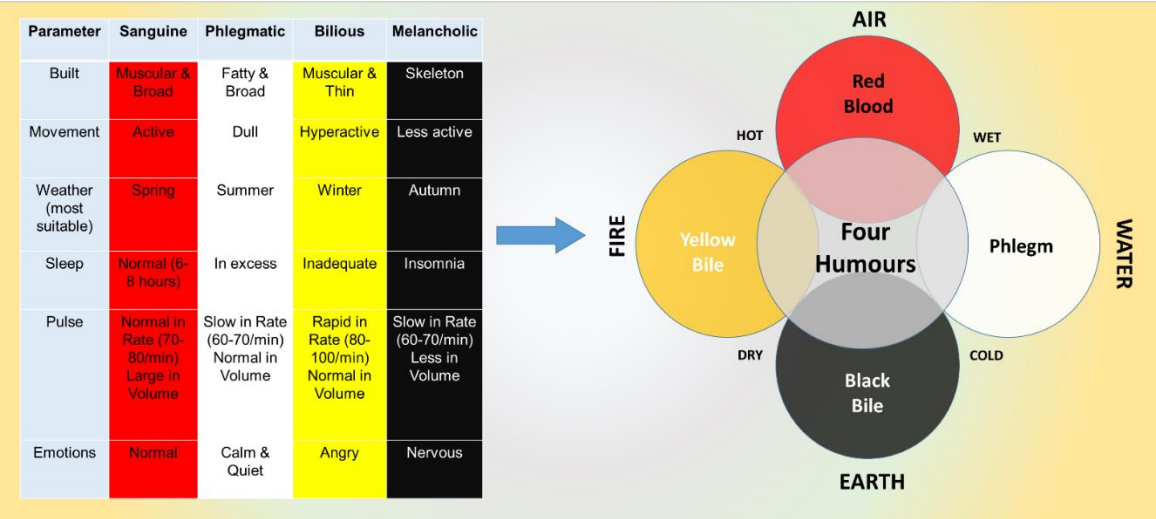

Parameter	Sanguine	Phlegmatic	Bilious	Melancholic
Built	Muscular & Broad	Fatty & Broad	Muscular & Thin	Skeleton
Movement	Active	Dull	Hyperactive	Less active
Weather (most suitable)	Spring	Summer	Winter	Autumn
Sleep	Normal (6-8 hours)	In excess	Inadequate	Insomnia
Pulse	Normal in Rate (70-80/min) Large in Volume	Slow in Rate (60-70/min) Normal in Volume	Rapid in Rate (80-100/min) Normal in Volume	Slow in Rate (60-70/min) Less in Volume
Emotions	Normal	Calm & Quiet	Angry	Nervous

Figure 2: Depicts the fundamental basis of classification of an individual based on their built, movement, his/her suitability to a particular weather, pulse, emotions, sleep. Then, on this basis, they are classified as sanguine or phlegmatic or Bilious or Melancholic, and according to this classification, they are treated with a particular drug.

Khamira with Saccharides? A curse or boon

Unani medicine traditionally prepares sugar-based formulations like Ma'j_un (electuary) and Khamira (fermented confection) by adding drugs to or boiling them in sugar syrup. Boiling sucrose in water leads to partial hydrolysis, forming glucose and fructose, which may offer advantages such as preventing sucrose crystallization and lowering the glycemic index. Additionally, these sugars can form deep eutectic solvents, i.e., natural deep eutectic solvents (NADES), which improve the bioavailability of therapeutic compounds, as seen with honey and other sugar mixtures. NADES, introduced by Choi et al. in 2011, are natural solvents that dissolve bioactive components, enhance stability, and boost bioactivity. Honey, for example, can increase the levels of flavonoids and saponins in herbal medicines and improve their bioavailability. Similarly, honey-like mixtures of glucose, fructose, and sucrose have been shown to release beneficial plant compounds and provide storage stability. Most Unani electuaries require storage periods ranging from days to years to reach their "optimum temperament," a process noted by early scholars like Ibn Sina and Haly Abbas. During storage, fermentation occurs, breaking down complex components, enhancing drug bioavailability, and potentially reducing sucrose content.

Furthermore, fermented electuaries may have a lower glycemic index due to the conversion of sucrose into simpler sugars like fructose. Studies like the one by Cervera-Chiner et al.,

suggest that similar investigations on Unani formulations could confirm this effect after storage [12]. A normal heart derives ATP more from the oxidation of fatty acid than glucose metabolism. However, during cardiac ischaemia and hypertrophy, the heart generates more ATP from glucose metabolism rather than fatty acid oxidation [13]. We suspect that the Unani physicians, based on their observation during practice, might have utilized honey and sugar in Khamiras not only for taste masking or preservative action but also to achieve better therapeutic outcomes in heart failure, which they referred to as Zoaf-e-Qalb (as per their terminology) while unaware of the above-mentioned pharmacological implications.

Preparation of Khamiras

The general method used for preparing Khamirajat (singular: Khamira) aims to achieve a balanced consistency that is intermediate, being neither as thick as Majoon (electuary) nor as liquid as Sharbat (syrup) [14]. In Khamira, the drugs used are either in powdered or liquid form. Khamira preparations involve combining purified water with the drugs, though sometimes distillates (Arq) or fruit juices (Aabiyat) are used. The ratio of drugs to water, Arqiyat (aqueous distillate), or Aabiyat (fruit juice) varies. Once the desired amount of Joshanda is obtained as per USM guidelines, the base, or Qiwam, is prepared using pure sugar, with or without honey, and cooked over low heat to achieve the ideal Khamira consistency [15]. The Qiwam (base) of Khamira (Consistency) is evaluated by applying pressure between the thumb and index finger. A drop of the Khamira's Qiwam can be placed on the floor and monitored for two Tar. If the drop does not spread on the floor, it is deemed to be of high-quality Qiwam [15]. Once the Qiwam is prepared, it is continuously stirred over a flame until it changes to a white or whitish colour. At this point, the remaining components are added, along with silver or gold foil. When Khamira is stirred, it reacts with atmospheric carbon dioxide, causing it to swell, similar to the action of yeast, which is the origin of its name. The ingredients used in Khamira formulations come from plant, animal, and mineral sources. Crude ingredients like Abresham (Bombyx mori) and Daronj Uqrabi (Doronicum hookeri Hook.f.) are ground into coarse powder for decoctions or infusions. Nuts and dried fruits are finely ground using a Kharal (mortar and pestle) and added in small amounts to the Qiwam. A 40-mesh sieve is used for sieving the kernel powder. Precious stones, including Zammarrud (Emerald), Zahar Mohra (Mineral Stone), and Ambar Ash-hab (Ambra grasea), are finely pulverized and incorporated only after the Qiwam preparation. Zafran (Crocus sativus Linn.) and Musk (Moschus moschiferus Linn.) must be ground with Arq-Keora (Screw pine distillate), Arq-Gulab (Rose distillate), or Arq-Bed

Mushk (Distillate of Bed Mushk) and added during the final stage of Khamira preparation. Warq Nuqra (Silver leaf) is also added at the last stage of production. [16].Khamira contains preservatives such as Sat-e-leemu, Shab-e-yamani, and Sodium Benzoate [17]. The preparation of Khamira typically involves mixing medicinal ingredients with water or sugar, though different Unani texts suggest varying proportions of these components. Even the same type of Khamira can be prepared using different ratios based on the physician's practice. Thus, it is essential to compile and summarize these diverse formulations used by Unani practitioners, as each variation can influence the consistency, effectiveness, and properties of the Khamira.

Table 1. The different Drug/Water and Drug/Sugar ratios for Khamira preparation as recorded by physicians in different Unani books

Khamira	Weight of Drug (gms)	**Water/ Arqiyat/ Abiyat (ml)**	**Sugar/ Honey/Misri (rock sugar) (gm)**	***Distillate / Water Ratio***	Distillate/ sugar ratio	***Yield Of Joshanda***	Therapeutic application	Reference
Khamira Abresham Sada	215	1600	1000	1:7	1:5	-	It is used in *khafqan* (Palpitation) and other *Qalbi Amraz* (cardiac ailments. It is used as *Muqavvi Qalb* (Cardiac tonic).	[17]
Khamira Abresham Sada	316	2880	444	1:9	1:4	1/3		
Khamira Abresham Sada	478.75	2000	3000	1:4	1:6	3/4		
Khamira Abresham Sada	544	1008	960	1:2	1:2	-		
Khamira Abresham Sada	215	1600	1000	1:8	1:8	-		
Khamira Abresham Sada	520	2025	3000	-	1:4	3/4		
Khamira Abresham Hakim Arshad Wala	615	2960	1250	1:5	1:2	1/3	It is beneficial in *Amraz-e-Qalb* (cardiac ailments), *Khafqan* (Palpitation), *Malekholia* (Melancholia), and *Nazla* (Catarrh) in summer. [18,21]. It is used as *Muqavvi Jigar* (Liver) Tonic), *Muqavvi Qalb* (Heart Tonic), *Muqavvi Dimag* (Brain Tonic), *Muqavvi Azae raeesa* (Vital organs Tonic)	[15]
Khamira Abresham Hakim Arshad Wala	611	2928	960	1:5	1:2	1:3		
Khamira Abresham Hakim Arshad Wala	1691.72	7000	2500	1:4	1:1	3/4		
Khamira Abresham Hakim Arshad W#ala	608	2928	480	1:5	1:1	1/3		
Khamira Abresham Hakim Arshad Wala	609	2928	960	1:5	1:2	-		
Khamira Abresham Hakim Arshad Wala	1822.4	7100	2500	1:4	1:1	3/4		
Khamira Gaozaban Sada	160	2000	1500	1:12	1:9	670 ml	It is used in *Khafqan* (Palpitation). It is used as a *Muqavvi Basar* (Eye Tonic), *Muqavvi e Hafiza* (Memory Enhancer), *Muqavvi Qalb* (Heart Tonic), *Muqavvi e Dimag* (Brain Tonic)	[1,15]
Khamira Gaozaban Sada	144	1920	1200	1:13	1:8	-		
Khamira Gaozaban Sada	1020	10000	10000	1:10	1:10	1/5		
Khamira Gaozaban Sada	225	960	960	1:4	1:4	-		
Khamira Gaozaban Sada	114	1920	1200	1:13	1:8	1/3		
Khamira Gaozaban Sada	160	2000	1500	1:12	1:9	670		
Khamira Gaozaban Sada	1482.4	10000	8000	1:8	1:5	1/5		

CHAPTER - II

LITERATURE REVIEW

Cardiovascular effects of plant components in the selected Khamiras

The different plant components present in the three selected Khamiras have been listed and mentioned below (Table 2,3,4) [6,18] . Below, we have discussed the cardiovascular activity of various plant components present in the three selected Khamiras.

Table 1: List of plant components present in KAS [18]

SL.No	Name as per USM	Scientific name	source
1	Abresham Muqarraz	Bombyx mori cocoon	Animal
3	Berg Badranjboya	*Nepeta hindostana* (B.Heyne ex Roth) Haines	Plant
4	Berg Gaozaban	Leaf of *Borago officinalis* L.	Plant
5	Gule Khatmi	*Althaea officinalis* L.	Plant
6	Shakar Safaid	*Saccharum officinarum*	Plant
7	Sat Leemun	*Citrus aurantium* L.	Plant
8	Zafran	*Crocus sativus* L.	Plant
9	Natroon Banjawi	Sodium Benzoate	--

Table 2: List of plant components present in Khamira Gaozaban Sada [18]

SL.No	Name as per USM	Scientific name	source
1	Abresham muqarraz	*Bombyx mori* cocoon	Animal
2	Badranjboya	*Nepeta hindostana* (B.Heyne ex Roth) Haines)	Plant
3	Berg e Gaozaban	*Borago officinalis L.*	Plant
4	Burada Sandal Safaid	*Santalum album L.*	Plant
5	Behman Surkh	*Salvia haematodes L.*	Plant
6	Tukhm Balangu	*Lallemantia royleana* (Benth)Benth.	Plant
7	Tudri Surkh	*Cheiranthus cheiri L.*	Plant
8	Kishneez Khushk	*Coriandrum sativum L.*	Plant
9	Gule Khatmi	*Althaea officinalis L.*	Plant
10	Gule Gaozaban	Flower of *Borago officinalis L.*	Plant
11	Shakar safaid	*Saccharum officinarum*	Plant
12	Sat Leemun	*Citrus aurantium L.*	Plant
13	Natroon Banjawi	Sodium benzoate	

Table 3: List of plant components present in Khamira Aabreesham Hakim Arshad Wala [6]

SL.No	Name as per USM	Scientific name	Source
1	Ood Gharqi	*Aquilaria agallocha*	Plant
2	Sumbul ut teeb	*Nardostachys jatamansi*	Plant
3	Post Turanj	*Citrus medica*	Plant
4	Mastagi	*Pistacia lentiscus*	Plant
5	Qaranfal	*Syzygium aromaticum*	Plant
6	Dana Ilaichi Khurd	*Elettaria cardamomum*	Plant
7	Sazaj Hindi	*Cinnamomum tamala*	Plant
8	Burada Sandal Safaid	*Santalum album*	Plant
9	Aabresham	*Bombyx mori*	Animal
10	Ambar	*Ambra grasea*	Animal
11	Marwareed	*Mytilus margaritiferus*	Animal
12	Yaqoot	*Corundum*	Mineral
13	Yashab Sabz	*Jade, Green Jasper*	Mineral
14	Kehruba Shamai	*Pinus succinifera*	Plant
15	Marjan	*Corallium rubrium*	Animal
16	Mushk	*Moschus moschiferous*	Animal
17	Zafran	*Crocus sativa L.*	Plant
18	Warq-e-Nuqra (silver)	*Argentums*	Mineral
19	Warq-e-Tila (Gold)	*aurum*	Mineral
20	Arq-e-Gaozaban	*Borago officinalis*	Plant
21	Arq-e-Baidmushk	*Salix caprea*	Plant
22	Arq-e-Gulab	*Rosa damascene*	Plant
23	Arq-e-Keora	*Pandanus tectorius*	Plant
24	Aab-e-Seb Sheerien	*Malus sylvestris*	Plant
25	Aab-e-Anar Sheerien	*Punica granatum*	Plant
26	Aab-e-Behi Shereen	*Cydonia oblonga*	Plant
27	Aab-e-Baran	Rain Water	-
28	Nabat Safaid	*Saccharum officinarum*	plant

Abresham Muqarraz

In USM, silk, known as "abresham Muqirz" (with "Muqirz" meaning cut), is used as a raw medicinal ingredient in formulations like KAS, KAHAW, and KGS to treat various cardiac and neurological conditions. In USM, it is described as having a "hot" and "dry" temperament and is used for treating palpitations, hypertension, and cardiac disorders linked to arterial stiffening. Liver dysfunction (su-e-mizaj-e-jigar) affects Kilth-e-balgam (analogous to lipid abnormalities in modern terms), resulting in balgam-e-ghair tabaee. This abnormal condition can raise blood viscosity and potentially cause ischemia. Prolonged liver

dysfunction can lead to the transformation of Kilth-e-balgam into Sauda (Vata), a dry substance that may obstruct blood flow, further increasing ischemia and infarction risk. Bombyx mori cocoon extract, administered at a dose of 50 mg/100 g b.w., has been shown to improve lipid profiles, reduce aortic histopathology changes, and lower plaque formation in the aorta in New Zealand white rabbits with atherosclerosis induced by a cholesterol (1%) and coconut oil (4%) diet. The reduction in cholesterol and increase in HDL levels is likely due to the active component, sericin. [19].

Cocoon silk extract (CSE) ameliorated heart damage in Isoproterenol-induced cardiotoxicity in rats [20]. Similarly, ethanolic cocoon silk extract (ECSE) at doses of 250 and 500 mg/kg/day alleviated ISO-induced myocardial infarction in rats [21]. A standardized aqueous extract of Bombyx mori (BMAE) at doses of 30 and 60 mg/kg/day showed cardio-protection against doxorubicin (DOX)-induced cardiomyopathy in adult male wistar albino rats by showing significant antioxidant properties, reducing oxidative stress, lipid peroxidation, pro-inflammatory markers (IL-6), cardiac markers (CK-MB and LDH), and apoptotic markers (caspase-3 and TNF-α) accompanied by improved cardiac histological alterations [22]. Onsa-ard et al. demonstrated that sericin, a constituent of B.mori silk cocoon can reduce SBP by promoting arterial vasodilation and relaxing smooth muscle in the arterial walls by inhibiting calcium channels in a dose-dependent manner. Additionally, they may act as agonists for nitric oxide and prostacyclin, activating pathways that further relax smooth muscle [23]. Okazaki et al. explored how 4% sericin administered to mice fed with high-fat-diet showed no effect on b.w., food intake or fat mass. However, serum cholesterol, triglycerides, free fatty acids, phospholipids, VLDL, LDL and lipogenic enzymes decreased, causing an increase in serum adiponectin by 64%, and improved glucose tolerance, suggesting sericin's hypolipidemic effect is mediated by enhanced serine and reduced methionine concentration [24]. Limpeanchob et al. examined the effects of oral sericin at doses of 10, 100, and 1000 mg/kg in mice. The treatment lowered total and non-HDL cholesterol levels, while triglycerides and HDL remained unchanged. An in vitro model using Caco-2 cells demonstrated that sericin reduces intestinal cholesterol absorption and micelle formation, leading to decreased blood cholesterol levels [25]. Another study showed sericin can have a negative effect on the overall functioning of the digestive system, impeding the absorption of cholesterol in the intestines [26].

A study on hypercholesterolemic Wistar rats treated with sericin (1,000 mg/kg/day for 4 weeks) revealed elevated expression of proteins like ocular atrophy 1 (OPA1) and acetyl-

CoA acetyltransferase (ACAT1), while reducing NADH-ubiquinone oxidoreductase 75 kDa subunit (NDUFS1). These changes enhanced mitochondrial energy efficiency and structure, positively affecting fatty acid oxidation, electron transport, and pyruvate metabolism [27].

Badranjboya/ *Nepata hindostana*

Nepeta hindostana (Badranjboya) has demonstrated significant hypolipidemic and antioxidant effects, showing a protective role in managing hyperlipidemia [19]. Nepeta hindostana, demonstrated cardioprotective and anti-hypolipidemic effects against dyslipidemia induced by Triton WR 1339 (400 mg/kg, i.p.). Its methanolic extract, at a dose of 400 mg/kg, showed the highest efficacy, significantly reducing cholesterol levels and resulting in the lowest atherogenic index likely due to its antioxidant compounds [28].

Borago officinalis

Gaozaban has been used in USM in India. In the market, the crude drug is marketed as leaves (Berg-e-Gaozaban), flowers (Gul-e-Gaozaban), and single-seeded nutlets (Tukhm-e-Gaozaba) [29]. Borage (Borago officinalis L.), seeds are a notable source of gamma-linolenic acid (GLA), making up 16-28% of the oil content and 27-37% of the whole seed. GLA-rich oils from borage are used as dietary supplements to manage health conditions associated with GLA deficiency [30]. Borage oil has shown potential in lowering cholesterol, triglycerides, and phospholipids while increasing omega-6 fatty acids in tissues. It exhibits immunomodulatory, hypotensive, and antioxidant effects, likely through Ca++ channel blockade. Additionally, it may improve work performance by reducing blood pressure and stress responses and offer kidney protection by blocking angiotensin II receptors [31,32]. Another study emphasized the anti-hypertensive role of borago officinalis L [33]. Another study demonstrated anti-obesity effects by inhibiting lipid accumulation in 3T3-L1 adipocytes in a dose of 100-200 mg/kg by reducing weight gain, adipocyte size, and lipid storage. It also suppressed adipogenic gene expression (PPARγ, C/EBPα, SREBP-1c) and increased adiponectin levels, indicating its potential to decrease adipocyte hypertrophy and regulate fat metabolism [34].

Borage oil has been shown to reduce blood pressure in both Wistar Kyoto (WKY) and spontaneously hypertensive rats (SHR), likely due to the conversion of gamma-linolenic acid GLA into dihomogamma-linolenic acid (DGLA) and arachidonic acid (AA). The diet increased omega-6 polyunsaturated fatty acids, with elevated GLA, DGLA, and AA levels

in the plasma, liver, aorta, and renal artery tissues, suggesting these changes may underlie the blood pressure-lowering effects[35]

Althea officinalis L /Gule-e-Khatm

Marshmallow (Althaea officinalis L.) is a perennial herb from the Malvaceae family [36]. In this study, the safety and efficacy of Althaea officinalis (marshmallow) extract in common carp infected with *Aeromonas hydrophila* were assess*ed*. The addition of marshmallow extract at concentrations of 2.50 and 5.00 g/kg feed significantly reduced cholesterol and triglyceride levels, likely by affecting cholesterol production, absorption, and metabolism. Bioflavonoids in marshmallow extract may lower cholesterol by inhibiting HMG-CoA reductase, an enzyme critical for cholesterol synthesis. Additionally, soluble fibres like pectin and mucilage promote bile acid production and reduce cholesterol absorption in the colon. Fatty acids, including linoleic and oleic acids, further contribute to decreased LDL and cholesterol levels [37].In another report, it exhibited anti-inflammatory and anti-oxidant effects [38].

Saccharum Officinarum/ Shakar Safaid

Oral administration of Saccharum officinarum peel extract (SOPE) demonstrated significant anti-obesity and anti-atherosclerotic effects in high-fat diet-induced obese male rats, resulting in reduced systolic blood pressure (SBP), diastolic blood pressure (DBP), heart rate (HR) and oxidative stress. Additionally, SOPE administration alleviated haemorrhage in cardiac tissues and improved the histoarchitecture of the aorta, indicating its significant cardioprotective activity [39].

Arachidonic acid derivatives, such as prostacyclin (PGI2) and thromboxane A2 (TXA2), are crucial in endothelial dysfunction and thrombosis. Cyclooxygenase in the arterial wall converts these metabolites into 6-keto prostaglandin F1 alpha (6-keto-PGF1α) and thromboxane B2 (TXB2). The TXB2/6-keto-PGF1α ratio is essential for regulating blood flow and maintaining blood vessel integrity. Policosanols and D-003, a sugarcane wax derivative, exhibited anti-thrombotic effects. Administering D-003 (200 mg/kg) and policosanols (25 mg/kg) significantly, increased 6-keto-PGF1a levels, decreased TXB2 levels, and reduced venous thrombus weight. D-003 showed rapid effects within 30 minutes, peaking at 1-2 hours [40].

Citrus aurantium L/ Sat Leemun

Citrus aurantium (bitter orange) is widely used in food and dietary supplements, particularly for weight loss, due to its active component p-synephrine, which mimics adrenergic agents[41]. Neroli, the essential oil from Citrus aurantium L. var. amara has shown vasodilatory properties. Neroli-induced vasodilation was observed in aortic rings precontracted with prostaglandin F2 α. Thus, neroli-induced vasodilation involves both endothelial NO-sGC signalling and the modulation of smooth muscle calcium influx and release[42]. Homoeriodictyol (HE) and hesperetin-7-O-β-D-glucopyranoside (HG), isolated from Citrus aurantium, exhibited anti-inflammatory properties and inhibited foam cell formation in RAW264.7 macrophage cells. HE was more effective than HG in reducing lipopolysaccharide (LPS)-induced inflammatory markers such as nitric oxide (NO), interleukin-6 (IL-6), and tumor necrosis factor-α (TNF-α). Both compounds modulated inflammatory signalling pathways like ERK, JNK, P38, and NF-κB. Moreover, HE and HG reduced oxidized low-density lipoprotein (ox-LDL)-induced foam cell formation, crucial in atherosclerosis progression, by regulating genes and proteins such as PPARγ, ABCA1, ABCG1, and CD36. HE showed more substantial anti-inflammatory and anti-atherogenic potential compared to HG[43]. In L-NAME-induced hypertensive rats, limonin (50 and 100 mg/kg) effectively lowered blood pressure and improved cardiovascular function. It restored ACE activity, balanced Ang II levels, and increased ACE2. Limonin also reduced oxidative stress, enhanced antioxidant enzyme activity, and elevated nitric oxide metabolites (NOx). It suppressed inflammatory markers like TNF-α and IL-6 in heart tissue and plasma and regulated critical molecular targets such as AT1R, MasR, NF-κB, and gp91phox [44]. Naringin, a flavonoid from Citrus aurantium L., exhibited significant antiarrhythmic effects at cellular and organ levels. It shortened action potential duration (APD), reduced maximum depolarization velocity (Vmax), and inhibited L-type calcium (ICa.L) and late sodium currents (INa.L) in a dose-dependent manner. Additionally, it decreased peak sodium current (INa•P), delayed rectifier potassium current (IK), and transient outward potassium current (Ito). Naringin effectively counteracted early and delayed after depolarizations (EAD and DAD) triggered by anemone toxin II (ATX II) and CaCl2, respectively. In mouse hearts, it lowered the occurrence and duration of ATX II-induced ventricular tachycardia and fibrillation. The antiarrhythmic actions of naringin are attributed to its modulation of multiple ion channels[45,46] .

Crocus sativa L. or Zafran

In this study, a hydroalcoholic extract of Crocus sativus was administered at doses of 10, 20, and 40 mg/kg to rats with AngII-induced hypertension (300 ng/kg). The 10 and 20 mg/kg doses significantly reduced changes in mean arterial pressure (ΔMAP) and ΔSBP more effectively than Losartan. The antihypertensive effects of Crocus sativus may be partly due to its inhibition of the renin-angiotensin system (RAS), suggesting its potential as a therapeutic agent for AngII-induced hypertension [47]. Its aqueous extract (10 mg/kg) and two active constituents, crocin (200 mg/kg) and safranal (1mg/kg), reduced the MABP in normotensive and desoxycorticosterone acetate-induced hypertensive rats in a dose-dependent manner[48].In another study, Its aqueous extract (20, 40, 80 and 160 mg/kg IP) and safranal pretreatment (0.025, 0.050, 0.075 ml/kg IP) in wistar rats mitigated ISO-induced myocardial infarction through modulation of oxidative stress [49]. Crocin, a constituent of Crocus sative L., in a dose of 50, 100 and 200 mg/kg/ slow i.v attenuated the Ang-II induced an increased MAP, SBP and HR in rats. All the doses of crocin ameliorated acute hypertension through RAS[50] and demonstrated antiproliferative and antioxidant effects on bovine aortic vascular smooth muscle cells (BASMCs) by inhibiting AngII-induced proliferation. It blocked cell cycle progression, possibly by suppressing ERK1/2 activation and c-fos expression likely linked to crocetin's antioxidant properties[51]. Furthermore, Aqueous and ethanol extracts of *C. sativus* petals *C. sativus* petals' extract exhibited a reduction in blood pressure in anaesthetized rats[52].

Ood Gharqi (Aquilaria agallocha)

Aquilaria agallocha, known as agarwood, has traditional uses for treating pain and ischemic diseases and is mentioned in ancient texts like the Susruta Samhita and the 8th-century Sahih Muslim [53]. The alcohol extract of agarwood, produced via the whole-tree agarwood-inducing technique (WTAAE), demonstrated significant cardioprotective effects in rats with isoproterenol-induced myocardial ischemia. WTAAE improved abnormal ST elevation, reduced oxidative stress, and enhanced mRNA levels of the Nrf2-ARE pathway while decreasing apoptotic Bax family mRNA expressions, showing superior efficacy compared to other forms of garwood extracts [54]. Its methanol extract (in doses of 2.5, 5.0, 10, 30, 100, 300 µg/mL) in isolated rabbit hearts revealed positive inotropic and negative chronotropic effects, along with reduced coronary flow likely due to cardioactive glycosides in it. The inotropic action was blocked by metoprolol and verapamil, indicating the involvement of β1-adrenergic receptors and L-type Ca2+ channels [55].

Sumbul ut teeb (Nardostachys jatamansi):

Nardostachys jatamansi (D.Don) DC, known as Sumbul-ut-teeb, a Unani medicine used for centuries and is mentioned by Ibn-e-Sina (Avicenna) in his work Kitab al-Adwiya al-Qalbiya for treating cardiac diseases. Clinically, a dose of 3 g (1 capsule 3 times a day) significantly lowered SBP and DBP in patients with primary hypertension, likely due to its influence on the RAS system [56].

Both the ethanolic and methanolic extracts of Nardostachys jatamansi (250 and 500 mg/kg) demonstrated cardioprotective effects against doxorubicin-induced cardiac damage in rats by reducing oxidative stress. Additionally, the methanolic extract lowered HMG-CoA (3-hydroxy-3-methylglutaryl-coenzyme A) levels in doxorubicin-induced cardiotoxicity, indicating its cardioprotective, antioxidant, and hypolipidemic properties[57,58]. Its 70% hydroalcoholic extract (50 mg/kg) protected the heart from isoproterenol (ISO)-induced cardiotoxicity, with its cardioprotective effects attributed to its antioxidant and hypolipidemic properties. At a higher dose of 500 mg/kg b.w. it reduced lipid levels in Triton WR 1339-induced hyperlipidemic rats, showing hypolipidemic effect[57].

Post Turanj (Citrus medica):

Citrus medica L., commonly known as "Otroj" or Brain Citron, belongs to the Rutaceae family. Previous studies have shown that the peel extract of Citrus medica has strong anti-inflammatory properties in rats. The ethanolic extract of Citrus medica, at doses of 250 and 500 mg/kg, demonstrated a significant cardioprotective effect against isoproterenol (ISO)-induced cardiotoxicity in rats by improving lipid profile and showing intense anti-oxidant activity. It showed cardioprotective and hypolipidemic activity [59,60].

Mastagi (Pistacia lentiscus L.):

Mastagi, originating from the Greek word 'Mastakhi,' is a gum obtained from trees in regions like Sham (Syria) and Room (Italy). In USM, it is used as Muhallil (anti-inflammatory) and Mufarreh Qalb (heart-exhilarant) properties [61]. A 100 mg/kg of Pistacia vera L. (green pistachio) reduced DOX-induced cardiac severities through the reduction of 8-hydroxydeoxyguanosine and caspase 3/7 levels, total oxidant. Cardioprotective activity is attributed to antioxidant activity, which reduces cardiac apoptosis and DNA damage[62]. Its lyophilized extract exhibited a hypotensive effect in anaesthetized normotensive wistar rats, while the polymeric procyanidin glycoside (from 3 to 12 mg/kg) extracted from it also showed the same in a dose-dependent manner without affecting heart rate[63]. At a dose of

5 gm per day, pistacia lentiscus L. also showed hypolipidemic effec[64]. A six-week treatment with Chios Mastic gum, derived from the resin of Pistacia lentiscus var. chia, significantly reduced cardiac infarct size in hypercholesterolemic rabbits and showed substantial antiaromatic and hypolipidemic effects without affecting LDL oxidation or lipid peroxidation during reperfusion[65].

Clove/Qaranful (Syzygium aromaticum L.)

Clove, a dried flower bud and a traditional Unani drug is used for individuals with a cold temperament, women, and older people. In the USM, clove is recognized for its *Muhallil* (anti-inflammatory) and *Muqawwī-i-Qalb* (cardiotonic) properties, along with other documented benefits [66]. Clove is known to enhance blood circulation to the heart, making it a valuable tonic for the cardiovascular system [67].

Clove oil has been shown to inhibit platelet aggregation induced by platelet-activating factor (PAF), arachidonic acid, and collagen, with the most potent effects against PAF and arachidonic acid. In vivo studies on rabbits revealed that clove oil doses of 50–100 mg/kg offered complete protection against PAF and approximately 70% protection against arachidonic acid-induced pulmonary platelet thrombosis [68]. Clove oil also inhibited the production of thromboxane-A2 and 12-hydroxyeicosatetraenoic acid in human platelets treated with C-14 arachidonic acid [69].In another investigation it showed fibrinolytic activity and the inhibition of thrombin-induced platelet aggregation, indicating its potential to prevent atherosclerosis [70].

An in vivo study demonstrated that cloves reduced cardiac muscle tissue damage in rats and may improve blood circulation and increase body temperature. Eugenol, the primary compound in clove oil, exhibited dose-dependent vasodilatory and negative inotropic effects on cardiac muscle, as well as smooth muscle relaxation and hypotensive properties. Both eugenol and clove oil have shown effectiveness against fatty liver and dyslipidemia, primarily by reducing oxidative stress. Additionally, administering eugenol at 100 mg/kg, alongside gentamicin, significantly decreased gentamicin-induced oxidative damage [71].

Dana Ilaichi Khurd (Elettaria cardamomum)

Administration of cardamom powder was found to prevent obesity in rats induced by a high-fat diet [72]. A study showed that cardamom treatment (3 g/day for 12 weeks) significantly reduced SBP (from 154.2 to 134.8 mmHg) and diastolic blood pressure (from 91.8 to 79.6 mmHg) in individuals with stage 1 hypertension. It also improved fibrinolysis and

antioxidant status after 3 months [73]. It also reduced blood pressure in a dose of 3-100 mg/kg through cholinomimetic and calcium channel blocking mechanisms. It prevented phenylephrine (1 µM) and potassium (80 mM) induced contraction in the isolated rat aorta, showing vasodilatory action [74]. In a dose of 200 mg/kg b.w. it demonstrated cardioprotective effects in rats by attenuating doxorubicin (DOX)-induced myocardial injury, oxidative stress, apoptosis (caspase 3), inflammation (cardiac NFκB level), and promoting angiogenesis by increasing VEGF immunoreactivity [75].In a dose of 100 and 200 mg/kg, it ameliorated isoproterenol (ISO) and induced decreased arterial pressure, heart rate, contractility, and antioxidant levels, indicating a cardioprotective action[76]. Further, its aqueous extract prevented not only L-NAME-induced vascular remodelling, oxidative stress and hypertension [77] but also decreased the severity of fructose (10%)-induced metabolic hypertension and oxidative stress in a dose of 50, 100, and 200 mg/kg/day[77]

Sazaj Hindi (Cinnamomum tamala)

A study found that Cinnamomum tamala (CT) inhibits platelet aggregation and affects metabolites in the cyclooxygenase (COX) and lipoxygenase (LOX) pathways of arachidonic acid (AA). While its chloroform and n-hexane fractions had no impact on AA metabolism or platelet aggregation, the aqueous fraction inhibited AA metabolites through both COX (TXB2) and LOX (LP1) pathways. It also strongly inhibited AA, ADP, and PAF-induced platelet aggregation, though it was only partially effective against collagen-induced aggregation. The cardiovascular and anti-inflammatory properties of Cinnamomum tamala, especially in the aqueous fraction, may be due to the inhibition of AA metabolites, platelet aggregation, and enhanced antioxidant activity [78]. Further, ethanolic extract of CT at an oral dose of 200 and 400 mg/kg b.w. showed cardioprotective effects against doxorubicin-induced myocardial infarction in Wistar rats [79].

Burada Sandal Safaid (Santalum album L.)

Santalum album L. (SAL) has been shown to protect against ISO-induced heart failure. It exerts therapeutic effects by targeting multiple pathways, including anti-oxidative, anti-inflammatory, and anti-apoptotic mechanisms through YAP and PI3K-AKT signalling pathways, demonstrating a synergistic effect [80]. Sandalwood essential oil obtained from SAL in a dose of 100 mg/kg/day showed cardioprotective activity against DOX-induced cardiac toxicity in Male Sprague-Dawley rats. The oil ameliorated DOX, augmented cardiac injury biomarkers, altered ECG, deceased HR and antioxidants, and finally increased BP. It also mitigated inflammatory biomarkers like IL-1β, TNF-α, and NF-Kβ [81].SAL has also

been reported to show anti-hyperlipidemic and reduce atherogenic. It attenuated lipid profile in diabetic rats and increased cardioprotective high-density lipoprotein (HDL) [82].

Marwareed (Mytilus margaritiferus)

In USM, pearls, known as 'Marwareed,' are traditionally associated with beauty and strength. Calcinated and powdered forms are employed to treat cardiac conditions like heart weakness and myocardial degeneration [83]. In USM, as per their theory of temperament or Mizaj, pearls or Marwareed have been classified as drugs of typical temperament or Mo'tadil mizaj [84]. Water-soluble pearl powder exhibits cardioprotective and antiarrhythmic effects, enhancing cardiac contractility and aiding in sinus rhythm recovery, especially at higher doses i.e.,1 g/kg. In contrast, standard pearl powder shows minimal effects, likely due to its low water solubility, which limits the release of active components. Pearl hydrolysate significantly promotes human microvascular endothelial cell division, proliferation, and migration, suggesting its potential in maintaining vascular endothelium [85].

Yaqoot (Ruby)

Although we could not find any scientific evidence currently in support of the cardiovascular benefits of Yaqoot, it holds great significance in USM for similar applications. Yaqoot, a mineral found in metamorphic rocks, is a deep red, transparent or translucent type of corundum primarily composed of aluminium oxide with traces of Cr_2O_3, titanium, and manganese. In USM, it is known for its balanced temperament (Mo'tadil). It is often included in polypharmaceutical formulations for its cardiotonic (Muqawwi Qalb), exhilarant (Mufarrih), and heat-stimulating (Muharrik Hararat Gharizia) properties [86].

Marjan (Corallium rubrum L)

In the USM, animal-derived drugs, including marine products like marjān (Corallium rubrum L.), are widely used. Corals, composed of calcite and aragonite (polymorphs of calcium carbonate), are rich in $CaCO_3$ and contain carotenoids such as canthaxanthin. They also have measurable amounts of calcium (Ca), magnesium (Mg), sulfur (S), and strontium (Sr), with the red coral skeletons containing approximately 12 ppm of $MgCO_3$ and 3,100 ppm of sulfur. Other elements detected include sodium, potassium, phosphorus, boron, and trace amounts of barium, iron, lithium, manganese, and lead. Calcium derived from marjān is naturally absorbable and quickly metabolized. Unani medicine attributes several

properties to Corallium rubrum, such as being an exhilarant, mood elevator, and cardiotonic, which is beneficial for cardiac insufficiencies (Zoaf-e-Qalb). A study found that administering red coral at a dose of 50 mg/day for six months significantly reduced atherosclerosis induced by a high-cholesterol diet in rabbits, lowering plasma cholesterol by up to 65% and sphingomyelin levels. Additionally, it increased HDL levels and suppressed atheroma formation [87].

Musk

Natural musk, an essential remedy in USM, is obtained from the dried secretions of the preputial glands of male musk deer species like Moschus berezovskii, Moschus sifanicus, and Moschus moschiferus , possessing anti-inflammatory and cardiovascular effects mainly attributed to its water-soluble components [88]. Musk protected H9C2 cardiomyocytes from H_2O_2-induced damage by lowering reactive oxygen species (ROS) levels and boosting the activity of intracellular antioxidant enzymes [89]

Additionally, musk protected human umbilical vein endothelial cells (HUVECs) from H_2O_2-induced damage by boosting intracellular antioxidant enzyme activity and reducing oxidative stress [90]. Muscone, a primary component of musk, can stabilize mitochondrial membrane potential ($\Delta\Psi m$), decrease cellular permeability, and limit calcium (Ca^{2+}) influx, thereby preventing H_2O_2-induced apoptosis in human umbilical vein endothelial cells (HUVECs) both in vitro and in vivo [91]

It has been reported to improve cardiac remodelling and dysfunction, lowering inflammation by downregulating the expression of inflammatory markers, TGF-β1, TNF-α, IL-1β, and nuclear factor-κB (NF-κB). Additionally, it also mitigated myocardial apoptosis by increasing the Bcl-2/Bax ratio. Notably, it also promoted vascular endothelial function through the activation of Akt and eNOS phosphorylation[92]

Further, It also promoted angiogenesis in mice by upregulating hypoxia-inducible factor 1α (HIF-1α) and vascular endothelial growth factor A (VEGFA), which are essential for enhancing vascular growth and improving blood supply to the damaged heart tissue(Du et al., 2018).[93] Additionally, it mitigated MI by reducing macrophage-mediated chronic inflammation by inhibiting NF-κB and NLRP3 inflammasome activation, which subsequently blocks IL-1β, TNF-α, and IL-6, contributing to improved cardiac recovery post-MI [94].

An investigation reported that pretreatment with muscone before ischemia-reperfusion (I/R) injury in cardiomyocytes significantly reduced LDH release, MDA production, creatine kinase activity, caspase-3 activity, intracellular calcium concentration ($[Ca^{2+}]i$), apoptosis rate and Bax protein expression. It also helps maintain mitochondrial membrane potential (MMP) and Bcl-2 protein expression.[95]

Warg-e-Nuqra (Silver)

Both silver nanoparticles (AgNPs) and silver ions ($AgNO_3$) (dose 2.5mg/kg) were able to attenuate ISO-induced MI. However, AgNPs reduced oxidative stress more than silver ions. Moreover, ANPs augmented the expression of mitochondrial transcription factor A and PGC- 1α and decreased the expression of NF-κB while the $AgNO_3$ failed to do so. AgNPs offer better protection against ISO-induced MI than AgNO3 by reducing oxidative stress and NF-κB expression [96].

Warq-e-Tila (Gold)

AuNPs (gold nanoparticles) also display potential cardioprotective properties due to their anti-oxidative and anti-hypertrophic effects, which are exerted via the downregulation of β-adrenoceptors and the subsequent decrease in the ERK1/2-mediated hypertrophic pathway [97]. Au-NPs of sizes (5, 40, and 100 nm) decreased ISO-induced hypertrophy in rats. The 5 nm Au-NPs showed some cardioprotective effects but had minimal heart accumulation, likely due to their small size. Histological analysis indicated Au-NPs caused cardiac fibrosis and apoptosis in control groups but protected hypertrophied rats from these effects. In vitro tests using H9C2 cells and Au-NPs induced autophagy in treated cells, reducing LC3 II conversion, APG7, and caspase 12 levels in hyperthyroid rats but triggering inflammation in control groups. These findings offer insights into the potential use of Au-NPs in heart disease treatment [97]. In human umbilical vein and aortic endothelial cells (ECs) exposed to TNF-α, AuNP reduced the expression of cell adhesion molecules (CAMs), NF-κB via increased ubiquitination and also ROS production. The study indicates that AuNPs have anti-inflammatory effects on vascular ECs in vitro and can minimize arterial neointimal hyperplasia after vascular injury in vivo. In another study, AuNP (41.7 nm, 200 mg/kg/day, IP) derived from cyanobacteria mitigated ISO-induced (MI model) ECG alterations decreased arterial pressure [98].

Aab-e-Seb Sheerien (Malus sylvestris or Pyrus malus)

Malva sylvestris L. (MS) is a traditional herb known for its anti-inflammatory and antioxidant effects. MS extract pre-treatment prevented oxygen-glucose deprivation/re-oxygenation (OGD/Re) damage in H9c2 cells and protected against ischemia/reperfusion (I/R) injury in vivo. MS's cardioprotective effects are linked to the regulation of circular RNA (circRNA), specifically circ003593, which influences the NLRP3 complex and the reperfusion injury salvage kinase (RISK) pathway, offering therapeutic potential in ischemic heart disease [99].

Aab-e-Anar Sheerien (Punica granatum)

Pomegranate (*Punica granatum* L.) belongs to the family Punicaceae (also named Lythraceae). A novel extract obtained from non-edible byproducts i.e. peel and seeds (called PPE), extract of whole fruit (PFE) and Ellagic acid ameliorated Phenylephrine induced increased SBP. The PPE fraction also showed anti-fibrotic and anti-inflammatory effects and may be helpful in cardiac remodelling [100].

Ethanolic extract of pomegranate peel (100 mg/kg BW and 200 mg/kg BW) administered to Zucker diabetic fatty rats (ZDF, MetS rats, fa/fa), model of metabolic syndrome did not show changes in the troponin I (cTnI) and Galectin-3 (GAL-3) yet it did alleviate oxidative stress [101]. In one of the clinical studies, Pomegranate (200 ml daily for 4 weeks) alleviated hypercholestremia. It significantly reduced both systolic (SBP) and diastolic blood pressure (DBP) in T2DM patients, probably through reduction of oxidative stress, upregulation of antioxidant enzymes and modulation of transcription factors like NF-κB and PPARγ [102].

Pomegranate peel extract (mostly punicalagin) alleviated ISO-induced MI in rats. It may prevent MI through increased myocardial expression of eNOS, leading to nitric oxide-mediated Nrf2/ARE activation, thus upregulating antioxidant mechanisms, along with inhibition of apoptosis [103].

Pomegranate flower polyphenol (PFP) extract demonstrated vasodilation effects on rat aorta, particularly in endothelium-intact segments. The effect was partially inhibited by K+ channel blockers (TEA, glibenclamide, BaCl2) and an eNOS inhibitor (L-NAME), and PFP also reduced Ca^{2+} entry, especially under hyperglycemic conditions. These results suggest PFP's potential in managing hypertension, particularly in diabetic patients [104]

Pomegranate juice, given at 80 μM of polyphenols per ml per day, reduced cigarette smoke-induced cardiac hypertrophy in rats by lowering oxidative stress, inflammatory markers (IL-1β, TNFα), and fibrotic/atherogenic markers (fibronectin and leptin receptor) in the aorta. It also decreased aortic calcification and modulated Bradykinin receptors (Bdkrb1 and Bdkrb2), demonstrating its cardioprotective effects [105]. PPE (100 mg/kg b.w.) alleviated Alloxan-induced increases in plasma fibronectin and laminin, as well as left ventricular hydroxyproline and total collagen content. It also reduced ECM remodelling caused by diabetes, as indicated by normalized MMP activity, highlighting its potential in managing diabetes-induced cardiac ECM remodelling [106]

A standardized hydroethanolic extract of PPE (200 mg/kg) reduced plaque necrosis and increased collagen content in lesions while improving metabolic profiles, such as lowering blood glucose, cholesterol, and triglycerides, in an Apoe -/- murine model of advanced atherosclerosis. The reduction in plaque necrosis was linked to improved macrophage efferocytosis, which is associated with higher Mertk receptor expression. In vitro, the peel extract inhibited Mertk shedding, preserving macrophage efferocytosis efficiency and reducing inflammation in atherosclerosis [107].

Aab-e-Behi Sheerien (Cydonia oblonga or Pyrus cydonia)

Aqueous extracts of Quince (Cydonia oblonga Mill.) or COM demonstrated cardioprotective effects against Doxorubicin-induced cardiotoxicity by improving mitochondrial function. The extract reduced mitochondrial reactive oxygen species production, lipid peroxidation, swelling, membrane potential collapse, and cytochrome c release. The fruit extract of COM (0-600 μg/mL) inhibited triglyceride accumulation during adipogenesis in 3T3-L1 cells. Treatment with COM upregulated AMPKα phosphorylation and downregulated adipogenic transcription factors like SREBP-1c, PPARγ, and C/EBPα. It also reduced the expression of enzymes involved in lipid synthesis and storage while increasing the expression of hormone-sensitive lipase and CPT-1. These effects indicate that COM's anti-obesity activity is mediated through the AMPK signalling pathway [108]. COM demonstrated anti-atherosclerotic effects in a rat model of atherosclerosis induced by a high-fat emulsion and vitamin D3. The extract regulated blood lipids, reduced oxidative stress and exhibited anti-inflammatory and vascular protective properties. It lowered serum levels of pro-inflammatory markers (IL-1β, IL-6, TNF-α, CRP) while increasing the anti-inflammatory marker IL-10. Additionally, COM raised levels of NO, eNOS, and 6-keto-PGF1α and reduced ET-1 and TXB2 levels. It also inhibited the expression of EGFR, p-

PI3K, p-AKT, GSK-3β, Bax, and Caspase-3, suggesting its action through the EGFR/PI3K/AKT/GSK-3β pathway [109].

Further, various types of COM extract have shown an anti-hypertensive effect on blood pressure [110] [111] hypolipidemic effect [112]. In vitro, COM extract dose-dependently prolonged bleeding time in tail cutting and glass slide tests, reduced mortality in collagen-epinephrine-induced pulmonary thrombosis, and increased thrombolysis while shortening euglobulin lysis time (ELT). In vivo, it extended venous occlusion time in FeCl3-induced carotid artery thrombosis, reduced thrombus weight in arteries and veins, lowered serum TXB2 levels, and elevated 6-keto-PGF1α levels, indicating its anti-thrombotic activity, likely due to its antithromboxane effect [113].

Arq-e-Bedmushk (Salix caprea L.**)**

In USM, only distilled water (Arq Bedmushk) from Salix caprea is used for medicinal purposes. In Italy, its bud extracts have been used to alleviate oxidative stress-related disorders. Phenolic compounds such as vanillic acid, coniferyl alcohol, catechin, naringenin, and taxifolin have been isolated from their stem wood and knots. Nineteen compounds were identified in the aromatic hydrodistillate of its flowers, with hexahydrofarnesylacetone, 2-butyl-octanol, and 2-hexyl-1-octanol being the primary components. The ethanolic extract of its flowers has shown potent antioxidant effects. Bud extracts inhibit voltage-gated Ca^{2+} channels, reducing catecholamine secretion under oxidative stress conditions. The flower hydro distillate also exhibits notable antioxidant and anti-inflammatory activities[114] and a potent cyclooxygenase inhibitor[115]

Arq-e-Gulab (Rosa damascena)

Rosa damascena (RD) is valued as a cardiotonic agent, attributed to its fragrance and astringent properties. Traditional cardiotonic products derived from rose include rose water and “goleghand,” an electuary made from rose petals and sugar. Recent studies have also shown that rose exhibits inotropic effects and can improve cardiovascular function [116]

The ethanolic extract of RD (EERD) petals (500 mg/Kg b.w) exhibited a cardioprotective effect on ISO-induced MI in experimental rats[117]. Three doses i.e. 250, 500, and 1000 mg/kg of hydroalcoholic extract of RD (HERD) alleviated Ang-II induced hypertension causing a decreased SBP and MAP. 500 and 1000 mg/kg b.w. HERD significantly decreased AngII-induced bradycardia. The effect of HERD on the cardiovascular system is partly mediated by RAS suppression, especially on AngII [118]. Another study indicated that the

oil of R.D could decrease SBP [119]. RD relaxed guinea pig tracheal chains, suggesting its hypotensive effect may result from its vasodilatory properties. RD oil reduced sympathetic activity by 40% and adrenaline levels by 30% in humans, indicating that RD's hypotensive action may involve inhibiting sympathetic activity. Additionally, RD lowers blood pressure through the cholinergic system, as acetylcholine (Ach) suppresses cardiac and vascular smooth muscles. It also increases heart rate and contractility in isolated guinea pig hearts via beta-adrenergic receptors [120]. Previous reports indicate that both ISO and RD extract increased heart rate and contractility. However, ISO without propranolol led to a significantly higher increased heart rate compared to RD extract. The extract showed a more pronounced increase in heart contractility, both with and without propranolol and methacholine, compared to ISO, suggesting that RD has strong inotropic and chronotropic effects on the isolated guinea pig heart, potentially through β-adrenoceptor stimulation, calcium channel activation, or muscarinic receptor inhibition. Additionally, a newly discovered compound in RD, cyanidin-3-O-β-glucoside, significantly inhibited angiotensin I-converting enzyme (ACE) activity, indicating the plant's potential to improve cardiovascular function by reducing angiotensin II production [121].

Arq-e-Keora (Pandanus tectorius)

Pandanus tectorius (Pandanaceae), known as 'pandan laut,' is a commonly used herb in Malaysia and Indonesia. Pandanus tectorius fruit (PTF), containing tangeretin and ethyl trans-caffeate, has shown anti-atherosclerotic effects by inhibiting HMG-CoA reductase. The methanolic extract displayed the most potent inhibitory effect, surpassing that of pravastatin, a standard drug [122]. PTF showed an anti-hypercholesterolemia Scavenger Receptor Class B type 1 (SR-B1) pathway [123]. The caffeoylquinic acids 3-O-caffeoylquinic acid (3-CQA), 3,5-di-O-caffeoylquinic acid (3,5-CQA), and 3,4,5-tri-O-caffeoylquinic acid (3,4,5-CQA) isolated from PTF significantly inhibited lipid accumulation induced by oleic acid and reduced intracellular levels of total cholesterol (TC) and triglycerides (TG) in a dose-dependent manner in HepG2 cells. RT-qPCR analysis revealed that 3-CQA and 3,5-CQA increased the expression of lipid oxidation genes (PPARα, CPT-1, ACOX1), while 3-CQA, 3,5-CQA, and 3,4,5-CQA decreased lipogenic gene expression (SREBP-1c, SREBP-2, HMGR, ACC, FAS). Additionally, the n-butanol fraction of PTF (PTF-b) reduced retroperitoneal fat and improved the serum lipid profile. RT-qPCR showed that PTF-b upregulated PPARα and its target genes (ACO, CPT1, LPL, HSL), along with increasing LDLR, CYP7A1, and PPARγ expression. PTF-b treatment also

activated AMP-activated protein kinase (AMPK) and enhanced the activity of both serum and hepatic lipoprotein lipase (LPL)[124][125].

Behman Surkh (Salvia haematodes L.)

The aqueous extract of the root of Salvia haematodes was found to possess a significant cardiotonic effect [126]. It also exhibited positive chronotropic and inotropic effects on isolated rabbit hearts [127].

Tukhm Balangu (Lallemantia royleana (Benth)Benth.)

A polysaccharide (PS) isolated from Balangu Shirazi (Lallemantia royleana) seeds demonstrated protective effects against hypercholesterolemia-induced liver and kidney injury in adult rats. The treatment improved liver and kidney levels of MDA, advanced oxidation protein products, glutathione, superoxide dismutase (SOD), glutathione peroxidase, and vitamin C. These results suggest that the polysaccharide has potential applications in hyperlipidemia-induced atherosclerosis. [128].In another experiment, Its whole seeds (dose of 0, 5, 10, and 20%) showed hypolipidemic activities in cholesterol (0.5%) induced hyperlipidemic rats, leading to decreased serum cholesterol and TG levels but led to the increase in atherogenic index [129].

Tudri Surkh (Cheiranthus cheiri L.)

Wallflower (Erysimum cheiri), also known as Cheiranthus cheiri, from the Brassicaceae family, contains various cardiotonic steroids such as cheiroside A, cheirotoxin, and neouzarin, mainly found in its seeds. The seeds also have glucosinolates and isothiocyanates, including cheirolin and iberin, with cheirolin present in the essential oils of the flower, leaf, and fruit. Additionally, the herb contains flavonoids like isorhamnetin, kaempferol, and quercetin derivatives. The cardiac glycoside extract of wallflower shows digitalin-like effects. Due to the high levels of 11-α-hydroxycardenolides, research has suggested potential new pharmacotherapeutic applications for wallflower seeds beyond their cardiotonic properties [130]

Kishneez Khushk (Coriandrum sativum L.)

Silver nanoparticles (AgNPs) from Coriandrum sativum (CS) methanolic extract showed 58.29% clot lysis at 2.5 mg/ml, while the extract alone had 45.99% thrombolytic activity[131]. A 50 mg dose of CS demonstrated protective effects on the endothelium and antihypertensive properties against arsenic-induced hypertension (100 ppm in drinking water), likely due to its antioxidant activity. It resulted in a 51% reduction in SBP and

relaxated at concentrations of 0.003−5 mg/mL against phenylephrine (1μM) and high potassium (80 mM)-induced contractions. Moreover, CS had a positive effect on lipid peroxidation and eNOSIn another study, an oral dose of 1.0 or 2.0 g/kg·bw of CS demonstrated anti-hypertensive activity against high-fructose and high-salt diet (HFSD)-induced hypertension. This was achieved by reducing systolic blood pressure (SBP), diastolic blood pressure (DBP), and mean arterial pressure (MAP), while increasing serum levels of vasodilatory factors (PGI2, NO, and eNOS). Additionally, CS treatment decreased Na+ retention and serum uric acid (UA) levels and improved glucolipid profiles. The treatment also reduced the mRNA expression of NHE3, a Na+/H+ exchanger responsible for Na+ absorption, in the kidney and small intestine.[133].CS extract has been shown to potentially decrease blood lipid profile in rats [134–138]. It is interesting to note that the presence of antioxidants in CS, such as tocopherols and phenolics, protects the unsaturated fatty acids from peroxidation[139]. Further, it also improved cardiac hemodynamic parameters in experimental rats, including SBP, DBP, HR, and MAP, indicating its positive role in MI [138]. The cardioprotective effect of CS is attributed to its ant-hypertensive potential[140].

Pre-clinical studies of the selected Khamiras

Khamira Abreesham Sada (KAS) at 1000 mg/kg b.w. did not reduce L-NAME (185 mmol/kg) induced hypertension in Wistar rats, as it failed to lower the increased SBP significantly. In a similar study, KGS at 2000 mg/kg b.w. not only failed to decrease the L-NAME-induced SBP but also slightly increased it by the 14th day. KGS also slightly reduced the RR interval, serum sodium, and nitrite levels while significantly increasing serum potassium. However, KGS significantly reduced the elevated levels of adrenaline and noradrenaline induced by L-NAME on the 14th day. These findings suggest that KGS may act as a central sympathomimetic agent, similar to clonidine, but further investigation is needed [23].

KAHAW, administered orally at doses of 200, 400, and 800 mg/kg/day, effectively alleviated ISO-induced myocardial necrosis and decreased systolic, diastolic, and mean arterial pressures in male Wistar albino rats. It also reduced maximum positive and negative rates of developed left ventricular pressure (±LVdp/dt), and increased left ventricular end-diastolic pressure (LVEDP). These effects of KAHAW may be attributed to its anti-oxidant activity in rat myocardium. At 800 mg/kg/day, KAHAW significantly reversed most hemodynamic and antioxidant imbalances without significantly changing heart rate [141].

In another study, pre-treatment with KAHAW in a dose of 200mg/kg b.w. attenuated Doxorubicin-induced elevated activities of AST, LDH, MDA, depletion in GSH level, and catalase activity. It improved DOX-induced disruption of cardiac tissues, which showed marked cardioprotective activity [142]. The cardiovascular activity of phytoconstituents present in particular plant components of the three selected Kamiras have been mentioned in Table.5 and Figure 2

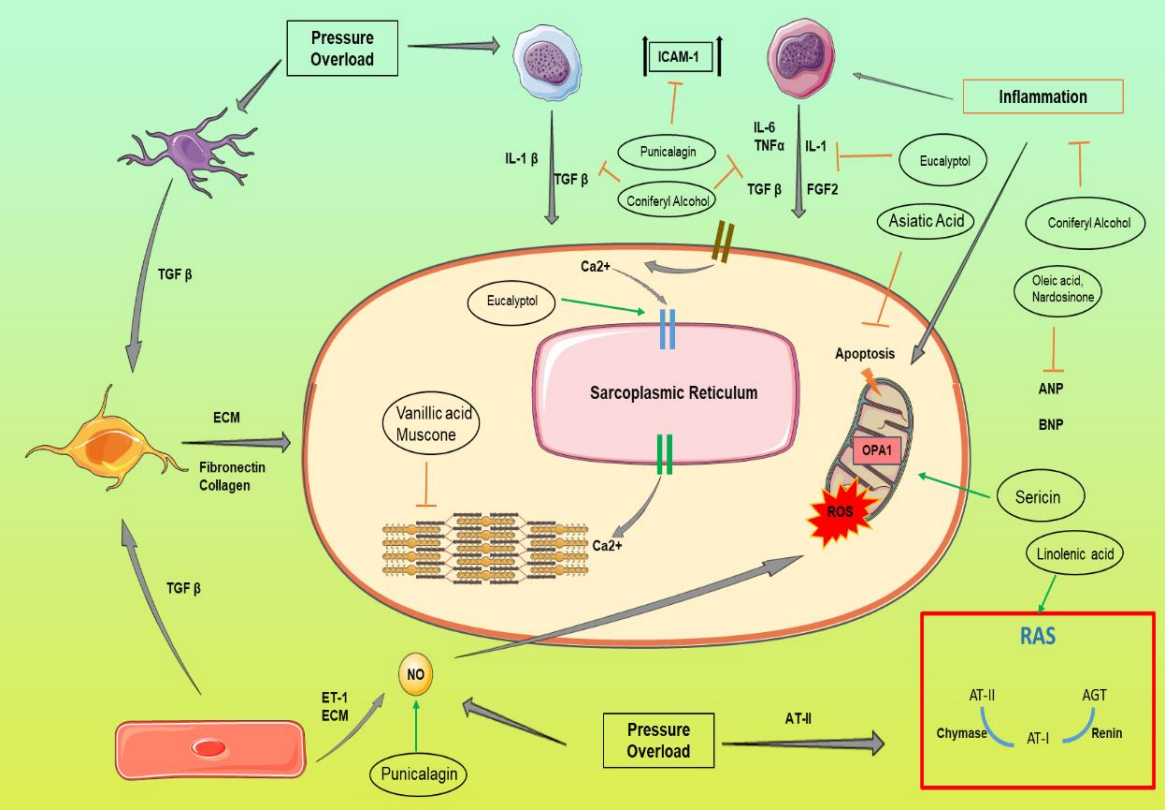

Figure 1: Depicts the mechanism of various phytoconstituents present in different plant components of KGS, KAS and KAHAW in the management cardiovascular disorders.

Table 4: The reported disease model, dose and cardiovascular activity of phytoconstituents present in plants which constitutes the 3 Khamiras

Name of the Khamira	Name of Plant	Phytochemicals	Disease	Disease Model	Dose	cardiovascular activity	Reference
KAHAW, KGS, KAS	Abresham Muqarraz	Sericin	hypercholestremia	6% cholesterol diet induced rats	Invivo: 1000 mg/kg,	upregulation of mitochondrial proteins like ocular atrophy 1 (OPA1) and acetyl-CoA acetyltransferase (ACAT1), downregulation of NADH-ubiquinone oxidoreductase 75 kDa subunit (NDUFS1). Enhanced mitochondrial energy efficiency and structure, positively affecting fatty acid oxidation, electron transport, and pyruvate metabolism	[27]
KAS and KGS	Berg Badranjboya (Nepeta hindostana (B.Heyne ex Roth) Haines)	Asiatic acid	heart failure	Invivo: transverse aortic constriction (TAC) in mice Invitro: H2O2 induced apoptosis in neonatal rat cardiomyocytes	100 mg/kg/day	Reduced Bax/Bcl-2 ratio, oxidative stress and cleaved caspase-9/3 levels, inhibited the activation of the JNK	[143] [144]
KAS, KGS and KAHAW	Berg Gawzaban (Borago officinalis L.)	Gamma-Linolenic Acid	Hypertension	Spontaneously hypertensive rats	11% by weight of sesame oil (SES) or BORage oil	Plasma aldosterone (PA) and SBP decreased, Plasma Renin (PRA) increased, PA/PRA ratio and Ang-II density in adrenal gland decreased	[145] [146]
		Zerumbone	Cardiac hypertrophy	Norepinephrine induced human embryonic stem cell (hESC)-derived cardiomyocytes	anti-NE effect (IC50=16.70 ±2.659 μM) on beating rates in hESC-CMs Invivo:70 mg kg−1 d−1 and 35 mg kg−1 d−1	Induction of high molecular weight KEAP1, which impeded the interaction of CUL3 with KEAP1, leading to the inhibition of NRF2 ubiquitination and its accumulation and translocation into the nucleus. Inhibition of HO-1 expression blocked the effect of zerumbone in attenuating cardiomyocyte hypertrophy.	[147] [148]
KAS and KGS	Gule Khatmi (Althaea officinalis L.)	Vanllic acid	Cardioprotective effects	Doxorubicin induced cardiotoxicity in male albino wistar rats	10, 20 and 40 mg/kg/ day	Decreased levels of CK-MB, LDH, cardiac troponin-I, SGOT, MDA, and cardiac TLR4, Increased FRAP value	[149]

Name of the Khamira	Name of Plant	Phytochemicals	Disease	Disease Model	Dose	cardiovascular activity	Reference
KAS and KGS	Shakar Safaid (Saccharum officinarum)	Luteolin	Cardioprotective effects		50 and 100 mg/kg b.w.	Improved heart rate, R wave amplitude, and attenuated QT interval prolongation. Decreased Plasma BNP, CK-MB, CTnT, and LDH,MDA, Bax, Caspase-3, cleaved caspase-3 expressions and increased SOD, Bcl-2, Pro-caspase-3	[150]
KGS and KAS	Sat Leemun (Citrus aurantium L.)	Limonene	Cardiac hypertrophy	Invivo: aortic banding surgery in C57/BL6 male mice to establish a pressure overload-induced cardiac hypertrophy model Invitro: neonatal rat cardiac myocytes (NRCMs) stimulated with phenylephrine to induce cardiomyocyte hypertrophy	Invivo: 80 mg/kg b.w. Invitro: 50µM	increased levels of SIRT6 protein, PPARα Activity: Enhanced, activated Ubiquitin-Specific Peptidase 10 (USP10)	[151]
KGS	Behman Surkh (Salvia haematodes L.)	Eucalyptol	angina pectoris and myocardial ischemia	Invivo: Rat Model with Vasopressin-Induced Ischemia Invitro: Phenylephrine-induced contraction of aortic rings and endothelium-denuded rings	Invivo:80 µL/kg administered sublingually via a spray to anaesthetized rats. Invitro: 0.019, 0.19, 0.65, 1.3, and 2.60 mM for isolated aortic ring experiments	Increased coronary blood flow, plasma NO, eNOS expression, decreased Mean BP, MDA, TNF-α, IL-6. Invitro: increased Vasorelaxation of aortic rings, decreased Phenylephrine-Induced Contractions (indicating reduced vasoconstriction)	[152]
KGS	Tudri Surkh (Cheiranthus cheiri L.)	Strophanthidin	end-stage failing human myocardium	Trabeculae from the left or right ventricle	(0.01 to 1 µmol/L	positive inotropic effects, increases in intracellular [Na+] as well as increasing [Ca^{2+}]i-transients and SR- Ca^{2+} load	[153]

Name of the Khamira	Name of Plant	Phytochemicals	Disease	Disease Model	Dose	cardiovascular activity	Reference
KGS	Tukhm Balangu (Lallemantia royleana (Benth)Benth.	oleic acid	Hypertensive cardiac remodelling	Invivo: Angiotensin II (Ang II)-induced hypertensive cardiac remodelling in mice Clinical: patients with and without left ventricular hypertrophy	Clinical dose: Plasa Invivo dose: 160 mg/kg b.w.	decrease d FGF23 expression and cardiac hypertrophy and fibrosis markers ANP, BNP, α-SMA, Col1a1, Col3a1. Oleic acid inhibited the translocation of Nurr1, preventing it from promoting FGF23 transcription and reducing the activation of pathways like PLCγ-NFAT1 and TGF-β/β-Catenin, which are connected with cardiac remodelling.	[154]
KAHAW	Aquilaria agallocha	Kaempferol	Hypertension and cardiac hypertrophy	L-NAME induced hypertension and cardiac hypertrophy in rats.	20 and 40 mg/kg b.w.	reduced SBP, left ventricular malfunction, and hypertrophy, superoxide formation, MDA, cat, plasma NO restoration, decreased TNF-α and IL-6, downregulation of TNFR1, TNFR2, PI3K, Akt1, Smad2/3, p-NF-κB, and TGF-β1	[155]
KAHAW	Nardostachys jatamansi	Nardosinone	Cardiac hypertrophy	AngII-induced cardiac cell hypertrophy in the myoblast cell line H9c2, derived from embryonic rat heart	25, 50, 100, and 200 μmol/L	Decreased cell surface area, especially 100 μmol/L, decreased ANP, BNP and β-MHC expression, e inhibited PI3K/Akt/mTOR and MEK/ERK pathway.	[156]
KAHAW	Citrus medica	citral	vasorelaxation	1)phenylephrine-induced contraction of endothelium-intact and denuded rings from WKY rats 2) K+-induced contraction	IC50 endothelium-intact and -denuded rings were 1.42 ± 0.26 mM and 1.33 ± 0.18 mM IC50 vasorelaxant value was 0.69 ± 0.08 mM in KCl-contracted aortic rings	vasorelaxation of the thoracic aorta by affecting the NO/cyclic GMP pathway. citral reduced the calcium influx by the blockade of voltage-dependent l-type Ca^{2+} channels ,	[60]

Name of the Khamira	Name of Plant	Phytochemicals	Disease	Disease Model	Dose	cardiovascular activity	Reference
					0.6 mM and 6 mM of citral completely abolished calcium response		
KAHAW	Pistacia lentiscus	α-pinene	Hypertension	1) phenylephrine precontracted Phenyl ephrine aorta and SMA 2) L-NAME induced SMA contraction 3)PE-precontracted SMA wereexposed to ODQ 3 µM 4) PE-precontracted blood vessel with a TRPA1 antagonist (A-967079, 1 µM)	1) a-pinene 0.1, 1, 10, 30, 100, 300, and 1,000 µM 2)1–300 µM 3) .1–300 µM 4)0.1–300 µM	relaxations in male SMA was mediated by 1) endothelium, 2) eNOS-derived NO,and 3) guanylyl cyclase (GC) activity. Moreover, a-pinene activated the transient receptor potential ankyrin-1 (TRPA1) channel. Vasorelaxation of aorta	[157]
KAHAW	Syzygium aromaticum L.	Eugenol	Hypertension	Mesenteric artery rings with intact endothelium induced contraction with U46619, a thromboxane A2 receptor agonist, L-NAME, indomethacin, TRAM-34 and apamin, inhibitors of intermediate (IKCa) and small conductance (SKCa) Ca2+-activated K+ channels, , or HC-067047, a TRPV4 blocker	Invivo: 5 mg/kg b.w.	Invitro: increased activation of TRPV4 channels in endothelial cells, NO production,IKCa (intermediate conductance calcium-activated potassium channels) channel activity Invivo: decreased blood pressure, Heart rate (transienteffect)	[158]

Name of the Khamira	Name of Plant	Phytochemicals	Disease	Disease Model	Dose	cardiovascular activity	Reference
KAHAW	Elettaria cardamomum	1, 8-cineole	Hypertension	Hypertension induced by chronic nicotine administration in Male Sprague–Dawley rats	0.01, 0.1 and 1 mg/kg 1,8-cineole	increased plasma nitrite concentration, decreased SBP, lipid peroxidation	[159]
KAHAW	Cinnamomum tamala	cinnamaldehyde	Cardiac hypertrophy	aortic banding induced cardiac hypertrophy in C57/BL6 mice (pressure load)	50 mg/kg b.w.	Amelioration of systolic and diastolic abnormalities decreased cardiac fibrosis Decreased expression of ANP,BNP and β-MHC. Cinnamaldehyde blocked pressure overload activation of extracellular signal-regulated kinase (ERK) signaling pathway,	[160]
KGS and KAHAW	Santalum album L	α-santalol	Pressure lowering effect	Healthy volunteers	20% (w/w) of alpha santalol in peanut oil	Decreased pulse rate and systolic blood pressure in comparison to control group	[161]
KAHAW	Ambra grasea	Ambrein	Cardiovascular disorder	Adrenalin, noradrenaline, acetylcholine., isoprenaline, nicotine,histamine, atropine,atenolol, verapamil induced cardiovascular disorder	50-200 mg/kg	Positive inotropic effect	[162]
KAHAW	Pinus succinifera	Cinnamic		Invivo: transverse aortic constriction (TAC) induced pressure overload and left ventricular hypertrophy Invitro: Phenylephrine induced hypertrophy in Neonatal rat cardiomyocytes (NRCMs)	Invivo: 120 mg/kg and 300 mg/kg per day. Invitro: 100 μM	Increased Nppa and Nppb expression, reduced cardiomyocyte hypertrophy, restoration of FTO levels and reduced m6A RNA modification, thereby lowering hypertrophic signaling, improved mitochondrial function, reduced mitochondrial superoxide generation and increased mitochondrial integrity, membrane potential, and ATP levels.	[163]

Name of the Khamira	Name of Plant	Phytochemicals	Disease	Disease Model	Dose	cardiovascular activity	Reference
KAHAW	Moschus moschiferous	Muscone		Angiotensin II (Ang II)-Induced Cardiac Hypertrophy in mice	2 mg/kg and 4 mg/kg per day	reduced COL1A1, COL3A1, α-SMA levels, indicating lessened fibrosis. Decreased expression of ANP, BNP, and β-MHC, suppressed phosphorylation of STAT3, SMAD2, SMAD3, ERK, JNK, and p38,	[163]
KAS and KAHAW	Crocus sativa L.	Crocin	Gestational hypertension	L-NAME induced gestational hypertension	50 mg/kg/day	increased Nrf-2 (nuclear factor erythroid 2–related factor 2) and HO-1 (heme oxygenase-1) , decreased IL-1β (interleukin-1β), IL-6, and TNF-α, lowered blood pressure and decreased placental growth factor (PlGF) and soluble fms-like tyrosine kinase-1 (sFlt-1), both of which are associated with preeclampsia and gestational hypertension	[164]
KAHAW	Salix caprea	Coniferyl alcohol	Renovascular hypertension	Invivo: two-kidney, one-clip (2K1C) model in mice Invitro: Ang II-induced hypertrophy in H9C2 cardiomyocytes	20 mg/kg and 40 mg/kg per day	reduced the expression of TNF-α, IL-17, COX2, and MMP9 in both cardiac tissues and cardiomyocytes, decreased Systolic and diastolic pressures	[115,165]
KAHAW	Rosa damascene	Citronellol	Myocardial ischaemia	DOX induced myocardial ischemia in rats	25 mg/kg, 50 mg/kg, and 100 mg/kg	Increased eNOS,PPAR-γ,IL-10,VEGF, decreased NF-κB1, lipid biomarkers	[166]
KAHAW	Pandanus tectorius	Squalene	-	effects of squalene on healthy rats	1000 mg/kg of squalene	Decreased Blood pressure Plasma leptin Glucose Cholesterol Triglycerides B.w. Body fat Increased: Testicular weight, Testosterone levels	[167]
KAHAW	Malus sylvestris	quercetin	Hypertension	Invivo: angiotensin II (Ang II) induced vascular dysfunction	Invivo: 2.5 mg/kg/day and 5 mg/kg/day	reduction in blood pressure, pulse wave velocity (PWV), and abdominal aortic thickness, upregulation of p53 and p21, decreased Proliferating Cell Nuclear	[168] [169]

Name of the Khamira	Name of Plant	Phytochemicals	Disease	Disease Model	Dose	cardiovascular activity	Reference
				and hypertension in male C57BL/6 mice Invitro: Ang II stimulated VSMCs mimicking mimic vascular injury and proliferation		Antigen (PCNA), Cyclin-Dependent Kinase-4 (CDK4), and Cyclin D1	
KAHAW	Punica granatum	Punicalagin		Invivo: Atherosclerosis in LDLR–/– mice induced by feeding a high-fat diet (HFD) Aortic stenosis induced by constricting the rat abdominal aorta with a U-shaped clip	Mouse model of atherosclerosis: 250 mg/kg/day and 500 mg/kg/day. Rat model of aortic stenosis: 500 mg/kg/day Endothelial cells (ECs) subjected to oscillatory shear stress (OSS): 50 μg/mL	Increased eNOS activity, SMα-actin expression in VSMCs, decreased Phospho-Smad1/5 , ICAM-1, VCAM-1, E-selectin Cyclin A, pRb in ECs, Reduced Macrophage infiltration in atherosclerotic plaques: Reduced Plasma TC and TG levels, Decreased Migration of VSMCs, IL-6 and c-fos expression in VSMCs Decreased LPS-induced expression of pro-inflammatory cytokines (IL-1β, IL-6, TNF-α, MCP-1) and iNOS in macrophages	[102]
KAHAW	Cydonia oblonga	chlorogenic acid	Blood pressure lowering effect	healthy male and female volunteers	400 mg of single intake	Decreased blood pressure systolic and distolic	: [170] : [171]

Conclusion:

Khamiras, from its period of inception during the mughal era till presently, has been used in the management of cardiovascular disorders by the Unani physician called Hakeem. In this article, we have put forward scientific evidences which indicate that, the presence of sugar in Khamiras is not only for preservative or delivery purpose rather it was added by unani physicians with some specific aim to manage weak heart or Zoaf-e-Qalb (as per their terminology), though they were probably unaware of its therapeutic applications. As discussed, the shifting of the weak heart from using fatty acid to glucose can be co-related with presence of sugar in it. Though we could not find scientific evidences for the cardiovascular activity of certain components like Aab-e-Baran (Rain Water), Yashab Sabz (Green jasper) in KAHAW, yet we have included these in the component list. Other plant components of KAS, KAHAW and KGS containing natural chemical compounds with their relevant pharmacological action in cardiovascular in vitro/in vivo disease models complemented their traditional use. KGS and KAS have only been tested against only one model of vascular dysfunction i.e., L-NAME model while KAHAW has been tested against both ISO and DOX induced cardiac dysfunction. Moreover, from the traditional point of view these selected khamiras have also been indicated for Khafqan (palpitation) too, which in USM, is described as a type of abnormal heartbeat characterized by Sari (rapid), mutwatir (continuous) and muztarib (irregular) heart beat which closely resembles to arrhymia of moden pathology. Although, we could not find any scientific report on the effect of these Khamiras in arrrhythmia. As per our literature review, further pre-clinical and clinical studies as per conventional rules and regulations are warranted for their evidence-based application in cardiovascular disorders specially hypertension, cardiac hypertrophy and arrhythmia in Unani hospitals. This is essential keeping in view probable potential for low cost-effective therapy, which is much relevant for developing countries like India.

References (Chapter I and II)

[1] E. Poulakou-Rebelakou, M. Karamanou, A. George, The impact of ancient Greek medicine in India: the birth of Unani medicine, Acta Med Hist Adriat 13 (2015) 323–328.

[2] T. Siddiqi, Unani medicine in India during the Delhi Sultanate, Indian J Hist Sci 15 (1980) 18–24.

[3] F. Jabin, A guiding tool in Unani Tibb for maintenance and preservation of health: a review study, Afr J Tradit Complement Altern Med 8 (2011) 140–143. https://doi.org/10.4314/ajtcam.v8i5S.7.

[4] M. Aleem, M. Imran Khan, Q. Islam Usmani, A. Ahmad, Review on Darunaj-aqrabi (Doronicum hookeri C.B. Clarke): an Unexplored Medicinal Plant of Unani System of Medicine, JoAYUSH (2020). https://doi.org/10.37591/joayush.v9i2.2108.

[5] V. Miller, L. Nambiar, M. Saxena, D. Leong, A. Banerjee, J.P. Werba, J.R. Faria Neto, K.C. Quinto, M. Moniruzzaman, S. Khandelwal, Exploring the Barriers to and Facilitators of Using Evidence-Based Drugs in the Secondary Prevention of Cardiovascular Diseases: Findings From a Multistakeholder, Qualitative Analysis, Gh 13 (2018) 27. https://doi.org/10.1016/j.gheart.2017.08.001.

[6] S. Ahmad, S. Rehman, A. Ahmad, K. Siddiqui, S. Shaukat, M. Khan, Y. Kamal, T. Jahangir, Khamiras, a natural cardiac tonic: An overview, J Pharm Bioall Sci 2 (2010) 93. https://doi.org/10.4103/0975-7406.67009.

[7] C.W. Tsao, A.W. Aday, Z.I. Almarzooq, C.A.M. Anderson, P. Arora, C.L. Avery, C.M. Baker-Smith, A.Z. Beaton, A.K. Boehme, A.E. Buxton, Y. Commodore-Mensah, M.S.V. Elkind, K.R. Evenson, C. Eze-Nliam, S. Fugar, G. Generoso, D.G. Heard, S. Hiremath, J.E. Ho, R. Kalani, D.S. Kazi, D. Ko, D.A. Levine, J. Liu, J. Ma, J.W. Magnani, E.D. Michos, M.E. Mussolino, S.D. Navaneethan, N.I. Parikh, R. Poudel, M. Rezk-Hanna, G.A. Roth, N.S. Shah, M.-P. St-Onge, E.L. Thacker, S.S. Virani, J.H. Voeks, N.-Y. Wang, N.D. Wong, S.S. Wong, K. Yaffe, S.S. Martin, on behalf of the American Heart Association Council on Epidemiology and Prevention Statistics Committee and Stroke Statistics Subcommittee, Heart Disease and Stroke Statistics—2023 Update: A Report From the American Heart Association, Circulation 147 (2023). https://doi.org/10.1161/CIR.0000000000001123.

[8] R. Gupta, I. Mohan, J. Narula, Trends in Coronary Heart Disease Epidemiology in India, Annals of Global Health 82 (2016) 307. https://doi.org/10.1016/j.aogh.2016.04.002.

[9] F.D. Fuchs, P.K. Whelton, High Blood Pressure and Cardiovascular Disease, Hypertension 75 (2020) 285–292. https://doi.org/10.1161/HYPERTENSIONAHA.119.14240.

[10] M. Itrat, Methods of health promotion and disease prevention in Unani medicine, J Edu Health Promot 9 (2020) 168. https://doi.org/10.4103/jehp.jehp_618_19.

[11] W. Ahmad, G. Sofi, M.A. Alam, M. Zulkifle, B. Ahmad, Understanding Holism in the light of principle underlying practice of Unani Medicine, Reviews on Environmental Health 37 (2022) 189–199. https://doi.org/10.1515/reveh-2021-0009.

[12] M. Fazil, S. Nikhat, Why the "sugars" in traditional Unani formulations are a pivotal component: A viewpoint perspective, Journal of Integrative Medicine 20 (2022) 91–95. https://doi.org/10.1016/j.joim.2022.01.002.

[13] D.H. Tran, Z.V. Wang, Glucose Metabolism in Cardiac Hypertrophy and Heart Failure, JAHA 8 (2019) e012673. https://doi.org/10.1161/JAHA.119.012673.

[14] H. Kabir, Unani Murakkabat (Formulations): Need of Modification, J Homeop Ayurv Med 03 (2014). https://doi.org/10.4172/2167-1206.1000146.

[15] Muzayyana Khan, Shariq Shamsi, Roohi Zaman, Khamira: An important dosage form of unani system of medicine, (2019). https://doi.org/10.13140/RG.2.2.21210.59844.

[16] M.A. Alam, Z.A. Zaheer Ahmed, A.H. Ansari, S.A. Shamim Ahmed, D.M. Danish Mand, M.T. Alam, Iksir-e-Badan (Elixir): unique influence from Unani medicine-a review., (2014).

[17] Hamdard Pharmacopoeia of Eastern Medicine - Indian books and Periodicals, (n.d.). https://www.ibpbooks.com/hamdard-pharmacopoeia-of-eastern-medicine/p/4138 (accessed November 13, 2024).

[18] Md.A. Shaharyar, R. Bhowmik, O. Afzal, A.S.A. Altamimi, S.I. Alzarea, W.H. Almalki, S.Z. Ali, P. Mandal, A. Mandal, M. Ayoob, I. Kazmi, S. Karmakar, Anti-Hypertensive Activity of Some Selected Unani Formulations: An Evidence-Based Approach for Verification of Traditional Unani Claims Using LC-MS/MS for the Evaluation of Clinically Relevant Blood Parameters in Laboratory Rats, JCM 11 (2022) 4628. https://doi.org/10.3390/jcm11154628.

[19] A. Sarasa Bharati, M. Ali, Effect of crude extract of Bombyx mori coccoons in hyperlipidemia and atherosclerosis, J Ayurveda Integr Med 2 (2011) 72. https://doi.org/10.4103/0975-9476.82527.

[20] T. Mahmood, H. Siddiqui, R. Dixit, P. Bagga, S. Hussain, Protective Effect of *Bombyx mori* L Cocoon (Abresham) and its Formulations against Isoproterenol-Induced Cardiac Damage, Trop. J. Pharm Res 14 (2015) 63. https://doi.org/10.4314/tjpr.v14i1.10.

[21] R.K. Srivastav, H.H. Siddiqui, T. Mahmood, F. Ahsan, Evaluation of cardioprotective effect of silk cocoon (Abresham) on isoprenaline-induced myocardial infarction in rats, Avicenna J Phytomed 3 (2013) 216–223.

[22] M.S. Khan, M. Singh, M.A. Khan, D.S. Arya, S. Ahmad, Scientific validation of cardioprotective attribute by standardized extract of Bombyx mori against doxorubicin-induced cardiotoxicity in murine model, EXCLI J 13 (2014) 1043–1054.

[23] A. Onsa-Ard, D. Shimbhu, J. Tocharus, M. Sutheerawattananonda, R. Pantan, C. Tocharus, Hypotensive and vasorelaxant effects of sericin-derived oligopeptides in rats, ISRN Pharmacol 2013 (2013) 717529. https://doi.org/10.1155/2013/717529.

[24] Y. Okazaki, S. Kakehi, Y. Xu, K. Tsujimoto, M. Sasaki, H. Ogawa, N. Kato, Consumption of Sericin Reduces Serum Lipids, Ameliorates Glucose Tolerance and Elevates Serum Adiponectin in Rats Fed a High-Fat Diet, Bioscience, Biotechnology, and Biochemistry 74 (2010) 1534–1538. https://doi.org/10.1271/bbb.100065.

[25] N. Limpeanchob, K. Trisat, A. Duangjai, W. Tiyaboonchai, S. Pongcharoen, M. Sutheerawattananonda, Sericin Reduces Serum Cholesterol in Rats and Cholesterol Uptake into Caco-2 Cells, J. Agric. Food Chem. 58 (2010) 12519–12522. https://doi.org/10.1021/jf103157w.

[26] T. Morita, A. Oh-hashi, K. Takei, M. Ikai, S. Kasaoka, S. Kiriyama, Cholesterol-Lowering Effects of Soybean, Potato and Rice Proteins Depend On Their Low Methionine Contents In Rats Fed a Cholesterol-Free Purified Diet, The Journal of Nutrition 127 (1997) 470–477. https://doi.org/10.1093/jn/127.3.470.

[27] K. Rujimongkon, S. Ampawong, D. Isarangkul, O. Reamtong, P. Aramwit, Sericin-mediated improvement of dysmorphic cardiac mitochondria from hypercholesterolaemia is associated with maintaining mitochondrial dynamics, energy production, and mitochondrial structure, Pharmaceutical Biology 60 (2022) 708–721. https://doi.org/10.1080/13880209.2022.2055088.

[28] S. Devi, R. Singh, Assessment of lipid lowering effect of Nepeta hindostana herb extract in experimentally induced dyslipidemia, Journal of Nutrition & Intermediary Metabolism 9 (2017) 17–23. https://doi.org/10.1016/j.jnim.2017.08.002.

[29] M.N. Khan, M. Tariq, J. Akhtar, M.A. Khan, STUDY OF A CONTROVERSIAL UNANI DRUG GAOZABAN-A, (2018).

[30] L. Casas-Cardoso, C. Mantell, S. Obregón, C. Cejudo-Bastante, Á. Alonso-Moraga, E.J.M. de la Ossa, A. de Haro-Bailón, Health-Promoting Properties of Borage Seed Oil Fractionated by Supercritical Carbon Dioxide Extraction, Foods 10 (2021) 2471. https://doi.org/10.3390/foods10102471.

[31] A.H. Gilani, S. Bashir, A. Khan, Pharmacological basis for the use of Borago officinalis in gastrointestinal, respiratory and cardiovascular disorders, Journal of Ethnopharmacology 114 (2007) 393–399. https://doi.org/10.1016/j.jep.2007.08.032.

[32] S.Y. Al-Okbi, S.M. El-qousy, S. El-Ghlban, H.F. Moawad, Role of Borage Seed Oil and Fish Oil with or without Turmeric and Alpha- Tocopherol in Prevention of Cardiovascular Disease and Fatty Liver in Rats, J. Oleo Sci. 67 (2018) 1551–1562. https://doi.org/10.5650/jos.ess18064.

[33] B. Baharvand-Ahmadi, M. Bahmani, P. Tajeddini, M. Rafieian-Kopaei, N. Naghdi, An ethnobotanical study of medicinal plants administered for the treatment of hypertension, J Renal Inj Prev 5 (2016) 123–128. https://doi.org/10.15171/jrip.2016.26.

[34] Y. Zheng, J. Lee, K.-O. Shin, K. Park, I.-J. Kang, Synergistic action of Erigeron annuus L. Pers and Borago officinalis L. enhances anti-obesity activity in a mouse model of diet-induced obesity, Nutrition Research 69 (2019) 58–66. https://doi.org/10.1016/j.nutres.2019.07.002.

[35] M.M. Engler, M.B. Engler, Dietary borage oil alters plasma, hepatic and vascular tissue fatty acid composition in spontaneously hypertensive rats, Prostaglandins, Leukotrienes and Essential Fatty Acids 59 (1998) 11–15. https://doi.org/10.1016/S0952-3278(98)90046-1.

[36] M. Sutovská, G. Nosálová, J. Sutovský, S. Franová, L. Prisenznáková, P. Capek, Possible mechanisms of dose-dependent cough suppressive effect of Althaea

officinalis rhamnogalacturonan in guinea pigs test system, Int J Biol Macromol 45 (2009) 27–32. https://doi.org/10.1016/j.ijbiomac.2009.03.008.

[37] M. Banaee, V. Soleimany, B. Nematdoost Haghi, Therapeutic effects of marshmallow (Althaea officinalis L.) extract on plasma biochemical parameters of common carp infected with Aeromonas hydrophila, Vet Res Forum 8 (2017) 145–153.

[38] G.A. Bonaterra, K. Bronischewski, P. Hunold, H. Schwarzbach, E.-U. Heinrich, C. Fink, H. Aziz-Kalbhenn, J. Müller, R. Kinscherf, Anti-inflammatory and Anti-oxidative Effects of Phytohustil® and Root Extract of Althaea officinalis L. on Macrophages in vitro, Front. Pharmacol. 11 (2020) 290. https://doi.org/10.3389/fphar.2020.00290.

[39] N. El-Sherif, E.B. Caref, M. Chinushi, M. Restivo, Mechanism of arrhythmogenicity of the short–long cardiac sequence that precedes ventricular tachyarrhythmias in the long QT syndrome, Journal of the American College of Cardiology 33 (1999) 1415–1423. https://doi.org/10.1016/s0735-1097(98)00700-1.

[40] S.E. Ali, Q. Yuan, S. Wang, M.A. Farag, More than sweet: A phytochemical and pharmacological review of sugarcane (Saccharum officinarum L.), Food Bioscience 44 (2021) 101431. https://doi.org/10.1016/j.fbio.2021.101431.

[41] I. Suntar, H. Khan, S. Patel, R. Celano, L. Rastrelli, An Overview on Citrus aurantium L.: Its Functions as Food Ingredient and Therapeutic Agent, Oxid Med Cell Longev 2018 (2018) 7864269. https://doi.org/10.1155/2018/7864269.

[42] P. Kang, K.-H. Ryu, J.-M. Lee, H.-K. Kim, G.H. Seol, Endothelium- and smooth muscle-dependent vasodilator effects of Citrus aurantium L. var. amara: Focus on Ca(2+) modulation, Biomed Pharmacother 82 (2016) 467–471. https://doi.org/10.1016/j.biopha.2016.05.030.

[43] C.-Y. Shen, J.-J. Lin, J.-G. Jiang, T.-X. Wang, W. Zhu, Potential roles of dietary flavonoids from Citrus aurantium L. var. amara Engl. in atherosclerosis development, Food Funct 11 (2020) 561–571. https://doi.org/10.1039/c9fo02336d.

[44] M. Iampanichakul, P. Potue, S. Rattanakanokchai, P. Maneesai, J. Khamseekaew, W. Settheetham-Ishida, P. Pakdeechote, Limonin ameliorates cardiovascular dysfunction and remodeling in hypertensive rats, Life Sciences 327 (2023) 121834. https://doi.org/10.1016/j.lfs.2023.121834.

[45] S. Maksoud, R.M. Abdel-Massih, H.N. Rajha, N. Louka, F. Chemat, F.J. Barba, E. Debs, Citrus aurantium L. Active Constituents, Biological Effects and Extraction Methods. An Updated Review, Molecules 26 (2021) 5832. https://doi.org/10.3390/molecules26195832.

[46] S.-H. Li, G.-L. Ma, S.-L. Zhang, Y.-Y. Yang, H.-F. Liu, A. Luo, J. Wen, Z.-Z. Cao, Y.-Z. Jia, Naringin exerts antiarrhythmic effects by inhibiting channel currents in mouse cardiomyocytes, Journal of Electrocardiology 80 (2023) 69–80. https://doi.org/10.1016/j.jelectrocard.2023.05.003.

[47] A.F. Plangar, A. Anaeigoudari, A. KhajaviRad, M.N. Shafei, Beneficial Cardiovascular Effects of Hydroalcoholic Extract from Crocus Sativus in Hypertension Induced by Angiotensin II, J Pharmacopuncture 22 (2019) 95–101. https://doi.org/10.3831/KPI.2019.22.012.

[48] M. Imenshahidi, H. Hosseinzadeh, Y. Javadpour, Hypotensive effect of aqueous saffron extract (Crocus sativus L.) and its constituents, safranal and crocin, in normotensive and hypertensive rats, Phytother Res 24 (2010) 990–994. https://doi.org/10.1002/ptr.3044.

[49] R. Mehdizadeh, M.-R. Parizadeh, A.-R. Khooei, S. Mehri, H. Hosseinzadeh, Cardioprotective effect of saffron extract and safranal in isoproterenol-induced myocardial infarction in wistar rats, Iran J Basic Med Sci 16 (2013) 56–63.

[50] M.N. Shafei, A. Faramarzi, A. Khajavi Rad, A. Anaeigoudari, Crocin prevents acute angiotensin II-induced hypertension in anesthetized rats, Avicenna J Phytomed 7 (2017) 345–352.

[51] S. Zheng, Z. Qian, N. Wen, L. Xi, Crocetin Suppresses Angiotensin II-Induced Vascular Smooth-Muscle Cell Proliferation Through Inhibition of ERK1/2 Activation and Cell-Cycle Progression, Journal of Cardiovascular Pharmacology 50 (2007) 519–525. https://doi.org/10.1097/FJC.0b013e31813c114e.

[52] R. Srivastava, H. Ahmed, R.K. Dixit, null Dharamveer, S.A. Saraf, Crocus sativus L.: A comprehensive review, Pharmacogn Rev 4 (2010) 200–208. https://doi.org/10.4103/0973-7847.70919.

[53] P. Shivanand, N.F. Arbie, S. Krishnamoorthy, N. Ahmad, Agarwood-The Fragrant Molecules of a Wounded Tree, Molecules 27 (2022) 3386. https://doi.org/10.3390/molecules27113386.

[54] C. Wang, D. Peng, Y. Liu, Z. Yu, P. Guo, J. Wei, Agarwood Alcohol Extract Ameliorates Isoproterenol-Induced Myocardial Ischemia by Inhibiting Oxidation and Apoptosis, Cardiology Research and Practice 2020 (2020) 1–10. https://doi.org/10.1155/2020/3640815.

[55] Q. Mahmood, M. Ahmad, M.S. Akhtar, Inotropic and chronotropic effects of methanol extract of Aquilaria agallocha on rabbit heart, Bangladesh Journal of Pharmacology 8 (2013) 311–316.

[56] M.D.A. Bhat, S.A. Malik, Efficacy of Nardostachys jatamansi (D.Don) DC in essential hypertension: A randomized controlled study, Complement Ther Med 53 (2020) 102532. https://doi.org/10.1016/j.ctim.2020.102532.

[57] G. Krishnamoorthy, M.M. Shabi, D. Ravindhran, S. Uthrapathy, V.G. Rajamanickam, G.P. Dubey, Nardostachys jatamansi: cardioprotective and hypolipidemic herb, Journal of Pharmacy Research 2 (2009) 574–78.

[58] M. Singh, M.A. Khan, K. Y. T., J. Ahmad, U.A. Fahmy, S. Kotta, N.A. Alhakamy, S. Ahmad, Effect of Nardostachys jatamansi DC. on Apoptosis, Inflammation and Oxidative Stress Induced by Doxorubicin in Wistar Rats, Plants 9 (2020) 1579. https://doi.org/10.3390/plants9111579.

[59] M. Al-Yahya, R. Mothana, M. Al-Said, K. El-Tahir, M. Al-Sohaibani, S. Rafatullah, Citrus medica "Otroj": Attenuates Oxidative Stress and Cardiac Dysrhythmia in Isoproterenol-Induced Cardiomyopathy in Rats, Nutrients 5 (2013) 4269–4283. https://doi.org/10.3390/nu5114269.

[60] N. Chhikara, R. Kour, S. Jaglan, P. Gupta, Y. Gat, A. Panghal, *Citrus medica* : nutritional, phytochemical composition and health benefits – a review, Food Funct. 9 (2018) 1978–1992. https://doi.org/10.1039/C7FO02035J.

[61] A.P. Ansari, P.A. Dar, N.Z. Ahmed, Chapter-5 Scientific Basis of Some Common Medicinal Plants used in Unani Medicine-a Rational Approach, Chief Editor (n.d.) 69.

[62] E. Ersöz, M.S. Aydın, Y. Hacanlı, N. Kankılıç, İ. Koyuncu, M.E. Güldür, E. Temiz, Y. Çakmak, K. Eği, R. Dikme, M. Padak, Cardioprotective Effect of Pistacia vera L. (Green Pistachio) Hull Extract in Wistar Albino Rats with Doxorubicin-Induced Cardiac Damage, Anatol J Cardiol 27 (2023) 135–145. https://doi.org/10.14744/AnatolJCardiol.2022.2452.

[63] A. Villar, M.J. Sanz, M. Paya, Hypotensive Effect of *Pistacia lentiscus* L, International Journal of Crude Drug Research 25 (1987) 1–3. https://doi.org/10.3109/13880208709060902.

[64] A. Triantafyllou, N. Chaviaras, T.N. Sergentanis, E. Protopapa, J. Tsaknis, Chios mastic gum modulates serum biochemical parameters in a human population, Journal of Ethnopharmacology 111 (2007) 43–49. https://doi.org/10.1016/j.jep.2006.10.031.

[65] I. Andreadou, S. Mitakou, S. Paraschos, P. Efentakis, P. Magiatis, L. Kaklamanis, M. Halabalaki, L. Skaltsounis, E.K. Iliodromitis, "Pistacia lentiscus L." reduces the infarct size in normal fed anesthetized rabbits and possess antiatheromatic and hypolipidemic activity in cholesterol fed rabbits, Phytomedicine 23 (2016) 1220–1226.

[66] S.A. Ara, S. Akhlaq, M. Haque, M. Fazil, U. Akram, B. Ahmad, A. Sayeed, U. Viquar, A.A. Khan, CLOVE/QURANFUL (Syzygium aromaticum L.): A REVIEW ON ITS POTENTIAL BENEFITS IN UNANI MEDICINE, BIOACTIVITIES AND CURRENT SCIENTIFIC APPLICATIONS, Ind. J. Unani Med 15 (2022) 112–120.

[67] R. Bahramsoltani, R. Rahimi, An Evaluation of Traditional Persian Medicine for the Management of SARS-CoV-2, Front. Pharmacol. 11 (2020) 571434. https://doi.org/10.3389/fphar.2020.571434.

[68] M. Mittal, N. Gupta, P. Parashar, V. Mehra, M. Khatri, Phytochemical evaluation and pharmacological activity of Syzygium aromaticum: a comprehensive review, International Journal of Pharmacy and Pharmaceutical Sciences 6 (2014) 67–72.

[69] S.A. Saeed, A.H. Gilani, Antithrombotic activity of clove oil, Journal of Pakistan Medical Association 44 (1994) 112.

[70] Y.-Y. Yang, M.-J. Lee, H.-S. Lee, W.-H. Park, Screening of antioxidative, anti-platelet aggregation and anti-thrombotic effects of clove extracts, Journal of Physiology & Pathology in Korean Medicine 25 (2011) 471–481.

[71] G. El-Saber Batiha, L.M. Alkazmi, L.G. Wasef, A.M. Beshbishy, E.H. Nadwa, E.K. Rashwan, Syzygium aromaticum L. (Myrtaceae): Traditional Uses, Bioactive Chemical Constituents, Pharmacological and Toxicological Activities, Biomolecules 10 (2020) 202. https://doi.org/10.3390/biom10020202.

[72] M.M. Rahman, M.N. Alam, A. Ulla, F.A. Sumi, N. Subhan, T. Khan, B. Sikder, H. Hossain, H.M. Reza, M.A. Alam, Cardamom powder supplementation prevents obesity, improves glucose intolerance, inflammation and oxidative stress in liver of high carbohydrate high fat diet induced obese rats, Lipids in Health and Disease 16 (2017) 1–12.

[73] S.K. Verma, V. Jain, S.S. Katewa, Blood pressure lowering, fibrinolysis enhancing and antioxidant activities of cardamom (Elettaria cardamomum), Indian J Biochem Biophys 46 (2009) 503–506.

[74] A.H. Gilani, Q. Jabeen, A. Khan, A.J. Shah, Gut modulatory, blood pressure lowering, diuretic and sedative activities of cardamom, Journal of Ethnopharmacology 115 (2008) 463–472. https://doi.org/10.1016/j.jep.2007.10.015.

[75] M. Abu Gazia, M.A. El-Magd, Ameliorative Effect of Cardamom Aqueous Extract on Doxorubicin-Induced Cardiotoxicity in Rats, Cells Tissues Organs 206 (2018) 62–72. https://doi.org/10.1159/000496109.

[76] S. Goyal, C. Sharma, U. Mahajan, C. Patil, Y. Agrawal, S. Kumari, D. Arya, S. Ojha, Protective Effects of Cardamom in Isoproterenol-Induced Myocardial Infarction in Rats, IJMS 16 (2015) 27457–27469. https://doi.org/10.3390/ijms161126040.

[77] K. S, A. V, B. Paul-Prasanth, V. M, R.S. A, U.D. P, Aqueous extract of large cardamom inhibits vascular damage, oxidative stress, and metabolic changes in fructose-fed hypertensive rats, Clin Exp Hypertens 43 (2021) 622–632. https://doi.org/10.1080/10641963.2021.1925682.

[78] S. Ahmed, S. Gul, H. Gul, M. Zia-Ul-Haq, S. Iram, H. Jaafar, M. Moga, Scientific basis for the use of Cinnamonum tamala in cardiovascular and inflammatory diseases, Exp Clin Card 20 (2014) 784–800.

[79] V. Nagaraju, K. Aruna, S. Vikas, D. Suryanarayana, Evaluation of cardioprotective activity of Ethanolic extract of dried leaves of Cinnamomum tamala in rats, Int J Biomed Adv Res 7 (2016) 181–186.

[80] B. Ding, L. Jiang, N. Zhang, L. Zhou, H. Luo, H. Wang, X. Chen, Y. Gao, Z. Zhao, C. Wang, Z. Wang, Z. Guo, Y. Wang, Santalum album L. alleviates cardiac function injury in heart failure by synergistically inhibiting inflammation, oxidative stress and apoptosis through multiple components, Chin Med 19 (2024) 98. https://doi.org/10.1186/s13020-024-00968-0.

[81] N.S. Younis, Doxorubicin-induced cardiac abnormalities in rats: attenuation via sandalwood oil, Pharmacology 105 (2020) 522–530.

[82] C.R. Kulkarni, M.M. Joglekar, S.B. Patil, A.U. Arvindekar, Antihyperglycemic and antihyperlipidemic effect of Santalum album in streptozotocin induced diabetic rats, Pharmaceutical Biology 50 (2012) 360–365.

[83] M. Rabbani, B.K. Muflih, K. Syakirin, Nature's Sustainable Aqua Gift—Pearl in Unani medicine, JOURNAL OF HALAL INDUSTRY & SERVICES 3 (2020).

[84] M.T. Ahsan, S. Zafar, Temperament of Drugs in Unani Medicine, Hamdard Medicus 55 (2012).

[85] Y. Song, W. Chen, K. Fu, Z. Wang, The Application of Pearls in Traditional Medicine of China and Their Chemical Constituents, Pharmacology, Toxicology, and Clinical Research, Front Pharmacol 13 (2022) 893229. https://doi.org/10.3389/fphar.2022.893229.

[86] A. Rahman, T. Tajuddin, K. Amin, Identification and standardization of a pharmacopoeial Unani formulation: estimation of marker compounds, Unani Medicus 01 (2011) 58–62.

[87] A. Mohd, Z. Mohammad, M. Md, H.K. Munawwar, Ethno-Pharmacological Profile of Corallium Rubrum L., an Important Marine Drug, in the Unani System of Medicine, Nps 27 (2021) 61–67. https://doi.org/10.20307/nps.2021.27.2.61.

[88] S. Lv, Z. Lei, G. Yan, S.A. Shah, S. Ahmed, T. Sun, Chemical compositions and pharmacological activities of natural musk (Moschus) and artificial musk: A review, J Ethnopharmacol 284 (2022) 114799. https://doi.org/10.1016/j.jep.2021.114799.

[89] H. Quan, X. Yang, P. Jin, L. Li, D. Jin, Y. Luo, Protective effect of Moschus and the alternative artificial moschus on H9c2 cardiomyocytes impaired by H2O2, J Chin Med Mater 41 (2018) 961–965.

[90] H. Quan, X. Yang, P. Jin, Comparative study on the protective effects of musk and its substitute artificial musk on H2O2-induced H9c2 myocardial cell injury, Chin Materia Medica 41 (2018) 961–5.

[91] Y. Hong, F. Jiang, Effects of muscone on human vascular endothelial cells apoptosis induced by oxidative stress, Chin J Tradit Chin Med Pharm 26 (2011) 2178–2180.

[92] X. Wang, H. Meng, P. Chen, N. Yang, X. Lu, Z.-M. Wang, W. Gao, N. Zhou, M. Zhang, Z. Xu, B. Chen, Z. Tao, L. Wang, Z. Yang, T. Zhu, Beneficial effects of muscone on cardiac remodeling in a mouse model of myocardial infarction, International Journal of Molecular Medicine 34 (2014) 103–111. https://doi.org/10.3892/ijmm.2014.1766.

[93] Y. Du, Y. Ge, Z. Xu, N. Aa, X. Gu, H. Meng, Z. Lin, D. Zhu, J. Shi, R. Zhuang, X. Wu, X. Wang, Z. Yang, Hypoxia-Inducible Factor 1 alpha (HIF-1α)/Vascular Endothelial Growth Factor (VEGF) Pathway Participates in Angiogenesis of Myocardial Infarction in Muscone-Treated Mice: Preliminary Study, Med Sci Monit 24 (2018) 8870–8877. https://doi.org/10.12659/MSM.912051.

[94] Y. Du, X. Gu, H. Meng, N. Aa, S. Liu, C. Peng, Y. Ge, Z. Yang, Muscone improves cardiac function in mice after myocardial infarction by alleviating cardiac macrophage-mediated chronic inflammation through inhibition of NF-κB and NLRP3 inflammasome, Am J Transl Res 10 (2018) 4235–4246.

[95] Q. Wu, H. Li, Y. Wu, W. Shen, L. Zeng, H. Cheng, L. He, Protective effects of muscone on ischemia–reperfusion injury in cardiac myocytes, Journal of Ethnopharmacology 138 (2011) 34–39. https://doi.org/10.1016/j.jep.2011.08.009.

[96] W. Arozal, E.R. Monayo, A.J. Barinda, D.P. Perkasa, V. Soetikno, N. Nafrialdi, M. Louisa, Protective effects of silver nanoparticles in isoproterenol-induced myocardial infarction in rats, Front Med (Lausanne) 9 (2022) 867497. https://doi.org/10.3389/fmed.2022.867497.

[97] N.K. Younis, J.A. Ghoubaira, E.P. Bassil, H.N. Tantawi, A.H. Eid, Metal-based nanoparticles: Promising tools for the management of cardiovascular diseases, Nanomedicine 36 (2021) 102433. https://doi.org/10.1016/j.nano.2021.102433.

[98] W.-C. Ko, S.-J. Wang, C.-Y. Hsiao, C.-T. Hung, Y.-J. Hsu, D.-C. Chang, C.-F. Hung, Pharmacological Role of Functionalized Gold Nanoparticles in Disease Applications, Molecules 27 (2022) 1551. https://doi.org/10.3390/molecules27051551.

[99] Y. Xiao, D.B. Oumarou, S. Wang, Y. Liu, Circular RNA Involved in the Protective Effect of Malva sylvestris L. on Myocardial Ischemic/Re-Perfused Injury, Front Pharmacol 11 (2020) 520486. https://doi.org/10.3389/fphar.2020.520486.

[100] G. Benedetti, L. Flori, J. Spezzini, V. Miragliotta, G. Lazzarini, A. Pirone, C. Meneguzzo, L. Tagliavento, A. Martelli, M. Antonelli, D. Donelli, C. Faraloni, V. Calderone, F. Meneguzzo, L. Testai, Improved Cardiovascular Effects of a Novel Pomegranate Byproduct Extract Obtained through Hydrodynamic Cavitation, Nutrients 16 (2024) 506. https://doi.org/10.3390/nu16040506.

[101] J. Niewiadomska, M. Kasztura, I. Janus, E. Chełmecka, D.M. Stygar, P. Frydrychowski, A. Wojdyło, A. Noszczyk-Nowak, Punica granatum L. Extract Shows Cardioprotective Effects Measured by Oxidative Stress Markers and Biomarkers of Heart Failure in an Animal Model of Metabolic Syndrome, Antioxidants (Basel) 12 (2023) 1152. https://doi.org/10.3390/antiox12061152.

[102] S. Eghbali, S.F. Askari, R. Avan, A. Sahebkar, Therapeutic Effects of Punica granatum (Pomegranate): An Updated Review of Clinical Trials, J Nutr Metab 2021 (2021) 5297162. https://doi.org/10.1155/2021/5297162.

[103] M. Gupta, P. Sharma, A.G. Mazumder, V. Patial, D. Singh, Dwindling of cardio damaging effect of isoproterenol by Punica granatum L. peel extract involve activation of nitric oxide-mediated Nrf2/ARE signaling pathway and apoptosis inhibition, Nitric Oxide 50 (2015) 105–113. https://doi.org/10.1016/j.niox.2015.09.002.

[104] Y. Wei, A.T. Khalaf, P. Ye, W. Fan, J. Su, W. Chen, H. Hu, R. Menhas, L. Wang, Z. Oglah, Therapeutic Benefits of Pomegranate Flower Extract: A Novel Effect That Reduces Oxidative Stress and Significantly Improves Diastolic Relaxation in Hyperglycemic In Vitro in Rats, Evid Based Complement Alternat Med 2022 (2022) 4158762. https://doi.org/10.1155/2022/4158762.

[105] M. Al Hariri, K. Zibara, W. Farhat, Y. Hashem, N. Soudani, F. Al Ibrahim, E. Hamade, A. Zeidan, A. Husari, F. Kobeissy, Cigarette Smoking-Induced Cardiac Hypertrophy, Vascular Inflammation and Injury Are Attenuated by Antioxidant Supplementation in an Animal Model, Front Pharmacol 7 (2016) 397. https://doi.org/10.3389/fphar.2016.00397.

[106] H. Dab, A. Chehidi, M. Tlili, A. Ben Saad, A. Khabir, L. Zourgui, Cardiac extracellular matrix modulation in a rat-diabetic model: biochemical and anti-oxidant beneficial effect of pomegranate (Punica granatum) peel extract, Biomarkers 27 (2022) 50–59. https://doi.org/10.1080/1354750X.2021.2006312.

[107] V. Manickam, U.K. Dhawan, D. Singh, M. Gupta, M. Subramanian, Pomegranate Peel Extract Decreases Plaque Necrosis and Advanced Atherosclerosis Progression in Apoe -/- Mice, Front Pharmacol 13 (2022) 888300. https://doi.org/10.3389/fphar.2022.888300.

[108] H.S. Lee, J.I. Jung, J.S. Hwang, M.O. Hwang, E.J. Kim, Cydonia oblonga Miller fruit extract exerts an anti-obesity effect in 3T3-L1 adipocytes by activating the AMPK signaling pathway, Nutr Res Pract 17 (2023) 1043–1055. https://doi.org/10.4162/nrp.2023.17.6.1043.

[109] A. Abulizi, J. Simayi, M. Nuermaimaiti, M. Han, S. Hailati, Z. Talihati, N. Maihemuti, M. Nuer, N. Khan, K. Abudurousuli, D. Dilimulati, N. Nueraihemaiti, N. Moore, W. Zhou, A. Wumaier, Quince extract resists atherosclerosis in rats by down-regulating the EGFR/PI3K/Akt/GSK-3β pathway, Biomed Pharmacother 160 (2023) 114330. https://doi.org/10.1016/j.biopha.2023.114330.

[110] U. Rahman, M. Saleem, M.H. Mahnashi, Y.S. Alqahtani, A.O. Alqarni, B.A. Alyami, M.N. Mushtaq, S. Qasim, Antihypertensive and safety studies of Cydonia oblonga M., Pakistan Journal of Pharmaceutical Sciences 34 (2021) 687–691.

[111] W. Zhou, W. Yiming, H. Ma, G. Mamat, A. Umar, [Anti-hypertensive Effect of Total Flavonoids of Cydonia oblonga Leaves and Its Mechanism Based on Anti-inflammatory Function], Zhong Yao Cai 38 (2015) 2134–2138.

[112] H.S. Lee, Y.E. Jeon, J.I. Jung, S.M. Kim, S.H. Hong, J. Lee, J.S. Hwang, M.O. Hwang, K. Kwon, E.J. Kim, Anti-obesity effect of Cydonia oblonga Miller extract in high-fat diet-induced obese C57BL/6 mice, Journal of Functional Foods 89 (2022) 104945.

[113] A. Umar, G. Iskandar, A. Aikemu, W. Yiming, W. Zhou, B. Berké, B. Begaud, N. Moore, Effects of Cydonia oblonga Miller leaf and fruit flavonoids on blood lipids and anti-oxydant potential in hyperlipidemia rats, Journal of Ethnopharmacology 169 (2015) 239–243.

[114] A. Ahmed, S. Akbar, W.A. Shah, Chemical composition and pharmacological potential of aromatic water from Salix caprea inflorescence, Chin. J. Integr. Med. (2017). https://doi.org/10.1007/s11655-017-2781-5.

[115] N. Tawfeek, M.F. Mahmoud, D.I. Hamdan, M. Sobeh, N. Farrag, M. Wink, A.M. El-Shazly, Phytochemistry, Pharmacology and Medicinal Uses of Plants of the Genus Salix: An Updated Review, Front. Pharmacol. 12 (2021) 593856. https://doi.org/10.3389/fphar.2021.593856.

[116] F. Ghorbani, E. Nazem, A. Imani, M. Faghihi, M. Keshavarz, Cardiotonic drugs from the Avicenna's point of view, Iranian Journal of Public Health 44 (2015) 153–4.

[117] S.N. Fathima, 42. Cardioprotective effects to chronic administration of rosa damascena petals in isoproterenol induced myocardial infarction: biochemical, histopathological and ultrastructural studies, (2019).

[118] M. Rahimi, M. Ghoreshi, B. Emami, M. Shafei, M. Hosseini, A. Khajavirad, Preventive effect of hydroalcoholic extract of Rosa damascena on cardiovascular parameters in acute hypertensive rats induced by angiotensin II, Int J Prev Med 9 (2018) 92. https://doi.org/10.4103/ijpvm.IJPVM_312_17.

[119] T. Hongratanaworakit, Relaxing effect of rose oil on humans, Natural Product Communications 4 (2009) 1934578X0900400226.

[120] A. Baniasad, A. Khajavirad, M. Hosseini, M.N. Shafei, S. Aminzadah, M. Ghavi, Effect of hydro-alcoholic extract of Rosa damascena on cardiovascular responses in normotensive rat, Avicenna Journal of Phytomedicine 5 (2015) 319.

[121] M.H. Boskabady, A. Vatanprast, H. Parsaee, M. Boskabady, Possible mechanism of inotropic and chronotropic effects of Rosa damascena on isolated guinea pig heart, DARU J Pharm Sci 21 (2013) 38. https://doi.org/10.1186/2008-2231-21-38.

[122] Y. Andriani, I. Pangestika, E. Oksal, H. Mohamad, H. Amir, T.S.T. Muhammad, M.E. Abd Wahid, Anti-atherosclerosis potency of Pandanus tectorius fruit rich by trangeretin and ethyl trans-caffeate, and their cytotoxicity against HepG2 cell line, in: IOP Publishing, 2019: p. 012155.

[123] C. Wu, Y. Tian, J. Yu, R. Zhang, X. Zhang, P. Guo, The pandanus tectorius fruit extract (PTF) modulates the gut microbiota and exerts anti-hyperlipidaemic effects, Phytomedicine 58 (2019) 152863. https://doi.org/10.1016/j.phymed.2019.152863.

[124] C. Wu, H. Luan, S. Wang, X. Zhang, H. Liu, P. Guo, Pandanus tectorius derived caffeoylquinic acids inhibit lipid accumulation in HepG2 hepatoma cells through regulation of gene expression involved in lipid metabolism, Yao Xue Xue Bao 50 (2015) 278–283.

[125] X. Zhang, C. Wu, H. Wu, L. Sheng, Y. Su, X. Zhang, H. Luan, G. Sun, X. Sun, Y. Tian, Y. Ji, P. Guo, X. Xu, Anti-hyperlipidemic effects and potential mechanisms of action of the caffeoylquinic acid-rich Pandanus tectorius fruit extract in hamsters fed a high fat-diet, PLoS One 8 (2013) e61922. https://doi.org/10.1371/journal.pone.0061922.

[126] A. Akbar, M. Tariq, M. Nisa, Pharmacological studies on Salvia haematodes Wall., Acta Tropica 42 (1985) 371–374.

[127] R. Tundis, N.G. Passalacqua, M. Bonesi, M.R. Loizzo, An Insight into Salvia haematodes L. (Lamiaceae) Bioactive Extracts Obtained by Traditional and Green Extraction Procedures, Plants 11 (2022) 781. https://doi.org/10.3390/plants11060781.

[128] null Mohammed Abdulameer Farhan, null Amal Feki, null Intissar Kammoun, null Malek Aroui, null Manel Naifar, null Rim Kallel, null Fatma Makni Ayadi, null Tahia Boudawara, null Choumous Kallel, null Adil Abaed Hassoni, I. Ben Amara, Hypocholesterolemic effects of a polysaccharide isolated from Balangu (Lallemantia royleana) seeds in Wistar rat fed on a cholesterol-containing diet, Cell Mol Biol (Noisy-Le-Grand) 68 (2022) 38–46. https://doi.org/10.14715/cmb/2022.68.10.6.

[129] A. Ghannadi, A. Movahedian, Z. Jannesary, Hypocholesterolemic effects of Balangu (Lallemantia royleana) seeds in the rabbits fed on a cholesterol-containing diet, Avicenna J Phytomed 5 (2015) 167–173.

[130] G. Mosleh, A. Azadi, S. Khademian, R. Heidari, A. Mohagheghzadeh, Anti-Inflammatory Activity and Quality Control of Erysimum cheiri (L.) Crantz, Biomed Res Int 2021 (2021) 5526644. https://doi.org/10.1155/2021/5526644.

[131] P. Pram, N. Mishra, M. Vaithilingam, M.K. Samuel, M. Mohanan, N. Kothari, S.D. Chandrasekaran, Green Synthesis of Silver Nanoparticles using Coriandrum sativum and Murraya koenigii Leaf Extract and its Thrombolytic Activity, Cardiovasc Hematol Agents Med Chem 22 (2024) 230–239. https://doi.org/10.2174/0118715257279159240118050207.

[132] R. Rana, M.H. Mehmood, B. Shaukat, S. Shahid, A. Malik, B. Murtaza, Evaluation of the Cardiovascular Effects of Coriandrum sativum and Citrus limon to Treat Arsenic-Induced Endothelial Damage and Hypertension in Rats, Life (Basel) 12 (2022) 1842. https://doi.org/10.3390/life12111842.

[133] X. Wang, Y. Liu, Y. Wang, X. Dong, Y. Wang, X. Yang, H. Tian, T. Li, Protective Effect of Coriander (Coriandrum sativum L.) on High-Fructose and High-Salt Diet-Induced Hypertension: Relevant to Improvement of Renal and Intestinal Function, J Agric Food Chem 70 (2022) 3730–3744. https://doi.org/10.1021/acs.jafc.2c00267.

[134] S.K. Chaudhary, N. Maity, N.K. Nema, S. Bhadra, B.P. Saha, P.K. Mukherjee, Angiotensin Converting Enzyme Inhibition Activity of Fennel and Coriander Oils from India, Natural Product Communications 8 (2013) 1934578X1300800531. https://doi.org/10.1177/1934578X1300800531.

[135] N. Sharma, P. Sharma, N. Jasuja, S. Joshi, Ameliorative efficiency of Coriandrum sativum seed extract on atherosclerosis and oxidative stress in male albino hyperlipidemic rabbits, Res. J. Pharm. Biol. Chem. Sci 5 (2014) 26–39.

[136] F. Zeb, M. Safdar, S. Fatima, S. Khan, S. Alam, M. Muhammad, A. Syed, F. Habib, H. Shakoor, Supplementation of garlic and coriander seed powder: Impact on body mass index, lipid profile and blood pressure of hyperlipidemic patients., Pakistan Journal of Pharmaceutical Sciences 31 (2018).

[137] N. Afsheen, Optimization of Cardioprotective Potential of Various Concentrations of Medicinal Plants by Using Response Surface Methodology, PVJ 39 (2019) 13–18. https://doi.org/10.29261/pakvetj/2018.111.

[138] N. Dhyani, A. Parveen, A. Siddiqi, M.E. Hussain, M. Fahim, Cardioprotective Efficacy of *Coriandrum sativum* (L.) Seed Extract in Heart Failure Rats Through Modulation of Endothelin Receptors and Antioxidant Potential, Journal of Dietary Supplements 17 (2020) 13–26. https://doi.org/10.1080/19390211.2018.1481483.

[139] X. Wang, C. Zhu, T. Peng, W. Zhang, J. Zhang, H. Liu, C. Wu, X. Pan, C. Wu, Enhanced stability of an emulsion enriched in unsaturated fatty acids by dual natural antioxidants fortified in both the aqueous and oil phases, Food Hydrocolloids 82 (2018) 322–328.

[140] F. Hussain, N. Jahan, K.- Rahman, B. Sultana, S. Jamil, Identification of Hypotensive Biofunctional Compounds of *Coriandrum sativum* and Evaluation of Their Angiotensin-Converting Enzyme (ACE) Inhibition Potential, Oxidative Medicine and Cellular Longevity 2018 (2018) 4643736. https://doi.org/10.1155/2018/4643736.

[141] S. Goyal, M.K. Siddiqui, K.M. Siddiqui, S. Arora, R. Mittal, S. Joshi, D.S. Arya, Cardioprotective effect of "Khamira Abresham Hakim Arshad Wala" a unani formulation in isoproterenol-induced myocardial necrosis in rats, Exp Toxicol Pathol 62 (2010) 61–74. https://doi.org/10.1016/j.etp.2009.02.115.

[142] A.S. Nazmi, S.J. Ahmad, A. Rashikh, M. Akhtar, K.K. Pillai, A.K. Najmi, Protective effects of 'Khamira Abresham Hakim Arshad Wala', a unani formulation against doxorubicin-induced cardiotoxicity and nephrotoxicity, Toxicology Mechanisms and Methods 21 (2011) 41–47. https://doi.org/10.3109/15376516.2010.529188.

[143] V. Uddin Ahmad, S. Bano, N. Bano, A triterpene acid from Nepeta hindostana, Phytochemistry 25 (1986) 1487–1488. https://doi.org/10.1016/S0031-9422(00)81318-7.

[144] J. Du, D. Yu, J. Li, L. Si, D. Zhu, B. Li, Y. Gao, L. Sun, X. Wang, X. Wang, Asiatic acid protects against pressure overload-induced heart failure in mice by inhibiting mitochondria-dependent apoptosis, Free Radical Biology and Medicine 208 (2023) 545–554. https://doi.org/10.1016/j.freeradbiomed.2023.09.015.

[145] M.M. Engler, M. Schambelan, M.B. Engler, D.L. Ball, T.L. Goodfriend, Effects of Dietary -Linolenic Acid on Blood Pressure and Adrenal Angiotensin Receptors in

Hypertensive Rats, Experimental Biology and Medicine 218 (1998) 234–237. https://doi.org/10.3181/00379727-218-44292.

[146] J.S. Charnock, G.L. Crozier, J. Woodhouse, Gamma-linolenic acid, black currant seed and evening primrose oil in the prevention of cardiac arrhythmia in aged rats, Nutrition Research 14 (1994) 1089–1099. https://doi.org/10.1016/S0271-5317(05)80262-3.

[147] Y.-H. Liao, P.J. Houghton, J.R.S. Hoult, Novel and Known Constituents from *Buddleja* Species and Their Activity against Leukocyte Eicosanoid Generation, J. Nat. Prod. 62 (1999) 1241–1245. https://doi.org/10.1021/np990092+.

[148] J. Huang, H. Chen, S. Lan, L. Qin, Z. Xun, S. Han, H. Zhao, Y. Ci, C. Xu, W. Zhu, X. Lu, J. Chen, Q. Zheng, E. Li, X. Chen, C. Lu, R. Qian, S. Chen, X. Li, N. Sun, Discovery of zerumbone as a new agent for cardiac hypertrophy by high-throughput screening using human embryonic stem cell-derived cardiomyocytes, (2022). https://doi.org/10.21203/rs.3.rs-574349/v1.

[149] B. Yalameha, H.R. Nejabati, M. Nouri, Cardioprotective potential of vanillic acid, Clin Exp Pharma Physio 50 (2023) 193–204. https://doi.org/10.1111/1440-1681.13736.

[150] Y. Zhang, C. Ma, C. Liu, F. Wei, Luteolin attenuates doxorubicin-induced cardiotoxicity by modulating the PHLPP1/AKT/Bcl-2 signalling pathway, PeerJ 8 (2020) e8845. https://doi.org/10.7717/peerj.8845.

[151] L. Liu, S. Huang, H. Qiu, X. Cen, Y. Guo, D. Li, Y. Ma, M. Xu, Q. Tang, Limonin stabilises sirtuin 6 (SIRT6) by activating ubiquitin specific peptidase 10 (USP10) in cardiac hypertrophy, British J Pharmacology 179 (2022) 4516–4533. https://doi.org/10.1111/bph.15899.

[152] F. Senatore, V. De Feo, Essential Oils from *Salvia* spp. (Lamiaceae). II. Chemical Composition of the Essential Oil from *Salvia pratensis* L. subsp. *haematodes* (L.) Briq. Inflorescences, Journal of Essential Oil Research 10 (1998) 135–137. https://doi.org/10.1080/10412905.1998.9700864.

[153] W.A. Keshk, N.A. Soliman, D.A. Ali, W.S. Elseady, Mechanistic evaluation of AMPK/SIRT1/FXR signaling axis, inflammation, and redox status in thioacetamide-induced liver cirrhosis: The role of Cichorium intybus linn (chicory)-supplemented diet, Journal of Food Biochemistry 43 (2019) e12938. https://doi.org/10.1111/jfbc.12938.

[154] T. Liu, H. Wen, H. Li, H. Xu, N. Xiao, R. Liu, L. Chen, Y. Sun, L. Song, C. Bai, J. Ge, Y. Zhang, J. Chen, Oleic Acid Attenuates Ang II (Angiotensin II)-Induced Cardiac Remodeling by Inhibiting FGF23 (Fibroblast Growth Factor 23) Expression in Mice, Hypertension 75 (2020) 680–692. https://doi.org/10.1161/HYPERTENSIONAHA.119.14167.

[155] C.Y. Chen, Y.S. Tsai, C.T. Chen, H.C. Yeh, H.T. Li, Flavonoids from the Flowers of Aquilaria agallocha, Chem Nat Compd 55 (2019) 722–723. https://doi.org/10.1007/s10600-019-02789-2.

[156] M. Du, K. Huang, L. Gao, L. Yang, W. Wang, B. Wang, K. Huang, D. Huang, Nardosinone protects H9c2 cardiac cells from angiotensin II-induced hypertrophy, J. Huazhong Univ. Sci. Technol. [Med. Sci.] 33 (2013) 822–826. https://doi.org/10.1007/s11596-013-1205-9.

[157] L. Jin, Z. Xie, P. Lorkiewicz, S. Srivastava, A. Bhatnagar, D.J. Conklin, Endothelial-dependent relaxation of α-pinene and two metabolites, myrtenol and verbenol, in isolated murine blood vessels, American Journal of Physiology-Heart and Circulatory Physiology 325 (2023) H1446–H1460. https://doi.org/10.1152/ajpheart.00380.2023.

[158] D. Peixoto-Neves, Q. Wang, J.H. Leal-Cardoso, L.V. Rossoni, J.H. Jaggar, Eugenol dilates mesenteric arteries and reduces systemic BP by activating endothelial cell TRPV 4 channels, British J Pharmacology 172 (2015) 3484–3494. https://doi.org/10.1111/bph.13156.

[159] H.K. Moon, P. Kang, H.S. Lee, S.S. Min, G.H. Seol, Effects of 1,8-cineole on hypertension induced by chronic exposure to nicotine in rats, Journal of Pharmacy and Pharmacology 66 (2014) 688–693. https://doi.org/10.1111/jphp.12195.

[160] L. Yang, Q.-Q. Wu, Y. Liu, Z.-F. Hu, Z.-Y. Bian, Q.-Z. Tang, Cinnamaldehyde attenuates pressure overload-induced cardiac hypertrophy, Int J Clin Exp Pathol 8 (2015) 14345–14354.

[161] Evaluation of the Effects of East Indian Sandalwood Oil and α-Santalol on Humans after Transdermal Absorption, Planta Med 70 (2004) 3–7. https://doi.org/10.1055/s-2004-815446.

[162] E.N. Ncube, L. Steenkamp, I.A. Dubery, Ambrafuran (AmbroxTM) Synthesis from Natural Plant Product Precursors, Molecules 25 (2020) 3851. https://doi.org/10.3390/molecules25173851.

[163] Y. Liu, J. Xu, C. Yang, Y. Li, M. Chen, S. Liu, X. Zheng, P. Luo, R. Li, D. Xiao, Z. Shan, Muscone inhibits angiotensin II–induced cardiac hypertrophy through the STAT3, MAPK and TGF-β/SMAD signaling pathways, Mol Biol Rep 51 (2024) 39. https://doi.org/10.1007/s11033-023-08916-1.

[164] X. Chen, J. Huang, Y. Lv, Y. Chen, J. Rao, Crocin exhibits an antihypertensive effect in a rat model of gestational hypertension and activates the Nrf-2/HO-1 signaling pathway, Hypertens Res 44 (2021) 642–650. https://doi.org/10.1038/s41440-020-00609-7.

[165] Q. Wu, Q. Zhou, C. Wan, G. Xin, T. Wang, Y. Gao, T. Liu, X. Yu, B. Zhang, W. Huang, Mechanism Actions of Coniferyl Alcohol in Improving Cardiac Dysfunction in Renovascular Hypertension Studied by Experimental Verification and Network Pharmacology, IJMS 25 (2024) 10063. https://doi.org/10.3390/ijms251810063.

[166] S. Munir, R. Hafeez, W. Younis, M.N.H. Malik, M.U. Munir, W. Manzoor, M.A. Razzaq, L.B. Pessoa, K.S. Lopes, F.A.D.R. Lívero, A. Gasparotto Junior, The Protective Effect of Citronellol against Doxorubicin-Induced Cardiotoxicity in Rats, Biomedicines 11 (2023) 2820. https://doi.org/10.3390/biomedicines11102820.

[167] Y. Liu, X. Xu, D. Bi, X. Wang, X. Zhang, H. Dai, S. Chen, W. Zhang, Influence of squalene feeding on plasma leptin, testosterone & blood pressure in rats, Indian J Med Res 129 (2009) 150–153.

[168] S. Gupta, S. Saxena, Endophytes: Saviour of apples from post-harvest fungal pathogens, Biological Control 182 (2023) 105234. https://doi.org/10.1016/j.biocontrol.2023.105234.

[169] F. Ali, D. Wang, Y. Cheng, M. Wu, M.Z. Saleem, L. Wei, Y. Xie, M. Yan, J. Chu, Y. Yang, A. Shen, J. Peng, Quercetin attenuates angiotensin II-INDUCED proliferation of vascular smooth muscle cells and p53 pathway activation in vitro and in vivo, BioFactors 49 (2023) 956–970. https://doi.org/10.1002/biof.1959.

[170] A. Kostecka-Gugała, Quinces (Cydonia oblonga, Chaenomeles sp., and Pseudocydonia sinensis) as Medicinal Fruits of the Rosaceae Family: Current State of Knowledge on Properties and Use, Antioxidants 13 (2024) 71. https://doi.org/10.3390/antiox13010071.

[171] L. Li, C. Su, X. Chen, Q. Wang, W. Jiao, H. Luo, J. Tang, W. Wang, S. Li, S. Guo, Chlorogenic Acids in Cardiovascular Disease: A Review of Dietary Consumption, Pharmacology, and Pharmacokinetics, J. Agric. Food Chem. 68 (2020) 6464–6484. https://doi.org/10.1021/acs.jafc.0c01554.

CHAPTER-III

ANTI-HYPERTENSIVE ACTIVITY OF SOME SELECTED UNANI FORMULATIONS: AN EVIDENCE-BASED APPROACH FOR VERIFICATION OF TRADITIONAL UNANI CLAIMS USING LC-MS/MS FOR THE EVALUATION OF CLINICALLY RELEVANT BLOOD PARAMETERS IN LABORATORY RATS

Anti-Hypertensive Activity of Some Selected Unani Formulations: An Evidence-Based Approach for Verification of Traditional Unani Claims Using LC-MS/MS for the Evaluation of Clinically Relevant Blood Parameters in Laboratory Rats

1. Introduction

Among the many serious medical conditions, hypertension is one where there is an increased risk for the heart, brain, kidney and other organs. Hypertension plays a pivotal role behind CVD mortality and disease burden worldwide. One of the World Health Organization's global non-communicable diseases (NCD) main goals, adopted in 2013, was to reduce the occurrence of hypertension to 25% by 2025 compared to 2010 [1]. Over the last decade, the combination therapies constituting multiple biologically active components have replaced the single component-based therapies. Considering the insufficiency of the single drug anti-hypertensive treatment in chronic conditions, a multiple drug regimen, addressing different anti-hypertensive targets at the same time, has become increasingly popular for clinicians [2].

The World Health Organization (WHO) has recognized the Unani system of medicine as a form of alternative medicine used by people globally.It considers a person's entire body, mind and spirit. It sees the human body as one cohesive system made up of four basic parts with four different temperaments. The physical qualities and inherent disposition of a person are reflected in their temperament. The human body is susceptible to several ailments due to temperamental imbalances [3]. Contemplation of unani literature points out that some of the formulations have been used for centuries in the management of cardiovascular diseases. In the Unani system of medicine, polyherbal formulations are generally named on the basis of the chief ingredient present (i.e., the ingredient which is considered to be mainly responsible for preparation's purpose—OR—sometimes the component present in the maximum quantity). An example is Habb-e-jadwar (HJ), where jadwar (5.136 mg per 240 mg of a pill) or Delphinium denudatum Wall. root is the main component. Similarly, Khamira Abreesham Sada (KAS), containing Abreesham (2.193 mg per g of KAS) or Bombyx mori cocoon as the main component. A total of 27.75 mg of *Rosa damascene* Herrm. is present per g of Mufarreh Shaikh ur Rais. Khamira Gawzaban Sada contains "Gawzaban", i.e., *Borago officinalis* L., which is the main component. As per the label claim of this commercial unani product, 17.544 mg of Borago officinalis L. (leaf and flower) per g weight of the KGS and 26.4 mg of Berberis aristata DC (fruit) per g weight of the DMM arepresent as the chief components in their respective formulations [4,5]. The

complete composition of these formulations are mentioned in Table 1, Table 2, Table 3, Table 4 and Table 5 [4,5,6]. Khamira Gozaban Sada (KGS)and Khamira Abreesham Sada (KAS) have been reported to be used exclusively as Muqavvi Qalb (cardiac tonic) and Khafqan (palpitations) [4,5] while Dawaul Misk Motadil (DMM) has been reported to be used as Muqavvi Qalb (cardiac tonic),Muqavvi Jiger (liver tonic) and particularly in Khafqan Saudavi (melancholic palpitations) [5]. Mufarreh Shaikhurais has been used as Mufarreh Qalb (refrigerant), Dafe Khafqan (relieves palpitations) and Muqavvi Qalb (cardiac tonic) [5]. Similarly, Habb-e-Jadwar (HJ) has been useful as Zofe Bah (sexual weakness), Jiryan (spermatorrhea), Sual (cough) and Nazla Muzmin (chronic cold) [5]. These formulations are frequently prescribed in almost all of the Unani hospitals in and around India. In India, the Unani system of medicine has been in practice since 1350 AD. At present this medical practice is still in use and is believed to be effective with minimal adverse events. Very few scientific studies are actually available on these polyherbal preparations. Our study was to contribute scientific input in the pursuit of creating scientific literature about this particular age-old system of medical practice. We have collected information from the Unani practitioners who still believe in the efficacy of this system of therapy, where efficacy may vary but adverse events are infinitesimally insignificant [7].

Table 1. Composition of Khamira Gozaban Sada (KGS) as per label claim.

SL.No	**Composition**	**Part Used**	**Quantity**
1	Abresham muqarraz	-	21.93 mg
2	Badranjboya (*Nepeta hindostana* (B.Heyne ex Roth) Haines)	Flower	153.51 mg
3	Berg e Gawzaban (*Borago officinalis* L.)	Leaf	131.58 mg
4	Burada Sandal Safaid (*Santalum album* L.)	Heart wood	109.65 mg
5	Behman Surkh (*Salvia haematodes* L.)	Root	87.72
6	Tukhm Balangu (*Lallemantia royleana* (Benth)Benth.	Seed	109.65 mg
7	Tudri Surkh (*Cheiranthus cheiri* L.)	Seed	43.86 mg
8	Kishneez Khushk (*Coriandrum sativum* L.)	Fruit	131.58 mg
9	Gule Khatmi (*Althaea officinalis* L.)	Flower	43.86 mg
10	Gule Gawzaban (*Borago officinalis* L.)	Flower	43.86 mg
11	Shakar safaid (*Saccharum officinarum*)	Crystal	8.722 g
12	Sat Leemun (*Citrus aurantium* L.)	Crystal	17.54 mg
13	Natroon Banjawi	-	5.26 mg

Table 2. Composition of Dawa ul Misk Motadil (DMM) as per label claim.

SL.No	Composition	Part Used	Quantity
1	Zarishk (*Berberis aristata* DC)	Fruit	132.0 mg
2	Tabasheer Safaid (*Bambusa arundinace* willd.)	Silicacious concretion	88 mg
3	Sandal safaid (*Santalum album* L.)	Heart wood	88 mg
4	Sandal Surkh (*Pterocarpus santalinus* L.f.)	Heart wood	88 mg
5	Kishneez Muqashshar (*Coriandrum sativum* L.)	Dried seed	88 mg
6	Gule Gawzaban (*Borago officinalis* L.)	Flower	88 mg
7	Amla (*Embelica officinalis*)	Dried fruit	88 mg
8	Tukhm Khurfa (*Portulaca oleracea* L.)	Dried seed	88 mg
9	Gule Surkh (*Rosa damascene* Herrm.)	Flower	51 mg
10	Abresham Muqarraz (*Bombyx mori* cocoon)	Cocoon	51 mg
11	Darchini (*Cinnamomum zeylanicum* Blume)	Stem, Bark	51 mg
12	Behman Safaid (*Centaurea behen* L.)	Root	51 mg
13	Behan Surkh (*Salvia haematodes* L.)	Root	51 mg
14	Darunaj Aqrabi (*Doronicum hookeri* C.B.Clarke ex Hook.f)	Rhizome	51 mg
15	Ood Hindi (*Aquilaria agallocha* Roxb.)	Heart wood	36 mg
16	Badranjboya (*Nepeta hindostana* (B.Heyne ex Roth) Haines)	Whole plant	36 mg
17	Mastagi (*Pistacia lentiscus* L.)		30 mg
18	Ushana (*Usnea longissima* Ach.)	Thallus	30 mg
19	Dana Elaichi Khurd (*Elettaria cardamomum* L.)	Dried seed	30 mg
20	Qand Safaid (*Saccharum officinarum*)	Crystal	2.44 g
21	Shahad (Honey)	--	1.22 g
22	Aabe Seb Shinn (*Pyrus malus* L.)	Fruit	1.22 g
23	Zafran (*Crocus sativa* L.)	Stigma	51 mg
24	Amber (resin) without musk	-	14 mg

Table 3. Composition of Khamira Abresham Sada as per label claim.

SL.No	Composition	Part Used	Quantity
1	Abresham Muqarraz	Cocoon	603.3 mg
2	Berg Badranjboys ((*Nepeta hindostana* (B.Heyne ex Roth)) Haines)	Leaf	452.4 mg
3	Berg Gawzaban (*Borago officinalis* L.)	Leaf	262 mg
4	Gule Khatmi (*Althaea officinalis* L.)	Flower	111.6 mg
5	Shakar Safaid (*Saccharum officinarum*)	Crystal	9.049 g
6	Sat Leemun (*Citrus aurantium* L.)	Crystal	36.20 mg
7	Natroon Banjawi		9.049 mg
8	Zafran (*Crocus sativus* L.)	Stigma	5.279 mg

Table 4. Composition of Habb-e-Jadwar as per label claim.

SL.No	Composition	Part of the Plant	Quantity
1	Afyun (*Papaver somniferum* L.)	Fruit	25.68 mg
2	Jadwar (*Delphinium denudatum* Wall. ex Hook.f. and Thomson)	*Tuber*	5.136 mg
3	Zafran *(Crocus sativa* L.)	*Style and Stigma*	2.568 mg
4	Sheer Gao *(Cow Milk)*		6.420 mL
5	Narjeel *(Cocos nucifera* L.)	*Kernel*	102.72 mg
6	Bisbasa *(Myristica fragrans* Houtt)	*fruit coat*	
7	Behman safed (*Centaurea behen* L.)	*Root*	6.629 mg
8	Behman surkh *(Salvia heamatodes* L.)	*Root*	6.629 mg
9	Maghz Badam Shirin *(Prunus amygdalus L.)*	*Stem oil*	9.946 mg
10	Maghz Chilghoza *(Pinus gerardiana* Wall.)	*Kernel*	9.946 mg
11	Tukhme Khurfa *(Portulaca oleracea* L.)	*Seed*	9.946 mg
12	Roghan Balsan *(Commiphora opobalsamum* L.)	*Oil and Stem*	13.268 mg
13	Jawitri (*Myristica fragrans* Houtt.)	*Aril*	6.629 mg
14	Badranjboya (*Nepeta hindostana* (B.Heyne ex Roth) Haines)	*Whole plant*	6.629 mg
15	Banslochan (*Bambusa arundinacea* willd.)	Silicacious concretion	2.94 mg
16	Gond Keekar (*Acacia arabica*)	*Gum*	2.94
17	Misri (*Saccharum officinarum*)	*Cubes*	13.268 mg
18	Kaleera (*Cochlospermum religiosum* (L.) Alston)	Gum	2.94 mg
19	Ajwain Khurasani (*Hyoscyamus niger* L.)	Fruit	2.94
20	Beikh Luffah *(Atropa Belladona* L.)	Root	2.94
21	Jaiphal (*Myristica fragrans* Houtt.)	Seed	2.94
22	Warq Nuqra (silver)		7.210 mg
23	Ghee		q.s.

Table 5. Composition of Mufarreh Shaikhur Raees as per label claim.

SL.No	Composition	Part of the Plant	Quantity
1	Agar (*Aquilaria agallocha* Roxb.)	Heart wood	37 mg
2	Elaichi Khurd (*Elettaria cardamomum* L.)	Fruit	55.5 mg
3	Berg Gawzaban (*Borago officinalis* L.)	Leaf	92.5 mg.
4	Burada Sandal Surkh (*Pterocarpus santalinus* L.f.)	HeartWood	27.75 mg
5	Burada Sandal Safaid (*Santalum album* L.)	HeartWood	55.5 mg
6	Banslochan (*Bambusa arundinacea* willd)	Silicaceous concretion	55.5 mg

SL.No	Composition	Part of the Plant	Quantity
7	Behman Surkh (*Salvia haematodes* L.)	Root	37 mg
8	Tukhm Khurfa Siyah (*Portulaca oleracea* L.)	Seed	83.25 mg
9	Tukhm Kahu (*Lactuca sativa* L.)	Seed	83.25 mg
10	Qust Shireen (*Saussurea lappa* (Falc.) Lipsch.)	Root	37 mg
11	Zarambad (*Curcuma zedoaria* Roxb.)	Root Trunk	37 mg
12	Sartan Sokhta (*Scylla serrata* (Forskål, 1775) ash)	-	27.75 mg
13	Gule Surkh (*Rosa damascene* Herrm.)	Flower	138.75 mg
14	Maghz Tukhm Kharbooza *(Cucumis melo* L.)	-	83.25 mg
15	Maghz Tukhm Khayarain *(Cucumis sativus* L.)	-	83.25 mg
16	Maghz Kadu Shireen (*Cucurbita maxima* Duch ex.Lam)	-	83.25 mg
17	Kafoor (Camphor)	-	27.75 mg
18	Busad Sokhta Mehlool	-	27.75 mg,
19	Marwareed Mehlool	-	27.75 mg
20	Abresham Muqarraz	Cocoon	27.75 mg
21	Qwam Shakar Safaid (*Saccharum officinarum*)	Crystal	2.222 g
22	Rub Anar Shireen (*Punica granatum* L.)	Fruit	555 mg
23	Rub Behi (*Cydonia oblonga* Mill)	Fruit	555 mg
24	Rub Seb (*Malus sylvestris* (L.) Mill.)	Fruit	555 mg
25	Natroon Banjawi.	-	5.55 mg
26	Zafran (*Crocus sativa* L.)	Stigma	6.48 mg
27	Arq Gawzaban (*Borago officinalis* L.)	Distilled	0.07 mL
28	Warq Nuqra	-	9.25 mg

2. Materials and Methods

2.1. Chemicals

The L-NAME $C_7H_{15}N_5O_4$.HCl (Sigma Aldrich, Burlington, MA, USA, catalogue no: N5751) was purchased from Sigma Aldrich. The KGS (batch no: MKHO35A); KAS (batch no. 0KM0109); MSR (batch no. 0K00010); DMM (batch no. MDE019) and HJ (batch no.0KN0001) (Hamdard Laboratories, Mfg Lic. No. U-212/78/2014) were a kind donation from The Calcutta Unani Medical College and Hospital, 8/1,Abdul Halim Lane, Kolkata, West Bengal 700,016. The Na^+, K^+ and the Cl^- ELYTE-3 estimation kit was provided by Coral Clinical Systems; catalogue no: SOD/POT/CL (ELYTE-3)/15T/CR. The Griess

Reagent (catalogue no: SRL# 35657) and the protease inhibitor cocktail (Sigma Aldrich, Burlington, MA, USA, catalogue no:I3911-1BO) were donated by TAAB Biostudy Services. The aldosterone, $C_{21}H_{28}O_5$ (Sigma Aldrich, Burlington, MA, USA, catalogue no: A9477), adrenaline tartrate, $C_9H_{13}NO_3 \cdot C_4H_6O_6$ (Sigma Aldrich, Burlington, MA, USA, catalogue no: A0300000), noradrenaline, $C_8H_{11}NO_3 \cdot C_4H_6O_6 \cdot H_2O$ (Sigma Aldrich, Burlington, MA, USA, catalogue no: N1100000) and the Atrial Natriuretic peptide, $C_{64}H_{107}N_{25}O_{19}S_2$ (Sigma Aldrich, Burlington, MA, USA, catalogue no: SCP0022)were employed.

2.2. Animals and Experimental Protocol

Male Wistar albino rats (8–9 weeks) weighing 130–150 g were purchased from Chakraborty Enterprises (West Bengal, India). All of the animal experiments were approved by the IAEC (1938/PO/Rc/S/17/CPCSEA).To rule out any intercurrent infection, they were kept under observation for roughly ten days prior to the start of the experiment. The animals were kept in polypropylene cages with well-aerated stainless steel covers and were exposed to a regular 12-h light/dark cycle and ambient temperature.

2.3. Development of Hypertensive Model in Rats

Hypertension was artificially induced in the Wistar rats by intraperitoneal administration of L-NAME (N-nitro-l-arginine methyl ester) in a dose of 185 mmol/kg of body mass two times daily for 7 consecutive days [8].

2.4. Non-Invasive Blood-Pressure Measurement

Using the BIOPAC-MP36 system, the systolic blood pressure (SBP) was recorded non-invasively by inserting a cuff around the tails of the adult male rats (kept in approved animal restrainers) (BIOPAC System Inc., Goleta, CA, USA). The test-animals' body temperatures were artificially maintained at 37 °C using an animal-heating unit. A non-invasive blood-pressure device (NIBP 200A, Santa Barbara, CA, USA) for animal tail insertion and finally a data simulation device (MP36, Goleta, CA, USA) were employed to acquire the data. The blood pressure was recorded until consistent and repeatable results were achieved [8].

2.5. Surface Electrocardiogram (ECG) Measurement in Anesthetized Rats

Ketamine (60 $mg \cdot kg^{-1}$) and xylazine (10 $mg \cdot kg^{-1}$) were used to anesthetize the rats, as reported previously. Using a standard lead, an ECG was taken for 5 min, immediately after anesthesia. MP36 (BIOPAC, Goleta, CA, USA) was used to collect and analyze the ECG

signals. The RR-interval was measured on day 0 (self-control) i.e., before the L-NAME administration, day-7 (L-NAME) and day-14 (L-NAME +respective formulations) [9].

2.6. Allocation of Groups: Animals were Divided into Six Groups (n = 6)

Group I or hypertensive control group: L-NAME administered for 7 days and left untreated for the next 7 days

Group II or KASgroup: L-NAME administered (i.p) for 7 days and L-NAME + KAS(1000 mg/kg b.w) for the next 7 days.

Group III or DMM group: L-NAME administered (i.p) for 7 days and L-NAME + DMM(2000 mg/kg b.w) for the next 7 days.

Group IV or MSR group: L-NAME administered (i.p) for 7 days and L-NAME + MSR(300 mg mg/kg b.w) for the next 7 days.

Group V or HJ group: L-NAME administered (i.p) for 7 days and L-NAME + HJ(113 mg/kg b.w) for the next 7 days.

Group VI or KGS group: L-NAME administered (i.p) for 7 days and L-NAME +KGS (2000 mg/kg b.w) for the next 7 days.

The animals were divided into six groups (n = 6) and the entire protocol comprised of 14 days. The control group was treated with L-NAME for 7 consecutive days and left untreated for the next 7 days. The animals of Group II-VI were initially treated with L-NAME for the first 7 days and concurrently administered with the respective formulations for the next 7 days. The RR-interval and systolic blood pressure (SBP) were measured on the 0th, 7th and 14th day. All of the unani formulations were administered orally using water as the vehicle.

Schematic representation of experiment

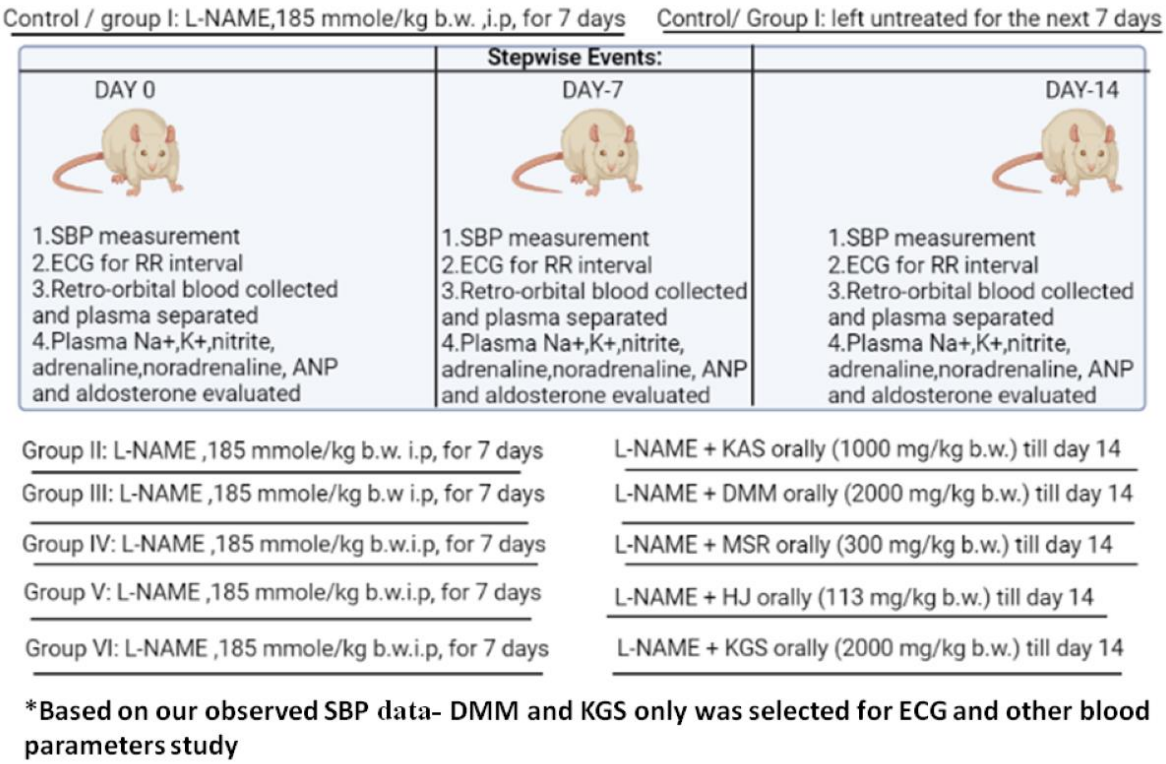

***Based on our observed SBP data- DMM and KGS only was selected for ECG and other blood parameters study**

2.7. Preparation of 0.2M Phosphate Buffer Solution pH 7.5

A total of 27.22 gm of potassium dihydrogen phosphate was dissolved in 930 mL of water, the pH was adjusted to 7.5 using 300 gm/L solution of potassium hydroxide and finally, the volume was made upto 1000 mL with water [10].

2.8. Collection of Plasma for Quantification of Biomarkers

Less than 1 mL of the blood samples from the retro-orbital plexus was collected and separated by centrifugation for 10 min at 3500 rpm in a cold centrifuge (4 °C). The plasma was collected separately in two parts. The first part was analyzed for sodium [11,12], potassium by Elyte 3 kit [13] and nitrite by Griess Assay [14] for the respective groups while the second part contained the protease inhibitor cocktail for the adrenaline, noradrenaline, ANP and aldosterone estimation by LC-MS/MS. The protease-inhibitor cocktail powdered product was dissolved by adding 1ml of deionized water into the bottle to make a 100 times concentrated-stock solution. The buffer was diluted to make 100 mL of 1× (1:100) protease inhibitor solution. A total of 10 µL of the protease inhibitor solution was added to 2 mL of the plasma sample and immediately mixed [15]. The samples were stored at −20 °C.

2.9. LC-MS/MS Methodology

To acquire data with a very low limit of quantification, which is essential for recording extremely minute changes in the blood concentration of hormones and neurotransmitters following the administration of test substances, is only possible with a LC-MS/MS triple-quadruple quantification. Shimadzu LC was used with a binary pump, on-line degasser, and a thermostatic autosampler (SIL-20AC). The LC was coupled to an Ab Sciex API-4000 QTRAP mass spectrometer equipped with an electrospray ionization (ESI) source. The Analyst Software 1.6.3 was used for the data acquisition. The separation was achieved using Phenomenex Kinetex (5µ C18 100A 50 × 3 mm)

2.9.1. *Chromatographic Conditions*

The injection volume was 10 µL. The mobile phases A and B were eluted in a linear gradient at a flow rate of 0.5 mL/min, while the column was kept at a constant temperature of 25 °C. The ionization source was electrospray ionization (ESI) in the positive and negative ion modes. Nitrogen was used as the curtain gas and was maintained at a flow of 20.00 psig with GS1 and GS2 gas at 40.00 and 45.00 psig, respectively. The gas temperature was set at 400 °C and the capillary voltage was −4500.00 V. The declustering potential was applied for parent ionization and the collision energy for the product ionization. Multiple reaction monitoring was the final stage of the detector response of the mass spectrometry. ESI was taken as the ion source. adrenaline, noradrenaline, aldosterone and atrial natriuretic peptide were extracted from the plasma matrix, using solid phase extraction (solid phase extraction cartridge). For the assessment of the aldosterone, tolbutamide was taken as the internal standard (IS), while propranolol served as an internal standard (IS) for ANP, adrenaline and noradrenaline.

3. Statistical Analysis

An average of three readings were taken over a period of 2 h and the variation was observed in the second place of the decimal. The mean ± standard deviation was used to represent all of the data. GraphPad Prism 9.0 was used to undertake the statistical data analysis (Graph Pad, San Diego, CA, USA). One-way ANOVA was applied to assess all of the serum parameters, and Tukey's test was used for post-hoc analysis. A statistically significant value was defined as $p < 0.05$.

4. Results

Figure 1 and Figure 2 represents the non-invasive SBP and RR-interval. Figure 3a shows non-significant decrease in KAS, MSR and HJ on day 14, as compared to day 7, but a significant ($p < 0.05$) one was noted in DMM. Unexpectedly, an elevated SBP was found in the KGS-treated group on day 14. There was a significant lengthening of the RR-interval on day 7. The shortening of the RR-interval on day 14 was not seen in KGS, on the contrary it lengthened, while the control and the DMM group showed a significant decrease ($p < 0.05$) (Figure 3b). The increase in the serum sodium for the control, KGS and DMM groups on day 7 were significant, except for the KGS group; meanwhile, on day 14, all of the groups showed a non-significant slight reduction (Figure 4a). The plasma potassium did not much change on day 7for all of the groups, while on day 14 it significantly ($p < 0.05$) increased, but not in the control group (Figure 4b). In Figure 4c, the plasma nitrite was found to decrease significantly ($p < 0.05$) in the control and DMM group on day 7 after the L-NAME treatment, but the animals in the KGS group showed a non-significant decrease on day 7. On day 14, there was not much change in the plasma nitrite status in the animals of the KGS group, while the control and DMM groups displayed a significant ($p < 0.05$) increase. In Figure 5a,b, the plasma adrenaline and noradrenaline in both the DMM- and KGS-treated rats increased significantly ($p < 0.05$) on day 7, and similarly the decrease on day 14 was also noted to be significant ($p < 0.05$). In Figure 5a,b there was no significant change in the plasma ANP and aldosterone in both the DMM and KGS groups for day 7 and 14. Figure 5c depicts the % inhibition in both the DMM and KGS group on day 14, in comparison to day 7. Figure 6, Figure 7, Figure 8 and Figure 9 represent the MRM (Multiple Reaction Monitoring) chromatogram of ANP, noradrenaline, adrenaline and aldosterone. The adrenaline, noradrenaline and ANP were ionized in the positive mode for detection, while aldosterone was evaluated by ionizing in the negative mode. Similarly, Figure 6 represents the b.w. of animals and did not show much change (non-significantly) from day 0–14.

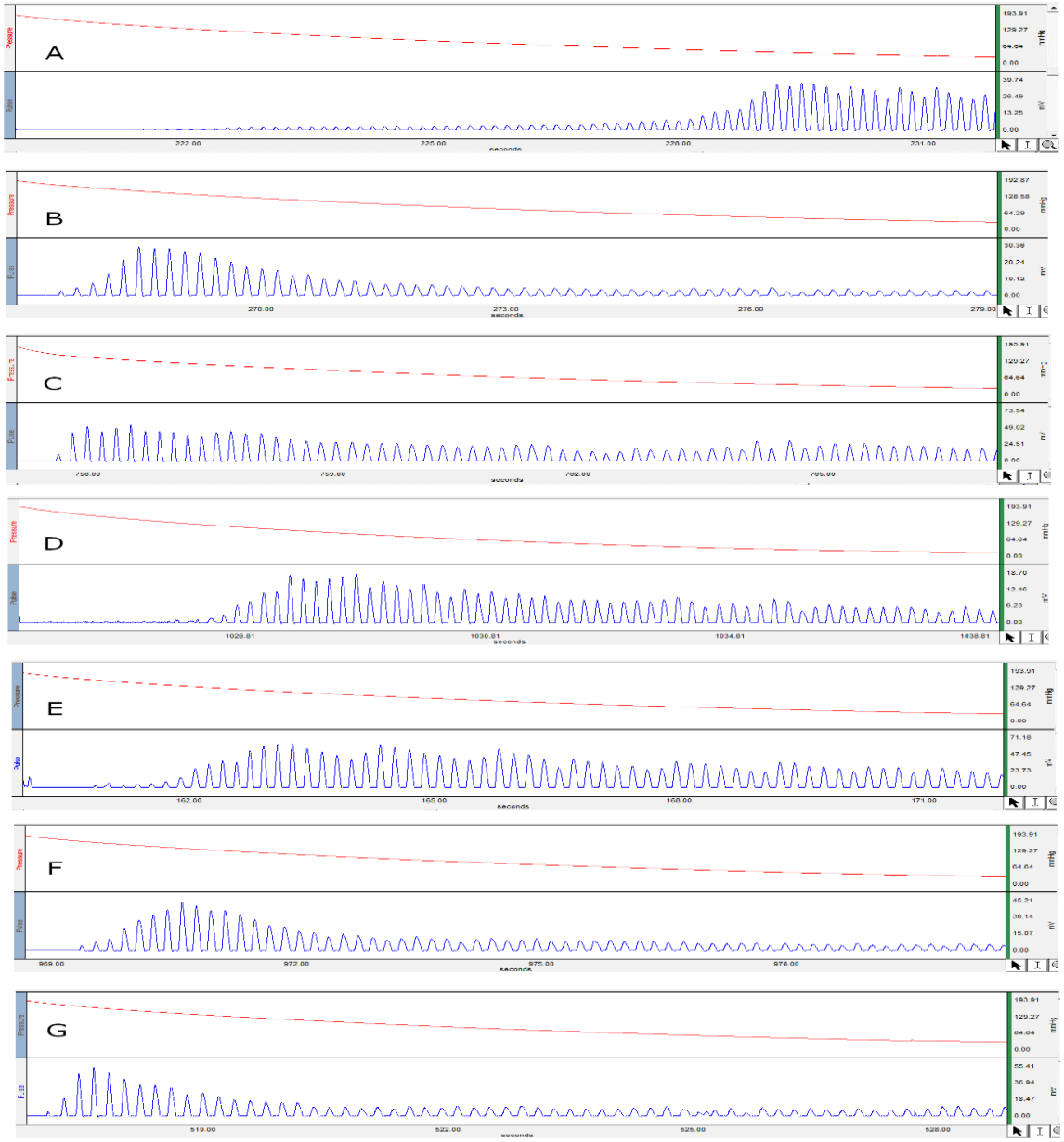

Figure 1. Represents the non-invasive systolic blood pressure. (**A**) Hypertensive control on day 0; (**B**) SBP on day 7 on treatment with L-NAME; (**C**) SBP of KAS on day 14; (**D**) SBP of DMM on day 14; (**E**) SBP of MSR on day 14; (**F**) SBP of HJ on day 14; (**G**) SBP of KGS on day 14.

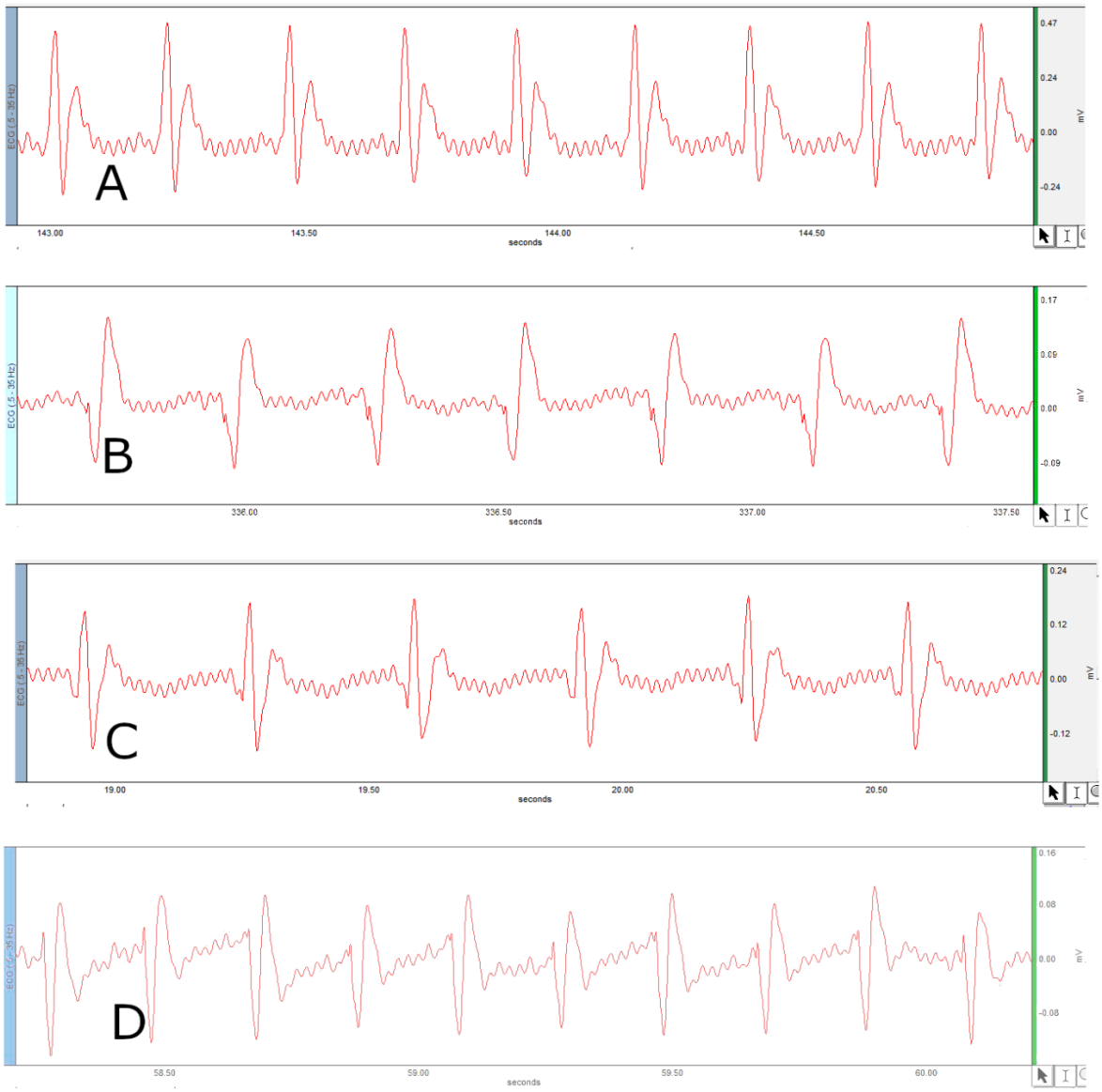

Figure 2. Represents RR-interval. (**A**) RR-interval of control on Day 0; (**B**) RR-interval on day 7 on treatment with L-NAME; (**C**) RR-interval of KGS on day 14; (**D**) RR-interval of DMM on day 14.

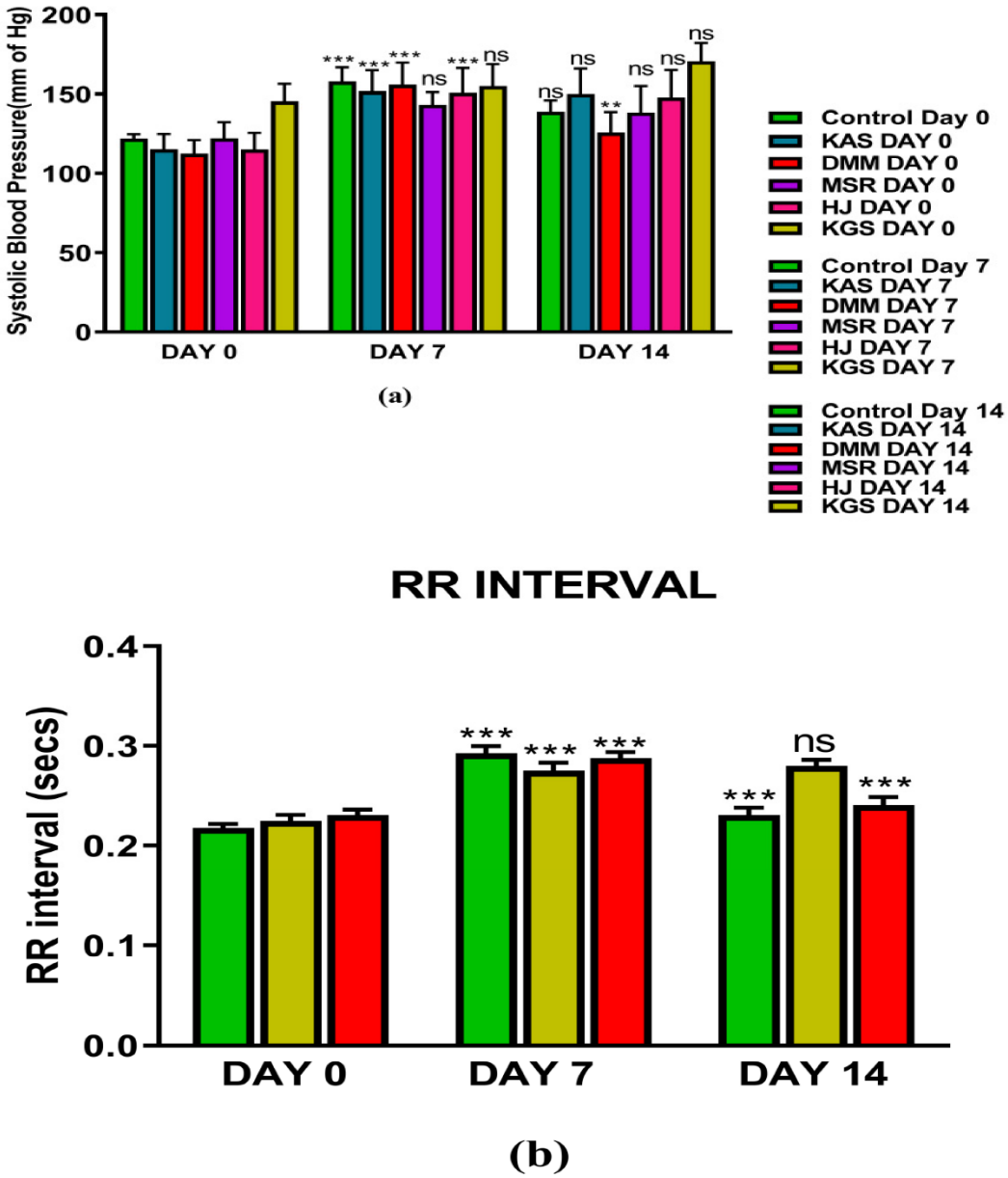

Figure 3. (**a**) Represents mean ± SD values of non-invasive systolic blood pressure of hypertensive control, KAS, DMM, MSR, HJ and KGS on day 0,7 and 14; (**b**) Represents RR-interval of DMM and KGS on day 0, 7 and 14. ** $p < 0.01$, *** $p < 0.001$, ns-non-significant. Day 0 vs. Day 7, and Day 7 vs. Day 14.

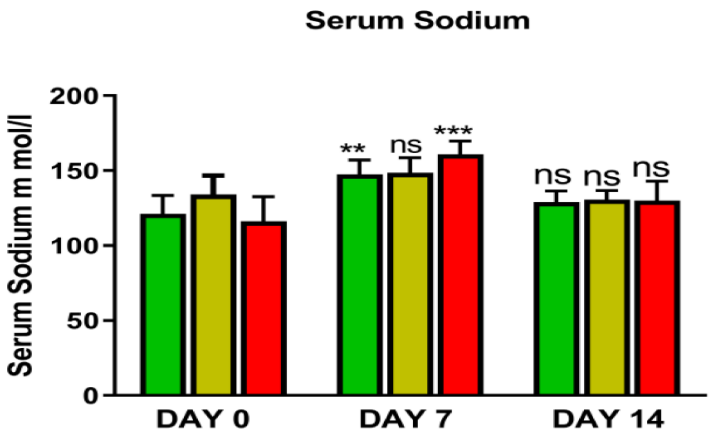

(a)

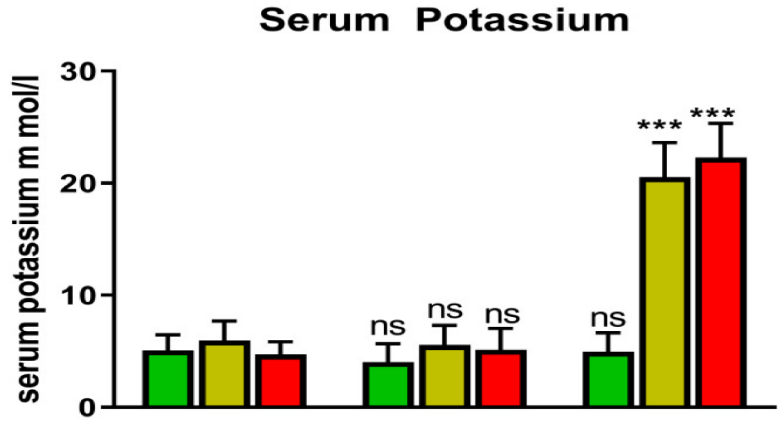

(b)

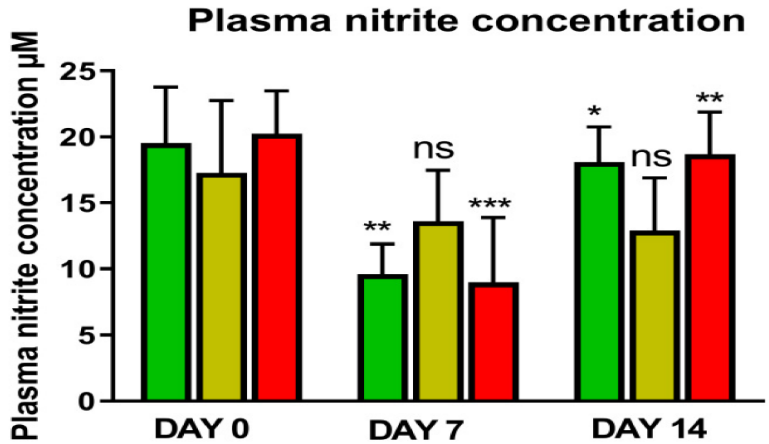

(c)

Figure 4. Represents (**a**) Plasma sodium; (**b**) Plasma potassium; (**c**) Plasma nitrite of control, KGS and DMM on day 0, 7 and 14. * $p < 0.05$, ** $p < 0.01$, *** $p < 0.001$, ns-non-significant. Day 0 vs. Day 7, and Day 7 vs. Day 14.

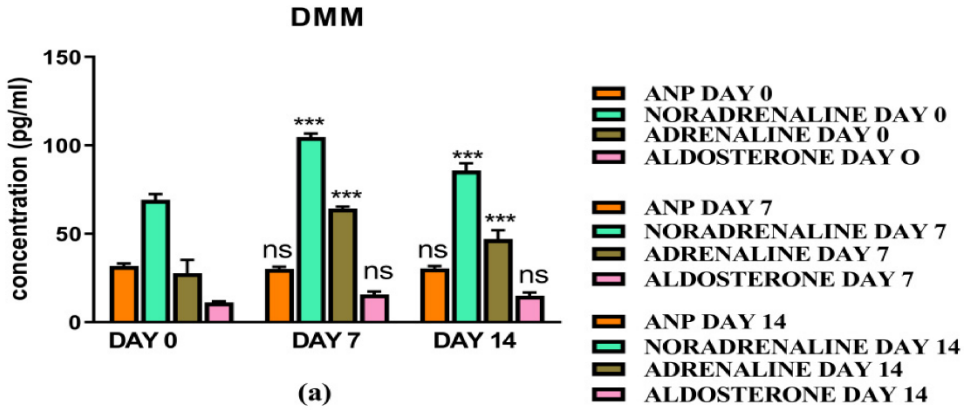

(a)

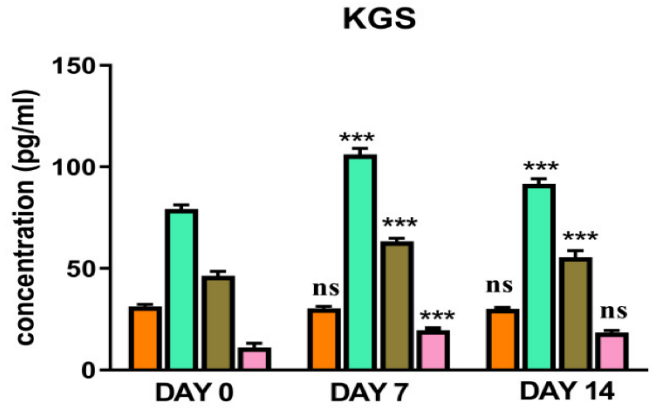

(b)

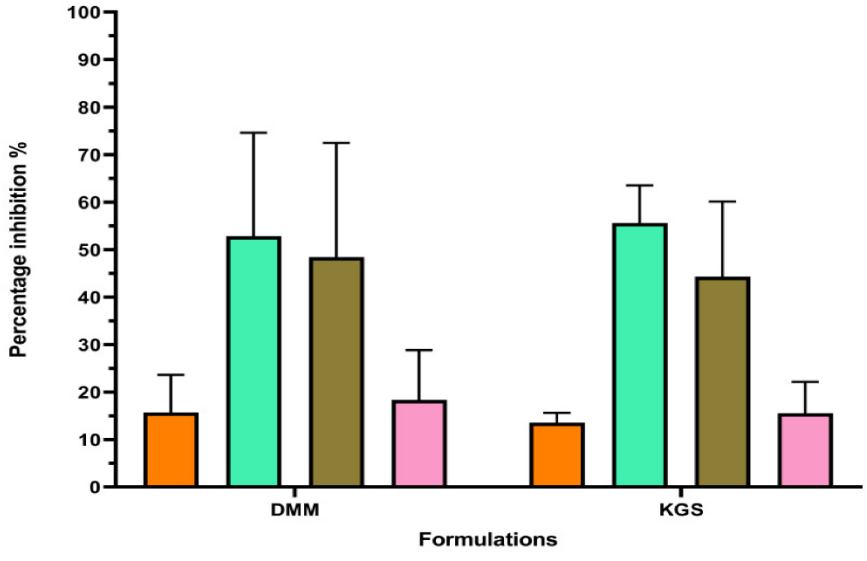

(c)

Figure 5. (**a**,**b**) Plasma concentration of ANP, noradrenaline, adrenaline and aldosterone on day 0, 7 and 14 in DMM- and KGS-treated rats; (**c**) % inhibition on day 14 as compared to day 7 by KGS and DMM. ns—non-significant, *** $p < 0.001$. Day 0 vs. Day 7, and Day 7 vs. Day 14.

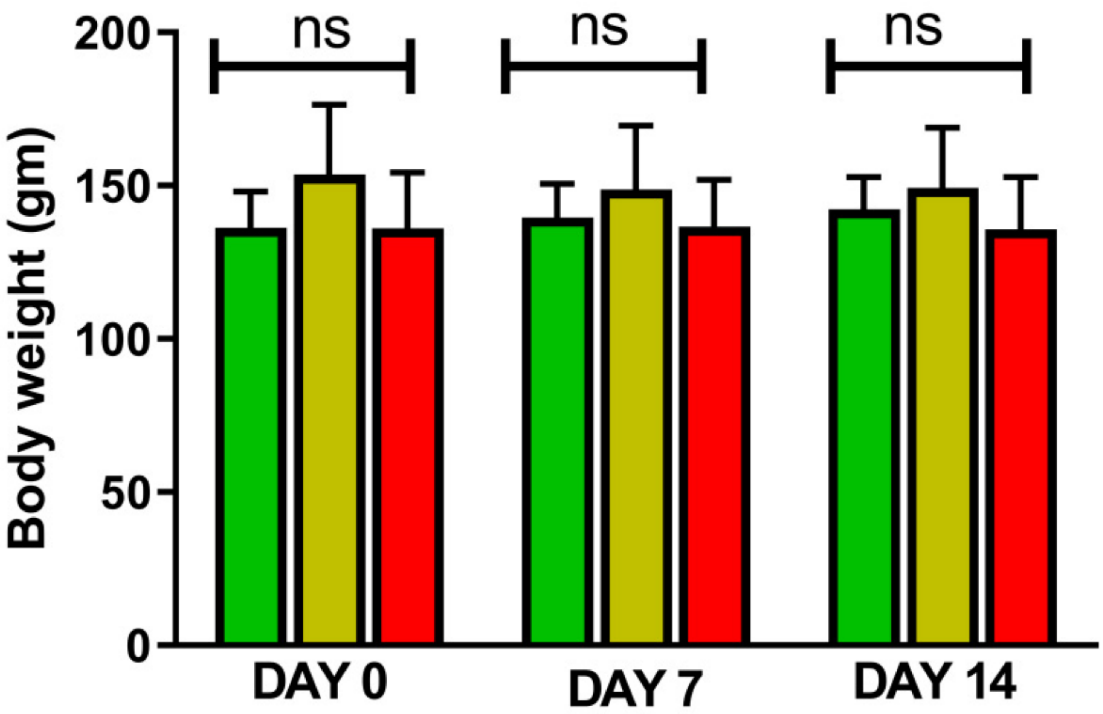

Figure 6. Represents mean ± SD of b.w. of rats on day 0,7 and 14. ns—non-significant. Day 0 vs. Day 7, and Day 7 vs. Day 14.

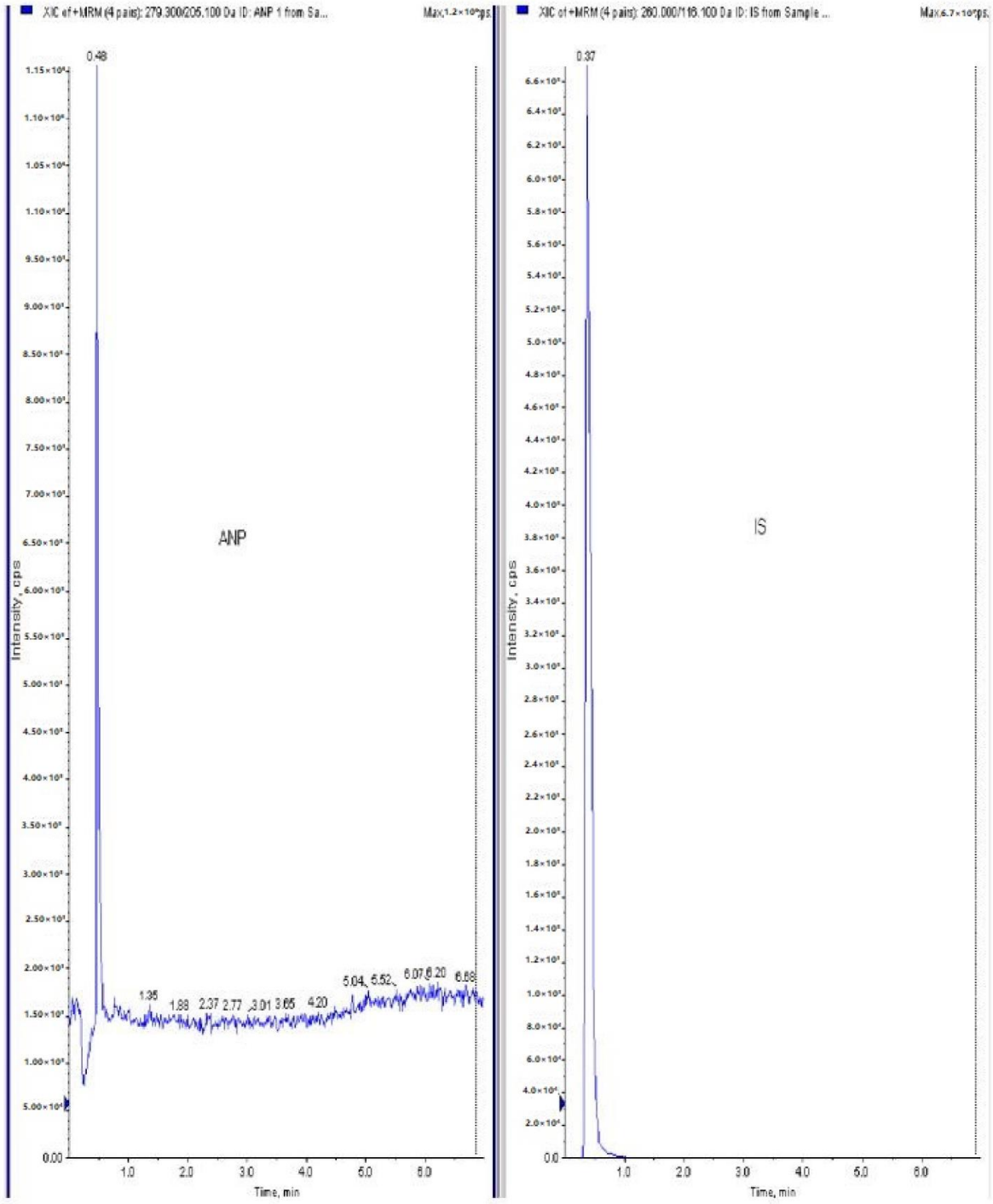

Figure 7. Raw data peaks obtained from LC-MS/MS quantitative measurements (MRM) of ANP using propranolol as internal standard (IS).

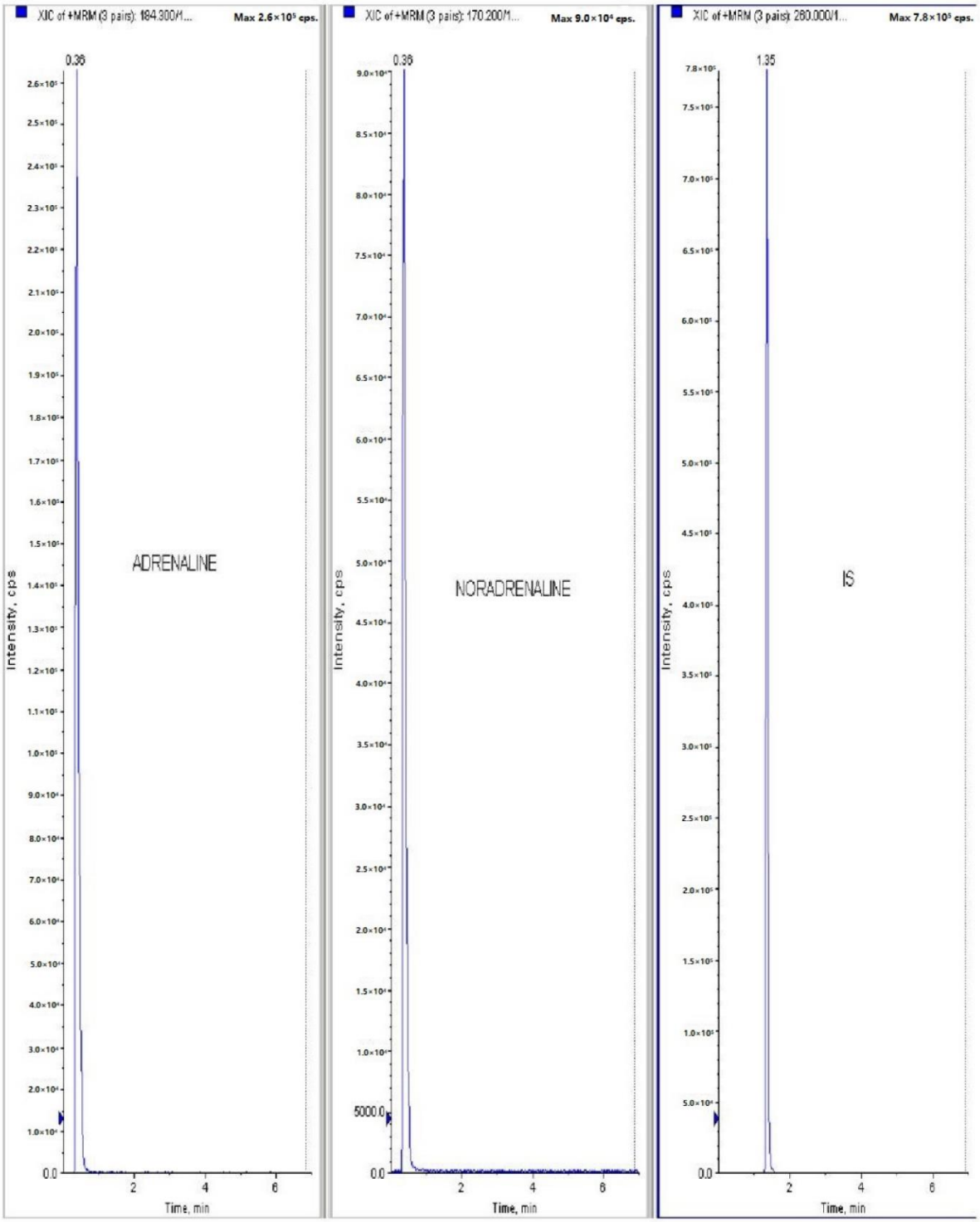

Figure 8. Raw data peaks obtained from LC-MS/MS quantitative measurements (MRM) of adrenaline and noradrenaline using propranolol as internal standard (IS).

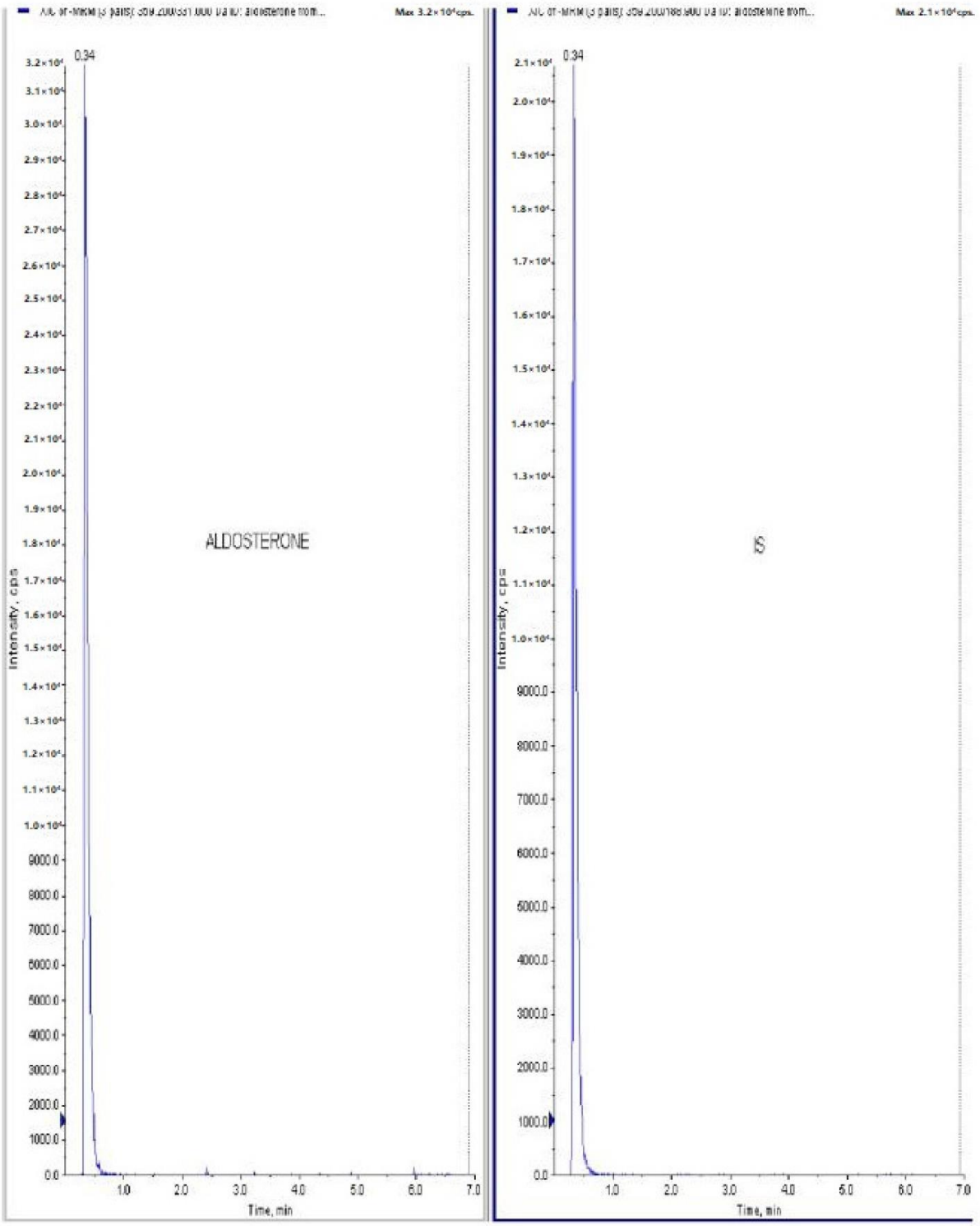

Figure 9. Raw data peaks obtained from LC-MS/MS quantitative measurements (MRM) of aldosterone using tolbutamide as internal standard (IS).

5. Discussion

Blood pressure is mainly modulated by cardiac output and total peripheral resistance (t.p.r). In this experiment, the systolic blood pressure of some of the selected unani formulations was measured against L-NAME-induced hypertension. L-NAME is a NOS (nitric oxide synthase)-inhibiting chemical moiety, which leads to NO (nitric oxide)-deficient artificial hypertension in experimental animals. However, the NOS distribution has been found in both the central and peripheral nervous system which modulates the cardiovascular functions through the autonomic system. NOS inhibition at the CNS level might also contribute to hypertension [16]. Apart from NO inhibition, other mechanisms through which L-NAME acts include SNS (sympathetic nervous system) activation, RAAS activation and oxidative stress. The adrenergic activation by L-NAME leads to the release of adrenaline and Noradrenaline, eventually exerting positive inotropic and chronotropic effect on the myocardium causing elevated blood pressure. It also acts by increasing Renin and Ang-II levels in the renal system, thereby augmenting plasma aldosterone and retaining Na+ and water [17].

The endothelium slowly releases a small amount of NO at baseline conditions, maintaining the constant vasodilation of the vascular smooth muscles [18]. The administration of L-NAME inhibits NOS, reducing the concentration of vasodilatory NO, causing vasoconstriction, eventually leading to an elevation in SBP. NO activates the soluble guanyl cyclase and this in turn causes the generation of cGMP. Nitric oxide oxidation leads to the production of nitrite found in the plasma [19]. It has been reported that bolus administration of L-NAME causes an increase in blood pressure with a concomitant decrease in heart rate or the lengthening of the RR-interval in ECG recordings [20]. The heart rate is reciprocally associated with the RR-interval (QRS-to-QRS interval) [21]. The presence of long RR-intervals may worsen CHD (coronary heart disease) and HF (heart failure), as well as elevating the SBP [22]. The recordings of the non-invasive SBP (Figure 1) and RR-interval (Figure 2) in this experiment on day 7 as compared to day 0 in all of the groups corroborate with the earlier reports of L-NAME administration [20].

5.1. Summary of Observation on Day 7

The SBP and RR-interval was found to increase significantly ($p < 0.05$) in all of the groups after 7 days of i.p. administration of L-NAME, except for the SBP of the MSR and KGS groups, which showed a non-significant increase.

5.1.1. DMM

Both the plasma adrenaline and noradrenaline increased after the L-NAME treatment on day 7 in the DMM group, which was consistent with previous scientific reports. The plasma potassium level did not sufficiently rise on the 7th day for the DMM group.

5.1.2. KGS

Both the plasma adrenaline and noradrenaline increased after the L-NAME treatment [17] on day 7 in the KGS group. The plasma potassium level did not sufficiently rise on the 7th day for the KGS group.

The concentration of noradrenaline was predominantly higher than adrenaline on day 7 in both of the groups, which might have contributed to the decreased HR or the lengthening of the RR- interval via β1 agonism. Through the dilation of the afferent arterioles and the constriction of the efferent arterioles, ANP increases the glomerular filtration rate (GFR) in the kidney. Further, at various regions of the nephron, ANP inhibits the salt and water reabsorption, while renin and the related plasma-aldosterone does the reverse [23]. Previous scientific reports suggest that the administration of L-NAME elevates plasma-ANP and induces its release through the enhancement of volume-load in conscious rats [24]. ANP is also released due to atrial stretch caused by the action of NA on α receptors or adrenaline on β receptors. On day 7, the L-NAME group showed a significant increase in NA, Adrenaline and SBP, while the ANP and aldosterone remained almost unaltered. A probable reason for this might be the insufficient stretching of the atrial walls to release ANP and a milder alteration of plasma Na+, as was evident in our Figure 4a, to trigger a significant increase in aldosterone. Unfortunately, we could not measure the atrial pressure or the parameters that give information about atrial stretch. It is interesting to mention that the literature also indicates that the plasma concentration of ANP is independent of the concentration of plasma adrenaline and noradrenaline [23].

5.2. Summary of Observations on Day 14

On day 14, the SBP of the animals treated with KAS, MSR and HJ showed a non-significant decrease.

5.2.1. DMM

The decrease in SBP was significant ($p < 0.05$) in the case of the DMM-treated rats. The RR-interval on day 14 significantly decreased in the DMM group. This change was conventional in the case of DMM, i.e., typical of an anti-hypertensive agent. The significant ($p < 0.05$) rise in the nitrite levels on day 14 indicate a different mechanism for DMM, exerting its vasodilatory effect by countering the L-NAME inhibition of NOS. The DMM also decreased plasma NA and adrenaline but showed an increased heart rate (shortening of the RR-interval) on day 14 (Figure 3b and Figure 5a). This can be explained by relating that an increase in the plasma catecholamines downregulates the adrenergic receptors, leading to diminished activity, according to some scientific reports [25]. It is probably that NA fails to achieve pharmacological action because of the higher concentration and the activity of adrenaline overshadows that of noradrenaline, leading to elevated HRs, a possible explanation for the increased HR produced by DMM on day 14 (Figure 3b). The plasma potassium levels were significantly elevated on the 14th day in the DMM-treated rats. Reports suggest that an increase in extracellular potassium is linked to the depolarization of smooth muscle cells, causing vasodilation [26]. The decrease in SBP and elevation of K+ on the 14th days can be extrapolated to our findings. However, the significant ($p < 0.05$) rise in the nitrite levels on day 14 (Figure 4c) indicate a different mechanism for the DMM, exerting its vasodilatory effect by countering the L-NAME inhibition of NOS. The DMM also decreased the plasma NA and adrenaline but showed increased heart rates (shortening of the RR-interval) on day 14 (Figure 5a). This can be explained by relating that an increased plasma catecholamine level downregulates the adrenergic receptors, leading to diminished activity, according to some scientific reports [25]. It is probably that NA fails to achieve pharmacological action because of the higher concentration, and because the activity of adrenaline overshadows that of noradrenaline, leading to elevated HRs, a possible explanation for an increased HR (shortening of the RR-interval) produced by DMM on day 14 (Figure 3b).

5.2.2. KGS

Unexpectedly, the KGS showed an enhancement in the SBP and RR-interval, in the KGS group, rather than decreasing on day 14, though not significantly. It is unclear why the RR and SBP increased non-significantly in the case of KGS. The observed decrease in the plasma concentration of adrenaline and noradrenaline from day 7 to day 14, following administration of the KGS appears to be similar to that of α2 agonist e.g., clonidine [27]. Strangely enough, the plasma nitrite did not increase on day 14, instead it decreased a bit in the case of KGS, which in another way supports the enhanced SBP in this group (Figure 4c). On the treatment of rats with KGS, on day 14, the noradrenaline and adrenaline decreased yet the concentration of noradrenaline was predominantly higher than adrenaline, which might explain a lower heart rate (increased RR-interval) (Figure 3b). Thus, it might be said that the KGS might not alter cardiac output (pharmacological action of noradrenaline) but may increase stroke volume and decrease the HR, indicating that it might exert a central sympathomimetic role. We do not have many reports to justify an elevated SBP and K+ in the KGS-treated rats on day 14 (Figure 3a and Figure 4b). So far, the convention is concerned that high plasma K+ indicates a smaller RR-interval which is expected to generate lower systolic blood pressure. In our study, we observed the reverse co-relationship between the RR-interval and K+. Therefore, it will be pertinent to mention in this context, one study claims an association of high plasma K+ accompanied by high blood pressure [28].

The plasma aldosterone did not change much from day 7 to day 14 in both the KGS- and DMM-treated rats. This is also quite evident from the non-significant slight decrease in Na+ level on day 14; such a small change may not be attributed to aldosterone. Thus, the KGS and DMM might not exploit the ANP and aldosterone balance and ultimately may not influence the Angiotensin-II release.

6. Conclusions

In our experiment, it is quite interesting to mention that KAS, MSR and HJ were unable to reduce the L-NAME-induced blood pressure, while DMM reduced the SBP. Perhaps, DMM acts through the inhibition of NOS as well as the adrenergic system. Our findings have also revealed a strange observation in the context of the way KGS acts, especially in elevating the SBP and K+ and slightly increasing the RR-interval. However, we have put forward a single previous report from the American Journal of Hypertension [28] which might help to

explain, at least in part, the observation in relation to KGS mentioned earlier. KGS has shown some of the remarkable pharmacological features similar to that of clonidine. This finding indicates that probably KGS acts as a central sympathomimetic agent. Thus, more detailed studies of KGS are needed to justify that the observed increase in SBP here maybe clinically correlated with its traditional use.

References

[1] Zhou, B.; Perel, P.; Mensah, G.A.; Ezzati, M. Global epidemiology, health burden and effective interventions for elevated blood pressure and hypertension. *Nat. Rev. Cardiol.* 2021, *18*, 785–802. [Google Scholar] [CrossRef] [PubMed]

[2] Zhou, X.; Seto, S.W.; Chang, D.; Kiat, H.; Razmovski-Naumovski, V.; Chan, K.; Bensoussan, A. Synergistic Effects of Chinese Herbal Medicine: A Comprehensive Review of Methodology and Current Research. *Front. Pharmacol.* **2016**, *7*, 201. [Google Scholar] [CrossRef] [PubMed] [Green Version]

[3] Yuan, H.; Ma, Q.; Ye, L.; Piao, G. The Traditional Medicine and Modern Medicine from Natural Products. *Molecules* **2016**, *21*, 559. [Google Scholar] [CrossRef] [PubMed] [Green Version]

[4] Ahmad, S.; Rehman, S.; Ahmad, A.M.; Siddiqui, K.M.; Shaukat, S.; Khan, M.S.; Kamal, Y.T.; Jahangir, T. Khamiras, a natural cardiac tonic: An overview. *J. Pharm. Bioallied Sci.* **2010**, *2*, 93–99. [Google Scholar] [CrossRef] [PubMed]

[5] Ministry of Health and Family Affairs. Part V. In *National Formulary of Unani Medicine (NFUM)*; Central Council for Research in Unani Medicine, Government of India, Ministry of Health and Family Welfare, Department of Health: New Delhi, India, 2006; pp. 76, 79, 110. [Google Scholar]

[6] Ministry of Health and Family Affairs. Part I. In *National Formulary of Unani Medicine (NFUM)*; Central Council for Research in Unani Medicine: New Delhi, India, 2006; pp. 19, 90. [Google Scholar]

[7] Ravishankar, B.; Shukla, V.J. Indian systems of medicine: A brief profile. *Afr. J. Tradit. Complement. Altern. Med.* **2007**, *3*, 319–337. [Google Scholar] [CrossRef] [Green Version]

[8] Gorain, B.; Choudhury, H.; Kundu, A.; Sarkar, L.; Karmakar, S.; Jaisankar, P.; Pal, T.K. Nanoemulsion strategy for olmesartan medoxomil improves oral absorption and extended antihypertensive activity in hypertensive rats. *Colloids Surf. B Biointerfaces* **2014**, *115*, 286–294. [Google Scholar] [CrossRef]

[9] Karmakar, S.; Padman, A.; Mane, N.S.; Sen, T. Hypokalemia: A potent risk for QTc prolongation in clarithromycin treated rats. *Eur. J. Pharmacol.* **2013**, *709*, 80–84. [Google Scholar] [CrossRef]

[10] Council of Europe; European Pharmacopoeia Commission; European Directorate for the Quality of Medicines & Healthcare. *European Pharmacopoeia*, 7th ed.; Council Of Europe: Strasbourg, Germany, 2010; p. 492. [Google Scholar]

[11] Maruna, R.F. Serum sodium determination; critical study on colorimetric determination and method. *Clin. Chim. Acta* **1957**, *2*, 581–585. [Google Scholar] [CrossRef]

[12] Trinder, P. Determination of serum sodium. *Analyst* **1951**, *76*, 596. [Google Scholar] [CrossRef]

[13] Suderman, H.J.; Delory, G.E. A rapid method for the determination of sodium in serum. *Can. J. Med. Sci.* **1952**, *30*, 302–307. [Google Scholar] [CrossRef]

[14] Lee, A.Y.; Choi, J.W.; Yokozawa, T.; Cho, E.J. Preventive effect of oligonol on nitric oxide and reactive oxygen species production through regulation of nuclear factor kappa B signaling pathway in RAW 264.7 macrophage cells against sodium nitroprusside. *RSC Adv.* **2019**, *9*, 3987–3993. [Google Scholar] [CrossRef] [PubMed] [Green Version]

[15] Shishkova, E.; Coon, J.J. Rapid preparation of human blood plasma for bottom-up proteomics analysis. *STAR Protoc.* **2021**, *2*, 100856. [Google Scholar] [CrossRef] [PubMed]

[16] Pechanova, O.; Vrankova, S.; Cebova, M. Chronic L-Name-Treatment Produces Hypertension by Different Mechanisms in Peripheral Tissues and Brain: Role of Central eNOS. *Pathophysiology* **2020**, *27*, 46–54. [Google Scholar] [CrossRef] [PubMed]

[17] Kvetnanský, R.; Pacák, K.; Tokarev, D.; Jeloková, J.; Jezová, D.; Rusnák, M. Chronic blockade of nitric oxide synthesis elevates plasma levels of catecholamines and their metabolites at rest and during stress in rats. *Neurochem. Res.* **1997**, *22*, 995–1001. [Google Scholar] [CrossRef] [PubMed]

[18] Hildebrand, S.; Ibrahim, M.; Schlitzer, A.; Maegdefessel, L.; Röll, W.; Pfeifer, A. PDGF regulates guanylate cyclase expression and cGMP signaling in vascular smooth muscle. *Commun. Biol.* **2022**, *5*, 298. [Google Scholar] [CrossRef] [PubMed]

[19] Chowdhary, S.; Ng, G.A.; Nuttall, S.L.; Coote, J.H.; Ross, H.F.; Townend, J.N. Nitric oxide and cardiac parasympathetic control in human heart failure. *Clin. Sci.* **2002**, *102*, 397–402. [Google Scholar] [CrossRef]

[20] Sung, J.H.; Jo, Y.S.; Kim, S.J.; Ryu, J.S.; Kim, M.C.; Ko, H.J.; Sim, S.S. Effect of Lutein on L-NAME-Induced Hypertensive Rats. *Korean J. Physiol. Pharmacol.* **2013**, *17*, 339–345. [Google Scholar] [CrossRef] [Green Version]

[21] Stauss, H.M. Heart rate variability: Just a surrogate for mean heart rate? *Hypertension* **2014**, *64*, 1184–1186. [Google Scholar] [CrossRef] [Green Version]

[22] Xu, H.; Li, J.; Zhong, G.; Li, L.; Huang, C.; Guo, P.; Chen, Y.; He, T. Characteristics of the Dynamic Electrocardiogram in the Elderly with Nonvalvular Atrial Fibrillation Combined with Long R-R Intervals. *Evid. Based Complement. Alternat. Med.* **2021**, *2021*, 4485618. [Google Scholar] [CrossRef]

[23] Ganguly, A. Atrial natriuretic peptide-induced inhibition of aldosterone secretion: A quest for mediator(s). *Am. J. Physiol.* **1992**, *263 Pt 1*, E181–E194. [Google Scholar] [CrossRef]

[24] Leskinen, H.; Vuolteenaho, O.; Leppäluoto, J.; Ruskoaho, H. Role of nitric oxide on cardiac hormone secretion: Effect of NG-nitro-L-arginine methyl ester on atrial natriuretic peptide and brain natriuretic peptide release. *Endocrinology* **1995**, *136*, 1241–1249. [Google Scholar] [CrossRef] [PubMed]

[25] Kotchen, T.A. Hypertensive vascular disease. In *Harrison's Principles of Internal Medicine*, 17th ed.; Tinsley, R.H., Anthony, S.F., Eds.; McGraw-Hill: New York, NY, USA, 1998; Volume 2, p. 1549, ISBN-10 1259834808. [Google Scholar]

[26] Martinez, D.V.; Rocha, R.; Matsumura, M.; Oestreicher, E.; Ochoa-Maya, M.; Roubsanthisuk, W.; Williams, G.H.; Adler, G.K. Cardiac damage prevention by eplerenone: Comparison with low sodium diet or potassium loading. *Hypertension* **2002**, *39*, 614–618. [Google Scholar] [CrossRef] [PubMed]

[27] *Essentials of Medical Pharmacology*; Tripathi, K.D. (Ed.) Jaypee Brothers Medical: New Delhi, India, 2013; ISBN 13 978-9350259375. [Google Scholar]

[28] Walsh, C.R.; Larson, M.G.; Vasan, R.S.; Levy, D. Serum potassium is not associated with blood pressure tracking in the Framingham Heart Study. *Am. J. Hypertens.* **2002**, *15 Pt 1*, 130–136. [Google Scholar] [CrossRef] [Green Version]

CHAPTER IV

LC-MS/MS METHOD DEVELOPMENT AND METHOD VALIDATION FOR THE ESTIMATION OF ADRENALINE, NORADRENALINE, ALDOSTERONE, AND ATRIAL NATRIURETIC PEPTIDE IN RAT PLASMA

1. Introduction:

Measuring the catecholamines adrenaline and noradrenaline in biological samples is particularly challenging due to their low concentrations and chemical instability. These compounds are highly sensitive to light and elevated pH, making them susceptible to spontaneous oxidation. Consequently, their analysis demands highly selective and sensitive bioanalytical techniques with stringent precautions to prevent analyte degradation [1-5].

Aldosterone is a challenging analyte to measure due to its low concentrations and the potential interference caused by metabolites in immunoassay techniques, especially in cases of renal dysfunction. Such analytical limitations can result in significant variability, with aldosterone immunoassays yielding up to two-fold differences in identical sample results. The use of LC-MS/MS provides a solution to these challenges by offering enhanced specificity [6-7]

Traditionally, the reference method for measuring serum aldosterone involved gas chromatography coupled with mass spectrometry after chemical derivatization. However, advancements in high-sensitivity triple quadrupole mass spectrometers have enabled the development of LC-MS/MS methods that eliminate the need for derivatization. Various sample preparation techniques have been employed, including protein precipitation followed by either online or offline solid-phase extraction (SPE), liquid–liquid extraction (LLE), and, more recently, supported liquid extraction (SLE). Notably, SLE methods present a significant advantage over LLE (Liquid liquid extraction) by requiring approximately half the initial sample volume to achieve comparable signal intensity [8-15]. Cyclic peptides are polypeptides arranged in a ring structure, stabilized by durable bonds such as disulfide linkages. The natriuretic peptide (NP) family, for example, consists of genetically distinct cyclic peptides with a characteristic amino acid ring formed by disulfide bonds. This unique configuration enhances their structural stability and conformational rigidity, resulting in greater biological activity compared to linear peptides. These properties make cyclic peptides valuable therapeutic candidates and effective agents for managing cardiovascular diseases [16]. One such cyclic peptide of importance is atrial natriuretic peptide, released from the cardiac atria as a result of stretching due to stress. A robust analytical method was developed and validated for quantifying Adrenaline, Noradrenaline, Aldosterone and Atrial Natriuretic peptide (ANP) in rat plasma using LC-ESI-MS/MS, using appropriate internal standard (IS). The method aimed to ensure high sensitivity and reproducibility.

2.0.Method Development of Adrenaline and Noradrenaline in rat Plasma Using LC-ESI-MS/MS (API-4000 QTRAP)

2.1. Chromatographic Conditions:

The separation was performed on a Phenomenex Kinetex 5µ C18 100A column (50 × 3 mm), utilizing a Shimadzu LC system with binary flow. The mobile phase comprised two components: (A) 0.1% formic acid in Milli-Q water with 10 mM ammonium acetate and (B) 0.1% formic acid in acetonitrile. A gradient flow was employed, starting with 15% B from 0.01 to 2 mins, then 85% B from 2.50 to 3.50 mins, and returning to 15% B from 4.0 mins to 6.50 mins. The total flow rate was set to 0.5 mL/min, with a sample injection volume of 10 µL. The column was maintained at ambient temperature.

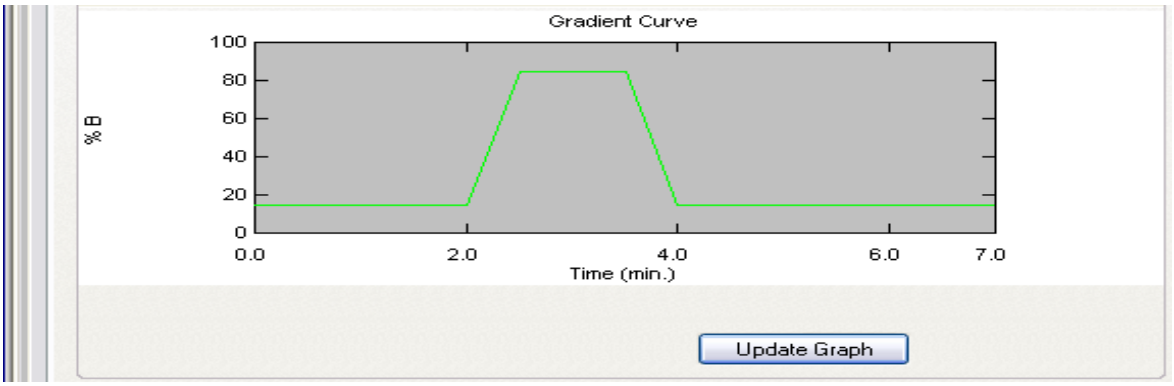

Figure 1: Gradient Curve Adrenaline and Noradrenaline

2.2.Sample Preparation:

Rat plasma (100 µL) was collected in tubes containing a protease inhibitor cocktail. The plasma was acidified with 10 µL of 2% formic acid and vortexed for 5 minutes, followed by dilution with 300 µL of 0.05 M ammonium acetate (pH 6.0). Solid-phase extraction (SPE) was employed to isolate the analytes, using SPE (Solid Phase Extraction) cartridges preconditioned with methanol and water. The loaded samples were washed with ammonium acetate solution and methanol to eliminate interferences. Elution of adrenaline and noradrenaline was achieved using 500 µL of methanol: ammonium hydroxide (95:5 v/v). The eluate was dried under nitrogen at 40°C and reconstituted in 200 µL of acetonitrile: water (50:50). A 10 µL aliquot was injected into the LC-MS/MS system.

2.3. Buffer solution preparation:

2.4. Preparation of 0.2M Phosphate buffer solution p^H 7.5

Dissolve 27.22gm of potassium dihydrogen phosphate in 930ml of water, adjust to p^H 7.5 with 300gm/l solution of potassium hydroxide and dilute to 1000ml with water.

2.5.Preparation of 0.05M Ammonium acetate solution p^H 6.0

Dissolve 3.854 g of ammonium acetate in 950 ml of deionized water. Adjust to pH 6.0 with acetic acid (AR Grade). Make up to 1lit. with deionized water and mix thoroughly.

2.6.Preparation of mixture of methanol and ammonium hydroxide (95:5 v/v)

5 ml of ammonium hydroxide (28%) was added to 95 ml methanol. Mixed thoroughly.

2.7. Mass Spectrometric Conditions:

Detection was conducted on an API 4000 QTRAP mass spectrometer (AB Sciex), utilizing an electrospray ionization (ESI) source in positive ion mode. Multiple reaction monitoring (MRM) transitions were used for quantification: adrenaline (Q1 184.3 m/z, Q3 166.1 m/z), noradrenaline (Q1 170.2 m/z, Q3 152.0 m/z), and propranolol (Q1 260.0 m/z, Q3 116.1 m/z). Key parameters included a source temperature of 400°C, ion spray voltage of 5500 V, and curtain gas at 20 psi.

Table 1: LC-MS/MS parameters for the estimation of Adrenaline and Noradrenaline

Adrenaline	**Q1 Mass (Da)**	**Q3 Mass (Da)**	**Dwell(msec)**	**Parameter**	**Start**
	184.3	166.1	200.00	DP	40.0
				CE	18.0
				CXP	15.0
Noradrenaline	**Q1 Mass (Da)**	**Q3 Mass (Da)**	**Dwell(msec)**	**Parameter**	**Start**
	170.2	152.0	200.00	DP	20.0
				CE	11.0
				CXP	15.0
Propranolol (IS)	**Q1 Mass (Da)**	**Q3 Mass (Da)**	**Dwell(msec)**	**Parameter**	**Start**
	260.0	116.1	200.00	DP	20.0
				CE	26.0
				CXP	15.0

2.8. Calibration and Quality Control:

Calibration curves were established over a range of 15.63 to 1000 pg/mL for both analytes, with quality control (QC) samples at LLOQ, LQC, MQC, and HQC levels. Linear regression demonstrated excellent correlation ($r^2 > 0.99$) for both adrenaline and noradrenaline, ensuring reliable quantitation.

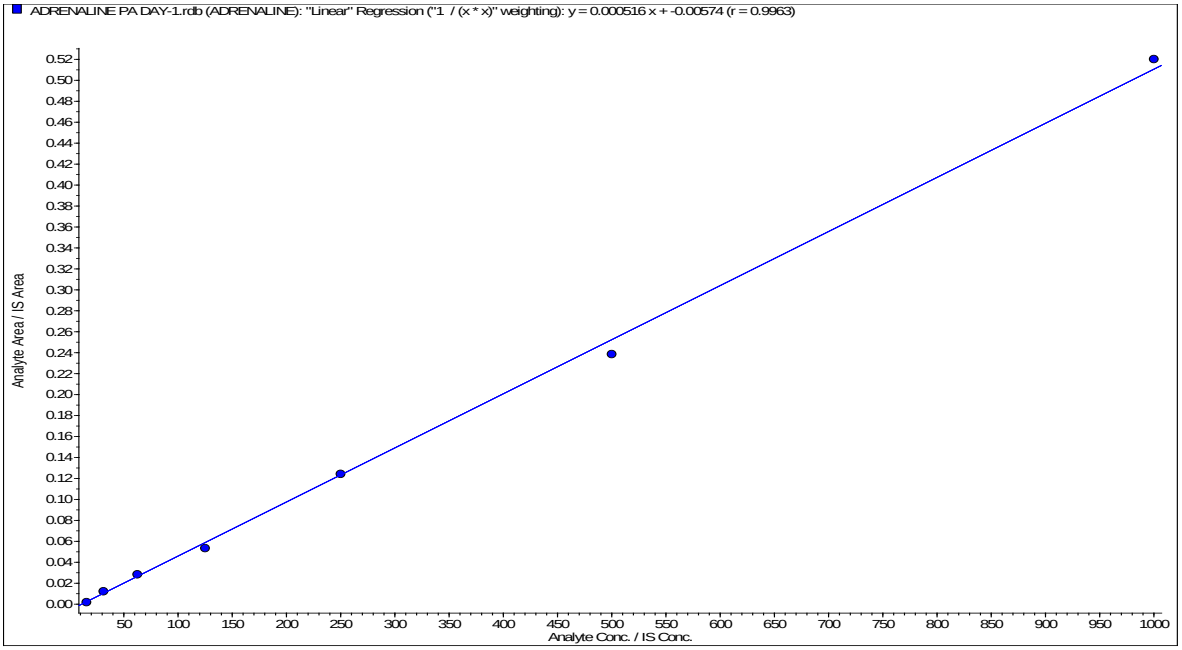

Figure 2: Calibration Curve of Adrenaline

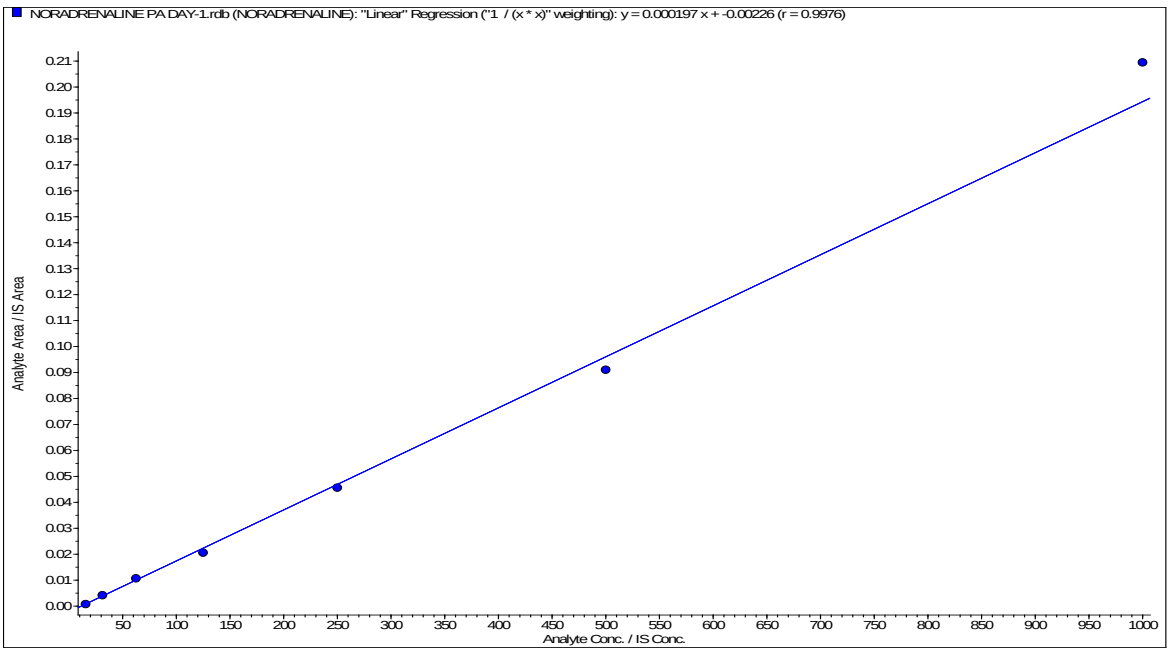

Figure 3: Calibration Curve of Noradrenaline

2.9.Plasma Calibration Standards (pg/ml):

Adrenaline: 15.63, 31.25, 62.50, 125.00, 250.00, 500.00, 1000.00
Noradrenaline: 15.63, 31.25, 62.50, 125.00, 250.00, 500.00, 1000.00

Table 2: QC points of Adrenaline and Noradrenaline

QC parameters	Adrenaline (pg/ml)	Noradrenaline (pg/ml)
LLOQ	15.63 pg ml	15.63 pg/ml
LQC	46.88 pg/ml	46.88 pg/ml
MQC	375.00 pg/ml	375.00 pg/ml
HQC	750.00 pg/ml	750.00 pg/ml

This method demonstrated exceptional precision, accuracy, and sensitivity, making it suitable for the biomarker studies of adrenaline and noradrenaline in biological matrices.

2.10. Method Validation of Noradrenaline

The method validation for the quantification of noradrenaline by LC-MS/MS was conducted following standard guidelines. The lower limit of quantification (LLOQ) was established at 15.63 pg/mL, with a limit of detection (LOD) of 4.1 pg/mL, meeting the acceptance criteria of 85–115% for accuracy and precision. Calibration curves were generated using seven concentration levels (15.63 to 1000 pg/mL), showing excellent linearity with mean R^2 values of 0.9963 and a coefficient of variation (CV) of 1.86% for the slope. The accuracy of the nominal concentrations ranged between 94.67% and 111.18%, demonstrating reliability across the calibration range.

The within- and between-run precision and accuracy were evaluated using quality control (QC) samples at LLOQ, low (LQC), medium (MQC), and high (HQC) concentrations. The precision, expressed as CV%, was consistently below 6% for all QC levels, while the accuracy was within the predefined acceptance criteria, with absolute biases ranging from 93.86% to 110.14%. The stability of noradrenaline under various conditions, including freeze-thaw, short-term, and long-term storage, was assessed. The results confirmed the analyte's stability with recovery rates ranging between 91.05% and 104.08%, adhering to the acceptance range of 85–115%.

Matrix effect evaluation showed minimal interference, with matrix factor values ranging between 0.88 and 0.99 across QC levels. The recovery rates for noradrenaline were consistent across LQC, MQC, and HQC levels, falling within 80–120%, ensuring the

method's robustness and reproducibility. These results affirm that the developed LC-MS/MS method is sensitive, precise, accurate, and stable for the determination of noradrenaline in biological matrices.

Table 3: Represents LLOQ and LOD of Noradrenaline with acceptance criteria of 85-115%

Noradrenaline	LLOQ	15.63	pg/ml
	LOD	4.1	pg/ml

Table 4: Represents Linearity data of Noradrenaline

Calibration concentration(pg/ml)	15.63	31.25	62.5	125	250	500	1000
Linearity 1	15.25	32.66	65.73	116.06	243.39	474.45	1076.69
Linearity 2	14.69	36.04	59.37	124.22	242.23	470.12	1054.25
Linearity 3	14.82	35.53	58.35	128.5	237.38	475.52	1052.28
Mean	14.92	34.74	61.15	122.93	241.00	473.36	1061.07
s.d.	0.29	1.82	4.00	6.32	3.19	2.86	13.56
c.v.	1.96	5.24	6.54	5.14	1.32	060.	1.28
nominal	95.46	111.18	97.84	98.34	96.40	94.67	106.11

Table 5: Represents the data associated with the calibration curve equation of Noradrenaline

	Slope(M)	Intersept-C	R square
Lin 1	0.00020	-0.00226	0.9976
Lin 2	0.00020	-0.00253	0.9954
Lin 3	0.00019	-0.00238	0.9958
MEAN	0.00019		0.9963
S.D.	0.000004		0.0012
C.V.%	1.86		0.12

Table 6: Represents the data for interday precision

	LLOQ	LQC	MQC	HQC
QC (pg/ml)	15.63	46.88	375	750
LIN 1	16.23	53.56	334.77	737.74
LIN 1	17.78	53.21	345.94	711.86
LIN 1	17.59	50.59	368.63	827.20
LIN 1	17.07	52.36	341.04	790.13
LIN 1	17.93	52.23	362.53	800.77
LIN 2	15.81	51.13	345.71	735.94
LIN 2	16.68	52.05	370.01	768.01
LIN 2	15.38	50.00	374.77	750.49
LIN 2	15.50	52.52	328.43	742.53
LIN 2	17.20	51.99	340.94	707.07

	LLOQ	LQC	MQC	HQC
LIN 3	17.35	52.02	352.35	707.20
LIN 3	17.40	49.92	340.24	768.78
LIN 3	17.47	50.13	354.73	778.64
LIN 3	16.90	52.16	354.21	775.42
LIN 3	16.93	50.62	392.88	785.72
Mean	16.88	51.63	353.81	759.17
S.D.	0.81	1.16	17.27	35.70
C.V.%	4.79	2.25	4.88	4.70
Absolute percent bias (%)	108.01	110.14	94.35	101.22

Table 7: Represents data for intraday precision

	LLOQ	LQC	MQC	HQC
QC (pg/ml)	15.63	46.88	375	750
	15.81	51.13	345.71	735.94
	16.68	52.05	370.01	768.01
	15.38	50.00	374.77	750.49
	15.50	52.52	328.43	742.53
	17.20	51.99	340.94	707.07
Mean	16.11	51.54	351.97	740.81
SD	0.79	1.00	19.75	22.35
CV	4.91	1.93	5.61	3.02
Absolute percent bias (%)	103.10	109.94	93.86	98.77

Table 8: Stability data of Noradrenaline After 3 Feeze Thaw Cycle with acceptance criteria of 85-115%

	Freeze Thaw Stability		Acceptance Criteria	Freeze Thaw	85-115%
LQC	MQC	HQC			
46.88	375	750	46.88	375	750
52.02	352.35	707.20	52.24	344.46	795.86
49.92	340.24	768.78	53.86	377.09	746.5
50.13	354.73	778.64	53.4	334.9	781.65
52.16	354.21	775.42	46.73	391.32	789.92
50.62	392.88	785.72	41.70	419.89	683.28
50.97	358.88	763.15	49.59	373.53	759.44
% Freeze thaw Stability			97.28	104.08	99.51

Table 9: Short term stability data obtained after 24 hrs with an acceptance criteria of 90-110%

	SHORT TERM STABILITY		ACCEPTANCE CRITERIA	SHORT TERM	90-110%
	Before 24hrs		After 24hrs		
46.88 (LQC)	375 (MQC)	750 (HQC)	46.88 (LQC)	375 (MQC)	750 (HQC)
52.02	352.35	707.20	45.1	387.77	750.86
49.92	340.24	768.78	46.47	308.13	743.58
50.13	354.73	778.64	52.88	310.01	703.67
52.16	354.21	775.42	46.51	313.25	752.08
50.62	392.88	785.72	49.3	387.99	732.01
50.97	358.88	763.15	48.05	341.43	736.44
Short term stability			94.28	95.14	96.50

Table 10: Long term stability of the analyte with an acceptance criteria of 90-110%

	LONG TERM STABILITY		ACCEPTANCE CRITERIA	LONG TERM	90-110%
46.88 (LQC)	375 (MQC)	750 (HQC)	46.88 (LQC)	375 (MQC)	750 (HQC)
52.02	352.35	707.20	49.87	333.12	755.11
49.92	340.24	768.78	42.01	349.5	742.86
50.13	354.73	778.64	49.44	330.05	745.44
52.16	354.21	775.42	45.32	365.94	760.92
50.62	392.88	785.72	45.39	333.83	731.4
50.97	358.88	763.15	46.41	342.49	747.15
Long term stability			91.05	95.43	97.90

Table 11: Matrix effect of IS with an acceptance criteria of 85-115%

Matrix Effect of IS	EXTRACTED PLASMA	AQUEOUS	% OF ME-OH	MATRIX FACTOR
SAMPLE				
LQC1	3333822.77	3481809.83	95.75	0.96
LQC2	3269190.75	3437768.49	95.10	0.95
LQC3	3229682.08	3303035.54	97.78	0.98
LQC4	3261091.84	3450567.86	94.51	0.95
LQC5	3337816.42	3410485.09	97.87	0.98

Matrix Effect of IS	EXTRACTED PLASMA	AQUEOUS	% OF ME-OH	MATRIX FACTOR
Mean	3286320.77	3416733.36	96.20	0.96
S.D.	47555.55	68535.45	1.55	0.02
C.V.%	1.45	2.01	1.61	1.61
MQC1	2878662.31	3282703.61	87.69	0.88
MQC2	3620937.46	3768564.41	96.08	0.96
MQC3	2826648.56	2923486.52	96.69	0.97
MQC4	3562518.74	3660070.63	97.33	0.99
MQC5	2961208.38	3112949.04	95.13	0.95
Mean	3169995.09	3349554.84	94.58	0.95
S.D.	388515.56	358460.14	3.94	0.04
C.V.%	12.26	10.70	4.16	4.51
HQC1	2851262.83	2904496.17	98.17	0.98
HQC2	3006162.33	3100040.68	96.97	0.97
HQC3	2969523.07	3177605.99	93.45	0.93
HQC4	2931869.41	3003949.26	97.60	0.98
HQC5	2331086.68	2584592.94	90.19	0.90
Mean	2817980.86	2954137.01	95.28	0.95
S.D.	278173.30	230615.78	3.38	0.03
C.V.%	9.87	7.81	3.55	3.55

Table 12: Matrix effect of the analyte

MATRIX EFFECT ANALYTE	EXTRACTED BL PLASMA	AQUEOUS	% OF ME	MATRIX FACTOR
SAMPLE				
LQC1	23435.39	23696.65	98.90	0.99
LQC2	23538.69	24693.73	95.32	0.95
LQC3	21389.61	23871.41	89.60	0.90
LQC4	22462.01	25090.81	89.52	0.90
LQC5	21588.82	22251.50	97.02	0.97
Mean	22482.90	23920.82	94.07	0.94
S.D.	1002.13	1096.08	4.31	0.04
C.V.%	4.46	4.58	4.58	4.58
MQC1	130149.67	131912.88	98.66	0.99
MQC2	127946.67	134276.04	95.29	0.95
MQC3	130697.18	133974.99	97.55	0.98
MQC4	123939.35	131286.29	94.40	0.94

MATRIX EFFECT ANALYTE	EXTRACTED BL PLASMA	AQUEOUS	% OF ME	MATRIX FACTOR
MQC5	129057.23	130032.95	99.25	0.99
Mean	128358.02	132296.63	97.03	0.97
S.D.	2686.28	1804.66	2.11	0.02
C.V.%	2.09	1.36	2.17	2.17
HQC1	381798.29	403682.51	94.58	0.95
HQC2	371978.19	396315.01	93.86	0.94
HQC3	386566.62	394389.10	98.02	0.98
HQC4	381617.66	389027.16	98.10	0.98
HQC5	387704.69	396303.72	97.83	0.98
Mean	381933.09	395943.50	96.48	0.96
S.D.	6204.81	5253.86	2.08	0.02
C.V.%	1.62	1.33	2.15	2.15

Table 13: Recovery of Analyte area with acceptance criteria of 80-120%

Dilluent Sample			Plasma sample		
LQC	MQC	HQC	LQC	MQC	HQC
23696.65	131912.88	403682.51	22449.30	121133.69	379136.96
24693.73	134276.04	396315.01	24289.48	122334.61	401341.53
23871.41	133974.99	394389.10	23247.19	122291.58	396911.66
25090.81	131286.29	389027.16	22304.22	123099.59	384158.32
22251.50	130032.95	396303.72	24081.68	121282.24	392059.86
23920.82	132296.63	395943.50	23274.37	122028.34	390721.67
% Recovery			97.30	92.24	98.68

Table 14: Bench Top Stability data after 24 hrs with acceptance criteria 90-110%

BENCH TOP STABILITY					
			After 24 Hours		
46.88 (LQC)	375 (MQC)	750 (HQC)	46.88 (LQC)	375 (MQC)	750 (HQC)
52.02	352.35	707.20	48.60	317.46	725.88
49.92	340.24	768.78	51.61	307.02	759.32
50.13	354.73	778.64	42.57	351.15	734.64
52.16	354.21	775.42	43.98	350.12	783.97
50.62	392.88	785.72	49.46	307.73	738.23
50.97	358.88	763.15	47.24	326.70	748.41
% Stability			92.69	91.03	98.07

Table 15: Recovery of IS with acceptance criteria of 80-120%

RECOVERY IS AREA					
Dilluent Sample			Plasma sample		
LQC	MQC	HQC	LQC	MQC	HQC
3481809.83	3282703.61	2904496.17	2833647.06	3347530.96	2673675.17
3437768.49	3768564.41	3100040.68	2869602.84	2945662.04	2701155.38
3303035.54	2923486.52	3177605.99	3582675.67	2861221.71	2410168.59
3450567.86	3660070.63	3003949.26	2795357.65	2912750.64	2492584.68
3410485.09	3112949.04	2584592.94	3295457.84	2969772.41	2698231.99
3416733.36	3349554.84	2954137.01	3075348.21	3007387.55	2595163.16
% Recovery			90.01	89.78	87.85

Table 16: Autosampler stability after 24 hrs with acceptance of 85-115%

			After 24 hr		
46.88	375	750	46.88	375	750
52.02	352.35	707.20	48.33	314.3	730.32
49.92	340.24	768.78	50.55	392.28	737.17
50.13	354.73	778.64	44.83	316.99	778.59
52.16	354.21	775.42	45.11	318.14	770.84
50.62	392.88	785.72	48.22	393.88	740.11
50.97	358.88	763.15	47.41	347.12	751.41
% Stability			93.01	96.72	98.46

2.11. Method Validation of Adrenaline

The bioanalytical method for adrenaline was validated using an LC-MS/MS system. The method demonstrated a lower limit of quantification (LLOQ) of 15.63 pg/mL and a limit of detection (LOD) of 3.91 pg/mL. The linearity of the method was confirmed across a concentration range of 15.63 to 1000 pg/mL, with a mean slope of 0.00051 and an R^2 value of 0.9950, meeting acceptance criteria of 85–115%. Within-run (intraday) and between-run (interday) precision and accuracy were evaluated for LLOQ, low-quality control (LQC), medium-quality control (MQC), and high-quality control (HQC) samples. The coefficients of variation (CV%) were below 5%, and absolute bias ranged from 92.82% to 113.04%, aligning with the acceptance criteria. Stability studies revealed robust freeze-thaw, short-term, and long-term stability, with percentage recoveries and biases well within acceptance criteria (85–115% for freeze-thaw and 90–110% for short- and long-term stability). The freeze-thaw stability after three cycles demonstrated stability with percent values of

102.80%, 103.21%, and 97.04% for LQC, MQC, and HQC, respectively. Short-term stability after 24 hours showed values of 99.30%, 94.05%, and 106.42%. Long-term stability results further confirmed method reliability with recovery values of 96.57%, 96.20%, and 103.77%. Matrix effects and recovery were also assessed, demonstrating minimal interference with an overall matrix factor close to 1. Recovery results for LQC, MQC, and HQC were consistent with values of 96.81%, 94.33%, and 89.96%, respectively, ensuring accurate quantification under the specified conditions.

Table 17: Represents LLOQ and LOD of Adrenaline with acceptance criteria of 85-115%

Adrenaline	LLOQ	15.63	pg/ml
	LOD	3.91	pg/ml

Table 18: Data for the calibration curve of Adrenaline

	Slope(M)	Intersept-C	R square
Lin 1	0.00052	-0.00574	0.9963
Lin 2	0.00050	-0.00602	0.9938
Lin 3	0.00050	-0.00641	0.9948
MEAN	0.00051		0.9950
S.D.	0.000009		0.0013
C.V.%	1.72		0.13

Table 19: linearity data table of adrenaline

Calibration concentration	15.63 pg/ml	31.25 pg/ml	62.5 pg/ml	125 pg/ml	250 pg/ml	500 pg/ml	1000 pg/ml
Lin 1	14.69	34.81	66.12	114.53	251.76	473.24	1018.47
Lin 2	14.83	35.46	62.65	105.71	261.34	483.02	1057.21
Lin 3	14.79	35.77	60.59	113.22	257.37	470.18	1064.2
Mean	14.77	35.35	63.12	111.15	256.82	475.48	1046.63
s.d.	0.07	0.49	2.79	4.76	4.81	6.71	24.63
c.v.	0.49	1.39	4.43	4.28	1.87	1.41	2.35
nominal	94.50	113.11	100.99	88.92	102.73	95.10	104.66

Table 20: Data of adrenaline between run (interday) precision

	LLOQ	LQC	MQC	HQC
QC	15.63	46.88	375	750
LIN 1	16.93	48.41	329.71	641.11
LIN 1	17.91	48.20	344.11	641.90
LIN 1	17.54	49.12	359.92	715.21
LIN 1	17.18	49.61	347.56	699.44

	LLOQ	LQC	MQC	HQC
LIN 1	16.99	50.08	353.07	697.18
LIN 2	17.67	49.86	353.43	736.94
LIN 2	17.35	49.38	371.13	681.24
LIN 2	17.89	48.61	383.48	700.21
LIN 2	17.55	49.43	336.40	685.10
LIN 2	17.88	48.66	354.45	680.61
LIN 3	17.27	48.74	371.61	686.03
LIN 3	17.67	47.62	343.55	778.63
LIN 3	17.88	50.40	349.66	703.03
LIN 3	16.83	48.84	351.70	698.18
LIN 3	17.59	48.81	394.96	697.16
Mean	17.48	49.05	356.32	696.13
S.D.	0.37	0.75	17.48	33.35
C.V.%	2.10	1.52	4.91	4.79
Absolute percent bias (%)	111.81	104.63	95.02	92.82

Table 21: Data for within run (intraday) precision

	LLOQ	LQC	MQC	HQC
	15.63	46.88	375	750
	17.67	49.86	353.43	736.94
	17.35	49.38	371.13	681.24
	17.89	48.61	383.48	700.21
	17.55	49.43	336.40	685.10
	17.88	48.66	354.45	680.61
Mean	17.67	49.19	359.78	696.82
SD	0.23	0.54	18.07	23.79
CV	1.29	1.09	5.02	3.41
Absolute percent bias (%)	113.04	104.92	95.94	92.91

Table 22: **S**tability study data of adrenaline After 3 Feeze Thaw Cycle with an acceptance criteria of 85-115%

			After 3 Freeze Thaw Cycle		
46.88	375	750	46.88	375	750
48.74	371.61	686.03	49.88	337.82	694.15
47.62	343.55	778.63	50.16	383.82	671.01
50.40	349.66	703.03	51.17	339.63	675.34
48.84	351.70	698.18	53.75	389.92	685.40
48.81	394.96	697.16	46.29	418.48	731.73
48.88	362.30	712.61	50.25	373.93	691.53
% Freeze thaw Stability			102.80	103.21	97.04

Table 23: Short term stability data of adrenaline obtained after 24 hrs with an acceptance criteria of 90-110%

			after 24 hours		
46.88	375	750	46.88	375	750
48.74	371.61	686.03	49.14	329.88	787.00
47.62	343.55	778.63	49.95	341.23	744.84
50.40	349.66	703.03	47.60	330.89	736.75
48.84	351.70	698.18	47.16	352.42	736.78
48.81	394.96	697.16	48.86	349.20	786.33
48.88	362.30	712.61	48.54	340.72	758.34
Short term stability			99.30	94.05	106.42

Table 24: Long term stability (7 days) of the analyte with an acceptance criteria of 90-110%

46.88	375	750	46.88	375	750
48.74	371.61	686.03	46.32	359.58	769.37
47.62	343.55	778.63	45.89	365.81	717.44
50.40	349.66	703.03	47.01	330.19	738.46
48.84	351.70	698.18	49.59	345.78	713.92
48.81	394.96	697.16	47.22	341.20	758.29
48.88	362.30	712.61	47.21	348.51	739.50
Long term stability			96.57	96.20	103.77

Table 25: Matrix effect of Internal standard Propranolol with an acceptance criteria of 85-115%

	EXTRACTED PLASMA	AQUEOUS	% OF ME-OH	MATRIX FACTOR
SAMPLE				
LQC1	3333822.77	3481809.83	95.75	0.96
LQC2	3269190.75	3437768.49	95.10	0.95
LQC3	3229682.08	3303035.54	97.78	0.98
LQC4	3261091.84	3450567.86	94.51	0.95
LQC5	3337816.42	3410485.09	97.87	0.98
Mean	3286320.77	3416733.36	96.20	0.96
S.D.	47555.55	68535.45	1.55	0.02
C.V.%	1.45	2.01	1.61	1.61
MQC1	2878662.31	3282703.61	87.69	0.88
MQC2	3620937.46	3768564.41	96.08	0.96
MQC3	2826648.56	2923486.52	96.69	0.97
MQC4	3562518.74	3660070.63	97.33	0.97
MQC5	2961208.38	3112949.04	95.13	0.95
Mean	3169995.09	3349554.84	94.58	0.95
S.D.	388515.56	358460.14	3.94	0.04
C.V.%	12.26	10.70	4.16	4.16
HQC1	2851262.83	2904496.17	98.17	0.98
HQC2	3006162.33	3100040.68	96.97	0.97

	EXTRACTED PLASMA	AQUEOUS	% OF ME-OH	MATRIX FACTOR
HQC3	2969523.07	3177605.99	93.45	0.93
HQC4	2931869.41	3003949.26	97.60	0.98
HQC5	2331086.68	2584592.94	90.19	0.90
Mean	2817980.86	2954137.01	95.28	0.95
S.D.	278173.30	230615.78	3.38	0.03
C.V.%	9.87	7.81	3.55	3.55

Table 26: Matrix effect on the analyte

	EXTRACTED BLOOD PLASMA	AQUEOUS	% OF ME	MATRIX FACTOR
SAMPLE				
LQC1	60194.83	60529.28	99.45	0.99
LQC2	59480.03	60813.50	97.81	0.98
LQC3	60369.16	60774.53	99.33	0.99
LQC4	59911.45	61137.07	98.00	0.98
LQC5	60659.33	60982.64	99.47	0.99
Mean	60122.96	60847.40	98.81	0.99
S.D.	450.44	229.05	0.83	0.01
C.V.%	0.75	0.38	0.84	0.84
MQC1	299807.07	351126.25	85.38	0.85
MQC2	295325.06	324844.47	90.91	0.91
MQC3	293130.18	337061.19	86.97	0.87
MQC4	289363.83	327162.42	88.45	0.88
MQC5	293543.59	344380.23	85.24	0.85
Mean	294233.95	336914.91	87.39	0.87
S.D.	3796.81	11163.79	2.36	0.02
C.V.%	1.29	3.31	2.71	2.71
HQC1	954393.76	968605.96	98.53	0.99
HQC2	950731.40	964830.46	98.54	0.99
HQC3	960198.21	965820.92	99.42	0.99
HQC4	954269.49	964406.10	98.95	0.99
HQC5	966009.24	975402.56	99.04	0.99
Mean	957120.42	967813.20	98.90	0.99
S.D.	6018.01	4547.01	0.37	0.00
C.V.%	0.63	0.47	0.38	0.38

Table 27: Recovery Analyte area of Adrenaline with acceptance criteria of 80-120%

Dilluent Sample			Plasma sample		
LQC	MQC	HQC	LQC	MQC	HQC
60529.28	351126.25	968605.96	54552.06	336830.49	869748.70
60813.50	324844.47	964830.46	54937.00	334535.37	879788.98
60774.53	337061.19	965820.92	54599.53	335210.35	876240.35
61137.07	327162.42	964406.10	55552.88	332286.66	885908.32
60982.64	344380.23	975402.56	55121.77	330142.92	885004.15
60847.40	336914.91	967813.20	54952.65	333801.16	879338.10
% Recovery			90.31	99.08	90.86

Table 28: Recovery of Internal standard Propranolol

Dilluent Sample			Plasma sample		
LQC	MQC	HQC	LQC	MQC	HQC
3481809.83	3282703.61	2904496.17	2833647.06	3347530.96	2673675.17
3437768.49	3768564.41	3100040.68	2869602.84	2945662.04	2701155.38
3303035.54	2923486.52	3177605.99	3582675.67	2861221.71	2410168.59
3450567.86	3660070.63	3003949.26	2795357.65	2912750.64	2492584.68
3410485.09	3112949.04	2584592.94	3295457.84	3169772.41	2698231.99
3416733.36	3349554.84	2954137.01	3075348.21	3047387.55	2595163.16
% Recovery			90.01	90.98	87.85

Table 29: Bench Top Stability data of adrenaline after 24 hrs with acceptance criteria 90-110%

			After 24 Hours		
46.88	375	750	46.88	375	750
48.74	371.61	686.03	47.04	355.47	754.53
47.62	343.55	778.63	48.10	369.07	795.23
50.40	349.66	703.03	40.42	352.96	789.73
48.84	351.70	698.18	48.18	347.57	739.49
48.81	394.96	697.16	47.16	331.51	729.77
48.88	362.30	712.61	46.18	351.32	761.75
% Stability			94.47	96.97	106.90

Table 30: Autosampler Stability data of adrenaline after 24 hrs with acceptance criteria 90-110%

			AUTOSAMPLER AFTER 24 HR		
46.88	375	750	46.88	375	750
48.74	371.61	686.03	47.83	359.14	794.75
47.62	343.55	778.63	46.38	337.77	761.28
50.40	349.66	703.03	48.44	365.47	724.30
48.84	351.70	698.18	46.78	348.02	708.67
48.81	394.96	697.16	48.06	341.08	721.35
48.88	362.30	712.61	47.50	350.30	742.07
% Stability			97.17	96.69	104.13

3.0.Analytical Method Development of Aldosterone by LC-ESI-MS/MS (API-4000 QTRAP)

A method was developed and validated for the quantitative assay of aldosterone in rat plasma, using Tolbutamide as an internal standard (IS). The primary goal was to establish a reliable analytical method for aldosterone analysis in rat plasma. The chemicals used in the

method included MS-grade acetonitrile (ACN), water from a Milli-Q purification system, MS-grade formic acid, methanol, and ammonium acetate.

The chromatographic analysis was performed on a Triple Quadrupole LC/MS/MS Mass Spectrometer (API 4000 Q-Trap) manufactured by AB Sciex Instruments. The column used was a Phenomenex Kinetex 5µ C18 (100A, 50 × 3 mm). The mobile phase consisted of two components: Component A, 0.1% ammonium hydroxide with 10 mM ammonium acetate in Milli Q water, and Component B, 0.1% formic acid in acetonitrile. The Shimadzu LC system was employed for liquid chromatography, with a binary flow pumping mode and a total flow rate of 0.5 mL/min. The injection volume was set at 10 µL, and the auto-sampler temperature was maintained at 15°C. The gradient elution program involved varying the concentration of Pump B at 30% from 0.01 to 0.1 mins and then 70% from 0.50 mins to 3.0 mins , again returning back to 30 % from 3.50 mins to 6.50 mins.

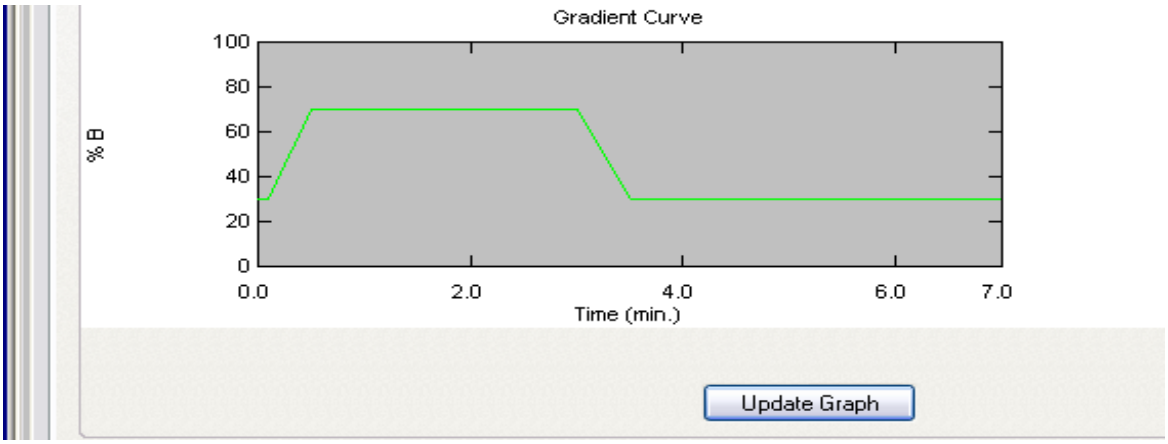

Figure 4: Gradient curve of Aldosterone

For mass spectrometry, the MRM (Multiple Reaction Monitoring) mode was used with negative polarity. Aldosterone and Tolbutamide (IS) were monitored at Q1/Q3 transitions of 359.2 /331.0 m/z and 269.0/170.0 m/z, respectively. The optimized ion source parameters included a Curtain gas of 20 psig, temperature of 400°C, GS1 at 40 psig, GS2 at 45 psig, and an IS voltage of -4500 V. Analyst software version 1.6.3 was utilized for data acquisition and processing.

Table 31: LC-MS parameter for plasma Aldosterone estimation

Aldosterone	**Q1 Mass (Da)**	**Q3 Mass (Da)**	**Dwell(msec)**	**Parameter**	**Start**
	359.2 m/z	331.0 m/z	200.00	DP	-40.0 V
				CE	-28.0 V
				CXP	-15.0 V
Tolbutamide (IS)	**Q1 Mass (Da)**	**Q3 Mass (Da)**	**Dwell(msec)**	**Parameter**	**Start**
	269.0 m/z	170.0 m/z	200.00	DP	-50.0 V
				CE	-31.0 V
				CXP	-15.0 V

The plasma extraction involved solid-phase extraction (SPE). Rat plasma (100 µL) was mixed with a protease inhibitor cocktail, acidified with 10 µL of 2% formic acid, and vortexed. The sample was alkalized with 300 µL of 5% ammonium hydroxide and subjected to further vortexing. This solution was applied to a pre-treated SPE cartridge, washed with water and ammonium hydroxide (95:5 v/v), followed by methanol. Aldosterone was eluted with a methanol:formic acid (98:2 v/v) mixture, dried under a nitrogen stream at 40°C, and reconstituted in methanol:acetonitrile (50:50). A 10 µL aliquot of the reconstituted sample was injected into the chromatographic system.

Plasma calibration standards for Aldosterone ranged from 1.56 to 100.00 pg/mL, with QC concentrations defined as LLOQ (1.56 pg/mL), LQC (4.68 pg/mL), MQC (37.50 pg/mL), and HQC (75.00 pg/mL). This method demonstrated accuracy and precision for Aldosterone quantification, providing a reliable approach for bioanalytical studies.

3.1.Method Validation of Aldosterone

Aldosterone was quantified using LC-MS/MS, with an LLOQ of 1.56 pg/mL and an LOD of 0.1 pg/mL. The acceptance criteria for accuracy were set at 85-115%. For the calibration curve data, the mean concentrations at seven levels (1.56, 3.12, 6.25, 12.5, 25, 50, and 100 pg/mL) were 1.453, 3.553, 6.347, 12.313, 23.887, 51.663, and 94.077 pg/mL, respectively. The % CV ranged from 0.708 to 4.479, demonstrating acceptable precision. The slope, intercept, and R^2 values across three calibration lines were 0.00765 ± 0.00074, -0.00528 ± 0.00081, and 0.9953 ± 0.00297, respectively, indicating robust linearity. For quality control (QC) samples at LLOQ, LQC, MQC and HQC levels, the mean concentrations were 1.604 ± 0.064, 4.627 ± 0.298, 35.793 ± 1.742, and 69.858 ± 2.004 pg/mL, respectively. The % CV

ranged from 2.869% to 6.435%, with absolute percent bias values of 102.82%, 98.87%, 95.45%, and 93.14%, indicating acceptable accuracy and precision. Freeze-thaw stability after three cycles showed concentrations of 4.62 ± 0.12, 36.64 ± 0.72, and 71.33 ± 1.78 pg/mL for LQC, MQC, and HQC, respectively, with stability values of 99.18%, 97.29%, and 98.55%. Short-term stability assessed at 24 hours yielded stability values of 98.40%, 107.99%, and 100.72% for LQC, MQC, and HQC, respectively, within the acceptable range of 90-110%. Long-term stability results were also acceptable, with mean concentrations of 4.53 ± 0.41, 37.73 ± 2.54, and 75.00 ± 3.34 pg/mL for LQC, MQC, and HQC, respectively, demonstrating stability values of 98.10%, 102.98%, and 105.15%. The matrix effect was evaluated by comparing extracted blank plasma with aqueous standards. For LQC, MQC, and HQC levels, the matrix effect values were 96.38% ± 1.00%, 92.94% ± 4.72%, and 96.61% ± 1.80%, respectively, with corresponding matrix factors of 0.96 ± 0.01, 0.93 ± 0.05, and 0.97 ± 0.02. These results confirmed that the matrix effect was within acceptable limits (85-115%). Overall, the method demonstrated adequate sensitivity, precision, accuracy, and stability under various conditions, making it suitable for the quantification of aldosterone in plasma samples.

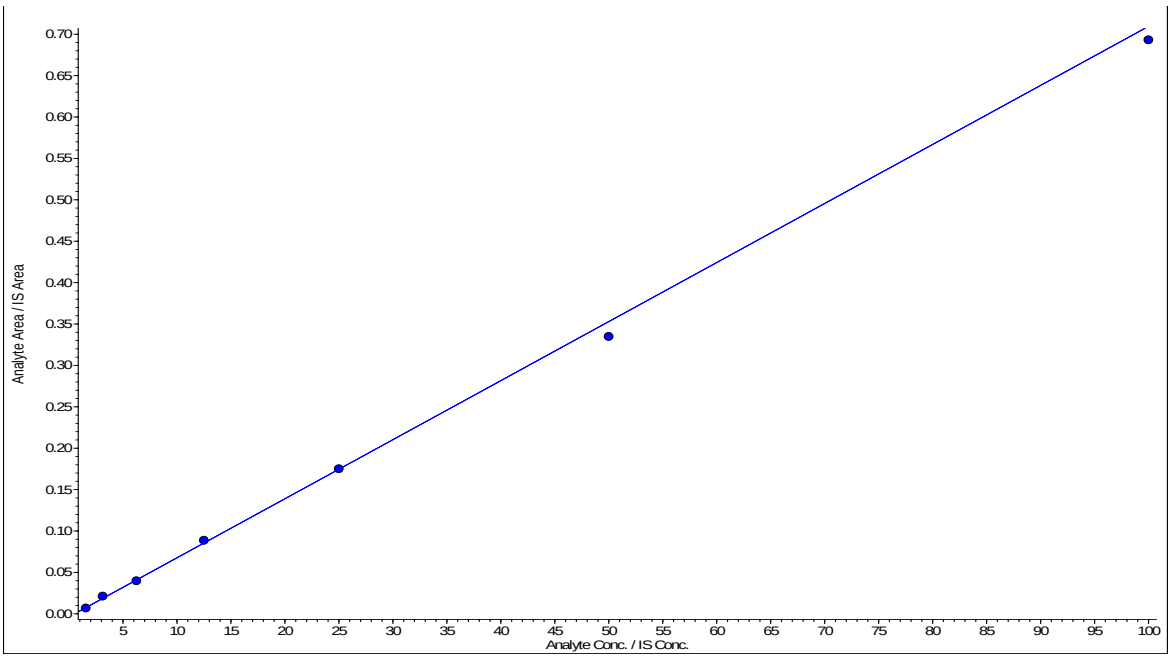

Figure 5: Calibration curve of Aldosterone

Table 32: Lower Limit of Quantification (LLOQ) and Limit of Detection (LOD) for aldosterone determined using LC-MS/MS with acceptance criteria set at 85–115%

1	LLOQ	1.56	pg/ml
2	LOD	0.1	pg/ml

Table 33: Linearity assessment of aldosterone calibration standards (1.56 to 100 pg/mL) analyzed over three independent runs, reporting mean values, standard deviation (S.D.), coefficient of variation (C.V.), and nominal accuracy

	1.56	3.12	6.25	12.5	25	50	100
Lin 1	1.43	3.6	6.55	12.01	23.6	51.97	93.46
Lin 2	1.45	3.58	6.4	11.98	23	55.56	91.07
Lin 3	1.48	3.48	6.09	12.95	25.06	47.46	97.7
mean	1.453	3.553	6.347	12.313	23.887	51.663	94.077
s.d.	0.025	0.064	0.235	0.552	1.059	1.059	1.059
c.v.	0.708	1.809	3.696	4.479	4.436	2.051	1.126
nominal	93.16	113.89	101.55	98.51	95.55	103.33	94.08

Table 34: Data for the calibration curve of aldosterone

	Slope(M)	Intersept-C	R square
Lin 1	0.00845	-0.00517	0.9947
Lin 2	0.00817	-0.00503	0.9932
Lin 3	0.00713	-0.00364	0.9974
MEAN	0.00765		0.9953
S.D.	0.00074		0.00297
C.V.%	9.613		0.298

Table 35: Inter-day precision and accuracy of aldosterone across four concentration levels (LLOQ, LQC, MQC, HQC) with absolute percent bias calculations.

	LLOQ	**LQC**	**MQC**	**HQC**
	1.56	4.68	37.5	75
LIN 1	1.57	4.79	36.24	67.61
LIN 1	1.55	4.78	34.42	67.96
LIN 1	1.57	4.84	36.44	70.80
LIN 1	1.55	4.81	34.23	69.08
LIN 1	1.65	4.96	34.16	67.52
LIN 2	1.59	4.71	39.97	69.01
LIN 2	1.54	4.37	35.42	68.56
LIN 2	1.57	4.49	34.01	69.16
LIN 2	1.59	4.23	34.52	71.05
LIN 2	1.50	4.33	34.27	70.49

	LLOQ	**LQC**	**MQC**	**HQC**
LIN 3	1.67	4.90	38.45	73.06
LIN 3	1.67	5.20	37.05	71.44
LIN 3	1.66	4.37	36.88	74.45
LIN 3	1.65	4.30	35.55	68.77
LIN 3	1.73	4.33	35.28	68.91
Mean	1.604	4.627	35.793	69.858
S.D.	0.064	0.298	1.742	2.004
C.V.%	3.963	6.435	4.866	2.869
Absolute percent bias (%)	102.82	98.87	95.45	93.14

Table 36: Intraday precision and accuracy of aldosterone across four concentration levels (LLOQ, LQC,MQC and HQC) showing mean, S.D., C.V. and percent bias

	LLOQ	**LQC**	**MQC**	**HQC**
	1.56	4.68	37.5	75
	1.59	4.71	39.97	69.01
	1.54	4.37	35.42	68.56
	1.57	4.49	34.01	69.16
	1.59	4.23	34.52	71.05
	1.50	4.33	34.27	70.49
Mean	1.56	4.43	35.64	69.65
SD	0.038	0.184	2.479	1.061
CV	2.461	4.159	6.957	1.523
Absolute percent bias (%)	99.87	94.57	95.03	92.87

Table 37: Freeze-thaw stability of aldosterone evaluated over three cycles at LQC, MQC, and HQC levels, with results expressed as percent stability and compared to acceptance criteria (85–115%).

4.68	37.5	75	4.68	37.5	75
4.90	38.45	73.06	4.8	35.96	67.94
5.20	37.05	71.44	4.64	35.52	73.06
4.37	36.88	74.45	4.62	35.62	68.02
4.30	35.55	68.77	4.37	34.96	71.92
4.33	35.28	68.91	4.48	36.18	70.51
4.62	36.64	71.33	4.58	35.65	70.29
% Freeze thaw Stability			99.18	97.29	98.55

Table 38: Short-term stability of aldosterone analyzed after 24 hours at room temperature, with concentrations assessed at LQC, MQC, and HQC levels, and stability expressed as percent relative to the acceptance criteria (90–110%)

			after 24 hours		
4.68	37.5	75	4.68	37.5	75
4.90	38.45	73.06	5.31	38.64	74.23
5.20	37.05	71.44	4.39	39.33	74.13
4.37	36.88	74.45	4.17	39.8	73.66
4.30	35.55	68.77	4.54	39.59	69.27
4.33	35.28	68.91	4.32	40.49	67.92
4.62	36.64	71.33	4.55	39.57	71.84
Short term stability			98.40	107.99	100.72

Table 39: Long-term stability of aldosterone evaluated under storage conditions, showing concentrations at LQC, MQC, and HQC levels, with percent stability relative to the acceptance criteria (90–110%).

4.68	37.5	75	4.68	37.5	75
4.90	38.45	73.06	4.4	38.08	77.99
5.20	37.05	71.44	4.26	33.97	77.9
4.37	36.88	74.45	4.19	35.57	75.79
4.30	35.55	68.77	5.07	40.88	75
4.33	35.28	68.91	4.74	40.17	68.3
4.62	36.64	71.33	4.53	37.73	75.00
Long term stability			98.10	102.98	105.15

Table 40: Matrix effect of IS for the evaluation for aldosterone, comparing extracted blank plasma and aqueous standards for LQC, MQC, and HQC levels. Results include percent matrix effect (% ME) and matrix factor, along with mean, S.D., and C.V. for each level

MATRIX EFFECT IS	EXTRACTED BLOOD PLASMA	AQUEOUS	% OF ME	MATRIX FACTOR
SAMPLE				
LQC1	6590353.9	6834150.91	96.43	0.96
LQC2	5920530.88	6050004.15	97.86	0.98
LQC3	6709165.76	6940713.36	96.66	0.97
LQC4	6081957.95	6381376.35	95.31	0.95
LQC5	6116928.49	6395470.48	95.64	0.96
Mean	6283787.40	6520343.05	96.38	0.96
S.D.	344768.80	364455.13	1.00	0.01
C.V.%	5.49	5.59	1.03	1.07
MQC1	6001966.21	6961703.14	86.21	0.86
MQC2	6164226.72	6349647.28	97.08	0.97
MQC3	6097938.94	6242233.98	97.69	0.98
MQC4	6059364.55	6530341.78	92.79	0.93

MATRIX EFFECT IS	EXTRACTED BLOOD PLASMA	AQUEOUS	% OF ME	MATRIX FACTOR
MQC5	5888375.21	6476763.71	90.92	0.91
Mean	6042374.33	6512137.98	92.94	0.93
S.D.	104370.31	275201.27	4.72	0.05
C.V.%	1.73	4.23	5.08	5.08
HQC1	5879121.47	6099028.77	96.39	0.96
HQC2	5847016.23	5903782.83	99.04	0.99
HQC3	5945961.54	6158802.85	96.54	0.97
HQC4	5980063.98	6361469.43	94.00	0.94
HQC5	6039885.57	6220764.56	97.09	0.97
Mean	5938409.76	6148769.69	96.61	0.97
S.D.	77390.77	168090.62	1.80	0.02
C.V.%	1.30	2.73	1.86	1.86

Table 41: Matrix effect evaluation for aldosterone, comparing extracted blank plasma and aqueous standards for LQC, MQC, and HQC levels. Results include percent matrix effect (% ME) and matrix factor, along with mean, S.D., and C.V. for each level.

MATRIX EFFECT ANALYTE	EXTRACTED BL PLASMA	AQUEOUS	% OF ME	MATRIX FACTOR
SAMPLE				
LQC1	203132.18	227317.91	89.36	0.89
LQC2	228935.93	230699.64	99.24	0.99
LQC3	201478.67	208381.47	96.69	0.99
LQC4	199668.57	214708.22	93.00	0.93
LQC5	219695.65	231605.49	94.86	0.95
Mean	210582.20	222542.55	94.63	0.95
S.D.	13013.44	10409.03	3.74	0.04
C.V.%	6.18	4.68	3.95	4.39
MQC1	1838709.24	1857318.02	99.00	0.99
MQC2	1831423.55	1895817.22	96.60	0.97
MQC3	1882180.68	1888675.57	99.66	1.00
MQC4	1843944.74	1899079.37	97.10	0.97
MQC5	1738817.61	1828141.62	95.11	0.95
Mean	1827015.16	1873806.36	97.49	0.97
S.D.	53067.97	30419.69	1.84	0.02
C.V.%	2.90	1.62	1.89	1.89
HQC1	3644359.79	4010037.36	90.88	0.91
HQC2	3688697.16	3730718.14	98.87	0.99
HQC3	3532229.96	3788752.99	93.23	0.99
HQC4	3632788.48	3718884.58	97.68	0.98
HQC5	3616121.80	3743975.16	96.59	0.97
Mean	3622839.44	3798473.65	95.45	0.97
S.D.	57346.65	121190.97	3.31	0.03
C.V.%	1.58	3.19	3.47	3.46

Table 42: Presents the LC-MS/MS recovery data for the analyte. The table includes analyte areas for diluent and plasma samples across three quality control levels: Low Quality Control (LQC), Medium Quality Control (MQC), and High Quality Control (HQC). The % recovery values were calculated by comparing the plasma sample analyte areas to the corresponding diluent sample areas within the acceptance criteria of 80-120%

Dilluent Sample			**Plasma sample**		
LQC	**MQC**	**HQC**	**LQC**	**MQC**	**HQC**
220041.29	1765903.94	3675626.32	212174.60	1784138.37	3650821.57
222031.98	1837524.96	3721476.92	201446.26	1877068.91	3651145.32
223770.32	1791555.28	3752157.00	199414.55	1771335.85	3500440.73
216100.60	1920496.16	3720121.65	196089.31	1707611.24	3684921.21
212858.04	1841756.86	3682166.23	185577.59	1769048.56	3786778.40
218960.45	1831447.44	3710309.62	198940.46	1781840.59	3654821.45
% Recovery			90.86	97.29	98.50

Table 43: Presents the LC-MS/MS recovery data for the Internal standard (IS). The table includes IS areas for diluent and plasma samples across three quality control levels: Low Quality Control (LQC), Medium Quality Control (MQC), and High Quality Control (HQC). The % recovery values were calculated by comparing the plasma sample IS areas to the corresponding diluent sample areas

Dilluent Sample			**Plasma sample**		
LQC	**MQC**	**HQC**	**LQC**	**MQC**	**HQC**
7305822.27	6976360.47	6444460.40	6839456.36	5510981.84	6045702.25
7440758.22	6162105.03	6969842.04	7105611.77	5734416.51	6561985.68
7403816.32	6030748.65	6367214.04	6594205.00	5803394.90	6263237.06
7316122.39	6098133.42	6193227.00	6601813.51	5927250.26	6015877.94
7478755.78	6146844.06	6661398.68	7613671.77	5964516.00	6326107.35
7389055.00	6282838.33	6527228.43	6950951.68	5788111.90	6242582.06
% Recovery			94.07	92.13	95.64

Table 44: Presents the bench-top stability data for aldosterone estimation using LC-MS/MS. The analyte concentrations were evaluated immediately (baseline) and after 24 hours at three levels: 4.68 pg/mL (low), 37.5 pg/mL (medium), and 75 pg/mL (high). The % stability was calculated by comparing the concentrations after 24 hours to the baseline values, with acceptance criteria of 90–110%.

			After 24 Hours		
4.68	**37.5**	**75**	**4.68**	**37.5**	**75**
4.90	38.45	73.06	5.06	39.58	75.77
5.20	37.05	71.44	5.09	39.39	78.41
4.37	36.88	74.45	4.41	40.10	80.65
4.30	35.55	68.77	4.65	39.76	78.94
4.33	35.28	68.91	4.32	39.63	77.55
4.62	36.64	71.33	4.71	39.69	78.26
% Stability			101.86	108.32	109.73

Table 45: Presents the Auto-Sampler stability data for aldosterone estimation using LC-MS/MS. The analyte concentrations were evaluated immediately (baseline) and after 24 hours at three levels: 4.68 pg/mL (low), 37.5 pg/mL (medium), and 75 pg/mL (high). The % stability was calculated by comparing the concentrations after 24 hours to the baseline values, with acceptance criteria of 85–110%.

			AFTER 24 hr		
4.68	**37.5**	**75**	**4.68**	**37.5**	**75**
4.90	38.45	73.06	4.8	34.67	67.02
5.20	37.05	71.44	4.25	33.99	66.73
4.37	36.88	74.45	5.01	35.77	65.89
4.30	35.55	68.77	4.92	35.47	67.19
4.33	35.28	68.91	5.05	34.89	67.51
4.62	36.64	71.33	4.81	34.96	66.87
% Stability			104.03	95.40	93.75

4.0.Analytical Method Development of Atrial Natriuretic Peptide (ANP) by LC-ESI-MS/MS (API-4000 QTRAP)

A robust method was developed in the positive mode for the quantitative determination of Atrial Natriuretic Peptide (ANP) in rat plasma using LC-ESI-MS/MS (API-4000 QTRAP). Propranolol served as the internal standard (IS) for the assay. High-performance liquid chromatography (HPLC) with a Phenomenex Kinetex 5µ C18 100A column (50 × 3 mm) was employed. The mobile phase consisted of 0.2% formic acid in Milli-Q water with 10 mM ammonium formate (phase A) and 0.2% formic acid in acetonitrile (phase B). A binary flow pumping system was used with a flow rate of 0.5 mL/min and an injection volume of 10 µL. The Shimadzu LC system parameters included a 0-minute equilibration time and a cooler temperature of 15°C to maintain sample stability. In case of gradient elution method mobile phase B concentration started with 80% from 0.01 to 0.10 minutes, 90% from 0.5 to 2.50 mins and returned back to 80% from 3.00 mins to 6.50 mins to optimize the separation

of ANP and propranolol. .Mass spectrometry detection was carried out using multiple reaction monitoring (MRM) in positive ion mode with Turbo Spray ionization. The mass transitions for ANP were 279.3 m/z → 205.1 m/z, and for propranolol (IS), m/z 260.0 m/z → 116.1 m/z. Critical mass spectrometer parameters included a declustering potential (DP) of 39.0 V for ANP and 20.0 V for propranolol, a collision energy (CE) of 10.0 V and 26.0 V, respectively, and a collision cell exit potential (CXP) of 15.0 V. Rat plasma samples were prepared by mixing with a protease inhibitor solution to prevent peptide degradation. Plasma extraction was performed using a solid-phase extraction (SPE) cartridge. Acidification with 2% formic acid facilitated protein precipitation, and the samples were subjected to interference elution using a water-acetonitrile mixture (60:40 v/v). ANP was eluted with 500 µl methanol, dried under nitrogen at 40°C, and reconstituted in a diluent (50:50 acetonitrile-water). The method was validated over a concentration range of 1.56–100.00 pg/mL for ANP, with quality control (QC) points defined at 1.56 pg/mL (LLOQ), 4.68 pg/mL (LQC), 37.50 pg/mL (MQC), and 75.00 pg/mL (HQC).

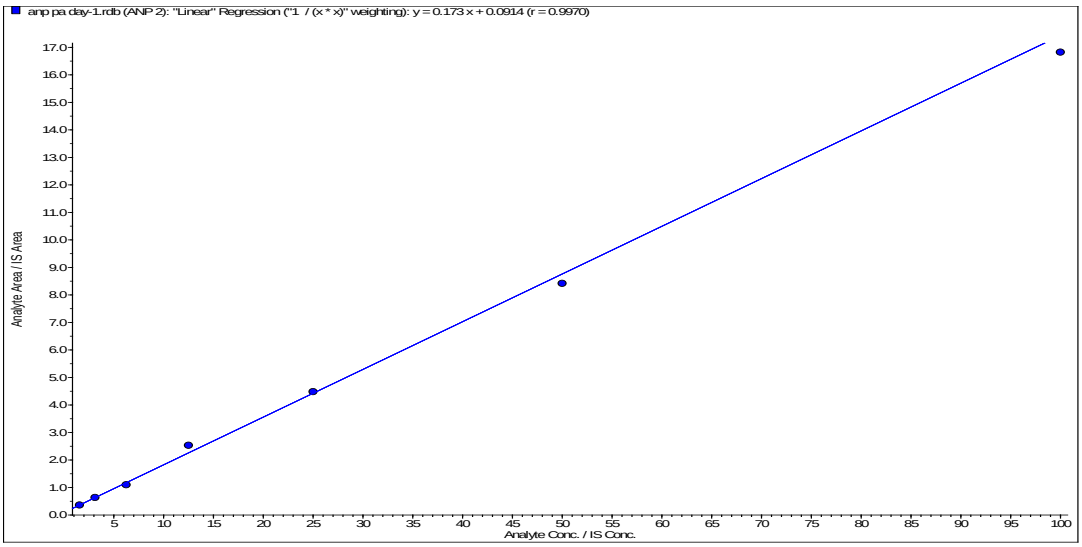

Figure 6: Calibration curve of ANP

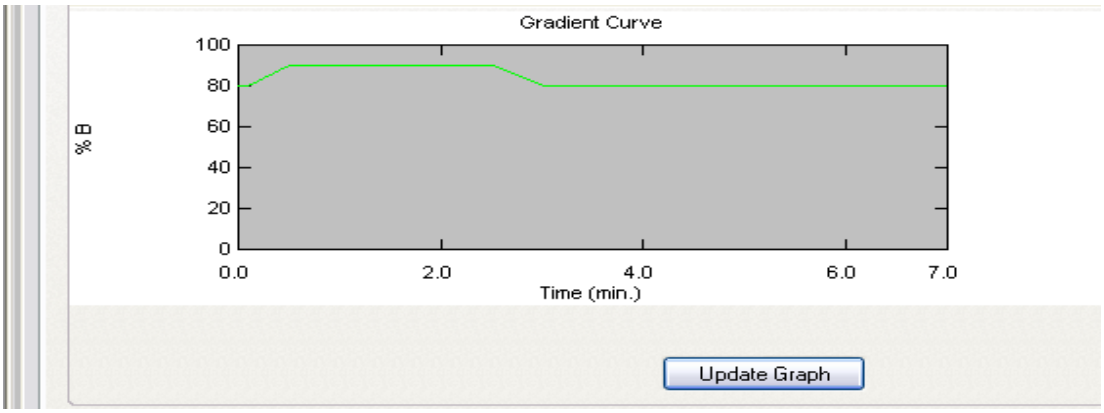

Figure7: Gradient Curve of ANP

Table 46: LC-MS parameters Q1/Q3 masses of ANP and Propanolol (IS)

ANP	**Q1 Mass (Da)**	**Q3 Mass (Da)**	**Dwell(msec)**	**Parameter**	**Start**
	279.3	205.1	200.00	DP	39.0
				CE	10.0
				CXP	15.0
Propranolol (IS)	**Q1 Mass (Da)**	**Q3 Mass (Da)**	**Dwell(msec)**	**Parameter**	**Start**
	260.0	116.1	200.00	DP	20.0
				CE	26.0
				CXP	15.0

4.1.Method Validation of ANP

The analytical method for ANP was validated following standard guidelines to assess its reliability and reproducibility. The lower limit of quantification (LLOQ) for ANP was established at 1.56 pg/mL, with a limit of detection (LOD) of 0.11 pg/mL. The calibration curves demonstrated excellent linearity across the concentration range of 1.56–100 pg/mL, with regression coefficients (R^2) of 0.9972 ± 0.0024, indicating strong correlation. The slope and intercept for the three linearity experiments averaged 0.01007 and 0.0111, respectively, with acceptable variability % CV 11.90 . Interday (between run) precision and accuracy were assessed at four concentration levels: LLOQ, LQC, 4.69 pg/mL, MQC, 37.50 pg/mL and HQC, 75.00 pg/mL. The mean concentrations were 1.54 ± 0.13 pg/mL (CV 8.20%) for LLOQ, 4.57 ± 0.34 pg/mL (CV 7.36%) for LQC, 37.38 ± 2.93 pg/mL (CV 7.83%) for MQC, and 76.32 ± 5.00 pg/mL (CV 6.56%) for HQC. Absolute percent biases ranged from 97.48% to 101.76%, reflecting acceptable accuracy. Intraday (Between run) precision and accuracy showed similar results, with maximum %CVs below at 7.95 and minimum % CV at 0.87 and biases within acceptable limits, confirming reproducibility. Stability studies demonstrated the robustness of the method. Freeze-thaw stability was confirmed over three cycles with recoveries of 102.01%, 98.50%, and 99.80% for LQC, MQC, and HQC, respectively, meeting the acceptance criteria of 85–115%. Short-term stability at room temperature for 24 hours yielded recoveries of 95.89% for LQC, 97.90% for MQC, and 101.85% for HQC. Long-term stability was also validated, with recoveries of 103.00% (LQC), 102.21% (MQC), and 104.49% (HQC), all within the acceptable range. Matrix effects were evaluated by comparing analyte responses in extracted blank plasma and aqueous standards. The mean matrix factor (MF) values were 0.93 ± 0.04 for LQC, 0.94 ± 0.03 for MQC, and 0.95 ± 0.04 for HQC, with negligible variability (CV < 5%). These findings confirm minimal matrix interference and high analytical accuracy. The method validation results underscore the robustness, precision, accuracy, and stability of the analytical procedure for ANP quantification in biological matrices.

Table 47: Lower Limit of Quantification (LLOQ) and Limit of Detection (LOD) for ANP determined using LC-MS/MS with acceptance criteria set at 85–115%

1	LLOQ	1.56	pg/ml
2	LOD	0.11	pg/ml

Table 48: Linearity assessment of ANP calibration standards (1.56 to 100 pg/mL) analyzed over three independent runs, reporting mean values, standard deviation (S.D.), coefficient of variation (C.V.), and nominal accuracy

	1.56	3.13	6.25	12.5	25	50	100
Lin 1	1.55	3.13	6.39	12.26	24.99	49.6	100.77
Lin 2	1.56	3.31	5.47	11.73	27.33	50.6	101.92
Lin 3	1.58	3.06	6.51	11.01	27.21	46.3	107.48
mean	1.56	3.17	6.12	11.67	26.51	48.83	103.39
s.d.	0.02	0.13	0.57	0.63	1.32	2.25	3.59
c.v.	0.98	4.07	9.29	5.38	4.97	4.61	3.47
nominal	100.21	101.17	97.97	93.33	106.04	97.67	103.39

Table 49: Data for the calibration curve of ANP

	Slope(M)	Intersept-C	R square
Lin 1	0.01050	0.001710	0.9999
Lin 2	0.01100	0.011100	0.9960
Lin 3	0.00872	0.048100	0.9956
MEAN	0.01007		0.9972
S.D.	0.0012		0.0024
C.V.%	11.90		0.24

Table 50: Inter-day precision and accuracy of ANP across four concentration levels (LLOQ, LQC, MQC, HQC) with absolute percent bias calculations.

	LLOQ	**LQC**	**MQC**	**HQC**
	1.56	4.69	37.50	75.00
LIN 1	1.59	4.73	37.22	80.32
LIN 1	1.46	4.94	39.72	80.22
LIN 1	1.52	4.85	36.96	79.91
LIN 1	1.40	4.62	39.28	79.10
LIN 1	1.43	4.63	39.42	80.24
LIN 2	1.57	4.24	34.85	73.15
LIN 2	1.70	4.45	35.89	71.95
LIN 2	1.59	4.10	34.81	73.66
LIN 2	1.37	4.08	36.22	72.75
LIN 2	1.49	4.57	35.44	72.67
LIN 3	1.32	4.15	38.01	73.84
LIN 3	1.76	5.30	42.61	72.65
LIN 3	1.64	4.52	32.50	80.96
LIN 3	1.54	4.63	42.75	67.20
LIN 3	1.66	4.77	35.00	86.16

	LLOQ	**LQC**	**MQC**	**HQC**
Mean	1.54	4.57	37.38	76.32
S.D.	0.13	0.34	2.93	5.00
C.V.%	8.20	7.36	7.83	6.56
Absolute percent bias (%)	98.46	97.48	99.68	101.76

Table 51: Intraday precision and accuracy of ANP across four concentration levels (LLOQ, LQC,MQC and HQC) showing mean, S.D., C.V. and percent bias

	LLOQ	**LQC**	**MQC**	**HQC**
	1.56	4.69	37.50	75.00
	1.57	4.24	34.85	73.15
	1.70	4.45	35.89	71.95
	1.59	4.10	34.81	73.66
	1.37	4.08	36.22	72.75
	1.49	4.57	35.44	72.67
Mean	1.54	4.29	35.44	72.84
SD	0.12	0.22	0.62	0.63
CV	7.95	5.04	1.76	0.87
Absolute percent bias (%)	98.97	91.43	94.51	97.11

Table 52: Freeze-thaw stability of ANP evaluated over three cycles at LQC, MQC, and HQC levels, with results expressed as percent stability and compared to acceptance criteria (85–115%)

			After Three Freeze Thaw Cycle		
4.69	37.50	75.00	4.69	37.50	75.00
4.15	38.01	73.84	5.07	40.47	80.45
5.30	42.61	72.65	4.10	43.24	78.53
4.52	32.50	80.96	4.84	32.28	73.55
4.63	42.75	67.20	4.54	32.56	78.22
4.77	35.00	86.16	5.29	39.45	69.28
4.67	38.17	76.16	4.77	37.60	76.01
% Freeze thaw Stability			102.01	98.50	99.80

Table 53: Short-term stability of ANP analyzed after 24 hours at room temperature, with concentrations assessed at LQC, MQC, and HQC levels, and stability expressed as percent relative to the acceptance criteria (90–110%)

	Before 24 hours		**after 24 hours**		
4.69	37.50	75.00	4.69	37.50	75.00
4.15	38.01	73.84	5.02	40.96	75.99
5.30	42.61	72.65	4.18	38.04	85.26
4.52	32.50	80.96	4.22	39.94	74.43
4.63	42.75	67.20	4.05	32.40	82.00
4.77	35.00	86.16	4.94	35.52	70.19
4.67	38.17	76.16	4.48	37.37	77.57
Short term stability			95.89	97.90	101.85

Table 54: Long-term stability of ANP evaluated under storage conditions, showing concentrations at LQC, MQC, and HQC levels, with percent stability relative to the acceptance criteria (90–110%)

4.69	37.50	75.00	4.69	37.50	75.00
4.15	38.01	73.84	4.67	36.72	82.89
5.30	42.61	72.65	4.69	40.54	81.58
4.52	32.50	80.96	4.84	37.46	79.39
4.63	42.75	67.20	4.98	39.25	85.22
4.77	35.00	86.16	4.89	41.11	68.81
4.67	38.17	76.16	4.81	39.02	79.58
Long term stability			103.00	102.21	104.49

Table 55: Matrix effect of IS for the evaluation for ANP, comparing extracted blank plasma and aqueous standards for LQC, MQC, and HQC levels. Results include percent matrix effect (% ME) and matrix factor, along with mean, S.D., and C.V. for each level

MATRIX EFFECT of IS	EXTRACTED PLASMA	AQUEOUS	% OF ME	MATRIX FACTOR
SAMPLE				
LQC1	915542.87	985250.32	92.92	0.93
LQC2	1022995.09	1092416.69	93.65	0.94
LQC3	906671.26	1027701.25	88.22	0.88
LQC4	1009582.09	1014652.43	99.50	0.99
LQC5	1012393.75	1106108.04	91.53	0.92
Mean	973437.01	1045225.75	93.16	0.93
S.D.	57204.66	51895.39	4.11	0.04
C.V.%	5.88	4.96	4.41	4.21
MQC1	1547764.59	1648884.32	93.87	0.94
MQC2	1469612.03	1599956.16	91.85	0.99
MQC3	1470440.21	1601900.79	91.79	0.92
MQC4	1500099.04	1586723.67	94.54	0.95
MQC5	1444830.86	1557980.14	92.74	0.93
Mean	1486549.35	1599089.02	92.96	0.94
S.D.	39426.23	32905.44	1.22	0.03
C.V.%	2.65	2.06	1.31	2.95
HQC1	1337339.88	1514847.12	88.28	0.88
HQC2	1487445.67	1539098.62	96.64	0.97
HQC3	1467534.19	1474076.11	99.56	0.99
HQC4	1422733.84	1516768.95	93.80	0.94
HQC5	1441376.46	1507828.24	95.59	0.96
Mean	1431286.01	1510523.81	94.78	0.95
S.D.	58027.30	23504.86	4.19	0.04
C.V.%	4.05	1.56	4.42	4.26

Table 56: Matrix effect evaluation for ANP, comparing extracted blank plasma and aqueous standards for LQC, MQC, and HQC levels. Results include percent matrix effect (% ME) and matrix factor, along with mean, S.D., and C.V. for each level.

MATRIX EFFECT ANALYTE	EXTRACTED BL PLASMA	AQUEOUS	% OF ME	MATRIX FACTOR
SAMPLE				
LQC1	95159.65	101341.26	93.90	0.94
LQC2	89009.99	93743.48	94.95	0.95
LQC3	93870.66	101348.15	92.62	0.93
LQC4	87908.88	92910.35	94.62	0.96
LQC5	80030.98	90742.23	88.20	0.88
Mean	89196.03	96017.09	92.86	0.93
S.D.	5981.36	4985.29	2.75	0.03
C.V.%	6.71	5.19	2.97	3.25
MQC1	610456.08	680559.26	89.70	0.90
MQC2	679491.88	738601.18	92.00	0.92
MQC3	612299.56	614573.67	99.63	0.99
MQC4	525286.64	605497.20	86.75	0.87
MQC5	624722.54	634608.05	98.44	0.98
Mean	610451.34	654767.87	93.30	0.93
S.D.	55287.22	55097.21	5.57	0.05
C.V.%	9.06	8.41	5.97	5.79
HQC1	998986.25	1170645.18	85.34	0.85
HQC2	950901.32	1073363.28	88.59	0.89
HQC3	1139078.89	1238560.26	91.97	0.92
HQC4	1102059.63	1288269.87	85.55	0.86
HQC5	1035290.15	1080224.17	95.84	0.99
Mean	1045263.25	1170212.55	89.46	0.90
S.D.	76112.42	94982.65	4.47	0.06
C.V.%	7.28	8.12	5.00	6.29

Table 57: Presents the LC-MS/MS recovery data for the analyte (ANP). The table includes analyte areas for diluent and plasma samples across three quality control levels:LQC, MQC and HQC. The % recovery values were calculated by comparing the plasma sample analyte areas to the corresponding diluent sample areas with an acceptance criteria of 80-120%

Dilluent Sample			Plasma sample		
LQC	**MQC**	**HQC**	**LQC**	**MQC**	**HQC**
106235.63	702404.89	1232241.76	93042.72	699573.85	1002646.95
103517.94	750385.61	1198580.07	93061.86	585131.08	1205503.04
107732.23	668638.79	1120883.37	99871.59	591644.04	1054642.19
104700.85	641243.60	1151538.98	88664.96	657481.62	990112.45
97167.14	719540.49	1185877.57	91820.24	642317.82	1147646.43
103870.76	696442.68	1177824.35	93292.27	635229.68	1080110.21
% Recovery			89.82	91.21	91.70

Table 58: Presents the LC-MS/MS recovery data for the Internal standard (IS). The table includes IS areas for diluent and plasma samples across three quality control levels: Low Quality Control (LQC), Medium Quality Control (MQC), and High Quality Control (HQC). The % recovery values were calculated by comparing the plasma sample IS areas to the corresponding diluent sample areas with an acceptance criteria of 80-120%

Dilluent Sample			Plasma sample		
LQC	**MQC**	**HQC**	**LQC**	**MQC**	**HQC**
1065201.86	1710656.79	1636765.06	769889.07	1596778.12	1558569.02
940232.04	1656255.66	1694875.23	912982.15	1511968.08	1644568.22
1051548.10	1784887.06	1582512.04	961916.42	1517293.10	1585699.94
1171344.34	1697737.92	1549854.43	1051841.06	1579885.96	1593282.34
1066834.32	1708473.43	1589028.43	1073060.86	1541790.05	1654643.35
1059032.13	1711602.17	1610607.04	953937.91	1549543.06	1607352.57
% Recovery			90.08	90.53	99.80

Table 59: Presents the bench-top stability data for ANP estimation using LC-MS/MS. The analyte concentrations were evaluated immediately (baseline) and after 24 hours at three levels: 4.69 pg/mL (low), 37.5 pg/mL (medium), and 75 pg/mL (high). The % stability was calculated by comparing the concentrations after 24 hours to the baseline values, with acceptance criteria of 90–110%.

			After 24 Hours		
4.69	37.50	75.00	4.69	37.50	75.00
4.15	38.01	73.84	4.93	32.81	80.64
5.30	42.61	72.65	4.52	41.30	73.35
4.52	32.50	80.96	4.67	34.73	86.24
4.63	42.75	67.20	4.79	39.62	83.01
4.77	35.00	86.16	5.29	40.38	76.97
4.67	38.17	76.16	4.84	37.77	80.04
% Stability			103.55	98.94	105.09

Table 60: Presents the Auto-Sampler stability data for ANP estimation using LC-MS/MS. The analyte concentrations were evaluated immediately (baseline) and after 24 hours at three levels: 4.69 pg/mL (low), 37.5 pg/mL (medium), and 75 pg/mL (high). The % stability was calculated by comparing the concentrations after 24 hours to the baseline values, with acceptance criteria of 85–110%.

			AUTOSAMPLER AFTER 24 Hours		
4.69	37.50	75.00	4.69	37.50	75.00
4.15	38.01	73.84	5.34	36.19	68.99
5.30	42.61	72.65	4.52	35.29	76.43
4.52	32.50	80.96	4.95	32.91	71.93
4.63	42.75	67.20	4.96	32.13	73.96
4.77	35.00	86.16	4.13	33.81	75.54
4.67	38.17	76.16	4.78	34.07	73.37
% Stability			102.27	89.24	96.33

5.0.Conclusion:

The developed methods for the quantification of adrenaline, noradrenaline, aldosterone and ANP was validated successfully, showing high sensitivity, specificity, precision, and accuracy. These methods ensured reliable detection and quantification of the above-mentioned biomolecules in biological samples, supporting their application in clinical and research settings.

References:

[1] Goeders, N.E. The Impact of Stress on Addiction. *Eur. Neuropsychopharmacol.* **2003**, *13*, 435–441. https://doi.org/10.1016/j.euroneuro.2003.08.004.

[2] Richard, J.C.; Andrew, B. The Handbook of Stress Science: Biology, Psychology and Health; Springer Publishing Company: 2010

[3] Morilak, D.A.; Barrera, G.; Echevarria, D.J.; Garcia, A.S.; Hernandez, A.; Ma, S.; Petre, C.O. Role of Brain Norepinephrine in the Behavioral Response to Stress. Prog. Neuropsychopharmacol. Biol. Psychiatry 2005, 29, 1214–1224 https://doi.org/10.1016/j.pnpbp.2005.08.007.

[4] Fotopoulou, M.A.; Ioannou, P.C. Post-Column Terbium Complexation and Sensitized Fluorescence Detection for the Determination of Norepinephrine, Epinephrine, and Dopamine Using High-Performance Liquid Chromatography. *Anal. Chim. Acta* **2002**, *462*, 179–185

[5] 5 Bicker, J.; Fortuna, A.; Alves, G.; Falcão, A. Liquid Chromatographic Methods for the Quantification of Catecholamines and Their Metabolites in Several Biological Samples—A Review. *Anal. Chim. Acta* **2013**, *768*, 12–34

[6] Jones, J.C.; Carter, G.D.; Macgregor, G.A. Interference by Polar Metabolites in a Direct Radioimmunoassay for Plasma Aldosterone. *Ann. Clin. Biochem.* **1981**, *18*, 54–59.

[7] Schirpenbach, C.; Seiler, L.; Maser-Gluth, C.; Beuschlein, F.; Reincke, M.; Bidlingmaier, M. Automated Chemiluminescence-Immunoassay for Aldosterone during Dynamic Testing: Comparison to Radioimmunoassays with and without Extraction Steps. Clin. Chem. 2006, 52, 1749–1755

[8] Siekmann, L. Determination of Steroid Hormones by the Use of Isotope Dilution-Mass Spectrometry: A Definitive Method in Clinical Chemistry. *J. Steroid Biochem.* **1979**, *11*, 117–123

[9] Taylor, P.J.; Cooper, D.P.; Gordon, R.D.; Stowasser, M. Measurement of Aldosterone in Human Plasma by Semiautomated HPLC–Tandem Mass Spectrometry. Clin. Chem. 2009, 55, 1155–1162.

[10] Guo, T.; Taylor, R.L.; Singh, R.J.; Soldin, S.J. Simultaneous Determination of 12 Steroids by Isotope Dilution Liquid Chromatography-Photospray Ionization Tandem Mass Spectrometry. *Clin. Chim. Acta* **2006**, *372*, 76–82

[11] Hinchliffe, E.; Carter, S.; Owen, L.J.; Keevil, B.G. Quantitation of Aldosterone in Human Plasma by Ultra High-Performance Liquid Chromatography Tandem Mass Spectrometry. *J. Chromatogr. B* **2013**, *913*, 19–23

[12] Turpeinen, U.; Hämäläinen, E.; Stenman, U.-H. Determination of Aldosterone in Serum by Liquid Chromatography–Tandem Mass Spectrometry. J. Chromatogr. B 2008, 862, 113–118.

[13] Van Der Gugten, J.G.; Dubland, J.; Liu, H.-F.; Wang, A.; Joseph, C.; Holmes, D.T. Determination of Serum Aldosterone by Liquid Chromatography and Tandem Mass Spectrometry: A Liquid–Liquid Extraction Method for the AB SCIEX API-5000 Mass Spectrometry System. J. Clin. Pathol. 2012, 65, 457–462

[14] Ray, J.A.; Kushnir, M.M.; Palmer, J.; Sadjadi, S.; Rockwood, A.L.; Meikle, A.W. Enhancement of Specificity of Aldosterone Measurement in Human Serum and Plasma Using 2D-LC–MS/MS and Comparison with Commercial Immunoassays. J. Chromatogr. B 2014, 970, 102–107.

[15] Van Der Gugten, Jessica Grace, Matthew Crawford, Russell P. Grant, and Daniel T. Holmes. "Supported liquid extraction offers improved sample preparation for aldosterone analysis by liquid chromatography tandem mass spectrometry." *Journal of clinical pathology* 65, no. 11 (2012): 1045-1048.

[16] Das, B.B.; Solinger, R. Role of Natriuretic Peptide Family in Cardiovascular Medicine. Cardiovasc. Hematol. Agents Med. Chem. 2009, 7, 29–42.

CHAPTER-V

KHAMIRA GOZABAN SADA, A TRADITIONAL LOW-COST UNANI PREPARATION IN THE MANAGEMENT OF DOXORUBICIN-INDUCED CARDIAC HYPERTROPHY: AN *IN VIVO*, *IN VITRO* AND MOLECULAR DOCKING APPROACH

Khamira Gozaban Sada, a traditional low-cost Unani preparation in the management of Doxorubicin induced cardiac hypertrophy: an *in vivo*, *in vitro* and molecular docking approach

1. Introduction:

DOX is a well-known anti-cancer agent, notoriously famous for inducing cardiac hypertrophy as a severe adverse effect affecting its clinical benefit. Further, left ventricular (LV) dysfunction and congestive heart failure (CHF) are a few irreversible features of DOX-induced cardiomyopathy [1]. The occurrence of chronic heart failure is around 1-2% in a population comprising adults and more than 10% of people of age greater than 70 years. Among many reasons, cardiac hypertrophy is clinically responsible for chronic heart failure, where the former event is often an outcome of chronic hypertension, myocardial infarction and drug adverse effects. Around 11% of patients on DOX therapy experience acute cardiotoxicity. DOX-induced cardiotoxicity is reported to occur in 1.7% of the population [2]. Molecular mechanisms often suggested for DOX-induced cardiotoxicity include RAAS [3], Oxidative stress, inflammation, mitochondrial dysfunction, autophagy, apoptosis, endoplasmic reticulum stress and even Ca^{2+} overload[4]. Cardiac hypertrophy (CH) is often the cause behind the development of heart failure[5].

ACE inhibitors (ACEI) are a pharmacological class of drugs often used in clinical practice. They have demonstrated consistent and beneficial therapeutic effects in treating heart failure resulting from various cardiovascular disorders. ACEI exhibits properties of scavenging free radicals and acting as antioxidants. Recent prospective clinical studies have demonstrated its effectiveness in preventing heart failure caused by anthracycline [6]. Khamira Gozaban Sada (KGS) is a low-cost, traditionally used medication which has been utilised as a cardiac tonic (Muqavvi Qalb) and for treating palpitations (Khafqan). This is particularly relevant in the current context [7]. The novelty of this research work lies in identifying low-cost therapeutic approaches for cardiovascular diseases, specifically for the needs of the Indian subcontinental population. This study emphasizes the scientific validation of low-cost-evidence-based medication, aiming to benefit the larger population through reverse pharmacology. Unani practitioners/physicians in Indian Unani hospitals have long been clinically using KGS for patients with symptoms of “weak heart” (as per their

terminologies). After much discussion with these unani physicians, we infer that by the term "weak heart" they indicated cardiac failure.

Therefore, the current study was designed to confirm these therapeutic claims of KGS, a low-cost medication used as a cardioprotective preparation, as mentioned in ancient Unani literature, where DOX was used to induce cardiac hypertrophy in laboratory animals as per existing protocol[8]. Further metabolite profiling of KGS was conducted using LC-qTOF-MS to identify tentative metabolites and quantify two specific metabolites present in it. In this experiment, the tentative identified bioactive metabolites in KGS were verified for possible interaction with ACE using target ligand-receptor interactions (molecular docking score).

2. Experimental Section

2.1. Chemicals

GLS PHARMA LTD supplied DOX (Doxoget) (batch no-DRLB2206G) Captopril (CAS no-62571-86-2), KGS (batch no. MKH139B; Hamdard Laboratories (India)) was donated by The Calcutta Unani Medical College and Hospital, Kolkata. Rat ACE ELISA Kit (Cat.No.E-EL-R2401, Elabscience Biotechnology Company Limited., Texas, United States of America),. Rat ANG II (Angiotensin II) ELISA Kit (Catalog No.: MBS705139 MyBiosource; San Diego, USA). Thiobarbituric acid (TBA) (CAS no 504-17-6) was supplied from HIMEDIA, MDA (Sigma cas no.100683-54-3), 10% Trichloro acetic acid (Himedia cas no-76-03-9).Tris buffer, pH 7.4 (Merck cas no: No: 77-86-1), sucrose (Sigma cas no 57-50-1), EDTA(K) (Sigma cas no. 25102-12-9), Bradford Reagent (Himedia ML-106-100ML), Bovine serum Albumin (BSA) (SKU MB083-100G, Himedia), Acetonitrile (Mass grade) (Cas no - 75-05-8), Phosphate buffer (10x) (SRL Cat no. 78529), Methanol (Mass grade) (Cas no.- 67-56-1), Ethyl acetate (Cas no.- 141-78-6), Folin-Ciocalteu, Gallic acid (Cas no.- 5995-86-8), Sodium Carbonate (Cas no.- 497-19-8), Formic acid (Cas no.- 64-18-6), Ketamine (Cas no.- 1867-66-9), Xylazine (Cas no.- 7361-61-7), Thiopental sodium (Cas no. 71-73-8), noradrenaline (Sigma cat no: N1100000), Atrial Natriuretic peptide (Sigma cat no: SCP0022), Aldosterone (Sigma cat no: A9477), Standard Rosmarinic acid (Sigma Aldrich, Cas no. 20283-92-5) and Standard Trehalose (Sigma Aldrich , Cas no. 6138-23-4) were used in this experiment.

2.2. Maintenance of experimental animals

In this study, 8-9 weeks old male rats (wistar albino) weighing 150-180 gms sourced from WBLDC Ltd. Buddha Park, Kalyani, Nadia-741235 with FSSAI registration no: 10012031000104. The procured rats were maintained in cages (polypropylene) with tops made of stainless steel for adequate ventilation. An optimal environmental condition consisting of a 12-hour light/dark cycle, a temperature of 25 ± 2°C, and a relative humidity of 50 ± 20% was maintained for animals. The study received approval from the IAEC with CPCSEA registration no: 1805/CPCSEA via proposal no JU/IAEC-22-20.

2.3. Development of DOX induced cardiac hypertrophy Model in Rats

After a one-week period of acclimatisation, the animals were assigned to 5 distinct groups (n = 6)

Normal control: The rats were administered with distilled water for 4 weeks, and 0.9% saline solution, 1 ml/kg of b.w. (i.p.) given in the last 2 weeks.

DOX group: animals received distilled water for 4 weeks and also 2.5 mg/kg b.w. of DOX (i.p.) in 6 equivalent injections alternatively in the last 2 weeks totalling to 15 mg/kg b.w .

DOX+KGS Low Dose group: animals received KGS (1000 mg/kg b.w./day) orally for 4 weeks and DOX (i.p) given concurrently in the last 2 weeks (as in DOX group).

DOX+KGS High Dose group: animals received KGS (2000 mg/kg b.w./day) orally for 4 weeks and DOX (i.p) given concurrently in the last 2 weeks (as in DOX group).

DOX + Captopril group: animals received captopril (50 mg/kg b.w./day) orally for 4 weeks and also DOX (i.p) given concurrently (as in DOX group) for the last 2 weeks. The reason for the selection of this drug has been mentioned in the discussion part. b. w. of rats was recorded on day 0 and on the 4^{th} week until they received their last dose. After 24 hr of the last DOX dosing, SBP, ECG was performed and blood from retro-orbital plexus was collected [8,9].

2.4. Systolic blood pressure recording using non-invasive technique.

SBP of adult male rats was measured non-invasively as reported earlier [10] using the blood-pressure device NIBP 200A, Santa Barbara, CA, USA and data acquisition was carried out utilising MP36 software, Goleta, CA, USA. The blood pressure measurements were documented until a state of consistency and reproducibility was attained.

2.5. Recording of ECG signals in Rats.

The rats were anaesthetized with a dose of 60 mg/kg b.w. ketamine and 10 mg/kg b.w. xylazine. ECG was performed accompanied by data acquisition using reported method[7]. QT interval was recorded and QTc interval was determined by using Bazett's formula.

$$QTc = QT/\sqrt{RR'}$$

2.6. Plasma collection and assessment of circulating plasma biomarkers.

Blood samples were collected from the rat retro-orbital plexus and centrifuged at 3500 rpm for 10 minutes at 4°C. The plasma was mixed with a protease inhibitor cocktail to measure noradrenaline, aldosterone, and ANP using LC-MS/MS [7]**. A** 1:100 diluted solution was prepared with deionized water and the protease-inhibitor powder. Rat Plasma were preserved at -20 ^{o}C**.**

2.7. Analysis of rat plasma angiotensin II and angiotensin Converting Enzyme (ACE)

For assessing rat plasma Ang-II, ELISA kits from MyBioSource, San Diego, USA (Catalog No.: MBS705139) was utilised. For ACE evaluation in rat plasma ELISA kit from Elabscience Biotechnology Company Limited., Texas, United States of America was used (Cat.No.: E-EL-R2401). All the ELISA based evaluations were carried out as per manufacturer's instruction.

2.8. Collection and homogenization of heart for histopathology and biochemical Assay

Following the collection of blood, the animals were euthanized by delivering a lethal dosage of thiopental sodium intraperitoneally (i.p). The hearts of rats were removed, meticulously cleansed, and subsequently rinsed in ice-cold phosphate-buffered saline with a pH of 7.4.

Then, the rat's hearts from different groups were weighed and subsequently immersed in a 10% formalin solution for fixation for the purpose histopathological examination. Further, for biochemical evaluation, cardiac tissue was cut into pieces and then placed in an isolation medium consisting of 10 mM Tris, 1 mM EDTA(K), 320 mM sucrose, pH 7.4[11,12]. Further, the isolation medium containing chopped cardiac tissue was homogenized in ice using tissue homogenizer (IKA, T-10 Basic Ultra-Turrax). The obtained cardiac tissue homogenate was further evaluated for MDA.

2.9. LC-MS/MS based quantification of circulating biomarkers.

An LC-MS/MS triple-quadrupole quantification system possesses the capability to collect data with an exceptionally low limit of quantification. This is essential for monitoring small variations in the concentrations of hormones and neurotransmitters in the bloodstream after administering the experimental agents. Thermostatic autosampler (SIL-20AC) and binary pump (Shimadzu LC) were utilised for analysis. The Ab Sciex API-4000 QTRAP with an electrospray ionisation (ESI) source, connected to the LC (Shimadzu). The data was acquired using Analyst 1.6.3 (software). Using gradient mobile phases, A and B, an elution was carried out at a column temperature of 25 °C, a flow rate of 0.5 mL/min, and 10 µl of injection volume.

ESI was employed as the ionization source, analysing in both positive/negative ion modes. For curtain gas, N_2 was used for maintaining a constant pressure of 20.00 psig and GS1 (40.00 psig) and GS2 (45.00 psig) were used [7].

2.10. Heart weight / Tail length ratio:

The mass (g) of the extracted heart was determined by weighing it after it had been blotted dry with tissue paper and stored in ice-cold saline (0.9% w/v). The HW/TL ratio was employed to assess DOX-induced cardiac hypertrophy in all experimental groups. The length of the tail was noted in centimetres (cm)[11].

2.11. Isolation of mitochondria and TMP estimation:

Briefly, the cardiac homogenate was subjected to centrifugation at 1300g /10 mins/ 4^{o}C. The post nuclear supernatant was subsequently centrifuged at 17000g /10 mins/ 4^{o}C. After centrifugation, the crude mitochondrial pellet was obtained. The resuspension of crude mitochondrial pellet was completed in isolation buffer and loaded onto a discontinuous gradient concentration of sucrose (1.2-1.0-0.8 M). This was again centrifuged 100,000g/60 mins/ 4 ^{o}C. An enriched mitochondrial pellet thus obtained was again rinsed twice with isolation buffer and centrifuged at 10,000 g/ 10 mins/ 4 ^{o}C. Finally, the obtained mitochondrial pellet was resuspended in isolation buffer. The TMP was calculated spectrophotometrically using the Bradford Assay reagent in Spectramax M5 (molecular devices, LLC, USA) at 595 nm with the help of a calibration curve of BSA. For all centrifugation process Sorvall Mx 150+ micro-ultracentrifuge was used[12].

2.12. Cardiac MDA estimation:

The technique developed by Slater and Sawyer (1971) was utilised for the quantification of malondialdehyde (MDA) in heart tissue. The supernatant (2 ml) obtained from the homogenate was mixed with 2.0 ml of 10% w/v trichloroacetic acid (TCA). An ice bath was used for chilling the mixture for 15 mins and the precipitate thus obtained was isolated by centrifugation at 2500 rpm and 4 ℃. 2 ml of the mixture solution and 2.0 ml of prepared TBA were mixed together. After heating it to 80℃/ 10 mins (water bath) the resultant solution was eventually cooled to room temperature using an ice bath (5 mins). Finally, produced colour was evaluated at 532 nm in comparison to blank using Spectramax M5 (molecular devices, LLC, USA). Finally the result was expressed as nmol of MDA /mg protein[13].

2.13. Histopathological Study:

Using 10% neutral buffered formalin, the heart tissues were fixed. Hematoxylin and eosin (H&E) and Masson's trichrome staining were used on cardiac sections ranging in thickness from 3-5 µm. Histological images of the cardiac sections were acquired using EVOS®-XL imaging system at a magnification of 40x. The results of histopathology were expressed in terms of total myofibril, cardiac hypertrophy, inflammation and fibrosis, and these parameters were allotted scores ranging from 0 to 6. The images of the cardiac sections that were obtained were evaluated using image J software version 1.4 (NIH, USA)[14]. For total myofibril, a score of 0-2 meant severe, 2-4 moderate, 4-6-mild while for the other 3 parameters namely cardiac hypertrophy, inflammation and fibrosis 0-2 denoted mild, 2-4 for moderate and 4-6 severe.

2.14. Development of Solvent Systems and Preparation of KGS extract

In this study, we systematically selected different solvent systems to optimize the extraction of KGS so as to obtain a high percentage yield. 100 g of KGS was subjected to maceration in 5 different solvent systems, namely Ethanol (Et), Methanol (MeOH), Et: Water (1:1), MeOH: water (1:1) and only aqueous, kept for 24 hr with continuous shaking (Mini Rotary Shaker RS-12R Remi). The different fractions were filtered with the help of Whatman filter paper No.1. The collected filtrates were concentrated by using a rotary evaporator (CCA-1110, EYELA, Japan) [15]. The concentrated crude extracts thus obtained were stored at -20°C. The % yield of KGS in different fractions was estimated by utilizing the formula yield (%) = (weight of extraction/weight of dry sample) × 100.

2.15. Estimation of TPC

The TPC in KGS extracts was estimated by utilising the Folin-Ciocalteu spectrophotometric method, in which gallic acid acted as the reference standard. A 20 µL aliquot of KGS extract (10 mg/mL) was thoroughly mixed with 100 µL of Folin-Ciocalteu reagent. Following the mixing of 80 µL of 7.5% Na_2CO_3, the resulting mixture was vortexed again and eventually incubated for 30 mins/45°C. The absorbance of the resulting mixture was measured at 750 nm (Spectramax M5 spectrophotometer, Molecular Devices). The TPC was calculated as gallic acid (mg) equivalents (GAE) per gm of KGS [16].

2.16. Condition of Liquid Chromatography-Quadrupole Time-of-Flight Mass Spectrometry (LC-qTOF-MS)

Methanolic extract of KGS (2 µL injection volume) was analysed using an Agilent 1290 Infinity LC system paired with an Agilent 6530C Q-TOF mass spectrometer consisting of a dual Agilent Jet Stream (AJS) and ESI source. Chromatography-based separation was conducted on a column set at 40 °C, utilizing a gradient of aqueous solution (0.1% formic acid) and organic phase (methanol). The gradient started with 95% aqueous having 0.3 mL/min of flow rate, progressing to 70% organic from 8 min to 14 min, then returning to initial conditions i.e. 95% aqueous in the 15 min. The MS was conducted in negative ionization mode, covering a mass range of 100–3000 m/z and 1 spectrum/second of the acquisition rate. Source parameters included a gas temperature of 300 °C, gas flow rate of 8 L/min, sheath gas temperature of 350 °C, sheath gas flow of 11 L/min, nebulizer pressure of 35 psi, and a capillary voltage of 3500 V. Skimmer, fragmentor and octopole RF peak voltages were fixed at 65 V, 175 V, and 750 V, respectively. The real-time mass calibration was achieved with reference masses enabled at 112.9855, 966.0007, and 1033.9881 m/z. The detected masses were matched with Metline, which is an Agilent database. For the targeted MS/MS experiment, the mass range covered was 100-1000 m/z at a fixed collision energy of 10.00 eV with an acquisition rate of 12 spectra/s. Analysis of peaks and spectra was conducted with Mass Hunter Workstation B.06.00 (Agilent Technologies, 2012), and tentative compounds were identified.

2.17. Molecular docking studies

To analyse the binding interactions between the identified phytocompounds from KGS and the active pockets of Angiotensin Converting Enzyme (ACE) molecular docking simulation was conducted using the Libdock module of Discovery Studio 3.0 software, Dassault

Systèmes, San Diego, USA[17]. Following the identification and cleaning of the phytocompounds, the Discovery Studio 3.0 workspace was used to minimize energy using the "Prepare Ligands" programme. ACE X-ray crystallographic structures (PDB ID: 1O86) was taken from the Protein Data Bank (http://www.rcsb.org/pdb) and were optimized for docking analysis[18,19]. The optimization technique involves inserting hydrogen atoms, removing water molecules, and eliminating other non-interacting heteroatoms [20]. The CHARMm force field was utilized to represent the protein and ligand structures. Docking investigations were conducted using the standard LibDock module. The most superior ligand configurations are preserved following a concluding phase of energy reduction, which permits adaptability in the placements of the ligands. A widely accepted concept is that a LibDockScore of ≥90 suggests a higher affinity of the small molecule ligands with the receptor and possesses greater ease of binding[17].

2.18. Method development for Quantification of Rosmarinic acid and Trehalose in KGS

A single method was developed and validated for simultaneous determination of Rosmarinic acid and Trehalose in KGS using Triple Quadrupole LC-ESI-MS/MS (AB Sciex, API-4000). Tolbutamide was used as the internal standard (IS). Chromatographic separation was achieved on a Phenomenex Kinetex 5µ C18 100A (50 × 3 mm) column with a binary mobile phase consisting of 0.1% formic acid with 10 mM ammonium acetate in Milli-Q water (Phase A) and 0.1% formic acid in methanol (Phase B). The Shimadzu LC system with a total flow rate of 0.5 mL/min, coupled with the API 4000 triple quadrupole mass spectrometer was operated in negative ion mode. The LC method parameters included an injection volume of 10 µL, an autosampler maintained at 15°C, and a binary flow pumping system. The gradient elution program ranged from 10% of phase B from 0.01 to 1.20 minutes and then 90% from 1.50 mins to 2.70 mins and returned to the starting composition of 10% from 3 to 3.5 mins. Key parameters such as declustering potential (DP) for MS level while collision energy (CE) and collision cell exit potential (CXP) for MS2 level were carefully tuned for each compound. Detection was performed via multiple reaction monitoring (MRM) with optimized precursor and product ion transitions: Rosmarinic acid (DP: -20.00 v, CE:-23.00 v and CXP: -4.00 v) Q1→Q3 (359.0 m/z → 160.9 m/z); Trehalose (DP: -112.00 v, CE:-52.00 v and CXP: -4.00 v) (339.3 m/z → 182.9 m/z) and Tolbutamide (IS) (DP: -30.00 v, CE:-25.00 v and CXP: -4.00 v) (269.1 m/z → 170.1 m/z). Further, other parameters included Curtain gas at 30.0 psig, Temperature at 400°C, GS1 at 55.00 psig and

GS2 at 45.00 psig , Ihe (Interface heater) was kept on, capillary voltage: -4500.00 v, CAD (collisionally activated dissociation) : 8.00 v, EP (Entrance potential): -11.00v and FP (Focusing Potential): -400.00 were maintained. Sample preparation involved methanolic extraction of 1 mg KGS while calibration curves were established over the range of 2.34–150 ng/mL for Rosmarinic acid and 3.13–200 ng/mL for Trehalose. Quality control (QC) levels included LLOQ (Ros: 2.34 ng/ml, Trehalose: 3.13 ng/ml) LQC (Ros: 7.03 ng /ml, Trehalose: 9.38 ng/ml) MQC (Ros:56.25 ng/ml, Trehalose:75 ng/ml), and HQC (Ros: 112.5 ng/ml, Trehalose: 150 ng/ml) ensuring robust quantitation. The analytical procedure was executed with the help of Analyst 1.5 software, and performance characteristics demonstrated the method's reliability for simultaneous quantification of Rosmarinic acid and Trehalose.

3.0. Statistical Analysis:

The data in this article are represented as the mean ± SD. Statistical evaluation was conducted using GraphPad Prism 9.0 (Graph Pad, San Diego, CA, USA). Initially, one-way ANOVA was employed, followed by Tukey's test to compare the different groups. In order for the data to achieve statistical significance, $p < 0.05$ was considered.

4. Result:

4.1. Percentage Yield and TPC of KGS

The % yield (w/w) obtained after extracting KGS in 5 different solvent systems are given in Table 1. It was found that KGS methanolic extract showed a higher % yield of 5.8±0.81 (w/w) and TPC of 147.68±2.05 mg gallic acid/g KGS extract in comparison to other solvent systems.

Table. 1: Represents the %yield (w/w) and TPC of KGS

Sl.NO	Name of the Solvent System	Ratio	% Yield (w/w)	TPC as mg gallic acid/g KGS extract
1	Ethanol	1	2.1 ± 0.29	89.46±1.71
2	Methanol	1	5.8±0.81	147.68±2.05
3	Ethanol + Water	1:1	2.5±0.74	94.67±1.24
4	Methanol + Water	1:1	3.9±0.43	133.07±1.94
5	Water	1	2.8±0.66	39.64±1.07

4.2. KGS attenuates DOX-induced decreased b.w., Systolic blood Pressure and altered ECG parameters.

Figure 1A-D represents b.w. (Fig.1A), SBP (Fig.1B), QTc (Fig.1C) and HW/TL ratio (Fig.1D) measured in 5 different animal groups, namely control, DOX, DOX+KGS Low Dose, DOX+KGS High Dose and DOX + Captopril. The control group (non-significant), DOX+KGS High Dose(non-significant) and DOX + Captopril (non-significant) showed an increase in b.w. while the DOX ($p<0.01$) and DOX+KGS Low Dose (non-significant) group exhibited a decrease in b.w. on day 28 compared to day 0. A statistically significant ($p<0.001$) decrease in SBP, prolongation of QTc ($p<0.01$) and increased HW/TL ratio ($p<0.001$) in the DOX group compared to control was observed. The SBP significantly ($p<0.01$) increased in the DOX+KGS High Dose group while decreased ($p<0.01$) in the DOX+ Captopril group as compared to the DOX group. The QTc significantly reduced in the ($p<0.05$) DOX+KGS High Dose and ($p<0.01$) DOX+Captopril group compared to the DOX group. Similarly, the HW/TL ratio significantly ($p<0.05$) reduced in the DOX+KGS High Dose and ($p<0.01$) the DOX+Captopril group. The KGS Low Dose group showed non-significant changes with regard to SBP,QTc and HW/TL.

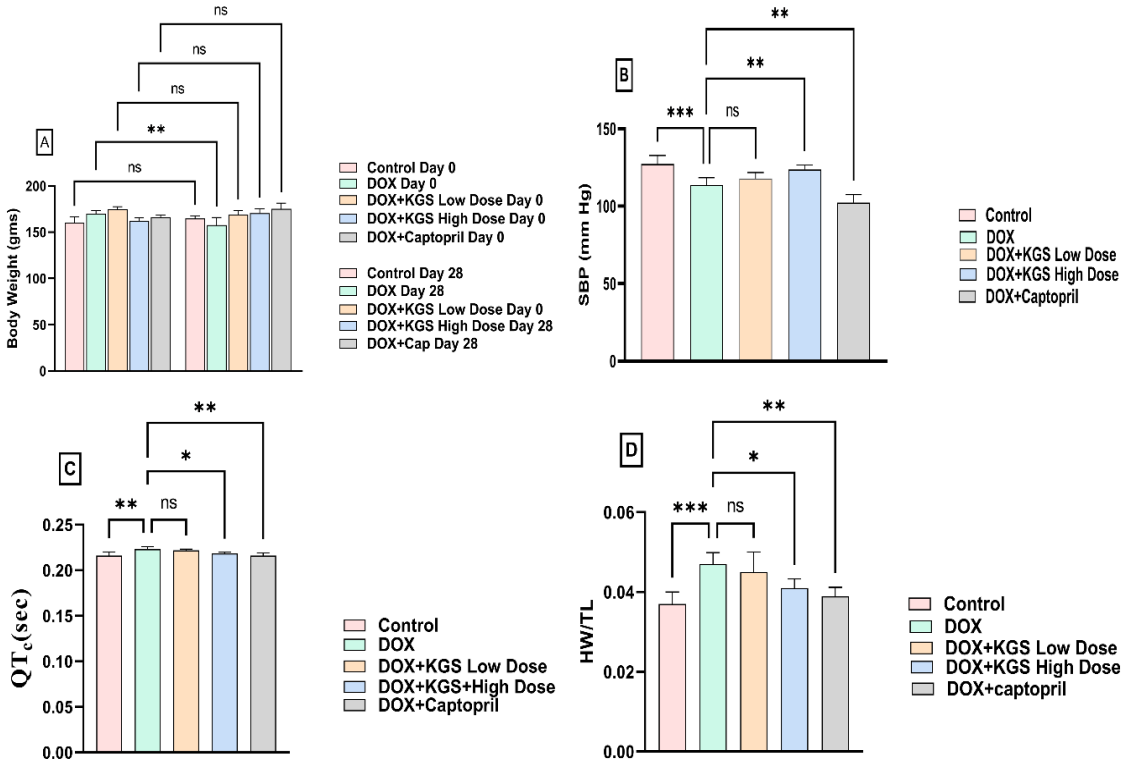

Figure 1: Represents (A) B.w. (B) SBP (C) QTc (D) HW/TL ratio of rats belonging to the Control, DOX, DOX + KGS Low Dose, DOX + KGS High Dose and DOX + Captopril groups. The statistically significant difference was denoted by ***$p<0.001$, **$p<0.01$,

*p<0.05, ns- non-significant. The b.w. of rats of each group on Day 0 was compared with b.w. on Day 28 of each group, while in the case of SBP, QTc and HW/TL ratio, the following comparisons were made Control Vs DOX group and DOX Vs DOX + KGS Low Dose, DOX Vs DOX + KGS High Dose and DOX Vs DOX+ Captopril group.

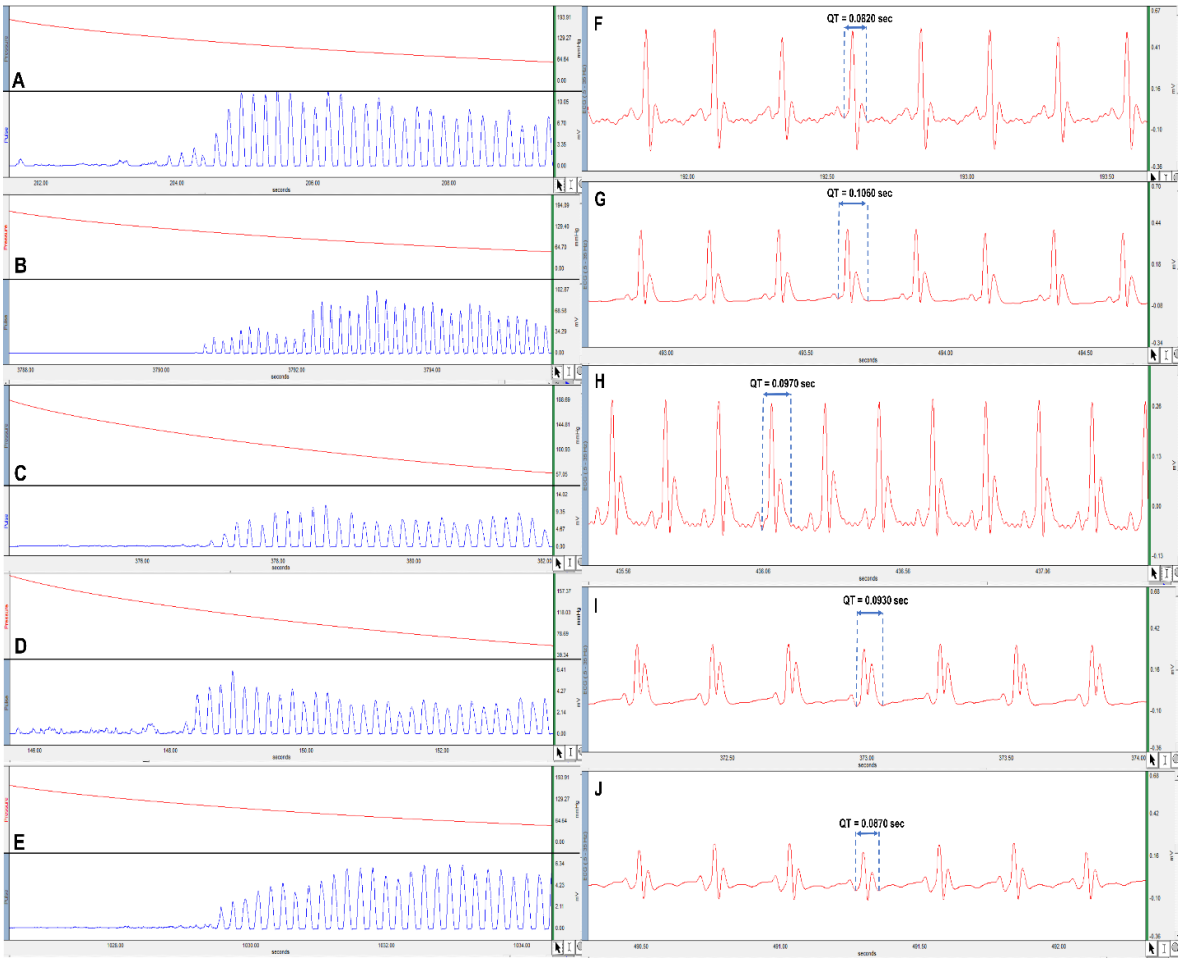

Figure 2: (A-E) Represents SBP, and (F-J) depicts ECG of rats showing QT interval where (A & F) is for the Control group (B & G) DOX group (C & H) DOX+KGS Low Dose group (D & I) DOX+ KGS High Dose group and (E & J) for DOX+Captopril group.

4.3. KGS attenuates DOX-induced cardiac MDA, TMP, plasma circulating biomarkers

Figure 3 represents a significantly ($p<0.01$) increased cardiac MDA (Fig 3A) and reduced ($p<0.001$) cardiac TMP (Fig 3B) in the DOX group when compared to control group. Further, a significantly ($p<0.05$) decreased cardiac MDA (both KGS low and high dose) and increased cardiac mitochondrial protein ($p<0.05$) was noted in the DOX +KGS High Dose and ($p<0.01$) DOX+Captopril group in comparison to the DOX group. For DOX+KGS Low dose, there was no significant change in TMP when compared to the DOX group.

Figure 3 shows circulating plasma biomarkers, namely plasma Angiotensin II, aldosterone, Noradrenaline, ANP and ACE in all the above-mentioned 5 animal groups. Plasma Ang-II ($p<0.001$) (Fig.3C), aldosterone ($p<0.01$) (Fig.3D), Noradrenaline ($p<0.01$) (Fig.3E), ANP ($p<0.001$) (Fig.3F) and ACE ($p<0.001$) (Fig.G) significantly augmented in the DOX group in comparison to the control group. All the above-mentioned evaluated plasma biomarkers significantly ($p<0.05$) decreased in the DOX+KGS High Dose group and DOX+Captopril group. The DOX+KGS Low Dose group showed non-significant changes in all the parameters mentioned above except cardiac MDA, where it exhibited a significant ($p<0.05$) decrease in comparison to the DOX group.

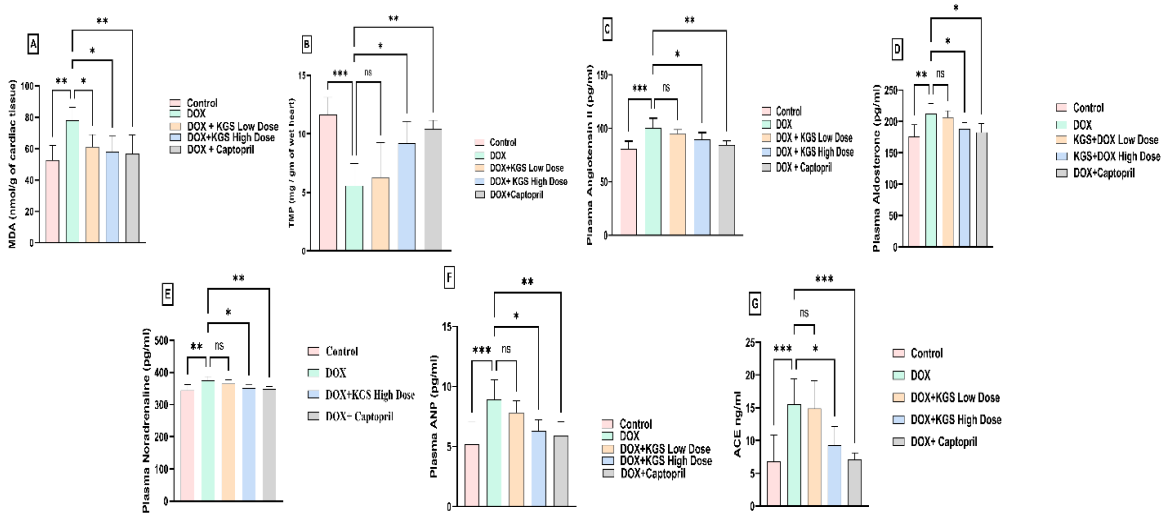

Figure 3: Represents (A) cardiac MDA level (B) TMP in the cardiac tissue of rat (C) Plasma Angiotensin II (D) Plasma aldosterone (E) Plasma Noradrenaline (F) Plasma ANP(G) Plasma ACE in the Control, DOX, DOX+KGS Low Dose, DOX+KGS High Dose and DOX+Captopril group. The comparison was made between Control Vs DOX group, DOX vs KGS+DOX Low Dose, DOX vs DOX+KGS High Dose group and DOX vs DOX + Captopril. The significance is denoted by ***$p<0.001$, **$p<0.01$, * $p < 0.05$.

4.4. KGS attenuates DOX-induced histopathological changes

Figure 4 represents H & E (fig 4A-4E) and massons's trichome (Fig.5F-5J) stained cardiac section of rats belonging to the Control, DOX, DOX+KGS Low Dose, DOX+KGS High Dose and DOX+Captopril groups. In these figures (Fig 4A-E), alterations in the 4 histopathological parameters, namely total myofibril, cardiac hypertrophy, inflammation and fibrosis, were labelled and shown. The variation in these 4 parameters was represented in fig.4K (total myofibril and cardiac hypertrophy) and Fig.4L (inflammation and fibrosis)

using histopathological scores ranging from 0 to 6. The total myofibril (Fig.4K) significantly ($p<0.001$) decreased while inflammation (Fig. 4L), fibrosis (Fig. 4L) and cardiac hypertrophy (Fig. 4K) significantly ($p<0.001$) augmented in the DOX group in comparison to the control. Furthermore, there was a significant ($p<0.05$) increase in the total myofibril and a decrease in cardiac hypertrophy, inflammation and fibrosis ($p<0.05$) in the DOX+KGS High Dose and ($p<0.01$) DOX+Captopril group compared to the DOX group. The DOX+KGS Low dose group showed statistically non-significant changes.

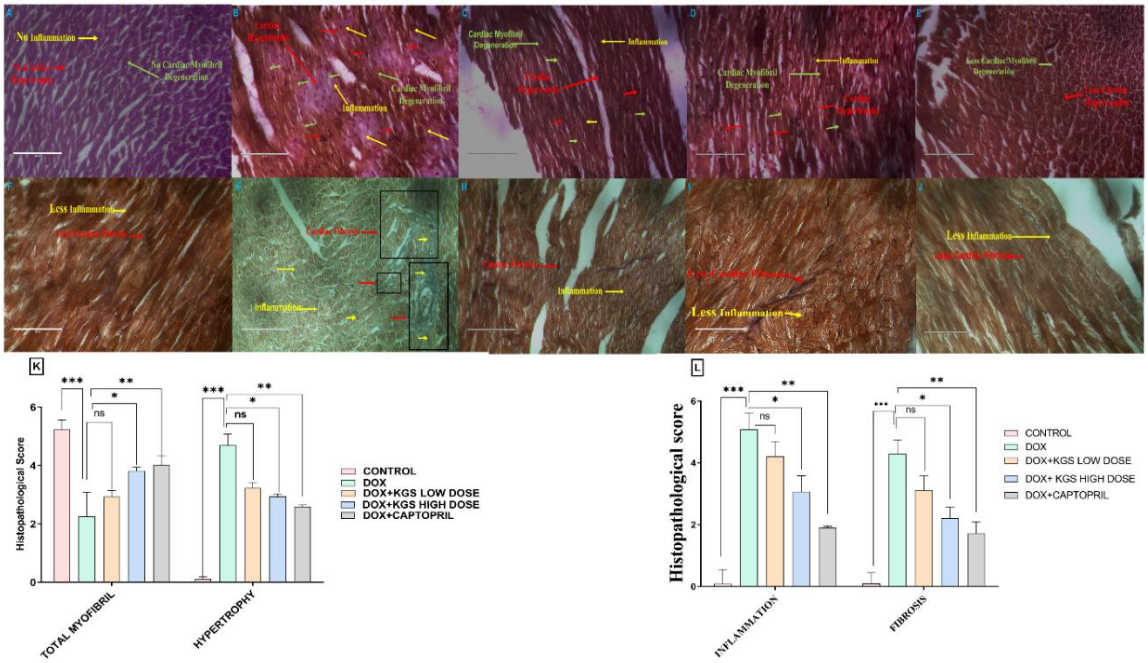

Figure 4: (A)-(E) represents histopathology of rat cardiac section stained with H & E where (A) represents the Control group (B) DOX group (C) DOX+KGS Low Dose group (D) DOX+KGS High Dose group (E) DOX+Captopril group while (F)-(J) represents Masson's Trichrome stained cardiac section in similar order. K represents total myofibril and cardiac hypertrophy, while L expresses inflammation and fibrosis of the 5 groups using a histopathological score. For K and L, statistical comparison was made between control vs DOX, DOX vs DOX+KGS High Dose group and DOX vs KGS Low Dose group and DOX vs DOX+Captopril. The level of statistical significance is denoted by ***$p<0.001$, **$p<0.01$, *$p<0.05$, ns- non-significant. Here, Red color denotes cardiac hypertrophy, Green- myofibril, yellow-Inflammation and Blue-cardiac fibrosis

4.5. LC-qTOF-MS-based metabolic profiling of KGS

The metabolites present in the KGS methanolic extract were analyzed with the help of LC-qTOF-MS in negative mode as shown in Table 2. Our analysis revealed that the metabolites detected in the methanolic extract of KGS were primarily phenolic acids, flavonoids, non-reducing sugars, fatty acids and organic acids. A list of 30 identified metabolites present in KGS has been mentioned in the table, along with its chromatogram in Figure 5. The obtained MS/MS fragmented masses of each metabolite obtained at a collision energy of 10.0 eV are also mentioned in table 2.

Table 2: Represents the LC-qTOF-MS based metabolite profiling of methanolic extract of the KGS.

Identity of the chemical moiety	**Class of the compound**	**Formula of the compound**	**Exact mass**	**Obtained m/z**	**Retention time (min)**	**Mass error (ppm)**	**Score**	**ms/ms fragment**
Trehalose	Non-reducing sugar	$C_{12}H_{22}O_{11}$	342.1161	341.1090	1.205	-0.23 .	99.86	221.0679, 179.0568, 161.0462, 19.0359
Tiliroside	glycosidic flavonoid	$C_{30}H_{26}O_{13}$	594.1363	593.1291	8.697	-1.69	94.36	551.0587, 499.1231, 445.137 397.0794 313.0751 275.0556 248.9577 221.071 165.975 130.944 100.9306
syringic acid	phenolic acid	$C_9H_{10}O_5$	198.052	197.0451	1.571	-4.33	93.95	177.1739, 151.4284, 133.6462
Rutin	Flavonoid	$C_{27}H_{30}O_{16}$	610.153	609.1458	7.332	-0.61	94.92	573.1369, 552.2641, 534.2501, 492.2419, 475.1781, 417.1146, 381.1819, 341.0942, 304.1757,

Identity of the chemical moiety	**Class of the compound**	**Formula of the compound**	**Exact mass**	**Obtained m/z**	**Retention time (min)**	**Mass error (ppm)**	**Score**	**ms/ms fragment**
								286.1660, 248.9630, 202.9987, 184.1334, 161.0439 101.0245
Rosmarinic acid	Polyphenolic acid	C_{18} H_{16} O_8	360.084	359.0767	5.85	-1.41	99.12	358.8499 310.1521 272.9934 203.0881 161.0153 100.9355
Rhoifolin or apigenin 7-O-β-neohesperidose	glycosidic flavonoid	C_{27} H_{30} O_{14}	578.1626	623.1607	7.931	-1.71	97.09	605.6889, 556.8641, 519.1540, 470.9122, 381.1871, 323.0724, 284.0963, 248.9658, 233.0366, 197.9558, 168.4002, 130.9411, 112.9867
Quinic acid	cyclitol	C_7 H_{12} O_6	192.062	251.0774	1.122	-7	98.5	206.9167 162.9309

Identity of the chemical moiety	**Class of the compound**	**Formula of the compound**	**Exact mass**	**Obtained m/z**	**Retention time (min)**	**Mass error (ppm)**	**Score**	**ms/ms fragment**
								114.988
Quercetin-3-O-glucoside (Isoquercetin)	glycosidic flavonoid	$C_{21}H_{20}O_{12}$	464.0967	463.089	6.782	2.55	93.83	419.0239 369.1615 301.0360 279.0890 243.0309 151.9135 112.9813
Palmitoleic acid	fatty acid	$C_{16}H_{30}O_2$	254.2242	313.238	12.99	-1.54	98.46	272.9333 216.9341 115.1448
Myristic acid	saturated fatty acid	$C_{14}H_{28}O_2$	228.2084	287.2223	10.86	-2.32	85.18	243.1381 190.9417 171.1025 102.9548
Lauraldehyde or dodecanal	long-chain fatty aldehyde	$C_{12}H_{24}O$	184.1824	243.1961	10.21	-1.87	97.68	222.5046, 196.9733, 181.1105, 109.8622
Isorhamnetin 3-O-beta-glucopyranoside-7-O-alpha-rhamnopyranoside	Glycosidic flavonoid	$C_{28}H_{32}O_{16}$	624.1681	623.1607	7.931	-1.53	97.2	616.7558, 571.1562, 517.2164
Isorhamnetin 3,7-diglycosides	Glycosidic flavanoid	$C_{27}H_{30}O_{15}$	594.1574	593.1503	7.848	-1.77	96.99	551.0587, 499.1231,

Identity of the chemical moiety	**Class of the compound**	**Formula of the compound**	**Exact mass**	**Obtained m/z**	**Retention time (min)**	**Mass error (ppm)**	**Score**	**ms/ms fragment**
								445.1370, 497.0794, 313.0751, 275.0556, 221.0710, 165.9750, 130.9440, 100.9306
Inositol	Cyclohexitol	$C_6 H_{12} O_6$	180.0637	225.0618	1.138	1.5	97.1	210.9493 182.9533 138.9660
Icariside B2	megastigmane glucoside	$C_{19}H_{30} O_8$	386.1923	431.1911	6.233	-4.48	93.77	395.1415 339.1342 275.1075 146.0832 112.9848
Hispidulin	Flavonoid	$C_{16}H_{12} O_6$	300.0628	359.0767	5.85	-1.8	99.12	355.3205 220.6994 194.9959 177.1744 167.2582 159.3538 133.6453 115.7195
Eupafolin	Flavonoid	$C_{16}H_{12} O_7$	316.058	315.0507	8.813	-0.83	99.29	311.7611 296.8930 293.7764

Identity of the chemical moiety	**Class of the compound**	**Formula of the compound**	**Exact mass**	**Obtained m/z**	**Retention time (min)**	**Mass error (ppm)**	**Score**	**ms/ms fragment**
								240.6196
d-Tartaric acid	Carboxylic acid	$C_4H_6O_6$	150.0158	149.0087	1.055	-3.93	85.61	149.0085
Cosmosiin or Apigenin 7-O-glucoside	Glycosidic flavanoid	$C_{21}H_{20}O_{10}$	432.1051	477.1034	7.481	-1.16	99.33	443.2437 385.2088 340.1787 317.0597 286.9704 262.4718 220.8345 181.0105 130.9440 112.9833
Caffeic acid	Polyphenol	$C_9H_8O_4$	180.0423	179.0349	2.637	0	99.15	290.0958, 177.1738, 134.6047, 111.8541
Aureusidin	Aurone/ flavonoid	$C_{15}H_{10}O_6$	286.0478	285.0404	9.213	0.08 .	98.41	282.0674,264.1298,238.608, 195.0842,179.2176,149.436, 111.9282
Astragalin (kaempferol 3-O-glucoside)	Flavonoid	$C_{21}H_{20}O_{11}$	448.1025	447.095	7.848	4.3	89.28	442.4617 264.1035
Aromadendrin 4'-glucoside	Flavanoid	$C_{21}H_{22}O_{11}$	450.1156	449.1083	6.233	-1.31	98.13	444.5273, 408.8262,

Identity of the chemical moiety	**Class of the compound**	**Formula of the compound**	**Exact mass**	**Obtained m/z**	**Retention time (min)**	**Mass error (ppm)**	**Score**	**ms/ms fragment**
								143.7824, 127.6102
Apigenin	Flavanoid	$C_{15}H_{10}O_5$	270.0525	315.0507	8.813	-1.03	99.4	311.7611,296.8930,293.7764,240.6196
8-Hydroxyluteolin 4'-methyl ether 8-glucoside	Flavonoid	$C_{22}H_{22}O_{12}$	478.1107	477.1034	7.481	-0.97	99.33	472.1055, 426.7096
4-Hydroxycinnamic acid	Non-flavonoid phenol	$C_9H_8O_3$	164.0475	163.0401	5.6	1.02	86.29	161.3663
1,5 dihydroxyxanthone	polyphenolic	$C_{13}H_8O_4$	228.0421	287.0557	7.315	-0.85	91.88	284.0717, 240.5335,159.3537
Dihydrokaempferol	Flavonoid	$C_{15}H_{12}O_6$	288.0632	287.0557	7.315	-0.67	91.88	284.0778
gamma-Linolenic acid	fatty acid	$C_{18}H_{30}O_2$	278.2234	277.2168	14.67	-4.19	98.87	274.3243, 254.1898, 230.7238, 202.9096,184.4413,115.7174
Homoplantaginin	flavonoid	$C_{22}H_{22}O_{11}$	462.1162	461.1089	7.931	-0.04	99.94	456.2788,325.6287

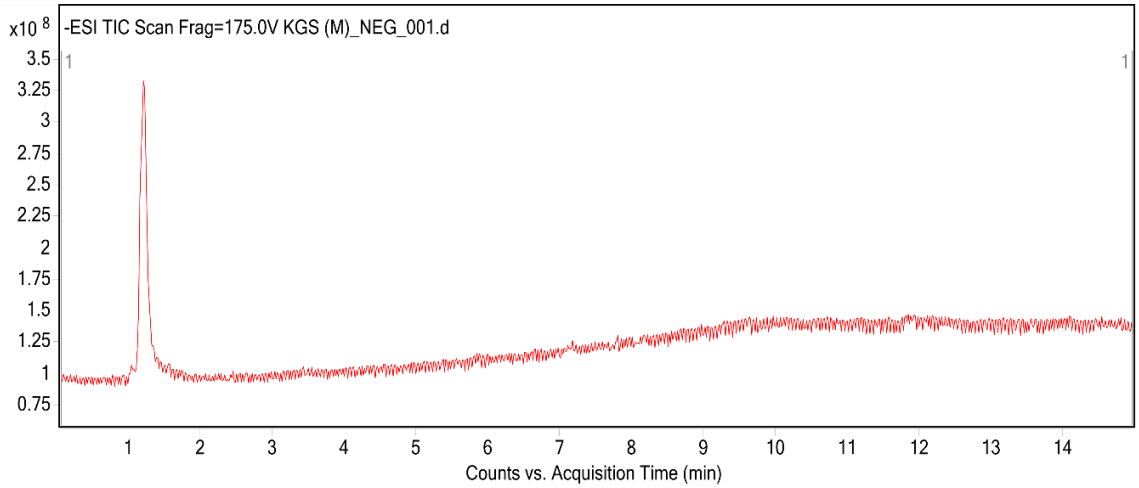

Figure 5: The figure represents the Total Ion chromatogram (TIC) from the LC-qTOF-MS-based metabolite profiling of KGS methanolic extract.

4.6. Ligand-Receptor Interaction analysis of bioactive metabolites in KGS

The docking results were evaluated using the LibDock score as the screening criterion. The LibDock score obtained against ACE (1O86) and the five best active constituents present in methanolic extract of KGS are shown in Figure 6.

Tiliroside LibDock score with ACE was higher than that of other active compounds (Table 3). The interactive amino acids of the macromolecules, along with their interactions viz. conventional -H Bond and hydrophobic interactions, are also shown (Figure 6G). Tiliroside, Rosmarinic acid, Cosmosiin, aromadendrin 4'-glucoside and rhoifolin were found to be the most stable compounds among other phytoconstituents obtained from KGS methanolic extract (Table 2). The most interactive amino acids were found to be TYR523, HIS353, VAL518, GLU384, HIS383 with 8.4179, 8.3164, 7.5713, 7.2133 and 6.4150 occurrence frequency (in %), respectively, according to ligand pose analysis (Figure 6G). The most predominant interactions in this analysis were found to be favourable (46.928 %), hydrogen (32.336 %) and followed by hydrophobic bond interactions (13.822 %) (Figure 6H). Heatmap analysis of the ligands and the active site amino acids of ACE indicated the involvement of different interactions with 59 amino acid residues. TRP220, ASP415, and GLN530 showed a predominantly favourable interaction. Meanwhile, ASP415, TRP220, and SER516 were found to interact with the ligand molecules with the most occurring hydrogen interactions. Besides, GLN530, THR166, and TRP220 amino acids interacted with the ligands through hydrophobic interactions (Figure 6I), resulting in activity. The docking result of the rest 25 metabolites is mentioned in the supplementary file.

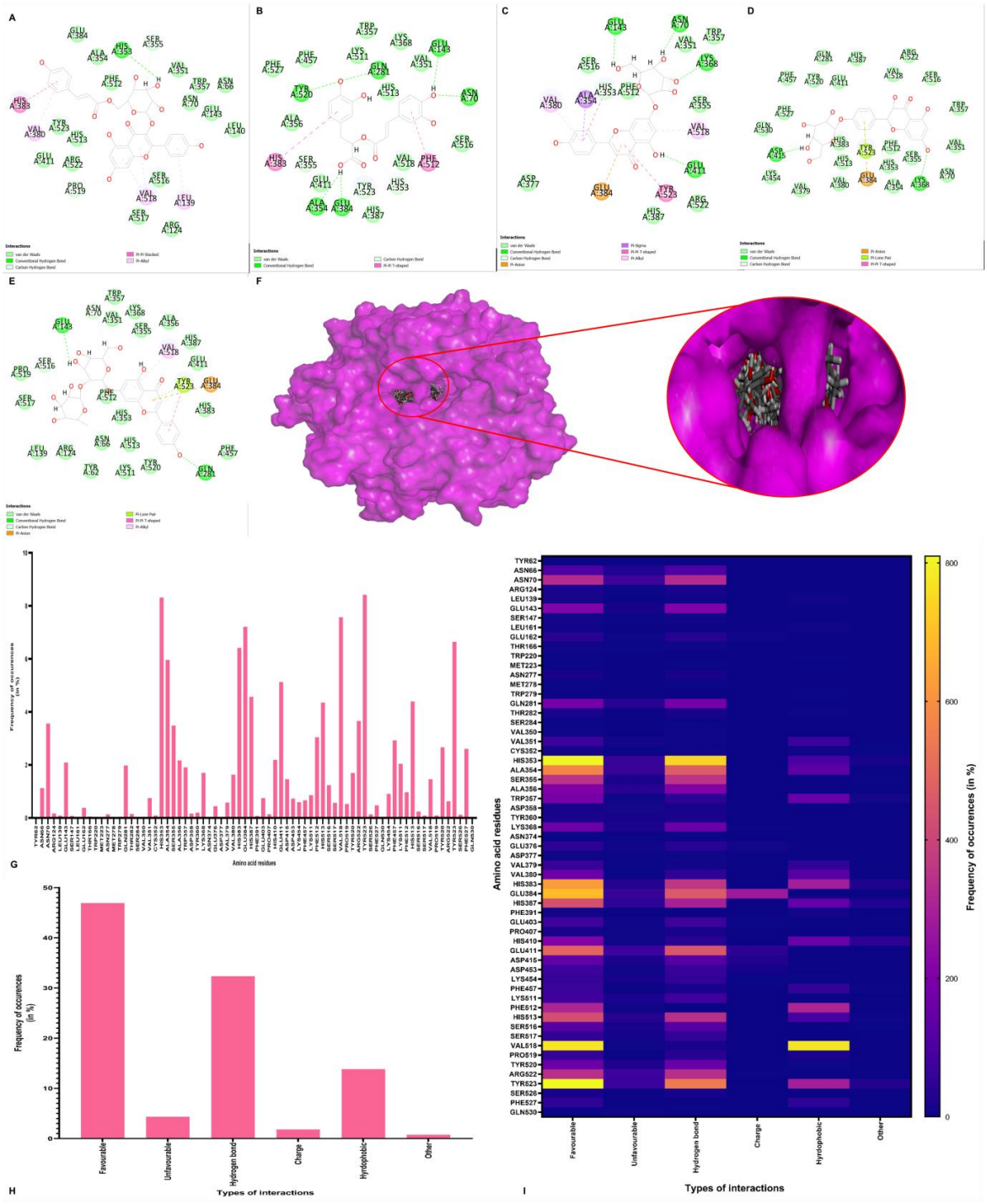

Figure 6: Docking analysis of the most active components with ACE where A. Tiliroside, B. Rosmarinic acid, C. Cosmosiin, D. aromadendrin 4'-glucoside E. rhoifolin, F. 3D docking representation of ACE with tentative bioactive metabolites obtained from KGS methanolic extract. G. represents most interactive amino acids present in the active sites of ACE found to interact with the ligands, H. Types of interactions between ACE and ligands, I. Heatmap analysis of the ligands and the active site amino acids of ACE.

Table 3: Docking analysis of the most active components with ACE.

Phytocomponents	ACE (1O86) activity		
	Libdock Score	Conventional -H Bond	Hydrophobic interactions
Tiliroside	146.864	HIS A:353	VAL A:518(2), LEU A:139, VAL A:380, HIS A:383
Rosmarinic acid	142.306	GLU A:173, ASN A:70, GLN A:281, TYR A:520, ALA A:354, GLU A:384	PHE A:512, HIS A:383
Cosmosiin	137.113	GLU A:143, ASN A:70, LYS A;368, GLU A:411	VAL A:518, ALA A:354, VAL A:380, HIS A:353, GLU A:384, TYR A:523
Aromadendrin 4'-glucoside	135.613	LYS A:368, ASP A:415	TYR A:523, GLU A:384
Rhoifolin	134.738	GLU A:143, GLN A:281	VAL A:518, GLU A:384, TYR A:523(2)

4.7. Quantification of Rosmarinic acid and Trehalose in KGS

Both Rosmarinic acid and Trehalose was quantified in KGS. Rosmarinic acid and Trehalose was found to be 0.110±0.017 and 0.077±0.005 mg/gm of KGS (table 4).

Table 4: Content of Rosmarinic acid and Trehalose in the KGS

SL.NO	Name of the quantified Chemical compound in KGS	Content in mg / gm of KGS
1	Rosmarinic Acid	0.110±0.017
2	Trehalose	0.077±0.005

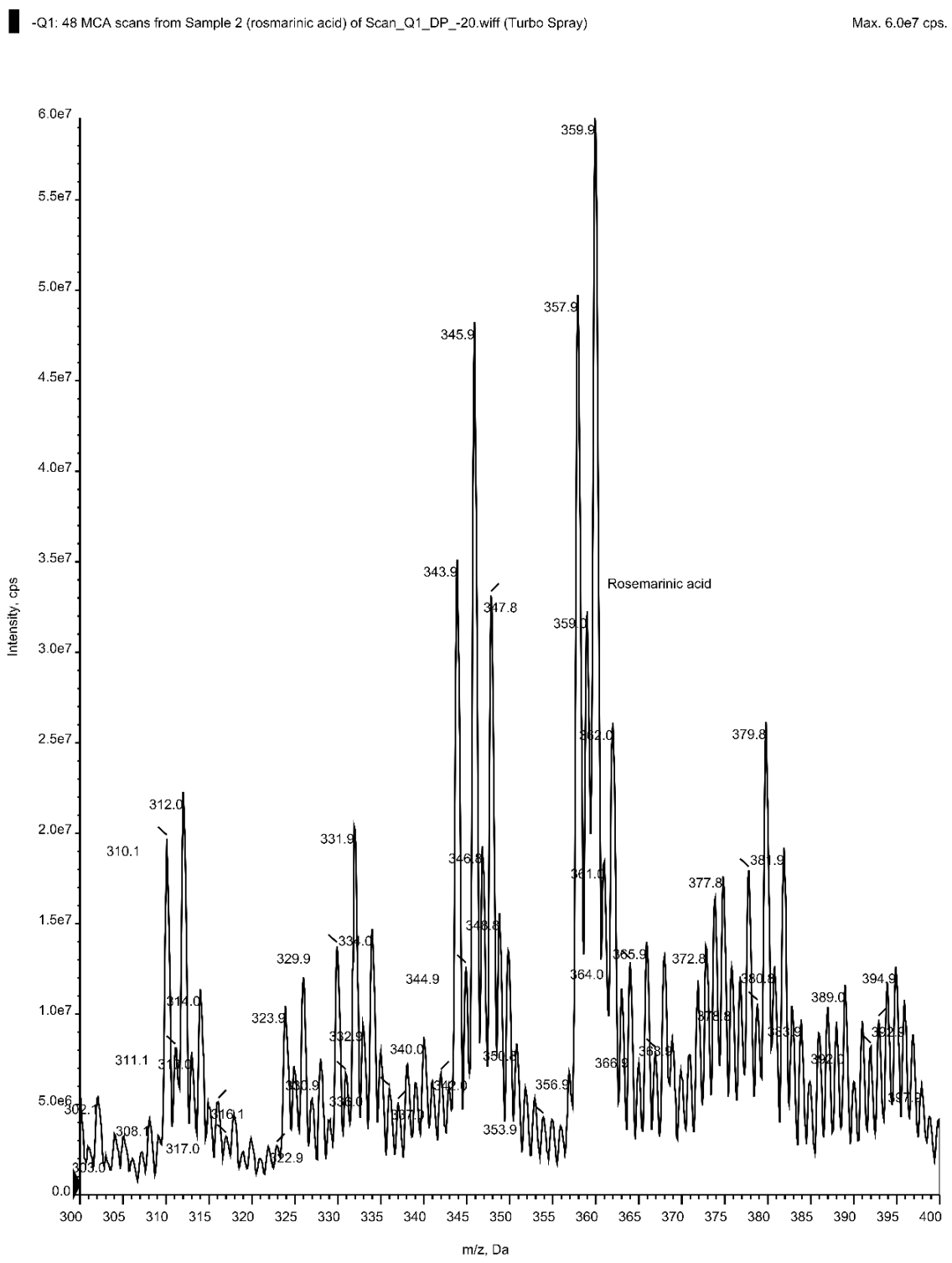

Figure 7A: Represents the parent ion (Q1) scan of KGS from 300 m/z Da to 400 m/z Da highlighting the Q1 mass of Rosmarinic acid.

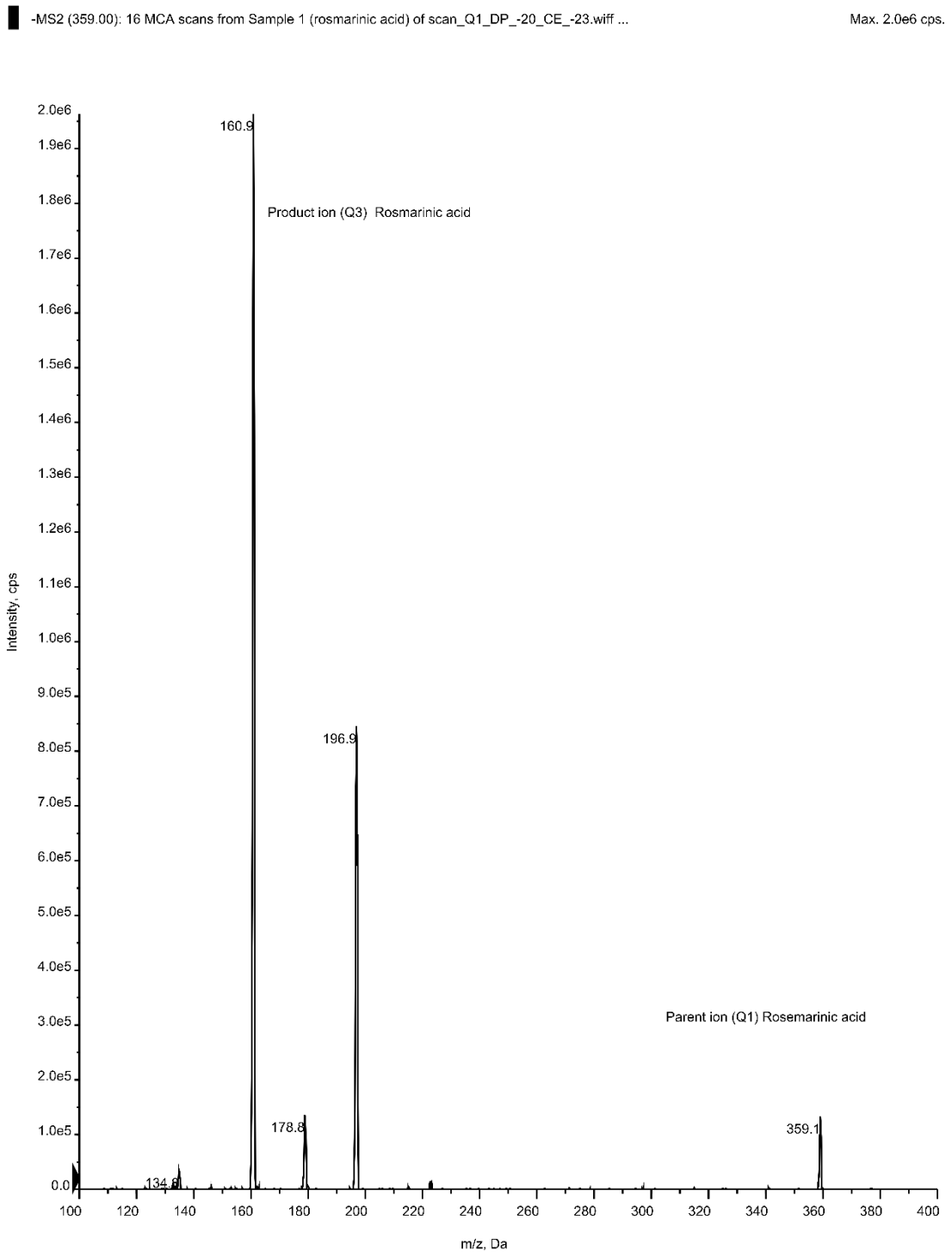

Figure 7B: Represents the Q3 scan of KGS from 100 m/z Da to 400 m/z Da highlighting the Q3 mass of Rosmarinic acid.

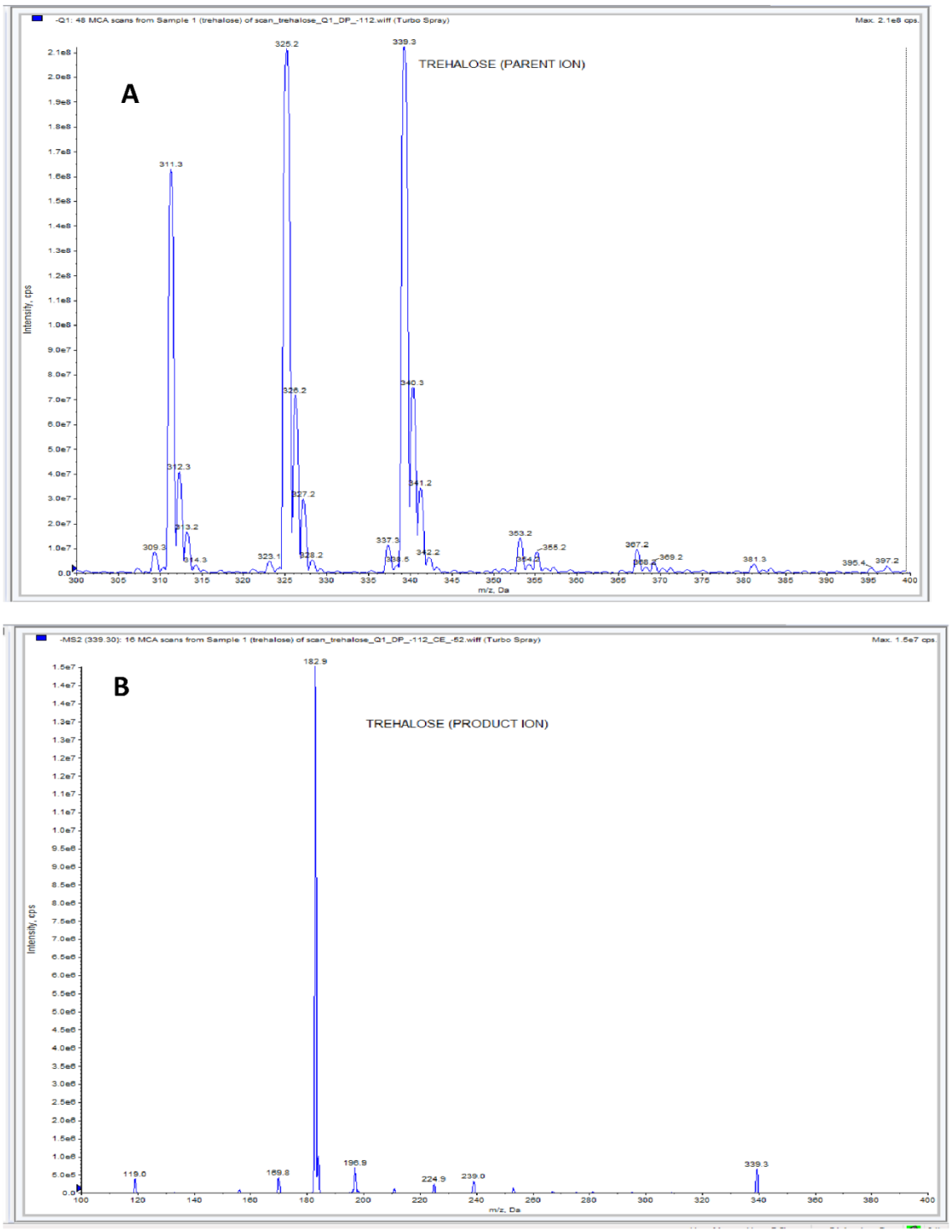

Figure 8: Represent the (A) Q1 scan from 200 to 400 m/z Da showing Q1 mass of Trehalose in KGS while (B) shows the Q3 scan of KGS from 100 to 400 m/z Da showing Q3 mass of Trehalose in KGS

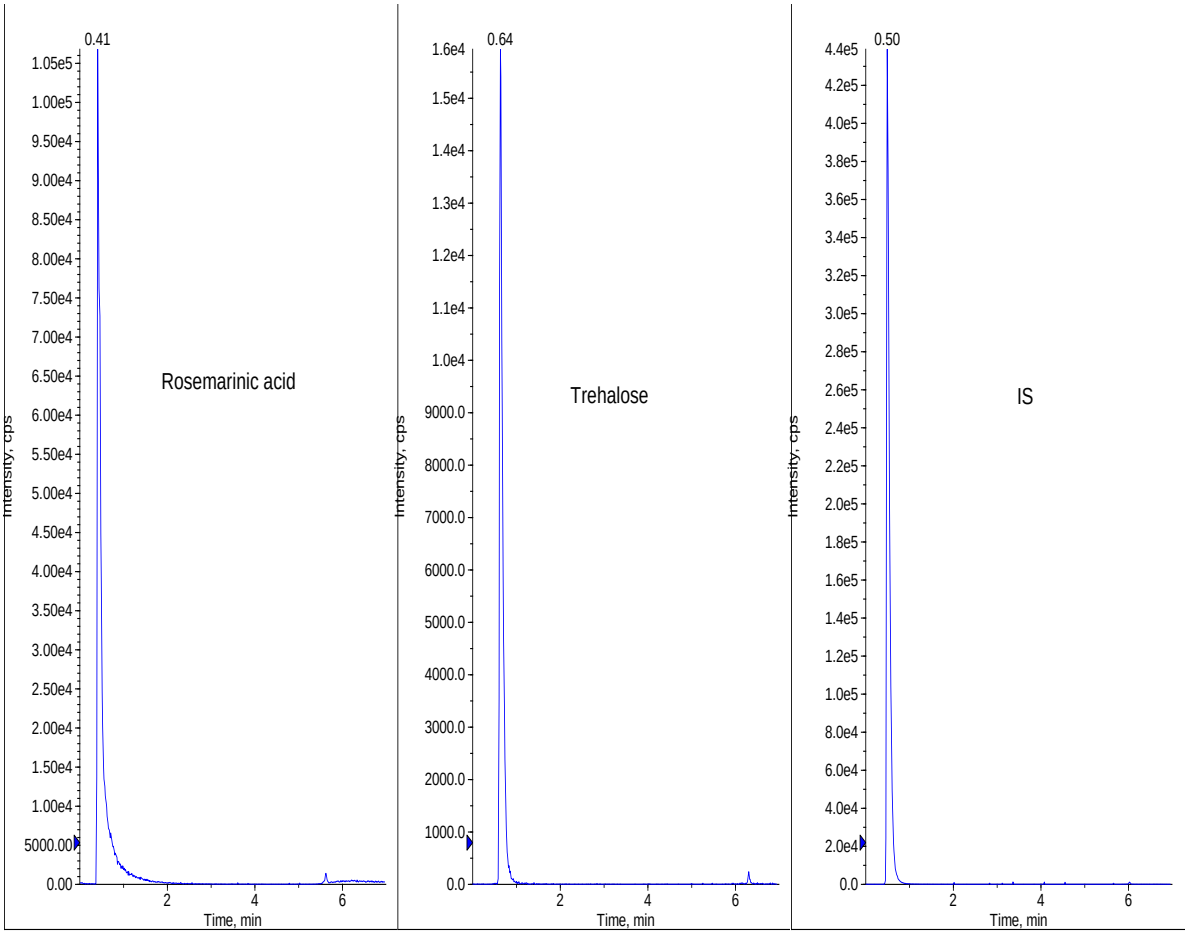

Figure 9: Represents the MRM of Rosmarinic acid, Trehalose and Tolbutamide (IS) in negative mode

4.7.1. Method Validation of Rosmarinic acid and Trehalose

As per International Conference on Harmonization Guidelines the above-mentioned quantitative method was validated through linearity, LOQs and LODs, precision, stability, and recovery estimation. The validation results were listed in Table 5, which depicts the correlation coefficient from 0.9947 to 0.9950 indicating high level of reproducibility. The findings indicated that the minimum concentration levels for reliable detection (LODs) and quantification (LOQs) of the analyte ranged from 0.05 to 2.34 ng/mL and 0.21 to 3.13 ng/mL, respectively, demonstrating the high sensitivity of this method. The % RSDs for intra-day precision and inter-day precision were recorded at less than 3.59% and 3.83%, respectively. In the case of stability and recovery of all the components, the % RSDs were less than 3.42%, and 2.82%, respectively. These data indicate that the developed LCMS/MS

method is precise, accurate, and sufficiently sensitive enough to quantify both compounds in KGS samples simultaneously.

Table 5: Represents the Regression equation, correlation coefficients, ranges of linearity and lower limit of detection (LOD) and Lower limit of quantitation (LOQ), Interday and intraday precision, stability and Recovery % RSD for the reference analytes.

Analytes used in the experiment	Regression equation	R^2	Linear range (ng/ml)	LOD (ng/ml)	LOQ (ng/ml)	Precision		Stability (RSD) n=5	Recovery % RSD
						Intra day	Interday		
Rosemarinic acid	Y=0.00216X+0.00166	0.9947	2.34-150	0.05	2.34	7.38	3.59	3.42	0.616
Trehalose	Y=0.00136X+0.00201	0.9950	3.13-200	0.21	3.13	3.83	4.18	2.82	2.996

5. Discussion:

It has been mentioned earlier that the current study was designed in pursuit of low-cost evidence-based traditional unani preparation and to confirm therapeutic claims as mentioned in ancient Unani literature where KGS preparation is being used as a cardio-protectant. To induce cardiac hypertrophy in laboratory animals, DOX was used as per the existing protocol. In the present investigation, KGS was observed to induce cardio-protective activity by attenuating impaired heart functions caused by DOX-induced cardiac hypertrophy. KGS's high dose significantly reduced DOX-induced abnormalities in SBP, b.w., QTc, HW/TL ratio, MDA, and circulating plasma biomarkers (mentioned in the method and result section). KGS high dose exhibited a reduction of DOX-induced histopathological changes and prevented DOX-induced cardiac mitochondrial protein loss. KGS low dose, as per our investigation, was unable to significantly mitigate DOX-induced cardiac hypertrophy. Out of the 5 different fractions, the % yield and TPC were best found in methanol. Further, metabolic profiling of the methanolic extract of KGS revealed tentative compounds such as Tiliroside, Rosmarinic acid, Cosmosiin; Aromadendrin 4'-glucoside and Rhoifolin, apart from other detected bioactive metabolites. Out of the 30 probable detected bioactive metabolites, the 5 compounds mentioned above showed acceptable interaction with ACE. Among these, Tiliroside showed the best interaction with ACE in molecular docking studies. LC-MS mediated quantification of Rosmarinic acid and Trehalose in KGS was carried out.

5.1. KGS attenuates DOX-induced decreased Systolic Blood Pressure and altered ECG parameter.

The weight loss in the DOX group (Fig 1A) rats is a characteristic of the oxidative stress of DOX, which culminated in heart failure[21]. Animals administered with DOX+ KGS high dose did not exhibit decreased b.w, suggesting protection against DOX toxicity, while the b.w. decreased in KGS low dose. The reason might be that the antioxidant activity of the polyphenolic contents of KGS protects against the oxidative stress of DOX. The observed decreased SBP (Fig 1B & 2G) and increased HW/TL ratio (Fig. 1D) in the DOX group probably indicate a negative inotropic effect with a possible correlation to increased cardiac mass owing to cardiac hypertrophy.

A probable reason for the lowering of SBP due to DOX treatment might be related to a decrease in total peripheral vascular resistance since earlier reports suggest DOX induces endothelial dysfunction[22]. Further, DOX is also known to cause myocardial dysfunction and disruption of calcium homeostasis, eventually leading to a negative inotropic effect on the heart[23]. The observed reduction in SBP in the DOX group might be due to the onset of cardiac hypertrophy[24], which is probably prevented by the presence of KGS in the DOX+KGS high-dose group (Fig 1B & 2I).

DOX has been reported to prolong QTc interval in rats [25]. A study suggests that prolonged QTc is linked to reduced LVEF (left ventricular ejection fraction) and stroke volume[26], which leads to lower cardiac output[27]. It has been mentioned earlier that DOX induces cardiac hypertrophy, which may be correlated with the observed significantly prolonged QTc (Fig.1C & Fig 2G) discussed above[26]. The presence of KGS in the DOX + KGS High dose group was associated with a significant decrease (compared to control) of the QTc (Fig 1C & 2I). It is crucial to note that in this particular circumstance, the observed increase in SBP (as mentioned earlier) in the DOX + KGS high dose group (Fig. 1B & 2D) probably indicates an improvement in cardiac function, stroke volume, and cardiac output. However, observed similar decrease of QTc in DOX+ Captopril group (Fig 1C & 2J) was not associated with increase in SBP as that of DOX + KGS High Dose group (Fig. 1B & 2D).

5.2. KGS attenuates the cardiac MDA level and TMP:

DOX significantly elevated MDA levels in the DOX group owing to oxidative stress in cardiomyocytes (Fig. 3A), which is one of the main reasons for cardiac damage. DOX is

known to bind with cardiolipin, a crucial phospholipid found in the cardiac cells, specifically located in the inner membrane of mitochondria—this binding causes lipid peroxidation, resulting in oxidation-induced destruction of mitochondrial proteins and DNA. A similar increase in cardiac MDA level in DOX-induced cardiotoxicity is available in the literature[28]. The presence of KGS was observed to significantly reduce MDA levels in the cardiomyocytes of both DOX+KGS Low Dose and DOX+KGS High Dose groups (Fig 3A). However, more protection against a rise in MDA in cardiac tissue was noted in DOX+KGS High Dose (Fig 3A).

Captopril, an ACE inhibitor (ACEI), is commonly prescribed as first-line therapy for heart failure based on clinical guidelines. Previous reports have demonstrated that ACEI can aid in the maintenance of cardiac energy equilibrium. Captopril has shown the ability to enhance myocardial energy metabolism through its maintenance of mitochondrial function, restoration of mitochondrial oxygen consumption, and reduction of cardiac preload. Captopril also reduces DOX-induced oxidative stress, which is the main reason for taking captopril as standard [29]. Pre-clinical studies have shown the potential preventive effects of captopril against DOX-induced cardiotoxicity [30].

Based on these scientific informations, captopril, an ACE inhibitor, was considered a standard drug or positive control for protection against DOX-induced cardiac hypertrophy. However, captopril exhibited no significant improvement against DOX-induced decreased SBP (Fig 1B & 2E). As discussed, in free radical-mediated cardiac damage due to DOX, the estimation of cardiac total mitochondria protein (TMP) is scientifically relevant. Accordingly, in our study, a significant protection against DOX-induced reduction in cardiac TMP was observed in the DOX+KGS High Dose and DOX+Captopril group (Fig 3B), where the protection was to a greater extent in the latter. The primary aetiology of DOX (DOX)-mediated cardiac damage is often attributed to overproduction of ROS, which causes oxidative damage to mitochondria and subsequently activates downstream proapoptotic cascade. DOX causes peroxidation of the lipid present in the mitochondrial membrane of cardiac cells, leading to derangement of mitochondria and apoptosis of cardiac cells, which is irreversible by nature[31]. Thus, in our study, a decrease in the cardiac TMP (Fig 3B) and an increase in MDA (Fig 3A) in the DOX group can be correlated. Therefore, in our findings, the presence of KGS in high doses is associated with elevated cardiac TMP and reduced cardiac MDA level despite DOX treatment indicating significant cardioprotective

activity, probably through quenching of ROS and protection against the cardiac mitochondrial depletion.

5.3. KGS attenuates DOX-induced histopathological changes

It is well known that DOX (DOX) causes damage and loss of cardiac myofibril, resulting in cardiac stiffness[2] which was also observed in our experiment (Fig 4K & 4G). Besides the loss of cardiac myofibril, the stiffness is also caused by DOX-induced cardiac fibrosis (4G & 4L), which was also observed in our findings[32] (Fig 4J). Cellular events like myofibroblast activation and collagen deposition due to pro-inflammatory cytokines in the damaged heart is known to create cardiac fibrosis[23,33]. The induced stiffness impairs the heart's contraction and relaxation ability, affecting cardiac output. Therefore, these changes in cardiac histopathology may be linked to the observed reduction in SBP (Fig. 1B & 2B) in the DOX group, as mentioned earlier in our study. However, the presence of KGS in the DOX+KGS high dose group prevented myofibril loss and significantly reduced inflammation (Fig. 4D & 4L) and fibrosis (4I & 4L), which may be related to the increased SBP as observed. Therefore, our histopathology study appears to suggest that KGS in high doses (Fig 4D & 4K), like captopril (Fig 4E & 4K) reduced the severity of DOX-induced cardiac hypertrophy. However, captopril exhibited better protection [34].

5.4. KGS attenuates DOX-induced alterations in circulating plasma biomarkers

Literature survey indicates DOX elevates Ang-II levels[35], either through increased renin activity leading to angiotensinogen synthesis and Ang-II or through enhanced ACE activity due to increased macrophage infiltration in cardiac cells[36]. Ang-II primarily exerts its activity through the AT_1 receptor and is responsible for vasoconstriction, increasing plasma aldosterone level and fluid and salt balance, thereby raising blood pressure[37,38], associated with enhanced fibrosis and inflammation of cardiac tissue. Additionally, elevated plasma Ang-II and AT1R expression[39] caused by DOX can induce cardiomyocyte apoptosis, leading to cardiac hypertrophy of myocardial tissue[40]. DOX-induced increased plasma aldosterone has been reported to overexpress AT1R, independent of the mineralocorticoid receptor pathway[41]. This cyclical event further worsens the Ang-II mediated cardiotoxicity and leads to heart failure[42]. In the DOX group, a significant elevation of plasma ANG-II (Fig. 3C) and aldosterone (Fig3D) was observed. At the same time, a significant reduction of the same in the DOX+ KGS High Dose group (Fig 3C and 3D) was also seen. The presence of KGS in the DOX+KGS high dose group indicates that

probably KGS might have reduced the plasma Ang-II through ACE inhibitory activity or directly inhibiting renin activity, leading to a decrease in aldosterone and eventually breaking the vicious cycle. It will be essential to mention in this context that KGS high-dose-mediated actions may be correlated with decreased fibrosis (Fig 4I & 4L) and inflammation (Fig. 4D & 4L) in our histopathology study mentioned earlier. In the DOX+Captopril group animals, a significant reduction in Ang-II and aldosterone levels in the blood was observed (Fig 3C and 3D).

DOX is reported to elevate plasma noradrenaline, which can be compared to our observation in the animals of the DOX group (Fig. 3E). This could be attributed to a compensatory sympathetic drive which gets activated due to reduced heart function[43]. Ang-II directly and via noradrenaline (from adrenal medulla) causes vasoconstriction[44]. A previous report suggests long-term noradrenaline infusion itself can cause left ventricular hypertrophy[45]. In this experiment, the DOX+KGS High Dose treated animals exhibited a significant decrease in plasma noradrenaline levels, probably suggesting that KGS might have contributed to reduced plasma noradrenaline either by inhibiting plasma Ang-II or by directly suppressing the SNS (sympathetic nervous system).

In our experiment, increased plasma ANP in the DOX group (Fig 3F) was observed, which was probably due to increased cardiac overload caused by DOX. This may cause an unusual rise in blood volume in the heart's atria, leading to enhanced mechanical stretching of the atrial wall. Further, the atria exert more pressure on the ventricles to circulate the increased blood volume, thus straining the ventricles. This increased workload may cause a progressive decrease in myocardial contractility, which can be linked to decreased myofibril content and probably reduced cardiac output, potentially leading to heart failure[43,46–48]. The observed reduction of plasma ANP in the DOX+KGS High Dose group (Fig.3F) might probably be due to the reduction of DOX-induced myocardial workload and subsequently decreased mechanical atrial stretch, thus protecting against the development of DOX-induced cardiac hypertrophic condition. In this observation, the presence of KGS in the DOX + KGS High Dose group (Fig.3F) is scientifically significant.

The role of ACE was suspected behind the decrease of plasma Ang-II as mentioned above, and to verify this, the plasma ACE level of rats belonging to all the 5 groups was evaluated. Captopril is a known drug to ameliorate Dox-induced cardiotoxicity, implying the role of ACE [34].

Cardiac ACE is recognized as a crucial factor in DOX-induced cardiac hypertrophy [36]. Administration of DOX has been reported to elevate plasma ACE, which is consistent with our finding [49] (Fig.3G). KGS at high doses was able to attenuate DOX-induced elevated plasma ACE. It appears that KGS at a high dose, to some extent, may act like an ACE inhibitor by inhibiting plasma ACE (Figure 3G), which can further be co-related with decreased plasma Ang-II and aldosterone, further strengthening the hypothesis. However, the significantly increased SBP in the DOX+KGS high dose group could not be directly correlated with the significantly decreased ACE levels. The increase in SBP by KGS (a multiple component preparation) might be attributed to the decrease in myofibril loss (Figure 4K) and oxidative stress (Fig 3A) or other mechanisms unknown to us that might have played a role in improving SBP, independent of ACE pathway.

KGS showed more % yield and TPC in the methanolic extract as compared to others (table 1) indicating presence of phenolic compounds.

From the metabolite profiling study, 30 metabolites tentatively present in the methanolic extract of KGS were identified (Figure 5, Table 2). Out of these 30 metabolites, Rosmarinic acid and Trehalose were quantified in KGS i.e. 0.110±0.017 and 0.077±0.005 mg/gm of KGS (Fig 7-9, Table 4 & 5). Further, to confirm the interaction of these 30 identified phytochemicals with ACE (as per our ACE inhibition test, Figure 3G), molecular docking studies was conducted.

It is conventionally accepted that lower binding between receptors and small molecule ligands results in greater LibDock scores, indicating more significant interactions and more potential activity of the components[17]. Upon conducting molecular docking studies on ACE (PDB ID: 1086), it was found that as per Libdock score of Tiliroside, it emerged as the most potent compound among all those identified. Several reports suggest the beneficial role of Tiliroside on ACE [50,51]. The useful activity may be attributed to the formation of multiple hydrogen and hydrophobic bonds with various amino acids in the ACE's active site (Figure 6A). Moreover, Rosmarinic acid [52], rhoifolin [53], cosmosiin [54], and Aromadendrin 4'-glucoside were tentatively detected in KGS and showed comparatively better docking scores than the rest (provided as supplementary document) against ACE. Further, Rosmarinic acid [55] and Trehalose [56] have been reported to show cardioprotective effect against DOX induced cardiac hypertrophy. In our experiment, the cardioprotective effect of KGS may be attributed to the presence of Rosmarinic acid and Trehalose. Additionally, the contribution of other bioactive metabolites mentioned earlier

might also be related to the observed protective activity of KGS, a low-cost medication. In this part of the discussion, it will be probably relevant to mention that multiple phytocomponents of KGS discussed so far might work in a better manner as earlier reports claim that the efficacy of plant extracts is often greater than the sum of their components [57].

6.0. Conclusion

From the above discussion, it appears that the higher dose of KGS might possess cardioprotective action against DOX-induced cardiac hypertrophy, which seems to confirm. To the best of our knowledge, this is the first time Rosmarinic acid (0.110±0.017 mg/gm KGS) and trehalose (0.077 ±0.005) have been quantified in KGS, a low cost traditional unani preparation. The cardio-protective action of KGS may be due to its oxidative stress-decreasing ability, preventing DOX-induced deterioration of cardiac function and partial restoration of histopathological alterations. It also seems relevant that the anti-cardiac hypertrophic activity of KGS High Dose is primarily mediated through ACE inhibition. The modulation of plasma Angiotensin-II and aldosterone levels by KGS High Dose provides significant evidence that KGS might possess some of the features of an ACE inhibitor, which was further complemented by a molecular docking study. However, the increased SBP and decreased plasma ACE in the DOX+KGS high dose group could not be related. The KGS Low Dose appears to exert no significant effect on DOX-induced cardiac hypertrophy. Accordingly, our laboratory experiments on rats hopefully provide scientific evidence for this traditional practice, demonstrating the potential of KGS as a cardio-tonic agent in managing maladaptive cardiac hypertrophy. The findings of this study are significant, particularly in the context of KGS being a low-cost, evidence-based medication, which is highly relevant for the densely populated Indian subcontinent. It is essential to mention that our findings will definitely contribute to enhancing and enriching the available scientific data concerning the cardiovascular therapeutic usage of this age-old Unani preparation.

References:

[1] Miyagawa, K.; Emoto, N.; Widyantoro, B.; Nakayama, K.; Yagi, K.; Rikitake, Y.; Suzuki, T.; Hirata, K.I. Attenuation of Doxorubicin-Induced Cardiomyopathy by Endothelin-Converting Enzyme-1 Ablation through Prevention of Mitochondrial Biogenesis Impairment. *Hypertension* **2010**, *55*, 738–746, doi:10.1161/HYPERTENSIONAHA.109.141903.

[2] Chatterjee, K.; Zhang, J.; Honbo, N.; Karliner, J.S. Doxorubicin Cardiomyopathy. *Cardiology* **2010**, *115*, 155–162, doi:10.1159/000265166.

[3] Toko, H.; Oka, T.; Zou, Y.; Sakamoto, M.; Mizukami, M.; Sano, M.; Yamamoto, R.; Sugaya, T.; Komuro, I. Angiotensin II Type 1a Receptor Mediates Doxorubicin-Induced Cardiomyopathy. *Hypertens. Res.* **2002**, *25*, 597–603, doi:10.1291/hypres.25.597.

[4] Shi, S.; Chen, Y.; Luo, Z.; Nie, G.; Dai, Y. Role of Oxidative Stress and Inflammation-Related Signaling Pathways in Doxorubicin-Induced Cardiomyopathy. *Cell Commun. Signal.* **2023**, *21*, 61, doi:10.1186/s12964-023-01077-5.

[5] Sheibani, M.; Azizi, Y.; Shayan, M.; Nezamoleslami, S.; Eslami, F.; Farjoo, M.H.; Dehpour, A.R. Doxorubicin-Induced Cardiotoxicity: An Overview on Pre-Clinical Therapeutic Approaches. *Cardiovasc. Toxicol.* **2022**, *22*, 292–310, doi:10.1007/s12012-022-09721-1.

[6] Hiona, A.; Lee, A.S.; Nagendran, J.; Xie, X.; Connolly, A.J.; Robbins, R.C.; Wu, J.C. Pretreatment with Angiotensin-Converting Enzyme Inhibitor Improves Doxorubicin-Induced Cardiomyopathy via Preservation of Mitochondrial Function. *J. Thorac. Cardiovasc. Surg.* **2011**, *142*, 396-403.e3, doi:https://doi.org/10.1016/j.jtcvs.2010.07.097.

[7] Shaharyar, M.A.; Bhowmik, R.; Afzal, O.; Altamimi, A.S.A.; Alzarea, S.I.; Almalki, W.H.; Ali, S.Z.; Mandal, P.; Mandal, A.; Ayoob, M.; et al. Anti-Hypertensive Activity of Some Selected Unani Formulations: An Evidence-Based Approach for Verification of Traditional Unani Claims Using LC-MS/MS for the Evaluation of Clinically Relevant Blood Parameters in Laboratory Rats. *J. Clin. Med.* **2022**, *11*, doi:10.3390/jcm11154628.

[8] Elblehi, S.S.; El-Sayed, Y.S.; Soliman, M.M.; Shukry, M. Date Palm Pollen Extract Avert Doxorubicin-Induced Cardiomyopathy Fibrosis and Associated Oxidative/Nitrosative Stress, Inflammatory Cascade, and Apoptosis-Targeting Bax/Bcl-2 and Caspase-3 Signaling Pathways. *Animals* **2021**, *11*, 1–28, doi:10.3390/ani11030886.

[9] Wu, R.; Yao, P.; Wang, H.; Gao, Y.; Yu, H.; Wang, L.; Cui, X.; Xu, X.; Gao, J. Effect of Fermented Cordyceps Sinensis on Doxorubicin-induced Cardiotoxicity in Rats. *Mol Med Rep* **2018**, *18*, 3229–3241, doi:10.3892/mmr.2018.9310.

[10] Anand, K.; Mandal, P.; Karmakar, S.; Bhowmik, R.; Shaharyar, M.A.; Mandal, A.; Sarkar, A.; De, A.; Chakraborty, S.; Ray, S.; et al. Evaluation of Cilnidipine-Loaded Self-Micro-Emulsifying Drug Delivery System (SMEDDS) by Quantification of Comparative Pharmacokinetic Parameters Using Validated LC-ESI-MS/MS Bioanalytical Method and Pharmacodynamic Assessment. *Ann. Pharm. Françaises* **2024**, doi:https://doi.org/10.1016/j.pharma.2024.07.007.

[11] Chowdhury, D.; Tangutur, A.D.; Khatua, T.N.; Saxena, P.; Banerjee, S.K.; Bhadra, M.P. A Proteomic View of Isoproterenol Induced Cardiac Hypertrophy: Prohibitin Identified as a Potential Biomarker in Rats. *J. Transl. Med.* **2013**, *11*, 130, doi:10.1186/1479-5876-11-130.

[12] Ahmad, F.; Alamoudi, W.; Haque, S.; Salahuddin, M.; Alsamman, K. Simple, Reliable, and Time-Efficient Colorimetric Method for the Assessment of Mitochondrial Function and Toxicity. *Bosn. J. Basic Med. Sci.* **2018**, *18*, 367–374, doi:10.17305/bjbms.2018.3323.

[13] Kwatra, M.; Kumar, V.; Jangra, A.; Mishra, M.; Ahmed, S.; Ghosh, P.; Vohora, D.; Khanam, R. Ameliorative Effect of Naringin against Doxorubicin-Induced Acute Cardiac Toxicity in Rats. *Pharm. Biol.* **2016**, *54*, 637–647, doi:10.3109/13880209.2015.1070879.

[14] El-Shoura, E.A.M.; Salem, M.A.; Ahmed, Y.H.; Ahmed, L.K.; Zaafar, D. Combined β-Sitosterol and Trimetazidine Mitigate Potassium Dichromate-Induced Cardiotoxicity in Rats through the Interplay between NF-KB/AMPK/MTOR/TLR4 and HO-1/NADPH Signaling Pathways. *Environ. Sci. Pollut. Res.* **2023**, *30*, 67771–67787, doi:10.1007/s11356-023-27021-1.

[15] Bashi, D.S.; Fazly Bazzaz, B.S.; Sahebkar, A.; Karimkhani, M.M.; Ahmadi, A. Investigation of Optimal Extraction, Antioxidant, and Antimicrobial Activities of Achillea Biebersteinii and A. Wilhelmsii. *Pharm. Biol.* **2012**, *50*, 1168–1176, doi:10.3109/13880209.2012.662235.

[16] Mehmood, A.; Javid, S.; Khan, M.F.; Ahmad, K.S.; Mustafa, A. In Vitro Total Phenolics, Total Flavonoids, Antioxidant and Antibacterial Activities of Selected Medicinal Plants Using Different Solvent Systems. *BMC Chem.* **2022**, *16*, 64, doi:10.1186/s13065-022-00858-2.

[17] Wang, C.; Zhou, Q.; Wu, S.-T. Scopolin Obtained from Smilax China L. against Hepatocellular Carcinoma by Inhibiting Glycolysis: A Network Pharmacology and Experimental Study. *J. Ethnopharmacol.* **2022**, *296*, 115469.

[18] Burley, S.K.; Berman, H.M.; Kleywegt, G.J.; Markley, J.L.; Nakamura, H.; Velankar, S. Protein Data Bank (PDB): The Single Global Macromolecular Structure Archive. *Methods Mol. Biol.* **2017**, *1607*, 627–641, doi:10.1007/978-1-4939-7000-1_26.

[19] Fan, Y.; Yu, Z.; Zhao, W.; Ding, L.; Zheng, F.; Li, J.; Liu, J. Identification and Molecular Mechanism of Angiotensin-Converting Enzyme Inhibitory Peptides from Larimichthys Crocea Titin. *Food Sci. Hum. Wellness* **2020**, *9*, 257–263, doi:10.1016/j.fshw.2020.04.001.

[20] Das, B.; Bhardwaj, P.K.; Sharma, N.; Sarkar, A.; Haldar, P.K.; Mukherjee, P.K. Evaluation of Mollugo Oppositifolia Linn. as Cholinesterase and β-Secretase Enzymes Inhibitor. *Front. Pharmacol.* **2023**, *13*, 990926, doi:10.3389/fphar.2022.990926.

[21] Renu, K.; V.G., A.; Tirupathi, T.P.; Arunachalam, S. Molecular Mechanism of Doxorubicin-Induced Cardiomyopathy – An Update. *Eur. J. Pharmacol.* **2018**, *818*, 241–253, doi:10.1016/j.ejphar.2017.10.043.

[22] Menna, P.; Salvatorelli, E.; Minotti, G. Cardiotoxicity of Antitumor Drugs. *Chem. Res. Toxicol.* **2008**, *21*, 978–989, doi:10.1021/tx800002r.

[23] Octavia, Y.; Tocchetti, C.G.; Gabrielson, K.L.; Janssens, S.; Crijns, H.J.; Moens, A.L. Doxorubicin-Induced Cardiomyopathy: From Molecular Mechanisms to Therapeutic Strategies. *J. Mol. Cell. Cardiol.* **2012**, *52*, 1213–1225, doi:10.1016/j.yjmcc.2012.03.006.

[24] Miyoshi, T.; Nakamura, K.; Amioka, N.; Hatipoglu, O.F.; Yonezawa, T.; Saito, Y.; Yoshida, M.; Akagi, S.; Ito, H. LCZ696 Ameliorates Doxorubicin-Induced Cardiomyocyte Toxicity in Rats. *Sci. Rep.* **2022**, *12*, 4930, doi:10.1038/s41598-022-09094-z.

[25] Kabir, S.; Lingappa, N.; Mayrovitz, H. Potential Therapeutic Treatments for Doxorubicin-Induced Cardiomyopathy. *Cureus* **2022**, *14*, e21154, doi:10.7759/cureus.21154.

[26] Dahou, A.; Toubal, O.; Clavel, M.A.; Beaudoin, J.; Magne, J.; Mathieu, P.; Philippon, F.; Dumesnil, J.G.; Puri, R.; Ribeiro, H.B.; et al. Relationship between QT Interval and Outcome in Low-Flow Low-Gradient Aortic Stenosis with Lowleft Ventricular Ejection Fraction. *J. Am. Heart Assoc.* **2016**, *5*, doi:10.1161/JAHA.116.003980.

[27] Berman, M.N.; Bhardwaj, A. Physiology, Left Ventricular Function. In *StatPearls*; Treasure Island (FL), 2019.

[28] Naderi, Y.; Khosraviani, S.; Nasiri, S.; Hajiaghaei, F.; Aali, E.; Jamialahmadi, T.; Banach, M.; Sahebkar, A. Cardioprotective Effects of Minocycline against Doxorubicin-Induced Cardiotoxicity. *Biomed. Pharmacother.* **2023**, *158*, 114055, doi:10.1016/j.biopha.2022.114055.

[29] Yu, S.; Qian, H.; Tian, D.; Yang, M.; Li, D.; Xu, H.; Chen, J.; Yang, J.; Hao, X.; Liu, Z.; et al. Linggui Zhugan Decoction Activates the SIRT1-AMPK-PGC1α Signaling Pathway to Improve Mitochondrial and Oxidative Damage in Rats with Chronic Heart Failure Caused by Myocardial Infarction. *Front. Pharmacol.* **2023**, *14*.

[30] Belger, C.; Abrahams, C.; Imamdin, A.; Lecour, S. Doxorubicin-Induced Cardiotoxicity and Risk Factors. *IJC Hear. Vasc.* **2024**, *50*, 101332, doi:https://doi.org/10.1016/j.ijcha.2023.101332.

[31] Li, W.; Zhang, Y.; Wang, X.; Cao, J.; Qian, W.; Ling, G.; Tan, N.; Jiang, J.; Sun, Q.; Li, C.; et al. Qishen Granule Protects against Doxorubicin-Induced Cardiotoxicity by Coordinating MDM2-P53-Mediated Mitophagy and Mitochondrial Biogenesis. *Oxid. Med. Cell. Longev.* **2022**, *2022*, 4344677, doi:10.1155/2022/4344677.

[32] Polegato, B.F.; Minicucci, M.F.; Azevedo, P.S.; Carvalho, R.F.; Chiuso-Minicucci, F.; Pereira, E.J.; Paiva, S.A.R.; Zornoff, L.A.M.; Okoshi, M.P.; Matsubara, B.B.; et al. Acute Doxorubicin-Induced Cardiotoxicity Is Associated with Matrix Metalloproteinase-2 Alterations in Rats. *Cell. Physiol. Biochem.* **2015**, *35*, 1924–1933, doi:10.1159/000374001.

[33] Baci, D.; Bosi, A.; Parisi, L.; Buono, G.; Mortara, L.; Ambrosio, G.; Bruno, A. Innate Immunity Effector Cells as Inflammatory Drivers of Cardiac Fibrosis. *Int. J. Mol. Sci.* **2020**, *21*, 1–27, doi:10.3390/ijms21197165.

[34] Ibrahim, M.A.; Ashour, O.M.; Ibrahim, Y.F.; EL-Bitar, H.I.; Gomaa, W.; Abdel-Rahim, S.R. Angiotensin-Converting Enzyme Inhibition and Angiotensin AT1-

Receptor Antagonism Equally Improve Doxorubicin-Induced Cardiotoxicity and Nephrotoxicity. *Pharmacol. Res.* **2009**, *60*, 373–381, doi:https://doi.org/10.1016/j.phrs.2009.05.007.

[35] Zheng, M.; Kang, Y.M.; Liu, W.; Zang, W.J.; Bao, C.Y.; Qin, D.N. Inhibition of Cyclooxygenase-2 Reduces Hypothalamic Excitation in Rats with Adriamycin-Induced Heart Failure. *PLoS One* **2012**, *7*, e48771, doi:10.1371/journal.pone.0048771.

[36] Okumura, K.; Jin, D.; Takai, S.; Miyazaki, M. Beneficial Effects of Angiotensin-Converting Enzyme Inhibition in Adriamycin-Induced Cardiomyopathy in Hamsters. *Jpn. J. Pharmacol.* **2002**, *88*, 183–188, doi:10.1254/jjp.88.183.

[37] Li, Q.; Feenstra, M.; Pfaffendorf, M.; Eijsman, L.; Van Zwieten, P.A. Comparative Vasoconstrictor Effects of Angiotensin II, III, and IV in Human Isolated Saphenous Vein. *J. Cardiovasc. Pharmacol.* **1997**, *29*, 451–456, doi:10.1097/00005344-199704000-00004.

[38] Aguilera, G. Role of Angiotensin II Receptor Subtypes on the Regulation of Aldosterone Secretion in the Adrenal Glomerulosa Zone in the Rat. *Mol. Cell. Endocrinol.* **1992**, *90*, 53–60, doi:10.1016/0303-7207(92)90101-B.

[39] Zong, W.N.; Yang, X.H.; Chen, X.M.; Huang, H.J.; Zheng, H.J.; Qin, X.Y.; Yong, Y.H.; Cao, K.; Huang, J.; Lu, X.Z. Regulation of Angiotensin-(1-7) and Angiotensin II Type 1 Receptor by Telmisartan and Losartan in Adriamycin-Induced Rat Heart Failure. *Acta Pharmacol. Sin.* **2011**, *32*, 1345–1350, doi:10.1038/aps.2011.96.

[40] Huang, C.Y.; Chen, J.Y.; Kuo, C.H.; Pai, P.Y.; Ho, T.J.; Chen, T.S.; Tsai, F.J.; Padma, V. V.; Kuo, W.W.; Huang, C.Y. Mitochondrial ROS-Induced ERK1/2 Activation and HSF2-Mediated AT1R Upregulation Are Required for Doxorubicin-Induced Cardiotoxicity. *J. Cell. Physiol.* **2018**, *233*, 463–475, doi:10.1002/jcp.25905.

[41] Hullin, R.; Métrich, M.; Sarre, A.; Basquin, D.; Maillard, M.; Regamey, J.; Martin, D. Diverging Effects of Enalapril or Eplerenone in Primary Prevention against Doxorubicin-Induced Cardiotoxicity. *Cardiovasc. Res.* **2018**, *114*, 272–281, doi:10.1093/cvr/cvx162.

[42] Xu, J.; Carretero, O.A.; Liao, T.D.; Peng, H.; Shesely, E.G.; Xu, J.; Liu, T.S.; Yang, J.J.; Reudelhuber, T.L.; Yang, X.P. Local Angiotensin II Aggravates Cardiac Remodeling in Hypertension. *Am. J. Physiol. - Hear. Circ. Physiol.* **2010**, *299*, H1328-38, doi:10.1152/ajpheart.00538.2010.

[43] Jeon, T.J.; Jong Doo, L.; Jong-Won, H.; Yang, W.I.; Sang Ho, C. Evaluation of Cardiac Adrenergic Neuronal Damage in Rats with Doxorubicin-Induced Cardiomyopathy Using Iodine-131 MIBG Autoradiography and PGP 9.5 Immunohistochemistry. *Eur. J. Nucl. Med.* **2000**, *27*, 686–693, doi:10.1007/s002590050563.

[44] Tripathi, K. *Essentials of Medical Pharmacology*; JP Medical Ltd, 2013; ISBN 9350259370.

[45] Morishima, M.; Ono, K. Serum MicroRNA-30d Is a Sensitive Biomarker for Angiotensin II-Induced Cardiovascular Complications in Rats. *Heart Vessels* **2021**, *36*, 1597–1606, doi:10.1007/s00380-021-01853-8.

[46] Dietz, J.R. Mechanisms of Atrial Natriuretic Peptide Secretion from the Atrium.

Cardiovasc. Res. **2005**, *68*, 8–17, doi:10.1016/j.cardiores.2005.06.008.

[47] Yuan, Y.; Fan, S.; Shu, L.; Huang, W.; Xie, L.; Bi, C.; Yu, H.; Wang, Y.; Li, Y. Exploration the Mechanism of Doxorubicin-Induced Heart Failure in Rats by Integration of Proteomics and Metabolomics Data. *Front. Pharmacol.* **2020**, *11*, 600561, doi:10.3389/fphar.2020.600561.

[48] Chen, D.S.; Yan, J.; Yang, P.Z. Cardiomyocyte Atrophy, an Underestimated Contributor in Doxorubicin-Induced Cardiotoxicity. *Front. Cardiovasc. Med.* **2022**, *9*, 812578, doi:10.3389/fcvm.2022.812578.

[49] Venkatesan, N.; Ramesh, C. V; Jayakumar, R.; Chandrakasan, G. Angiotensin I Converting Enzyme Activity in Adriamycin Induced Nephrosis in Rats. *Toxicology* **1993**, *85*, 137–148, doi:https://doi.org/10.1016/0300-483X(93)90038-T.

[50] Yi, X.; Xu, C.; Yang, J.; Zhong, C.; Yang, H.; Tang, L.; Song, S.; Yu, J. Tiliroside Protects against Lipopolysaccharide-Induced Acute Kidney Injury via Intrarenal Renin–Angiotensin System in Mice. *Int. J. Mol. Sci.* 2023, *24*.

[51] Radović, J.; Suručić, R.; Niketić, M.; Kundaković-Vasović, T. Alchemilla Viridiflora Rothm.: The Potent Natural Inhibitor of Angiotensin I-Converting Enzyme. *Mol. Cell. Biochem.* **2022**, *477*, 1893–1903, doi:10.1007/s11010-022-04410-7.

[52] Ferreira, L.G.; Evora, P.R.B.; Capellini, V.K.; Albuquerque, A.A.; Carvalho, M.T.M.; Gomes, R.A. da S.; Parolini, M.T.; Celotto, A.C. Effect of Rosmarinic Acid on the Arterial Blood Pressure in Normotensive and Hypertensive Rats: Role of ACE. *Phytomedicine* **2018**, *38*, 158–165, doi:https://doi.org/10.1016/j.phymed.2017.02.006.

[53] Guerrero, L.; Castillo, J.; Quiñones, M.; Garcia-Vallvé, S.; Arola, L.; Pujadas, G.; Muguerza, B. Inhibition of Angiotensin-Converting Enzyme Activity by Flavonoids: Structure-Activity Relationship Studies. *PLoS One* **2012**, *7*, e49493.

[54] Tundis, R.; Nadjafi, F.; Menichini, F. Angiotensin-Converting Enzyme Inhibitory Activity and Antioxidant Properties of Nepeta Crassifolia Boiss & Buhse and Nepeta Binaludensis Jamzad. *Phytother. Res.* **2013**, *27*, 572–580, doi:10.1002/ptr.4757.

[55] Zhang, X.; Zhu, J.X.; Ma, Z.G.; Wu, H.M.; Xu, S.C.; Song, P.; Kong, C.Y.; Yuan, Y.P.; Deng, W.; Tang, Q.Z. Rosmarinic Acid Alleviates Cardiomyocyte Apoptosis via Cardiac Fibroblast in Doxorubicin-Induced Cardiotoxicity. *Int. J. Biol. Sci.* **2019**, *15*, 556–567, doi:10.7150/ijbs.29907.

[56] Abu-Khudir, R.; Ibrahim, W.M.; Shams, M.E.; Salama, A.F. Trehalose Alleviates Doxorubicin-Induced Cardiotoxicity in Female Swiss Albino Mice by Suppression of Oxidative Stress and Autophagy. *J. Biochem. Mol. Toxicol.* **2021**, *35*, e22859, doi:10.1002/jbt.22859.

[57] Wagner, H.; Ulrich-Merzenich, G. Synergy Research: Approaching a New Generation of Phytopharmaceuticals. *Phytomedicine* **2009**, *16*, 97–110, doi:10.1016/j.phymed.2008.12.018.

CHAPTER VI

KHAMIRA GAOZABAN SADA, A LOW COST UNANI PREPARATION ALLEVIATES ISOPROTERENOL AND L-NAME INDUCED AUGMENTED CARDIAC WORKLOAD

Khamira Gaozaban Sada, a low-cost unani preparation, alleviates Isoproterenol and L-NAME-induced augmented cardiac workload.

1.0.Introduction

Cardiac hypertrophy, which can progress to heart failure, is a significant cause of morbidity and mortality worldwide. It represents a chronic physiological increase in cardiac muscle mass due to systolic or diastolic wall stress, often occurring during development, pregnancy, or in response to sustained exercise. While initially compensatory for increased cardiac workload, prolonged hypertrophy can lead to congestive heart failure, arrhythmias, and sudden death. Pathological cardiac hypertrophy may result from conditions such as hypertension, valvular disease, myocardial infarction, and cardiomyopathy. At the cellular level, it is characterized by an increase in cell size and reactivation of the fetal gene program, ultimately leading to heart failure. [1]. Cardiac hypertrophy is an adaptive response of the myocardium to pressure overload or stimulation by adrenergic agonists.[2]. It is well known that hypertension is a significant risk factor for cardiac hypertrophy [3]. In 2010, the global burden of hypertension was estimated at approximately 1.4 billion, and it is projected to exceed 1.6 billion by 2025. However, the blood pressure control rate among treated patients was only about 32.5% worldwide. This high prevalence of uncontrolled or poorly controlled blood pressure has contributed to the increase in hypertensive heart disease. It is estimated that the prevalence of left ventricular hypertrophy, as assessed by echocardiography, is around 40% in the hypertensive population. [4]. Regression of pathological hypertrophy is linked to improved cardiac function, better quality of life, and enhanced long-term health outcomes. However, less than 50% of patients respond positively to most therapies, and the reversibility of cardiac remodelling is influenced by factors such as age, sex, BMI, and the underlying cause of the disease [5]. L-NAME (Nω-nitro-L-arginine methyl ester) is a potent nitric oxide synthase (NOS) inhibitor used in rat models of hypertension. It induces marked and sustained hypertension, along with a decrease in heart rate, by causing nitric oxide (NO) deficiency, oxidative stress, inflammation, and endothelial dysfunction. The heart must work harder to overcome the increased peripheral resistance, significantly raising the cardiac workload. Consequently, L-NAME-induced arterial resistance can lead to increased cardiac workload and, ultimately, cardiac hypertrophy [6,7]. Isoproterenol (ISO)-induced cardiac hypertrophy, a model of catecholamine-induced hypertrophy, is one of the most widely used to mimic sustained adrenergic stimulation and serves as a key model for studying the pathogenesis of maladaptive cardiac hypertrophy. The activation of β-adrenergic signaling triggers various mechanisms in the heart that contribute to the

hypertrophic phenotype, including increased protein synthesis, proto-oncogene expression, elevated oxidative stress, and the activation of mitogen-activated protein kinases and phosphatidylinositol-3 kinases [1] Unani physicians have traditionally used Khamira Gaozaban Sada (KGS) as a Muqavvi Qalb (cardiac tonic) and for treating Khafqan (palpitations) [8].

This study investigates the effectiveness of KGS in alleviating increased cardiac work load induced through two different pathways, L-NAME, induced hypertension and ISO-induced cardiac hypertrophy, using *invivo* and *invitro* experiments. Further, molecular docking studies were performed to evaluate the interaction of tentative KGS metabolites with the eNOS and β1-adrenergic receptor.

2.0. Material and Methods

2.1. Material

L-NAME (Sigma Aldrich, Burlington, MA, USA, catalogue no: N5751)), Isoproterenol (51-30-9, TCI), Ketamine (Cas no.- 1867-66-9), Xylazine (Cas no.- 7361-61-7), Khamira Gaozaban Sada (batch no- MKH145A, Hamdard laboratories, India) ,citrate buffer (C9999, Sigma Aldrich), Phosphate bufferd Saline (Sisco Research Laboratories Pvt. Ltd., 78529), , Protease inhibitor cocktail (Sigma Aldrich, Burlington, MA, USA, catalogue no:I3911-1BO), eNOS Rabbit mAb (A20985), Poly Q stain 2 step detection kit goat antimouse/rabbit HRP with peroxidase Quench and DAB KIT (Lot: 441726T0916, Biocyc Biotechnologie, GmbH & Co.KG), Phosphate buffer (10x) (SRL Cat no. 78529),10% Trichloro acetic acid (Himedia cas no-76-03-9), Thiobarbituric acid (TBA) (CAS no 504-17-6) was supplied from HIMEDIA, MDA (Sigma cas no.100683-54-3), aspirin (50-78-2, Sigma Aldrich), sucrose (Sigma cas no 57-50-1), Bradford Reagent (Himedia ML-106-100ML), noradrenaline (Sigma cat no: N1100000), Atrial Natriuretic peptide (Sigma cat no: SCP0022), Aldosterone (Sigma cat no: A9477), Rat ANG II (Angiotensin II) ELISA Kit (Catalog No.: MBS705139 MyBiosource; San Diego, USA), DMEM (D5796, Sigma Aldrich) , FBS (9014-81-7, Sigma Aldrich) , Penicillin (113-98-4, Sigma Aldrich), Streptomycin (3810-74-0, Sigma Aldrich) trypsin (9002-07-7, Sigma Aldrich), H9C2 cells (National Centre for Cell Science, Pune) , DMSO (67-68-5, Pune), MTT (298-93-1, Sigma Aldrich) , Fluo-4 NW Calcium Assay Kit (Catalog #: F36206, ThermoFisher Scientific, USA), K_2HPO_4 (Sigma, Cat: 60356), 1 M KH_2PO_4 (Sigma, Cat: P0662), $MgCl_2$ (Sigma, Cat: M2670), Miconazole nitrate (Sigma, Cat: M3512), Human Liver Microsomes (HLM) (Xenotech LLC, Mixed Gender, Cat No: H2610, Lot No: 2310132), Tacrine HCl (Sigma,

Cat: A3773), Diclofenac Sodium (Sigma, Cat: D6899), Dextromethorphan HBr (Sigma, Cat: D9684), Midazolam HCl (Sigma-Aldrich, UC429), Bupropion, S-Mephenytoin (Cayman, Cat: 11913), Acetonitrile (Cas no - 75-05-8), $NaNO_2$ (7632-00-0, TCI), $AlCl_3$(7446-70-0, TCI), Quercetin standard (117-39-5, Sigma Aldrich), Formic acid (Cas no.- 64-18-6), ,Methanol (Cas no.- 67-56-1), Thiopental sodium (Cas no. 71-73-8)

2.2. Animals

Male Wistar rats weighing 150–180 g and aged 8-9 weeks, were used for both L-NAME and ISO models. The animals were housed in a 12-hour light/dark cycle, maintained at a temperature of 25 ± 2°C, with access to food and drinking water.. All the experiments involving animals were examined and approved by the Institutional Animal Ethics Committee (IAEC) of Dept. of Pharmaceutical Technology, Jadavpur University. Animals used in the ISO model received approval from the IAEC with CPCSEA registration no: 1805/CPCSEA via proposal no JU/IAEC-22-20 while the L-NAME Model animals were approved through 1938/PO/Rc/S/17/CPCSEA

2.3. Grouping of animals

2.3.1.L-NAME induced hypertension:

In the L-NAME-induced hypertension experiment, animals were divided into 4 groups (n=10), namely control, L-NAME group, L-NAME+KGS LD group and L-NAME+KGS HD group.

Control group: animals in the control group were administered purified water orally.

L-NAME group: L-NAME was administered i.p. in a dose of 185 mmol/kg b.w. two times daily for 7 consecutive days and left untreated for the next 7 days.

L-NAME+KGS Low Dose: L-NAME was administered i.p. in a dose of 185 mmol/kg of b.w. two times daily for 7 consecutive days and L-NAME + KGS (1000 mg/kg b.w) for the next 7 days.

L-NAME+KGS High Dose: L-NAME was administered i.p. in a dose of 185 mmol/kg of b.w. two times daily for 7 consecutive days and L-NAME + KGS (2000 mg/kg b.w) for the next 7 days.

Non-invasive blood pressure, ECG and blood collection were performed on days 0, 7 and 14 for all the respective groups in the L-NAME model [8].

2.3.2.ISO-induced cardiac hypertrophy

Animals were divided into 4 groups (n=6), namely control, ISO group, ISO+ KGS Low Dose group and ISO+ KGS High Dose group, with the following treatments

Control group: animals were administered with 0.9% saline/ s.c. for 14 days

ISO group: animals were administered with 3mg/kg/day/ s.c. of ISO for 14 days.

ISO + KGS Low Dose group: animals were administered with 3mg/kg/day/s.c. of ISO for 14 days along with KGS in a dose of 1000mg/kg b.w./day orally.

ISO + KGS High Dose group: animals were administered with 3mg/kg/day/s.c. of ISO for 14 days along with KGS in a dose of 2000mg/kg b.w./day orally [9].

At the end of the experiment (L-NAME and ISO model) i.e 15^{th} day, the animals were euthanised with an overdose of thiopental sodium intraperitoneally (i.p) and blood samples were collected into tubes for the estimation of biochemical parameters. At the same time, fresh cardiac tissues were collected and rinsed with cold saline. A portion of the cardiac tissue was utilised for mitochondrial protein extraction and MDA estimation. The remaining tissues were preserved at −80°C.

2.4. Measurement of non-invasive Systolic blood Pressure (SBP)

The SBP of adult male rats was assessed using the non-invasive blood pressure equipment (NIBP 200A, Santa Barbara, CA, USA). SBP was non-invasively evaluated by applying a cuff around the tails of the rats, secured in approved animal restrainers (BIOPAC System Inc., Goleta, CA, USA). Their body temperature was artificially maintained at 37°C using a heating apparatus. The data acquiring was performed using MP36, Goleta, CA, USA. SBP was assessed in rats participating in the L-NAME experiment on days 0, 7, and 14, whereas in the ISO-induced cardiac hypertrophy experiment, it was recorded on days 0 and 14 [8].

2.5.Measurement of RR and QTc interval in anaesthetised rats

The rats were anaesthetised with ketamine (60 mg/kgb.w.) and xylazine (10 mg/kg b.w.), as previously reported. ECG signals were obtained for a length of 5 minutes post-anaesthesia, utilising standard leads. The ECG signals were acquired and examined utilising MP36 software (BIOPAC, Goleta, CA, USA). In L-NAME-induced rats, the RR-interval was observed at three distinct time points: day 0, day 7, and day 14 across all respective groups. QT was assessed in ISO-induced cardiac hypertrophy on days 0 and 14. The QTc was calculated using Bazett's method, i.e., $QTc = QT/\sqrt{RR'}$ [8]

2.6.Immunohistochemistry in L-NAME Model

On the 15th day, animals were sacrificed, and hearts were extracted from each group for immunohistochemistry (IHC) analysis. Tissues were preserved in formalin for dehydration. After dehydration, tissues were placed in molten paraffin to obtain a paraffin block. Sections were made with microtome with 5–8 µm and were then placed on slide. Tissues were then rehydrated with distilled water, applied over the slide for 10 minutes, washed, and then discarded.

Paraffin-embedded rat heart tissue sections (5–8 µm) were deparaffinised, rehydrated and washed with milliQ water. Antigen retrieval was performed by heating the sections in citrate buffer (pH 6.0) at 95–99°C for 20 minutes, followed by cooling for 20 minutes and washing in PBS. To block endogenous peroxidase activity, sections were incubated in 3% hydrogen peroxide (in PBS) for 10 minutes and then washed in PBS. Sections were incubated with a primary antibody solution (1:200) against phosphorylated eNOS at room temperature for 1 hour in a humid chamber, followed by washing in PBS. A horseradish peroxidase (HRP)-conjugated secondary antibody was applied for 30 minutes in a humid chamber, followed by additional PBS washes. Chromogenic detection was performed using 3,3'-diaminobenzidine (DAB) (50 µl of liquid DAB chromogen and 1 ml of DAB substrate buffer, mixed) for 5 minutes, resulting in a brown precipitate indicative of positive eNOS staining. Sections were counterstained with hematoxylin for 1 minute and mounted. Positive staining was assessed by light microscopy, with brown staining indicating eNOS localisation. Negative controls were included by omitting the primary antibody to evaluate non-specific staining [10–12]

2.7.Preparation of Heart Tissue Homogenate

The homogenate of the heart of rats was obtained by homogenising 100 mg of heart tissue in 2 ml of 0.05 M phosphate buffer (pH 7.4), homogenised in ice using a tissue homogeniser (IKA, T-10 Basic Ultra-Turrax) and after that centrifuged at 15,000 rpm/30 mins/ 4°C. The resultant supernatant was preserved at −80°C for subsequent analysis [9].

2.8. Assessment of cardiac MDA

Briefly, 1.0 ml of phosphate buffer and 2 ml of 10% TCA were mixed with 1 ml of heart tissue homogenate and thoroughly mixed. To precipitate proteins, the mixture underwent centrifugation at 3000 rpm/ 10 mins. 2 ml of supernatant was collected, then 0.5 ml of 1% TBA was added, followed by one hour of heating at 95°C. The cardiac tissue was

homogenised in ice-cold 0.15 M HCl (10%), and the absorbance was assessed at 532 nm. Absorbance was employed to ascertain the concentration of TBARS, quantified as nmol/ml of MDA per mg of protein, utilising MDA as the standard [13].

2.9.Heart weight to tail length ratio

The excised cardiac tissues were washed with ice-cold PBS; subsequently, the adipose tissue, aorta and atria were separated, and the heart weight (mg) was measured. The HW/TL (mg/cm) was defined as the ratio of heart weight to Tail length.

2.10.Invitro membrane stability assay

Blood was drawn from a healthy, untreated goat, with sodium oxalate as an anticoagulant. Samples were kept at 4°C/24 hours for preservation. After 5 minutes of centrifugation at 2700 rpm, the supernatant was removed, and the cell suspension was washed with autoclaved isotonic saline. This process was repeated until the supernatant appeared clear and colourless. The cells were resuspended in 20% (v/v) PBS solution (10 mM, pH 7.4). A mixture was prepared with 0.5 mL of 20% RBC suspension, 1 mL of 0.15 M PBS (pH 7.4), and 2 mL of 0.25% sodium chloride, then left at room temperature for 15 minutes. Next, 0.5 mL of KGS crude extracts at concentrations of 250, 500, and 1000 µg/mL were added, with aspirin as the standard at equivalent concentrations. After incubation, samples were centrifuged at 5000 rpm for 5 minutes, and absorbance was measured at 530 nm [14]

2.11.Estimation of Total mitochondrial protein (TMP)

The cardiac homogenate underwent centrifugation at 1300g for 10 min at 4^{o}C. The post-nuclear supernatant underwent centrifugation at 17,000 g for 10 minutes at 4°C. The crude mitochondrial pellet was obtained following centrifugation. The crude mitochondrial pellet was resuspended in an isolation buffer and subsequently loaded onto a discontinuous sucrose gradient (1.2-1.0-0.8 M). The sample was subjected to centrifugation at 100,000 g for 60 mins at 4 °C. The resulting enriched mitochondrial pellet was subsequently rinsed twice with an isolation buffer at 10,000 g for 10 mins at 4 °C. The mitochondrial pellet was subsequently resuspended in an isolation buffer. The TMP was determined spectrophotometrically via the Bradford Assay reagent using a Spectramax M5 (Molecular Devices, LLC, USA) at 595 nm, utilising a calibration curve of BSA. The Sorvall Mx 150+ micro-ultracentrifuge was utilised for all centrifugation processes [15].

2.12.Histopathology

Hearts were subjected to histopathology to observe alterations in the structure and amount of fibrosis. Whole heart tissues were excised and cleaned with ice-cold PBS, then fixed in 4% formalin, routinely processed, and embedded in paraffin. Paraffin sections were cut into 5 μm thick sections and mounted on glass slides, then stained with hematoxylin and eosin (H & E), Masson trichrome stain. [14]. Histological images of the cardiac sections were acquired using a light microscope (Nikon Eclipse Ti). The images of the H& E and Masson's trichome stained sections were captured at 10X and 4X, respectively. The results of histopathology were expressed in terms of cardiomyocyte disarray, cardiac hypertrophy, myocyte injury (H & E) and fibrosis (MT); these parameters were allotted scores ranging from 0 to 6. The images of the cardiac sections that were obtained were evaluated using image J software version 1.4 (NIH, USA) [16]. A score of 0-2 denoted mild, 2-4 for moderate and 4-6 for severe.

2.13.Echocardiography

To investigate the cardiac structure and function, Fujifilm Visual Sonics Vevo LAZR-X 3100 system (Fujifilm Visual Sonics, Inc., Toronto, ON, Canada) was used. After anesthetising, rats were gently restrained on a three-axis micro-positioning stage for performing echocardiography. Rats were placed in the supine position on a heated pad to maintain a stable temperature (37°C). An echocardiographic examination was performed with a high conductive ultrasound gel and a linear transducer at 13-MHz (MX201) to obtain high-resolution two-dimensional and M-mode measurements. The pre-set mode used was "Rat cardiology (small animal)" with the parasternal long-axis view (PSALX). The echocardiographic measurements were performed using a digital image analysis package (Vevo Lab version 3.2.2) [17]

2.14. Measurement of circulating plasma biomarker

The plasma was collected, separated, and mixed with a protease inhibitor cocktail to quantify noradrenaline, ANP, and aldosterone using LC-MS/MS triple-quadruple. The protease-inhibitor cocktail was prepared as previously reported. Shimadzu LC was used with a binary pump, an on-line degasser, and a thermostatic autosampler (SIL-20AC). The LC was coupled to an Ab Sciex API-4000 QTRAP mass spectrometer equipped with an electrospray ionisation (ESI) source. The Analyst Software 1.6.3 was used for the data acquisition. The separation was achieved using Phenomenex Kinetex (5μ C18 100A 50 × 3 mm). The Chromatographic Conditions were as previously reported. Noradrenaline,

aldosterone and atrial natriuretic peptide were extracted from the plasma matrix. For the assessment of the aldosterone, tolbutamide was taken as the internal standard (IS), while propranolol served as an internal standard (IS) for ANP and noradrenaline [8].

2.15.Cell culture

H9C2 cells were procured from the National Centre for Cell Science (NCCS), Pune, India. Cells were grown in DMEM enriched with 10% FBS and antibiotics (100 U/mL penicillin and 100 U/mL streptomycin) at 37°C in a humidified environment containing 5% CO2 and subcultured using 0.05% trypsin.

2.16.MTT assay

KGS and ISO were diluted in DMEM (1 mg/mL). All cells were washed with phosphate buffer saline (PBS) and serum-starved for 2 hr before incubation with KGS or ISO. KGS was dissolved in dimethylsulfoxide (DMSO), and the final DMSO concentration was ≤0.05% (v/v) achieved.

In brief, H9C2 cells were preincubated with DMEM containing 10% FBS overnight in 96-well plates at a density of 5×10^4 cells per well. After cells were grown to 90% confluency, all cells were washed twice with PBS and serum-starved for 2 h. The cells were then incubated with KGS in a concentration of 0, 5,10,20,50,100 and 200 µg/ml for 6 hrs. , the supernatants were removed, and the formazan crystals were dissolved in 150 µL DMSO. H9C2 cells without KGS were considered as control (100% viability) and determined through MTT assay.

In another similar experiment, cells were incubated with KGS in 0, 5,10,20,50,100, and 200 ug/ml concentrations for 3 hr. As per the report, after 3 hrs, all the cells were treated with 10µM of ISO and further incubated for 6 hr. The medium was then removed, and solutions containing 5% MTT (100 µl) and DMEM were added to each well. The cells were further incubated at 37°C for 4 hours, the supernatants were removed, and the formazan crystals were dissolved in 150 µL DMSO (Sigma, USA). Absorbance was recorded at a wavelength of 490 nm and a reference wavelength of 630 nm using a microplate reader (Spectramax M5, Molecular Devices) [15]. The MTT assay involves the conversion of the water-soluble MTT to an insoluble formazan. The amount of blue formazan dye generated from MTT was proportional to the number of live cells. The values of the reaction were obtained after subtraction of matched blanks, and the ODs of the controls were taken as 100% for comparisons.[17,18].

2.17.Measurement of intracellular calcium

Calcium (Ca^{2+}) signalling in H9C2 cells was quantified using Fluo-4 NW Calcium Assay Kit (Catalog #: F36206, ThermoFisher Scientific, USA).

Briefly, H9C2 cells were cultured in a flat black clear bottom 96 well plates (Catalog #: 266120, ThermoFisher Scientific, USA) with a density of 5×10^4 cells per well in DMEM containing 10% FBS and incubated overnight at 37°C in 5% CO_2. After reaching 80-90% confluency, the cells were divided into the following groups: Control:

Control: Untreated H9C2 cells

ISO: cells were incubated with 10 µM of ISO for 6 hours.

$KGS_{200\ \mu g/mL}$ +ISO: cells were pre-treated with KGS at 200 µg/mL for 3 hours and then incubated with 10 µM of ISO for 6 hours.

After incubation, the culture medium was removed to avoid baseline fluorescence interference. Fluo-4 NW assay reagent was added to each well as per the manufacturer's protocol. Plates were incubated for 30 minutes at 37°C, followed by an additional 30 minutes in the dark at room temperature. The fluorescent intensity in each well was determined at excitation 494nm and emission 516nm. Fluorescence images were captured using a Zeiss LSM 700 Confocal Microscope (Carl Zeiss, Germany) at 20× magnification following cell mounting with DAPI solution [19].

2.18.CYP inhibition assay

CYP (1A2, 2C9, 2D6, 3A4, 2B6, and 2C19) Inhibition Assay Using HLM

2.18.1.Preparation of Reagents and Buffer

A stock solution of 1 M potassium phosphate buffer by titrating 1 M K_2HPO_4 (Sigma, Cat: 60356) with 1 M KH_2PO_4 (Sigma, Cat: P0662) to reach a pH of 7.4 was prepared. This stock solution was diluted by adding 30 mL of the 1 M buffer solution to 270 mL of deionised water to achieve a final concentration of 100 mM. The pH was adjusted to precisely 7.4, and this buffer was used throughout the CYP inhibition experiment. $MgCl_2$ (Sigma, Cat: M2670, FW: 203.3) was dissolved in deionised water to reach a concentration of 33.23 mM to achieve the required $MgCl_2$ concentration in the assay mix.

2.18.2.Preparation of KGS and Positive Control

KGS was dissolved in DMSO at 0.2,1 and 5 µg/mL concentration. The final concentration of the organic solvent in the assay did not exceed 1% (v/v). Miconazole nitrate (Sigma, Cat:

M3512) was taken as a positive control inhibitor for the CYP enzymes and was used in the concentrations at IC_{50} points (0.2, 1, and 5 µg/mL) for validation.

2.18.3.Preparation of HLM Solution

Human Liver Microsomes (HLM) (Xenotech LLC, Mixed Gender, Cat No: H2610, Lot No: 2310132) stock was prepared at 20 mg/mL. For the pre-incubation phase, HLM stock was diluted to achieve 1 mg/mL for CYP1A2, 2C9, 2D6, 3A4, 2B6, and 2 mg/mL for CYP2C19 in the final assay volume. After pre-incubation, for the 4 CYPs cocktail assay (CYP1A2, 2C9, 2D6, 3A4), HLM concentration was adjusted to 0.10 mg/mL, while for the CYP2C19 assay, it was adjusted to 0.20 mg/mL

2.18.4.CYP Enzyme Substrates and Cocktail Preparation

Individual substrates were prepared at the following concentrations CYP1A2: 10 µM Tacrine HCl (Sigma, Cat: A3773), CYP2C9: 35 µM Diclofenac Sodium (Sigma, Cat: D6899), CYP2D6: 6 µM Dextromethorphan HBr (Sigma, Cat: D9684), CYP3A4: 8 µM Midazolam HCl (Dormicum , Roche Molecular Biochemicals (Basel, Switzerland), CYP2B6: 20 µM Bupropion, CYP2C19: 200 µM S-Mephenytoin (Cayman, Cat: 11913). A cocktail of substrates for CYP1A2, 2C9, 2D6, 3A4, and 2B6 and a separate solution of S-Mephenytoin for CYP2C19 were prepared, maintaining the specified concentrations.

2.18.5.Pre-Incubation Step

Two sets of reactions were prepared for each test condition, i.e., one with NADPH (1.2 mM final concentration) and one without NADPH, to assess time-dependent inhibition. HLM was added (1 mg/mL for CYP1A2, 2C9, 2D6, 3A4, and 2B6; 2 mg/mL for CYP2C19), NADPH, and KGS (10 µg/ml) in a 20 µL reaction volume to initiate the pre-incubation. The mixture was incubated for 30 minutes at 37°C with gentle shaking to allow for any potential enzyme-inhibitor interactions.

2.18.6. Dilution and Incubation with Substrate

Following the 30-minute pre-incubation, the cocktail was diluted in each reaction mixture 10-fold with 100 mM potassium phosphate buffer (pH 7.4) containing the appropriate cocktail of substrates and $MgCl_2$ (3.3 mM). Further, the diluted reaction mixture was incubated at 37°C for an additional 10 minutes for CYP1A2, 2C9, 2D6, 3A4, and 2B6. For CYP2C19, the incubation period was extended to 20 minutes. This step enables enzyme-substrate interactions, allowing for product formation in the presence of the test inhibitor.

2.18.7.Reaction Termination and Sample collection for LC-MS analysis

The reaction was stopped by adding ice-cold acetonitrile with 0.1% formic acid to each sample in a ratio of 3:1 (acetonitrile volume). An internal standard, bucetin at 459.2 > 322.2 was added to each sample. The samples were cooled to 4°C and centrifuged at 2500 g for 15 minutes to precipitate proteins. Further, the supernatant was collected for LC-MS analysis.

2.18.8.LC-MS/MS Analysis

For this study, the Agilent 6495, coupled with Rapidfire and the Agilent LC 1260 Infinity II, was used. The mobile phases were as follows: Phase A consisted of water with 0.1% formic acid, while Phase B/C for four CYP enzymes (CYP1A2, 2C9, 2D6, 3A4) was composed of 80:20 MeCN: water with 0.1% formic acid. For CYP2C19, Phase B/C was 80:20 MeCN/MeOH: water with 0.1% formic acid. A Rapidfire C18 cartridge with a 4 µL volume was employed, operating in trap-and-elute mode. The flow rate was set at 1.0 mL/min, with a cycle time of 20 seconds. Transition monitoring was performed for each CYP enzyme product by monitoring specific Q1/Q3 transitions in multiple reaction monitoring (MRM) mode: For CYP1A2, the transition monitored was OH-Tacrine (215.1 > 197); for CYP2C9, it was OH-Diclofenac (312 > 229.9); for CYP2D6, Dextrophane (258.1 > 156.9); for CYP3A4, OH-Midazolam (342.2 > 202.8); for CYP2B6, OH-Bupropion (256.1 > 237.9); and for CYP2C19, OH-Mephenytoin (235.1 > 150.1). Finally, the IC_{50} values were determined using GraphPad Prism (ver 9.0.2) based on Dose-response inhibition (Nonlinear regression, 4 parameters) curve fitting [18,20].

2.19.Total Flavanoid content (TFC)

The amount of flavonoids in each KGS extract was measured by mixing 24 µL of the extract (10 mg/mL) with 28 µL of NaNO2 (50 g/L) and letting it stand for 5 minutes. Subsequently, 28 µL of AlCl3 (100 g/L) was introduced, and the mixture was permitted to react for 6 minutes. Subsequently, 120 µL of 1 M NaOH was then added to the mixture, and the absorbance was instantly assessed at 510 nm. The TFC was determined as mg QE per gram of dry weight [21].

2.20.Condition of LC-qTOF-MS for metabolite profiling of KGS

The methanolic extract of KGS (2 µL injection volume) was analysed with an Agilent 1290 Infinity LC system in conjunction with an Agilent 6530C Q-TOF mass spectrometer, accompanied by its source composed of dual Agilent Jet Stream (AJS) and ESI. Separation by chromatography was performed on a column maintained at 40 °C, employing a gradient

of an aqueous solution (0.1% formic acid) and methanol as an organic component. The gradient commenced with 95% aqueous at a flow rate of 0.3 mL/min, transitioning to 70% organic from 8 to 14 mins, and after that, reverting to the beginning conditions of 95% aqueous at 15 minutes. The mass spectrometry was performed in positive ionisation mode, spanning a mass range of 100–3000 m/z, having an acquisition rate of 1 spectra per second. The source parameters comprised of a gas temperature of 300 °C, a gas flow rate of 8 L/min, a sheath gas temperature of 350 °C, a sheath gas flow of 11 L/min, a nebuliser pressure of 35 psi, and a capillary voltage of 3500 V. The skimmer, fragmentor, and octopole RF peak voltages were set at 65 V, 175 V, and 750 V, respectively. Real-time mass calibration was accomplished using reference masses set at 112.9855, 966.0007, and 1033.9881 m/z. The identified masses were correlated with Metline, an Agilent database. The targeted MS/MS experiment encompassed a mass range of 100-1000 m/z, with a fixed collision energy of 10.00 eV and an acquisition rate of 12 spectra per second. Peaks and spectra were analysed using Mass Hunter Workstation B.06.00 (Agilent Technologies, 2012), resulting in the identification of tentative chemicals.

2.21.Molecular docking studies

To investigate the binding interactions between the identified phytocompounds from KGS and the active sites of Endothelial nitric oxide synthase (eNOS) and Beta-1 adrenergic receptor (β1AR), molecular docking simulations were performed utilizing the Libdock module of Discovery Studio 3.0 software, Dassault Systèmes, San Diego, USA [22]. After identifying and cleaning the phytocompounds, the Discovery Studio 3.0 workspace was utilized to decrease energy through the "Prepare Ligands" tool. The X-ray crystallographic structures of eNOS (PDB ID: 6CIE) and β1AR (PDB ID: 7BVQ) were obtained from the Protein Data Bank (http://www.rcsb.org/pdb) and optimized for docking analysis [23,24] [25]. The optimization strategy entails the incorporation of hydrogen atoms, the removal of water molecules, and the elimination of other non-interacting heteroatoms [26]. The CHARMm force field was utilised to model the structures of the protein and ligand. Docking studies were performed with the standard LibDock module. Optimal ligand configurations are maintained after a final phase of energy minimization, allowing for flexibility in ligand positioning. A LibDockScore of ≥90 is commonly seen as indicative of a higher affinity between small molecule ligands and the receptor, suggesting enhanced binding efficiency [22].

3.0.Result

3.1.KGS attenuates L-NAME-induced hypertension

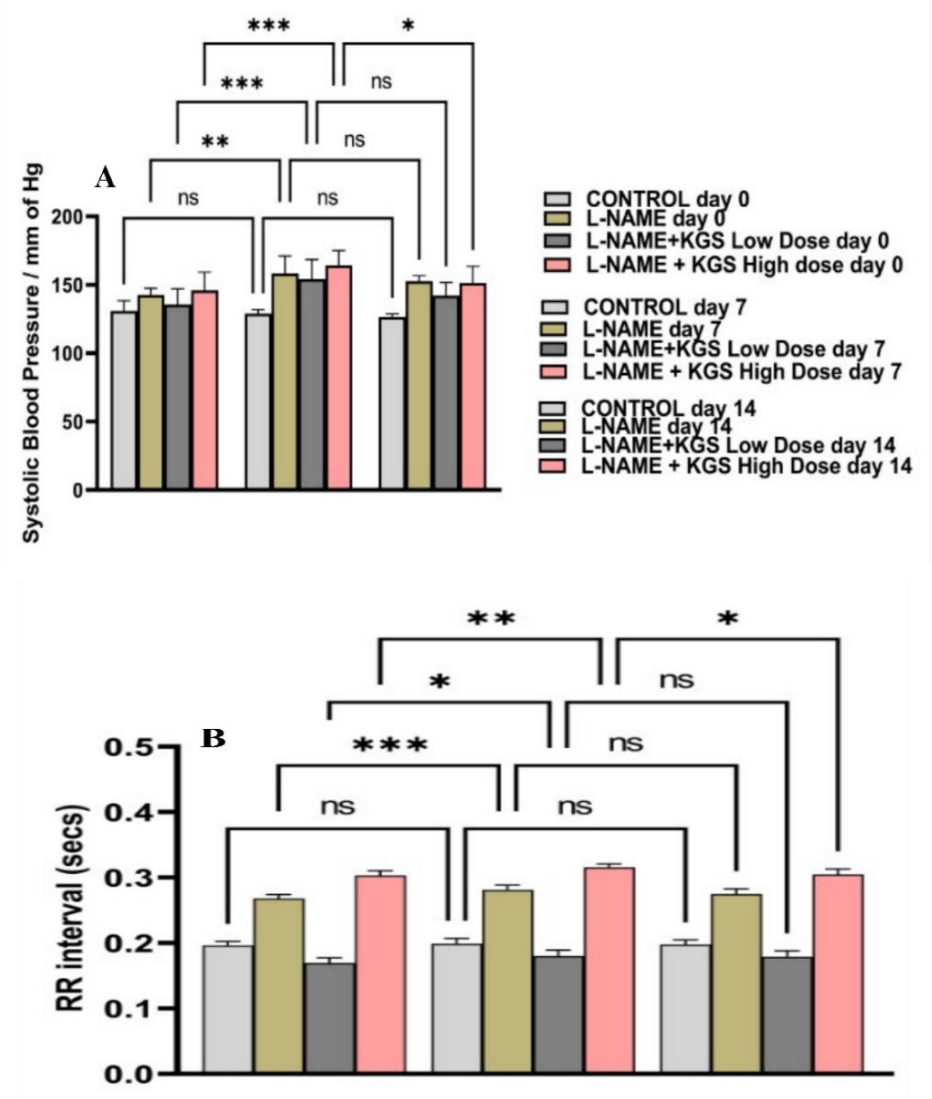

Figure 1: Represent (A)SBP and (B) RR interval in Control, L-NAME, L-NAME+KGS Low Dose group and L-NAME + KGS High Dose group. All the data are expressed as Mean ± SD. Statistical comparison was made between Day 0 Vs Day 7 and Day 7 Vs Day 14 between each group, where p*<0.05, p**<0.01, p***<0.001.

In Fig 1A and 2A-2D, except for the control, all the groups showed a significant ($p<0.05$) increase in SBP on day 7 as compared to day 0. There was a significant decrease in SBP on day 14 as compared to day 7 in only the L-NAME + KGS High Dose group, though a non-significant decrease was noted in the L-NAME+KGS Low Dose group. Similarly, in Fig. 1B and 2E-2H, except for control, there was a significant 7^{th}-day increase in RR interval when compared to day 0, while no groups showed a substantial decrease in the same except the L-NAME + KGS High Dose group.

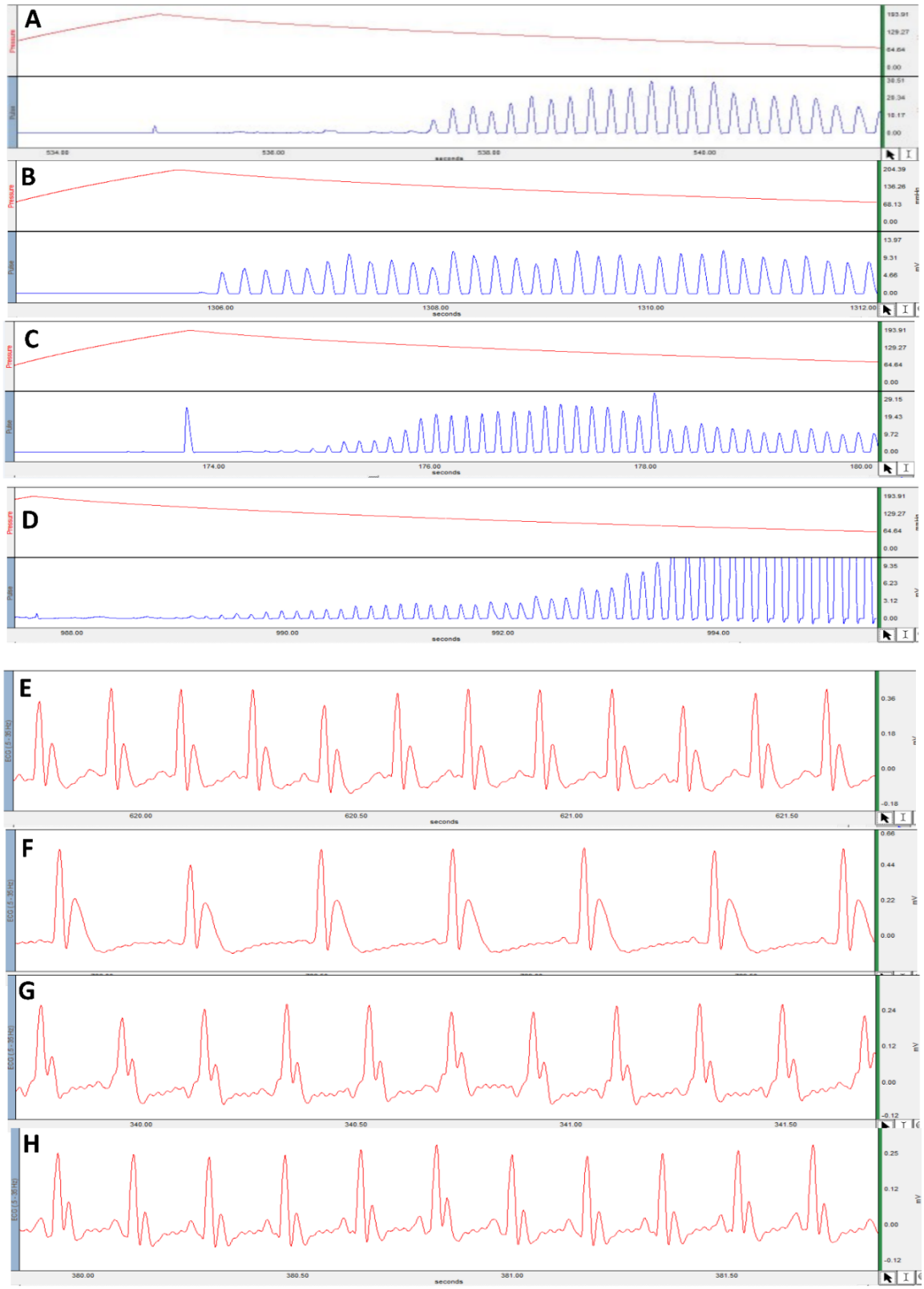

Figure 2: Represents the SBP and RR interval of Control (A & E), L-NAME (B & F), L-NAME+KGS Low Dose (C & G), L-NAME+ KGS High Dose (D & H) recorded using MP-36 software

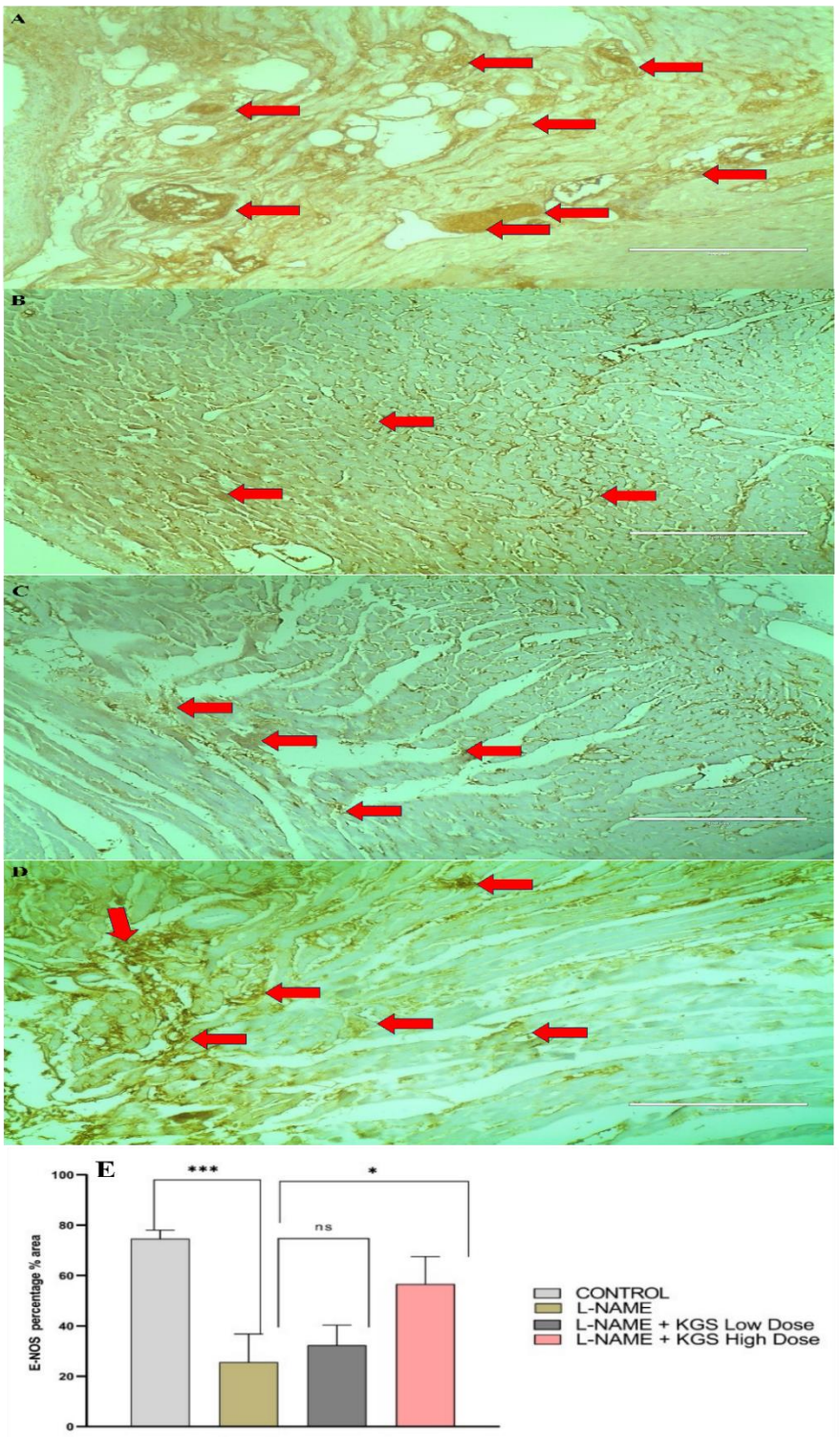

Figure 3: Represents the immunohistochemistry of cardiac sections from rats targeting eNOS, categorised as follows: (A) Control, (B) L-NAME, (C) L-NAME + KGS (Low Dose), and (D) L-NAME + KGS (High Dose)

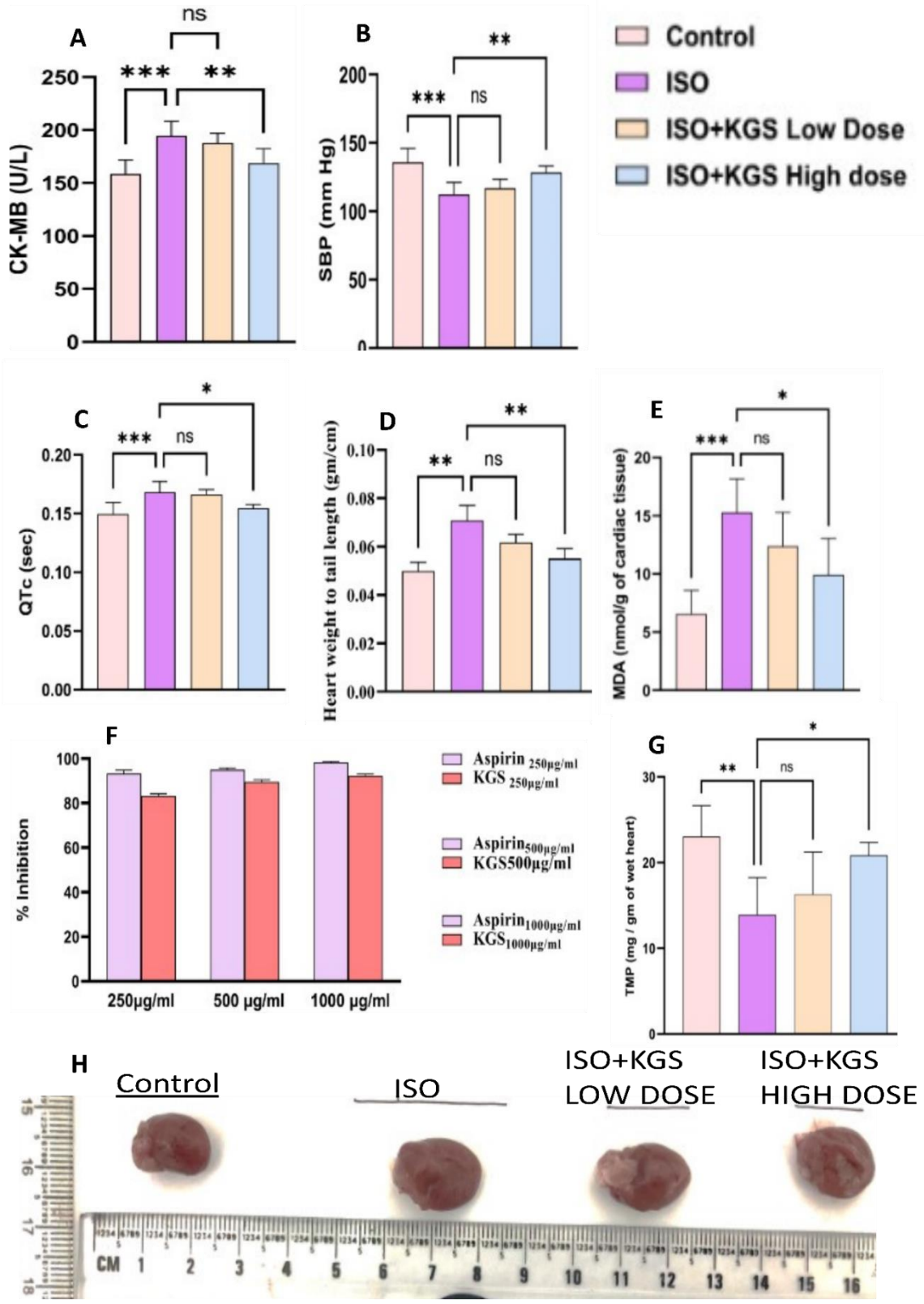

Figure 4: Represents mean±SD data of (4A) serum CK-MB levels (4B) SBP (4C) QTc interval, (4D) heart weight/tail length ratio and (4E) cardiac MDA (4F) % inhibition in goat blood assay and(4G) cardiac TMP (4H) images of the extracted heart from male wistar rats. Statistical Comparisons were made between the control Vs ISO group, ISO vs KGS low dose group and KGS High dose group

The administration of isoproterenol (ISO) significantly elevated ($p < 0.05$) serum CK-MB levels (Fig 4A), QTc interval (Fig 4C & 5B), heart weight/tail length ratio (Fig 4D & 4H), and cardiac MDA (4E) levels while significantly ($p<0.05$) decreasing SBP (Fig.4B & 5F)) and cardiac TMP (4G). Co-treatment with KGS demonstrated High-dose KGS significantly ($p<0.05$) reduced CK-MB, QTc interval (Figure 4c & 5D), and cardiac MDA levels ($p < 0.01$) heart weight/tail length ratio. Moreover, ISO-induced reductions in cardiac TMP levels and SBP were significantly ($p<0.05$) restored by KGS, particularly at the high dose (Fig 4B & 5H) ($p < 0.05$). In the goat RBC hemolysis assay, KGS showed dose-dependent inhibition, with maximum protection at 1000 µg/mL (4F). KGS Low dose was unable to make significant changes in the above invivo experiments.

Fig 4F demonstrates the anti-inflammatory efficacy of KGS through the induction of hypotonicity in goat red blood cells. The anti-inflammatory efficacy of KGS is quantified as the percentage suppression of RBC hemolysis. The anti-inflammatory effect measures the degree of protection offered to goat RBC by varying concentrations of KGS relative to the conventional drug aspirin. At a dose of 1000 µg/mL, KGS (92.33 ±0.67) exhibited the highest percentage of inhibition of red blood cell membrane rupture.

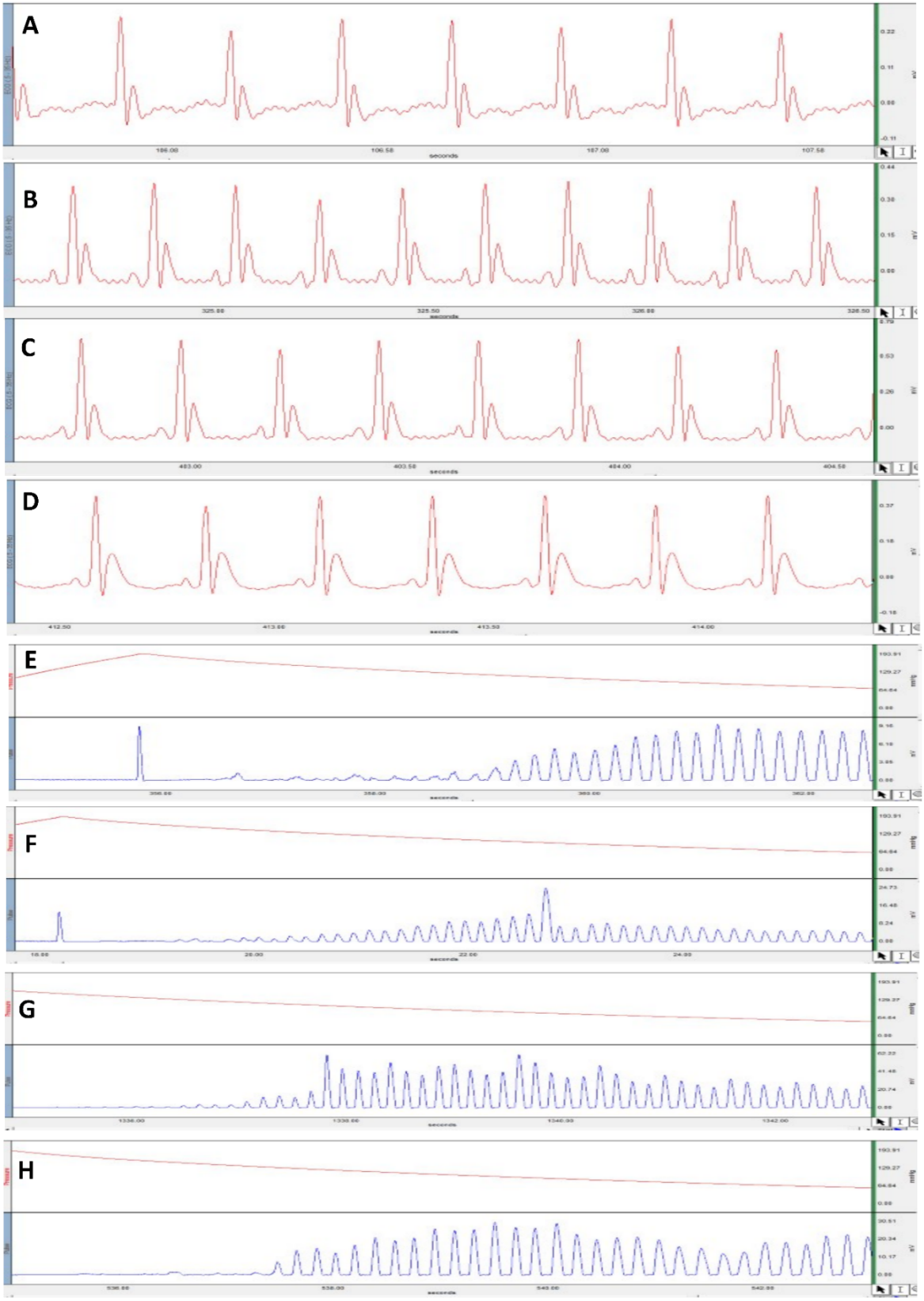

Figure 5: Represents the QT and SBP of Control (A & E), ISO (B & F), ISO+KGS Low Dose (C & G), ISO+ KGS High Dose (D & H) recorded using MP-36 software

3.2.KGS attenuates plasma circulating biomarkers

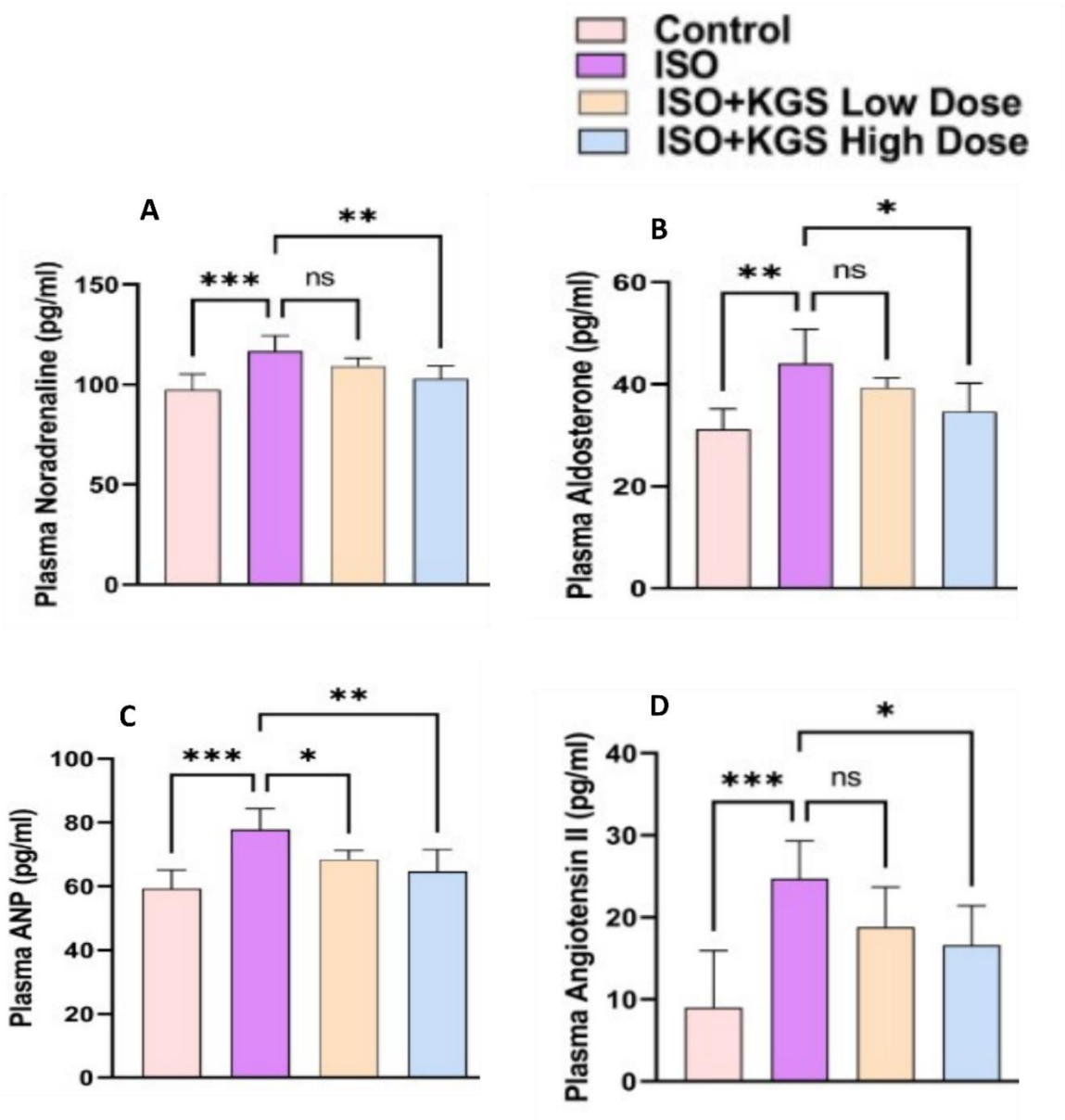

Figure 6: Represents mean±SD data of plasma (6A) noradrenaline (6B) Aldosterone (6C) ANP (6D) Angiotensin-II. Statistical Comparisons were made between the control Vs ISO group, ISO vs KGS low dose group, and the KGS High dose group

The administration of ISO significantly ($p<0.05$) increased plasma levels of noradrenaline, aldosterone, atrial natriuretic peptide (ANP), and angiotensin II compared to the control group. High-dose KGS significantly reduced plasma noradrenaline and ANP levels ($p < 0.01$), while aldosterone and angiotensin II levels showed significant reductions ($p < 0.05$ and $p < 0.01$, respectively. The KGS at a low dose did decrease these markers, but the changes were not statistically significant except in the case of plasma ANP level.

3.3.KGS improves ISO-induced histopathological alterations

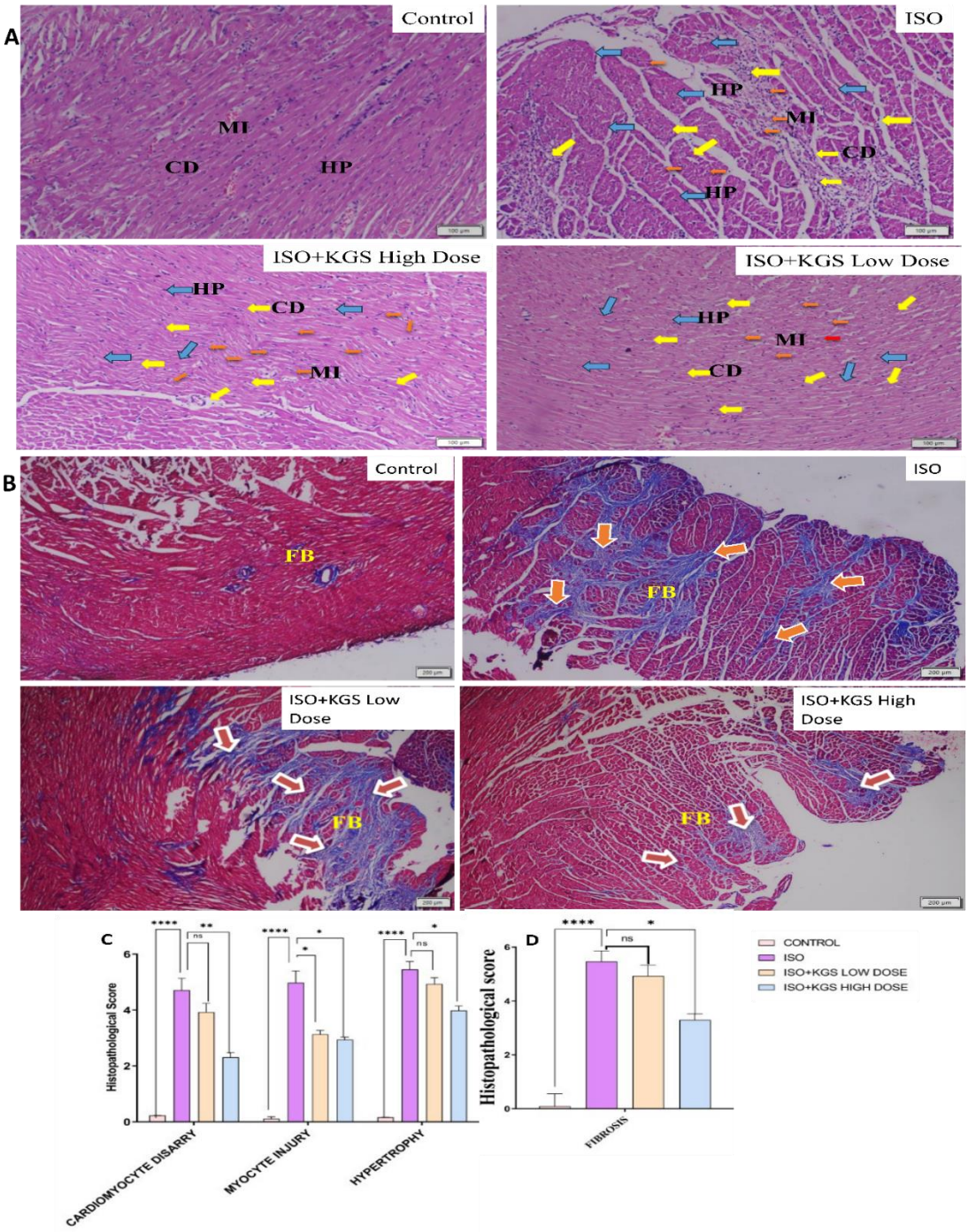

Figure 7: (A) H & E-stained heart section from different groups. KGS high-dose treatment reversed the (B) cardiomyocyte disarray (CD), myocyte injury (MI), and cardiac hypertrophy (HP) induced with ISO-exposed rat hearts. (C) Masson's Trichrome-stained heart sections from different groups. KGS high-dose treatment reduced the fibrosis caused by ISO-exposed rat hearts. FB in the yellow colour denotes fibrosis. (D) Changes in fibrosis across different groups are represented. All data are represented in mean±SD and statistical comparisons were made between control vs ISO; ISO vs ISO + KGS Low Dose and ISO+ KGS High Dose

Representative photomicrographs of H&E staining and Masson's trichrome (MT) staining of the left ventricle from the control and treated groups are shown in Figures 7A and 7B. In the H&E section, photomicrographs from the control group displayed intact left ventricular histoarchitecture and normal myocardial muscle fibers. In contrast, photomicrographs from the ISO-induced group revealed extensive damage, including loss of myofibrils, vacuolization, swelling, necrosis of myocardial cells, and neutrophil infiltration (ISO).In the KGS Low Dose treatment groups, protection with less myofiber loss and neutrophil infiltration compared to the ISO alone group was observed. Similarly, treatment with the KGS High Dose group provided significant protection with occasional myofiber loss and lower neutrophil infiltration compared to the ISO alone group. There was an significant ($p<0.0001$) increase in cardiomyocyte disarray, myocyte injury and cardiac hypertrophy.

Masson's trichrome staining was performed to evaluate the effects of KGS low and high doses on ISO-induced collagen accumulation and cardiac fibrosis. Interstitial collagen accumulation was assessed with representative photomicrographs of the left ventricle from the control and treated groups shown in Figure 7D. The control group displayed typical tissue architecture without collagen deposition. In contrast, the ISO-treated group exhibited significant fibrosis, characterized by extensive collagen deposition in the interstitial regions of the left ventricle. Treatment with KGS high dose significantly reduced myocardial fibrosis, with less interstitial collagen accumulation compared to the ISO-alone group. However, the KGS low-dose group did not prevent collagen accumulation or fibrosis.

3.4.KGS improves Echocardiographic parameters

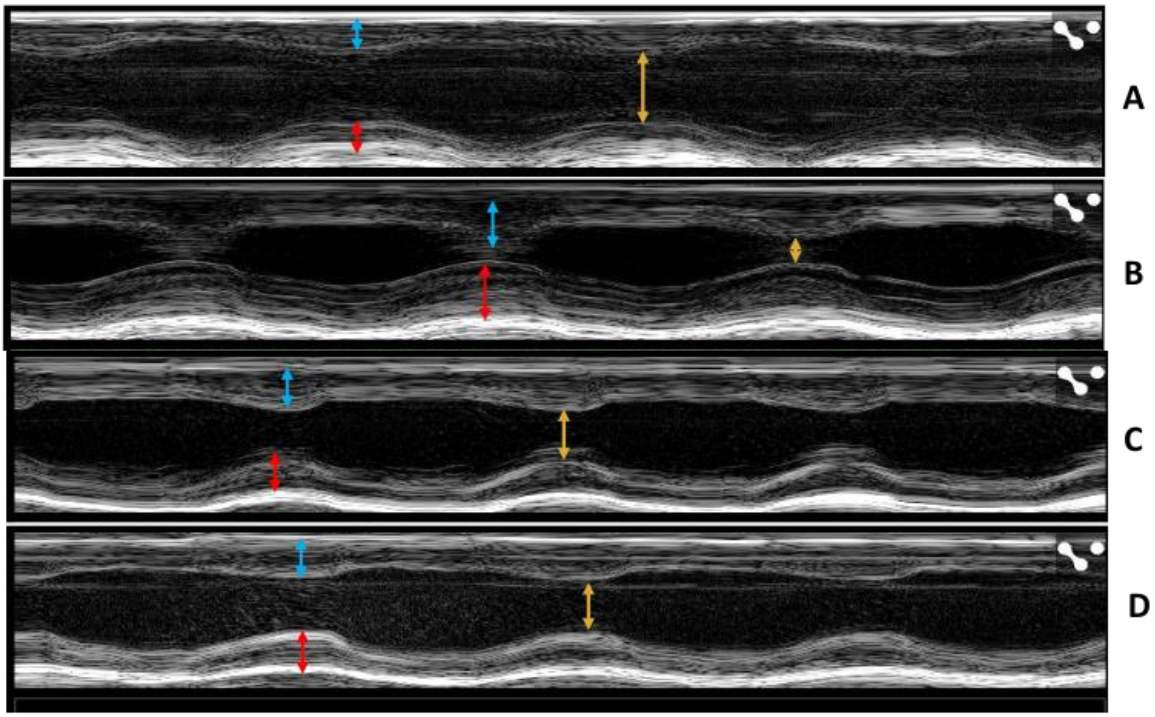

Figure 8: The image shows the left ventricle of the heart in motion-mode (M-mode) after 2 weeks (A) Control (B) Isoproterenol (C) Iso+KGS Low Dose (D) ISO+KGS High Dose. The orange line represents systolic diameter, the blue line shows left ventricular anterior wall thickness during systolic while the red line shows left ventricular posterior wall thickness during systolic

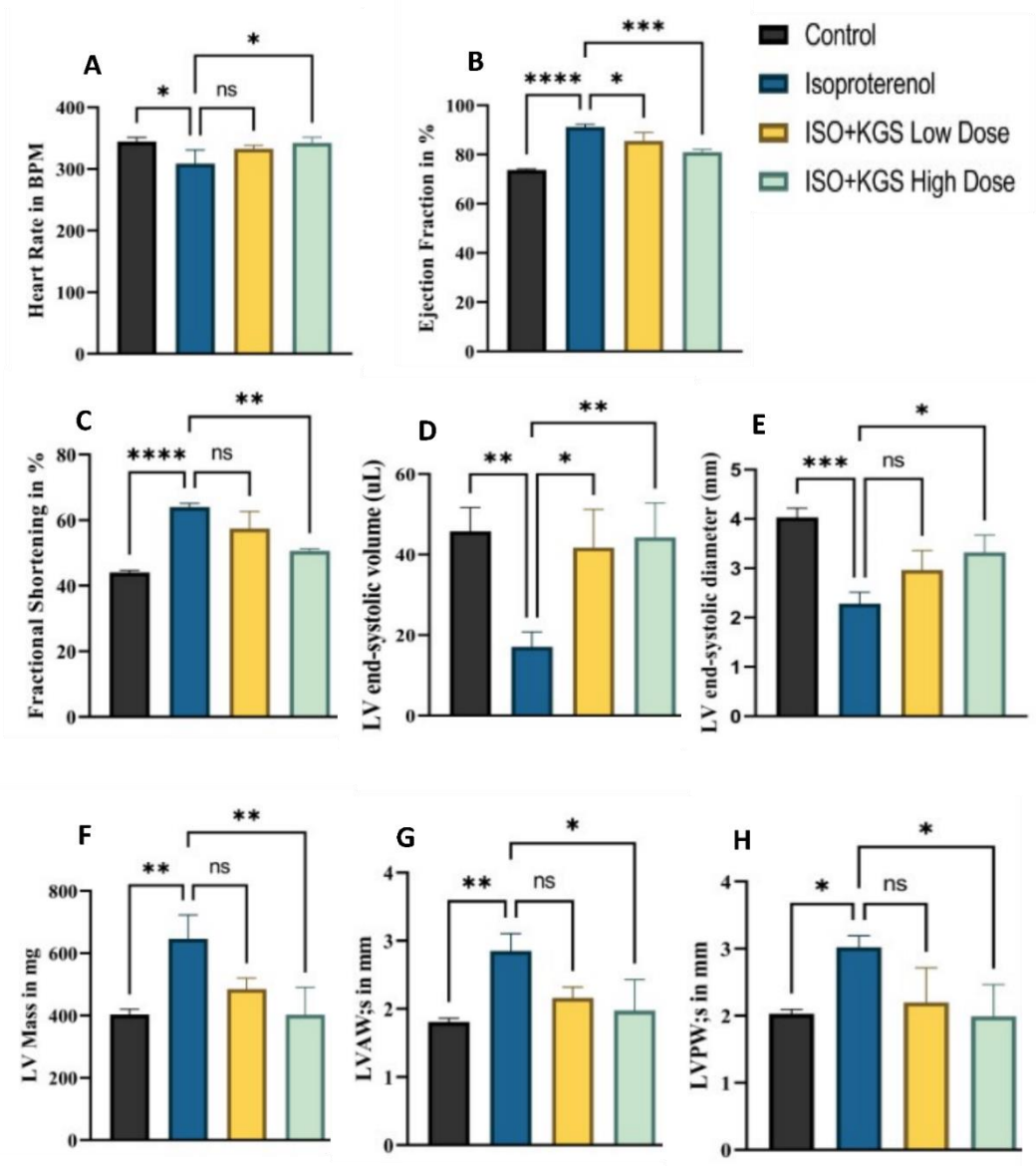

Figure 9: The graph shows different parameters of heart altered in 2 weeks of study period (Mean ± SD, n = 3). The data was analysed with one-way ANOVA followed by Tukey's test for different parameters of heart. *p<0.05, **p<.01, ***p<0.001 ,****p<0.0001, ns-non-significant.

Cardiac function was assessed by echocardiography on the 15th day, following 14 consecutive days of ISO administration. Representative M-mode echocardiography images from each experimental group are shown in Figure 8, while cardiac function parameters are presented in Figure 9. Significant reductions were observed in heart rate ($p<0.05$), left ventricular end-systolic diameter (LVESD) ($p<0.001$), and LV end-systolic volume (LVESV) ($p<0.01$). Additionally, a significant increase was noted in LV mass ($p<0.01$), LVAW,s ($p<0.05$), LVPW,s ($p<0.05$), ejection fraction ($p<0.0001$), and fractional shortening ($p<0.0001$) in the ISO-induced group compared to controls. Treatment with KGS

High Dose for 14 days significantly restored the ISO-induced decreases in heart rate ($p<0.05$), LVESD ($p<0.05$), and LVESV ($p<0.05$), while preventing increases in LV mass ($p<0.01$), LVAW,s ($p<0.05$), LVPW,s ($p<0.05$), ejection fraction ($p<0.001$), and fractional shortening ($p<0.01$) compared to the ISO-alone group.

3.5.MTT assay and intracellular calcium in H9C2 cells

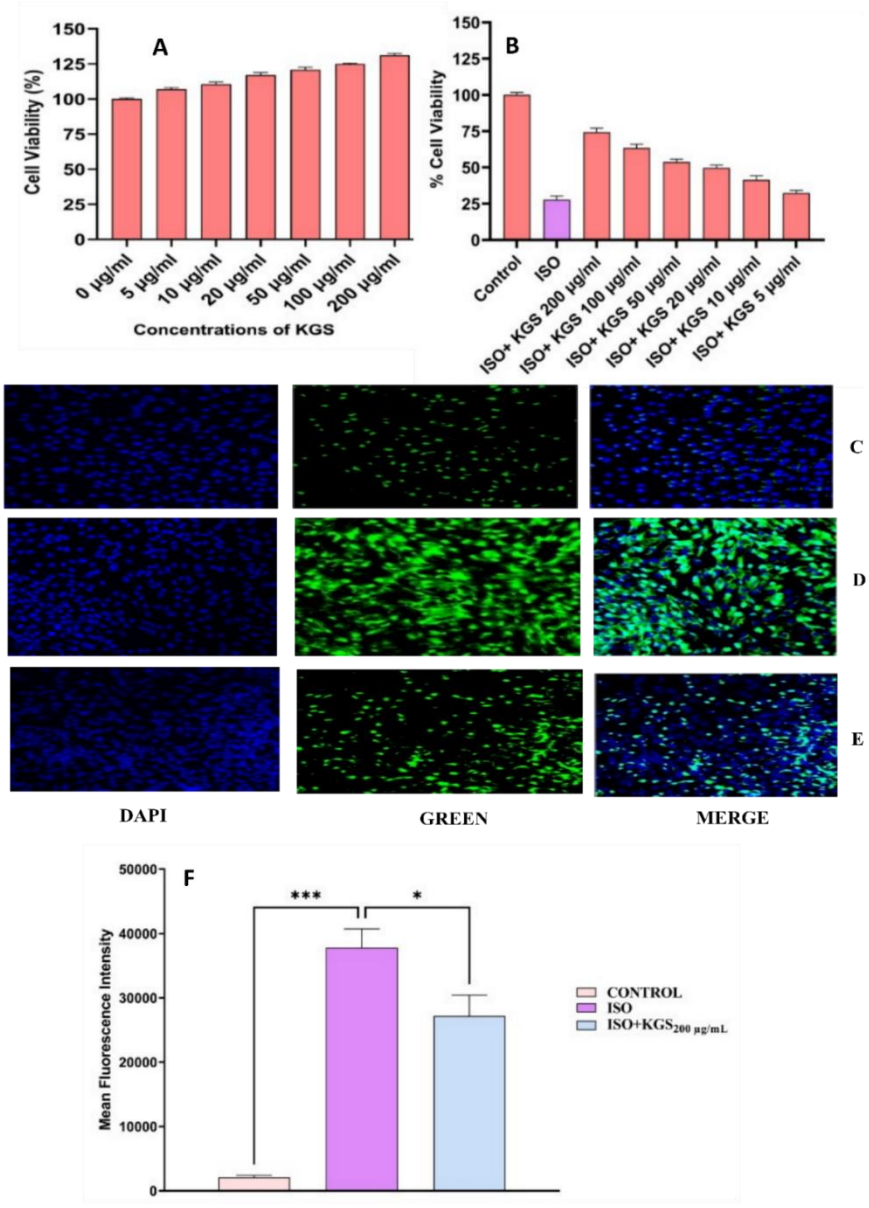

Figure10: Represents the MTT assay performed using H9C2 cells. (A) The control group represents untreated cells (100% viability). In contrast, the other groups of cells are incubated with different concentrations of KGS (0, 5, 10,20, 50,100 and 200 µg/mL) (B) Represents the protective effect of KGS on H9C2 cells where the % cell viability of the control group is taken as 100%, the purple bar indicates H9C2 cells treated with only 10

µM ISO. In contrast, in other groups, the cells were incubated with both ISO and various concentrations of KGS (200,100,50,20,10,5 µg/mL) (C) Representing the control group showing fluorescence due to intracellular calcium in H9C2 cells documented using a Zeiss LSM 700 Confocal microscope (Carl Zeiss 700, Germany) at 20X magnification (D) Represents the cells treated with 10 µM of ISO only (E) Fluorescence of cells co-incubated with ISO and KGS at 200 µg/mL. (F) Shows the intracellular calcium plotted in the graph using Mean fluorescence intensity (MFI) of the control group (untreated), 10 µM ISO group and ISO+ KGS 200 µg/ml. Statistical comparison was made between the Control Vs ISO group and ISO vs ISO+ KGS 200 µg/ml with Mean ±SD.

In Figure 10A, KGS treatment at concentrations ranging from 5 to 200 µg/mL for 6 hours did not reduce cell viability. In fact, % cell viability of H9C2 cells increased in a dose-dependent manner. KGS was found non-toxic till the tested concentration of 200 µg/ml. In Figure 10B, pre-treatment with KGS for 3 hours, followed by ISO exposure for 6 hours, demonstrated a dose-dependent protective effect of KGS against ISO-induced cytotoxicity. The ISO-only group exhibited significantly reduced % cell viability compared to the control. However, KGS pre-treatment mitigated this reduction, with a concentration of KGS 200 µg/mL showing the most pronounced protective effects, restoring the cell viability. Figure 10C, 10D and 10E represent the fluorescence due to intracellular calcium using Fluo-4 NW in Control, ISO alone and ISO+KGS 200 µg/mL, respectively. The mean Fluorescence intensity (MFI) was assessed using Image J software version 1.4 (NIH, USA). Treatment with 10 µM ISO to H9C2 cells (Fig 10D) significantly ($p<0.001$) increased MFI in ISO group cells as compared to control (Fig 10C). In contrast, co-incubation with KGS at a dose of 200 µg/ml (Fig 10E) significantly ($p<0.05$) reduced the MFI when compared with ISO-alone treated cells.

3.6.CYP inhibition assay in Human Liver Microsomes

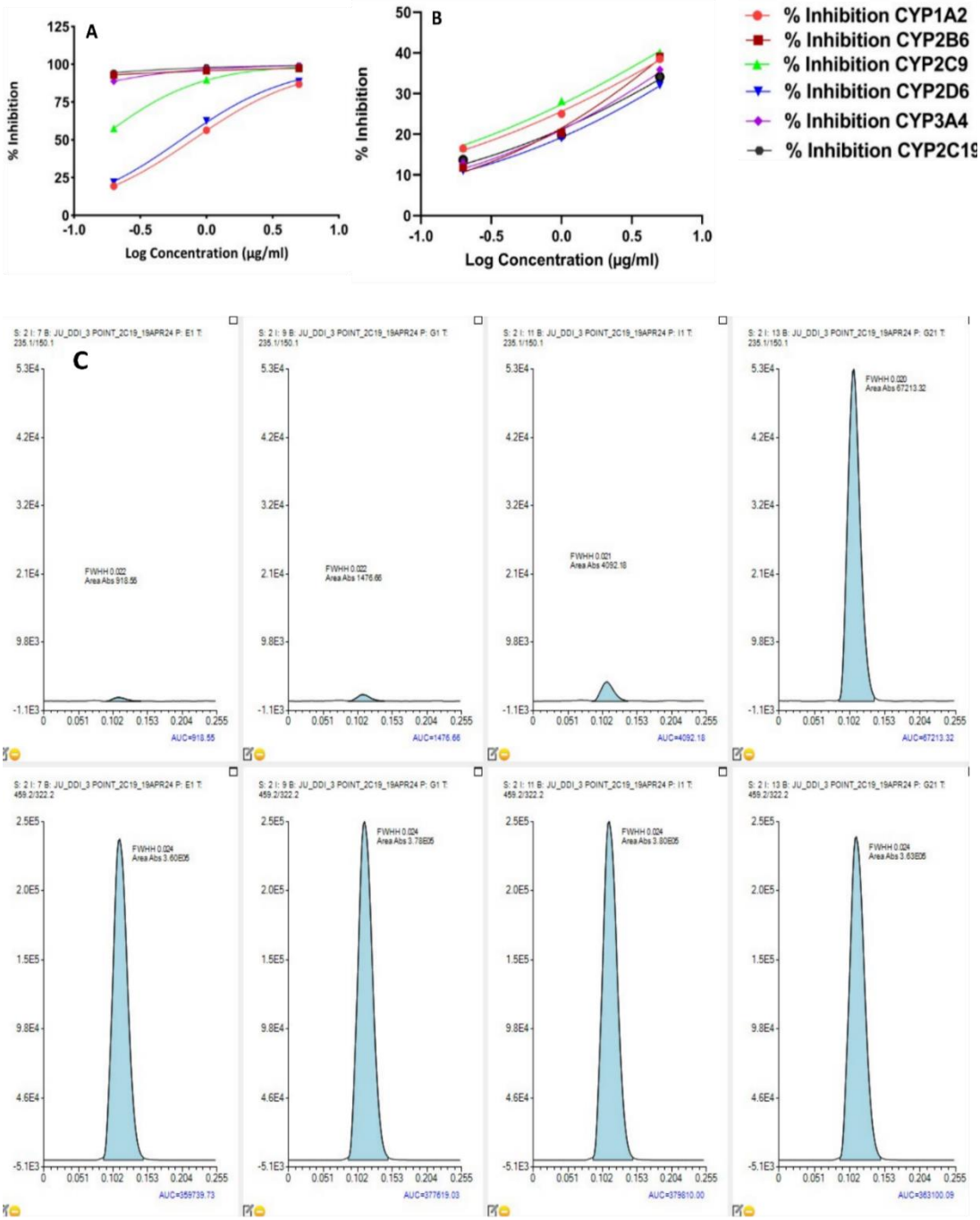

Figure 11: (A) and (B) shows the % inhibition of CYP450 enzymes i.e. CYP1A2, CYP2B6, CYP2C9, CYP2D6, CYP3A4, CYP2C19 where the IC_{50} (µg/ml) was estimated. The IC_{50} (µg/ml) for the (A) positive control Miconazole for inhibiting CYP1A2, CYP2B6, CYP2C9, CYP2D6, CYP3A4, CYP2C19 were 0.79, <0.20, <0.20 , 0.64 , <0.20 , <0.20 while for (B) KGS it was found to be more than 5 µg/ml for all the CYPs. (C) Represents the Q1 and Q3 MRM of CYP2C19 substrate OH-Mephynotoin: 235.1> 150.1;Internal standard: 459.2>322.2

Table 1: Shows the IC_{50} (µg/ml) value of KGS and positive control Miconazole

Compound	CYP1A2	CYP2B6	CYP2C9	CYP2D6	CYP3A4	CYP2C19
KGS	>5.00	>5.00	>5.00	>5.00	>5.00	>5.00
Miconazole	0.79	<0.20	<0.20	0.64	<0.20	<0.20

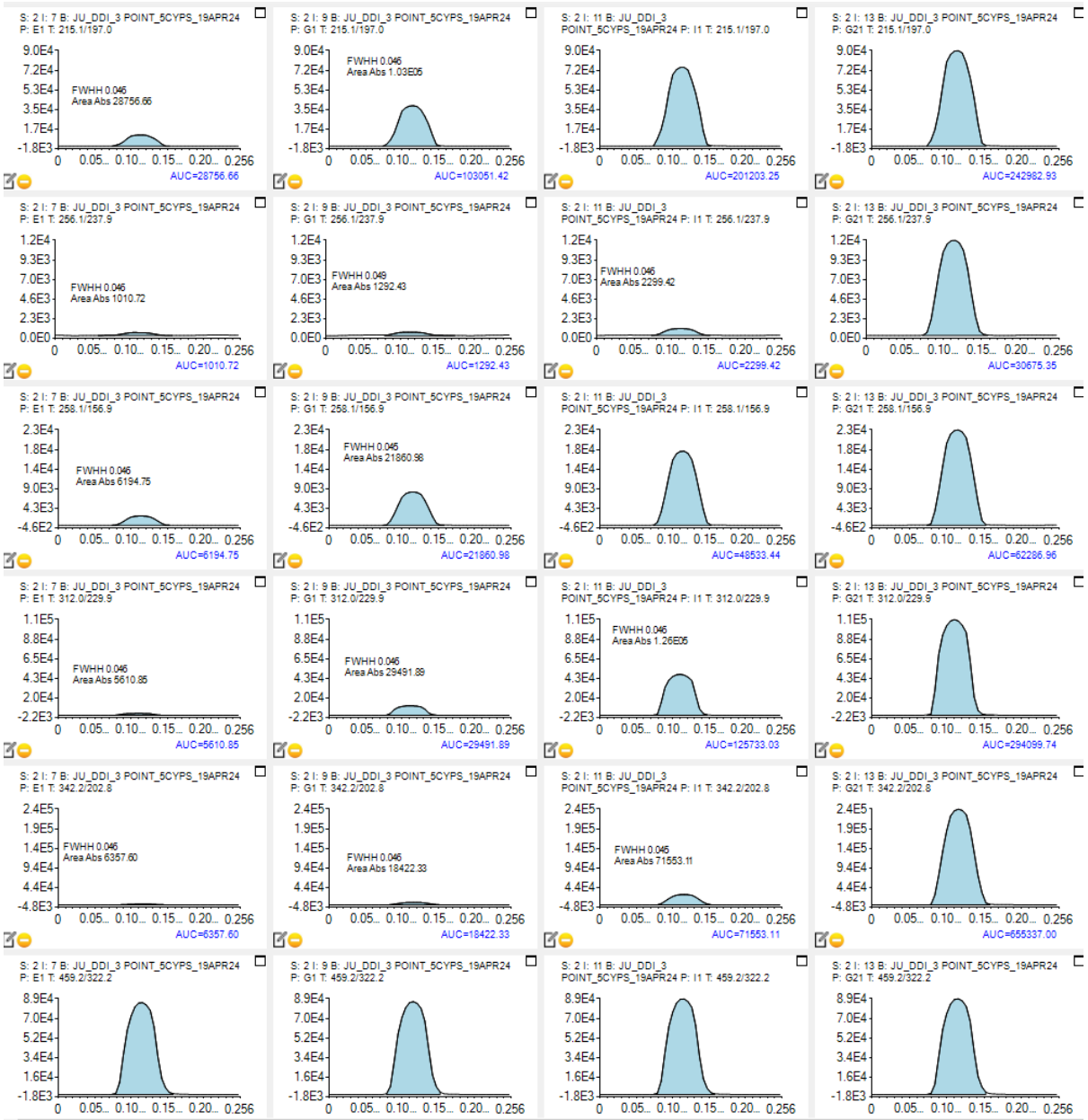

Figure 12: Represents the Q1 and Q3 MRM of different CYP substrates and internal standards. For 5CYPS-: OH-Tacrine: 215.1> 197.0; OH-Bupropion: 256.1>237.9; Dextrophane: 258.1> 156.9; OH-Diclofenac: 312.0>229.9; OH-Midazolam: 342.2> 202.8; Internal standard: 459.2>322.2

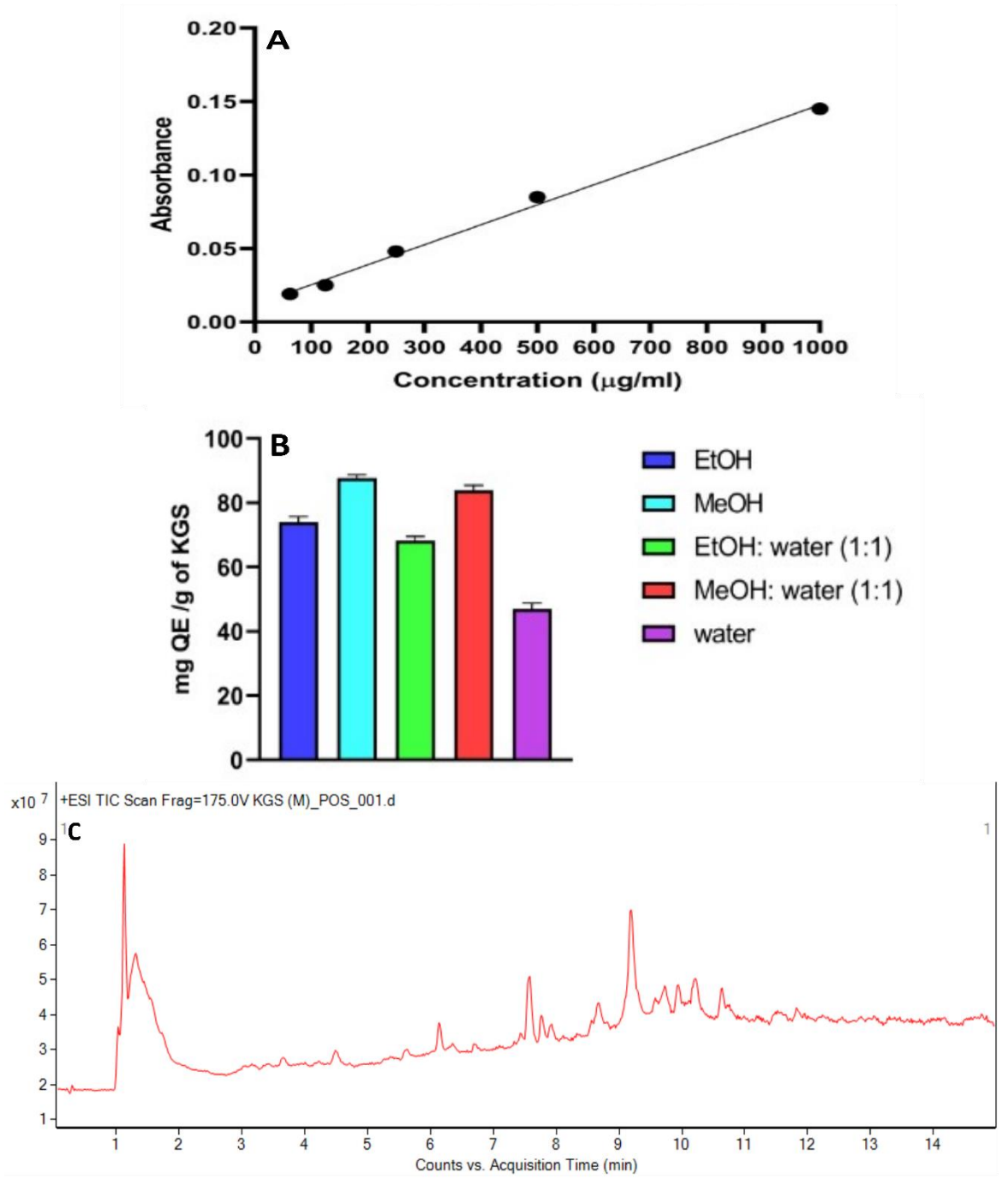

Figure13: (A) Represents the Standard calibration curve of Quercetin (B) Total Flavanoid content (TFC) present in KGS was estimated in 5 different solvent fractions, namely EtOH, MeOH, EtOH: Water (1:1) and MeOH: Water (1:1) and water (C) The Total Ion Chromatogram obtained from the metabolite analysis of KGS in positive mode

The TFC present in KGS in (Fig 13 A & 13B) EtOH, MeOH, EtOH: Water (1:1) and MeOH: Water (1:1) and water are 74.03±1.71, 87.68 ±1.05, 68.31 ±1.24, 83.91 ±1.51, 47.00 ±1.75 mg Quercetin per gm of KGS. Out of the 5 fractions, the methanolic extract showed the best yield of TFC

3.7. Metabolites in KGS

Table 2: List of 19 metabolites present in KGS using LC-qTOF-MS in positive mode

Identity of the chemical moiety	Class of the compound	Formula of the compound	Exact mass	Obtained m/z	Retention time (min)	Mass error (ppm)	Score	ms/ms fragment
Vanillic acid	polyphenol	$C_8 H_8 O_4$	168.0431	169.0502	7.446	4.82	93.22	138.1278, 100.1126
Uridine	pyrimidine nucleoside	C9 H12 N2 O6	244.0711	245.0783	9.577	6.28	89	227.1432 199.1495 159.0761 131.087 105.0705
palmitic acid	long-chain fatty acids	C16 H32 O2	256.24	274.2739	11.492	-0.96	99.56	257.1498 229.9915 208.9362 184.1053 165.0133 135.1168 107.0843
Nonenal	Organic compound	C9 H16 O	140.1198	158.1537	1.236	-1.96	99.17	141.0137 126.1255 101.059
cinnamic acid	Organic compound	C9 H8 O2	148.0529	166.0868	10.63	3.37	88.52	136.9839 120.0802 105.0163
Isoscopoletin	hydroxycoumarin	C10 H8 O4	192.0413	193.0495	6.680	-4.83	85.67	178.0327 160.9912 150.0367 117.0021
Hexadecanal	organic compound	C16 H32 O	240.2446	258.2785	11.33	-3.14	97.85	240.9273 202.1166 171.0063 131.0896 102.9693

Identity of the chemical moiety	Class of the compound	Formula of the compound	Exact mass	Obtained m/z	Retention time (min)	Mass error (ppm)	Score	ms/ms fragment
Heptadecanoic acid	long-chain fatty acid	C17 H34 O2	270.2552	288.2892	13.439	-2.35	97.7	271.1714 249.1841 220.9361 191.1723 174.1009 140.0762 112.1131
5-Hydroxymaltol	Organic compound (pyranones)	C6 H6 O4	142.0261	143.0335	3.417	-3.41	85.52	127.0391 101.0417
Coriandrone A	phenolic compounds	C16 H20 O5	292.131	310.1648	5.382	-0.4	99.92	251.0917 207.0649 185.043 149.021
Bisacumol	sesquiterpenoid	C15 H22 O	218.1679	219.1742	13.41	3.89	86.84	179.1507 149.0207 130.1158
7-Methoxycoumarin	coumarin	C10 H8 O3	176.047	177.0543	9.577	-1.72	99.22	160.9737 149.0274 131.0027 112.9913 100.9874
Diethyl phthalate	phthalates	C12 H14 O4	222.0891	245.0783	9.577	-0.46	99.78	227.1432 209.1317 205.1523 199.1495 189.0889 178.9534 167.0854 159.0761 140.9822 131.0870

Identity of the chemical moiety	Class of the compound	Formula of the compound	Exact mass	Obtained m/z	Retention time (min)	Mass error (ppm)	Score	ms/ms fragment
								120.0500 105.0705
Trehalose	disaccharides non-reducing sugar	C12 H22 O11	342.1167	365.1057	1.286	1.51	99.21	203.0534 185.0427
Tiliroside	glycosidic flavonoid	C30 H26 O13	594.1363	617.1253	8.711	-2	94.23	597.2227 585.3969 574.0371 555.9919 517.0426 459.8742 363.1641 333.1166 319.1122 145.0986
Methyl 2-(methylamino)benzoate	Organic compound	C9 H11 N O2	165.0795	166.0868	10.63	3.03	88.52	148.9565 136.9839 120.0802 112.1107 105.0163
Isorhamnetin 3-O-beta-glucopyranoside-7-O-alpha-rhamnopyranoside	Flavonoid	C28 H32 O16	624.1681	647.1576	7.979	-1.19	96.21	639.1403 629.2161 613.8057 605.5258 433.1273 364.9199

Identity of the chemical moiety	Class of the compound	Formula of the compound	Exact mass	Obtained m/z	Retention time (min)	Mass error (ppm)	Score	ms/ms fragment
								212.0929
Icariside B2	megastigmane glucoside	C19H30 O8	386.1924	409.1825	6.231	-4.31	94.57	396.5395 365.0938 333.003 309.1158 251.1256 245.0492 230.1108 202.1787 153.0915 129.053
Hispidulin	Flavonoid	C16H12 O6	300.0628	323.0539	5.615	-3.44	89.54	304.8846 291.0452 275.9837 258.1049 235.5595 210.9589 199.0135 145.0492 127.0381 110.9739

As indicated in Table 2, the metabolites found in the KGS methanolic extract were examined using LC-q TOF-MS in positive mode. It was observed that the metabolites identified in the methanolic extract of KGS were Polyphenols: Vanillic acid (RT-7.446 min), Pyrimidine Nucleosides: Uridine (RT-9.577 min), Long-Chain Fatty Acids such as Palmitic acid (RT-11.492 min) Heptadecanoic acid (RT-13.439 min), Organic Compounds like Nonenal (RT-1.236 min) Cinnamic acid (RT-10.63 min) Hexadecanal (RT-11.33 min) 5-Hydroxymaltol (RT-3.417 min) Methyl 2-(methylamino)benzoate (RT-10.63 min), Hydroxycoumarins like Isoscopoletin (RT-6.680 min) Phenolic Compounds: Coriandrone A (RT-5.382 min) Sesquiterpenoids: Bisacumol (RT-13.41 min) Coumarins: 7-Methoxycoumarin (RT-9.577 min) Phthalates: Diethyl phthalate (RT-9.577 min) Disaccharides (Non-Reducing Sugars): Trehalose (RT-1.286 min) Flavonoids: Tiliroside (RT-8.711 min), Isorhamnetin-3-O-beta-glucopyranoside-7-O-alpha-rhamnopyranoside (RT-7.979 min) Hispidulin (RT-5.615 min) Megastigmane Glucosides: Icariside B2 (RT-6.231 min) were detected. Table 2 shows a list of 19 metabolites present in KGS, accompanied by its TIC (Figure 13C). The MS/MS fragmented masses of each metabolite acquired at a collision energy of 10.0 eV are also listed in Table 2, consisting of primarily phenolics, flavonoids and organic compounds that were tentatively detected.

3.8. Molecular Docking interaction with eNOS (6CIE) and β1AR (7BVQ)

The docking outcomes were assessed utilising the LibDock score as the selection criterion. The LibDock scores for eNOS (6CIE) and β1AR (7BVQ) and the five most effective active components in KGS are illustrated in Figures 14 and 15, respectively. The docking data indicate that the LibDock score of Tiliroside with eNOS was markedly superior to those of other active compounds. The interacting amino acids of the macromolecules, together with their interactions, such as conventional hydrogen bonds and hydrophobic interactions, are presented below in Table 3. In addition to Tiliroside, Isorhamnetin-3-O-beta-glucopyranoside-7-O-alpha-rhamnopyranoside, Icariside B2, Trehalose and Heptadecanoic acid were identified as the most stable molecules among the phytoconstituents derived from KGS against eNOS. However, in the case of β1AR, Trehalose had superior stability and exhibited a more favourable Libdock score compared to other components. Regarding the other macromolecule, β1AR, in addition to Icariside B2, Hispidulin, Heptadecanoic acid, and Palmitic acid have notable docking scores relative to other chemical constituents (table 4). The interactions of different phytochemicals with eNOS (6CIE) and β1AR (7BVQ) are presented in Figures 14 and 15

Table 3: Docking analysis of the most active components with eNOS (6CIE)

Phyto- Compound	Lib Dock score	Hydrogen Bond	Hydrophobic Interaction
Tiliroside	188.453	ARG365(2), TRP356	PRO334, PRO451, PTO334, HEM501(2)
Isorhamnetin 3-O-beta-glucopyranoside-7-O-alpha-rhamnopyranoside	163.032	-	MET358, VAL185, VAL418, TRP356 (2), TRP178 (3), ALA181(2), MAT339, PHE473(2), LEU193(2), PHE353(2), CYS184 (4), PRO182
Icariside B2	150.986	GLY355, ARG250, GLN247	MAT339, VAL336(2), SER246, SER354, PRO334, TRP356, TYR357 HEM501
Trehalose	145.096	HEN501, GLN247(2), PRO334	GLEU361(2)
Heptadecanoic Acid	133.213	ASN338	TYR475, HEM501(2)

Table 4: Docking analysis of the most active components with β1AR (7VBQ)

Phyto- Compound	Lib Dock score	Hydrogen Bond	Hydrophobic Interaction
Trehalose	123.92	ALA 1225, SER1228, ASP1238(2), ASN1363	PHE1340, VAL1139, ASN1344
Icariside B2	123.267	ASN1363(2), TRP1364,	TRP1134 (2), PHE1218 (2), PHE1340, PHE1359
Hispidulin	120.483	THR1220	PHE1218 (2), VAL1139, VAL1142, PHE1341, ALA125 (2), SER1228, PHE1218 (3)
Heptadecanoic acid	112.037	THR1220, ASN1344,	
Palmitic acid	110.491	ASP1138,	ASN1363

Figure 14: Represents the 2D docking representation of eNOS with tentative phytomolecules present in KGS

Phytocomponents	6CIE activity
Vanillic acid	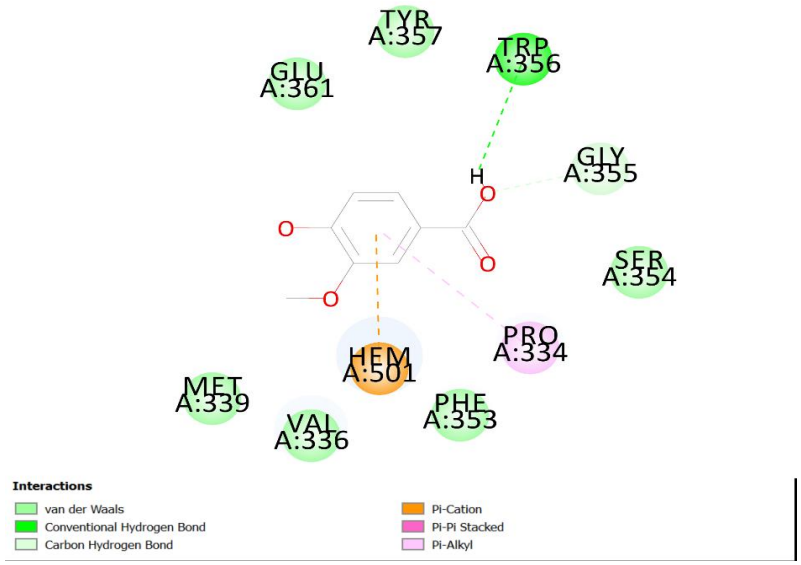
Trehalose	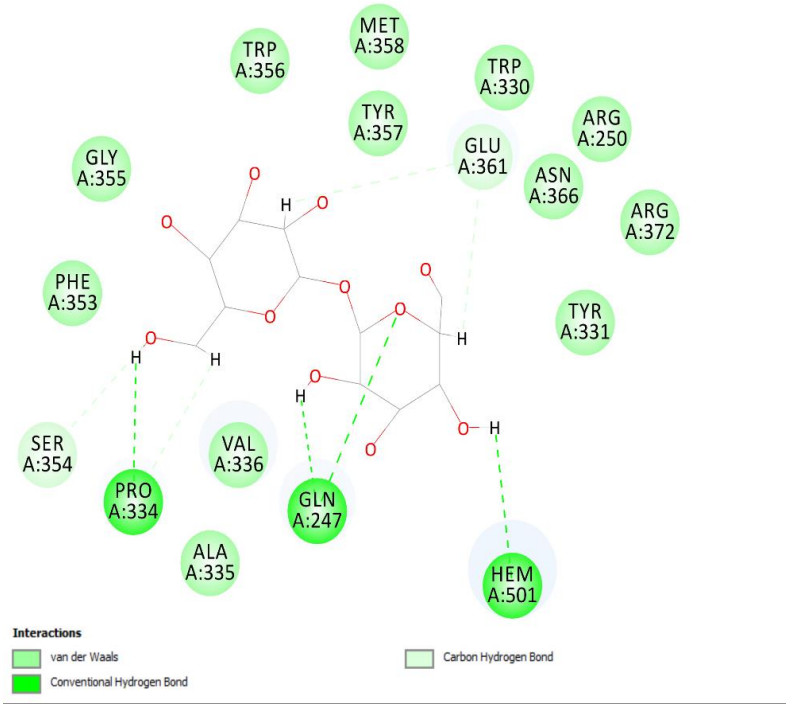

Uridine	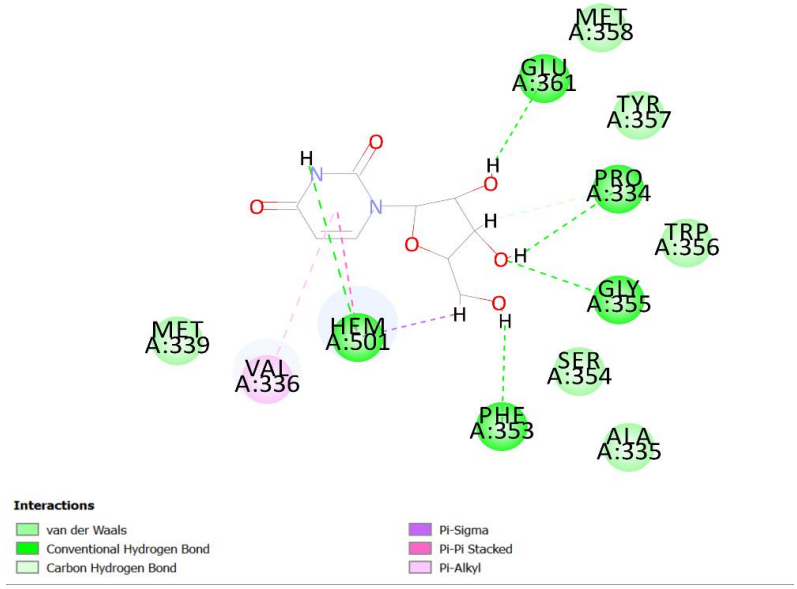
Tiliroside	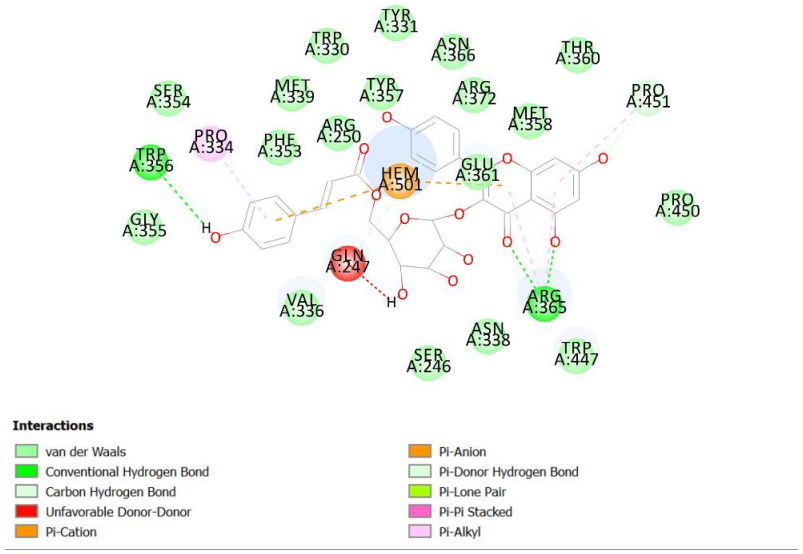

Palmitic	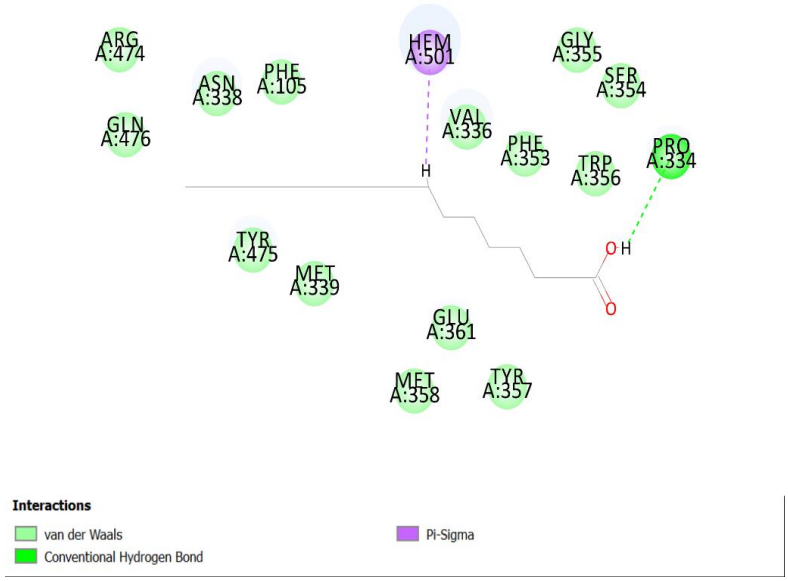
Noneal	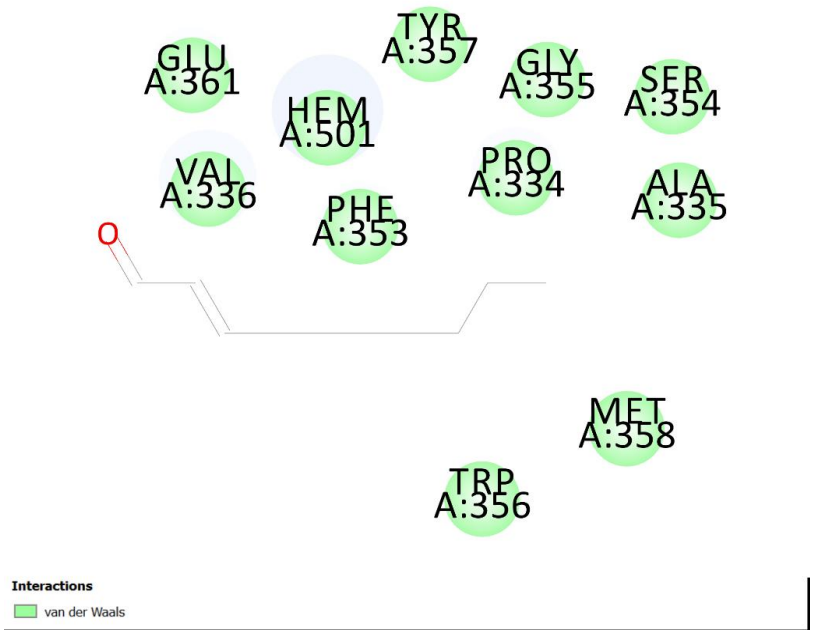

Cinnamic acid	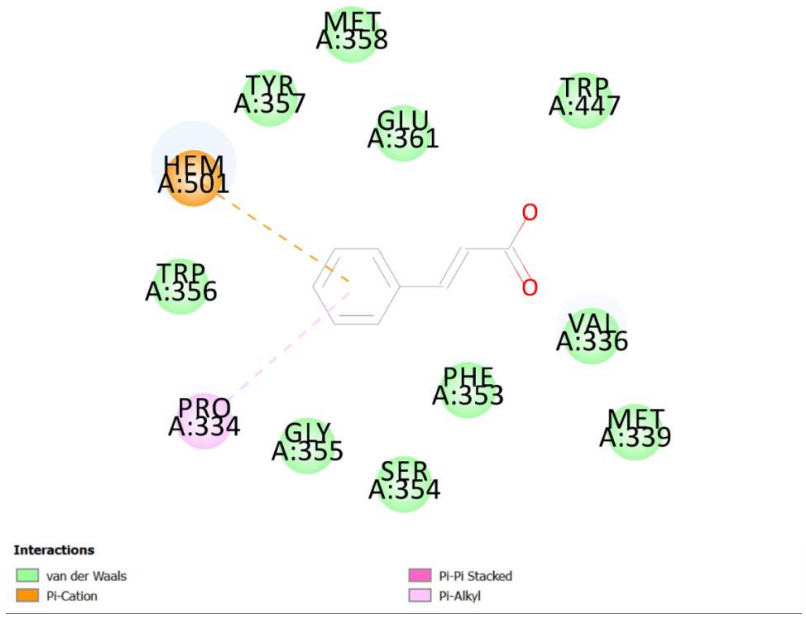
Isoscopoletin	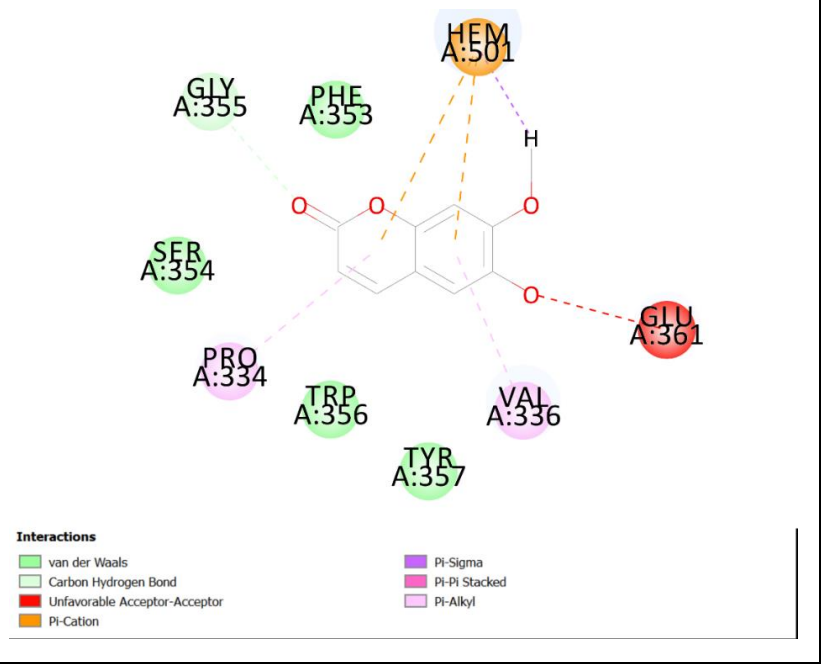

Hexadecanal	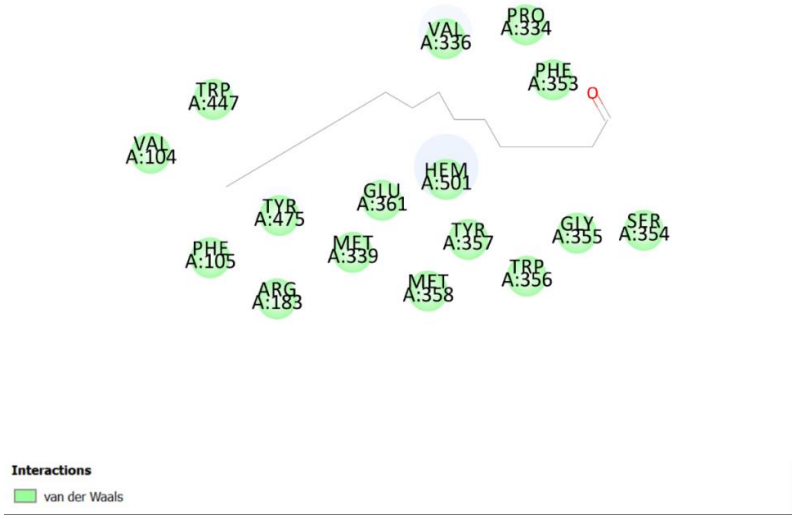
Heptadecanoic acid	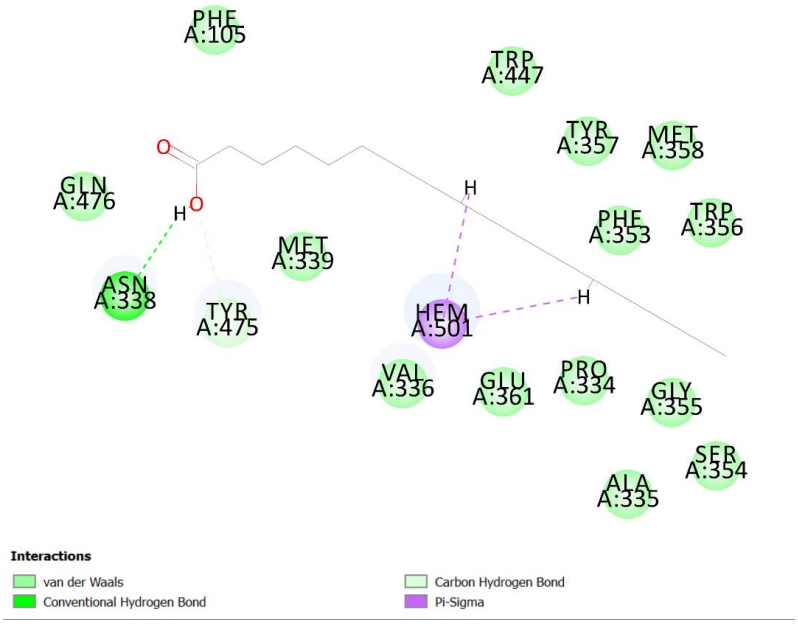

5-Hydroxymaltol	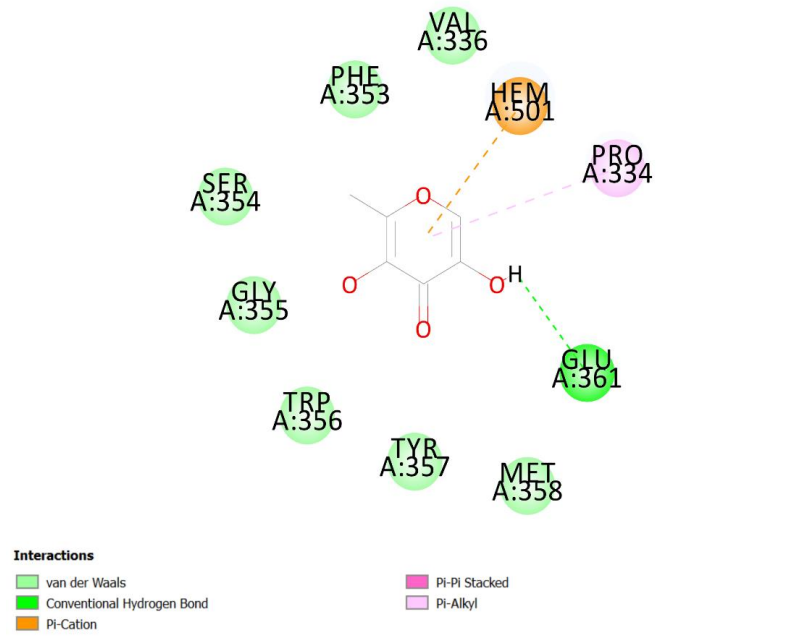
Coriandrone A	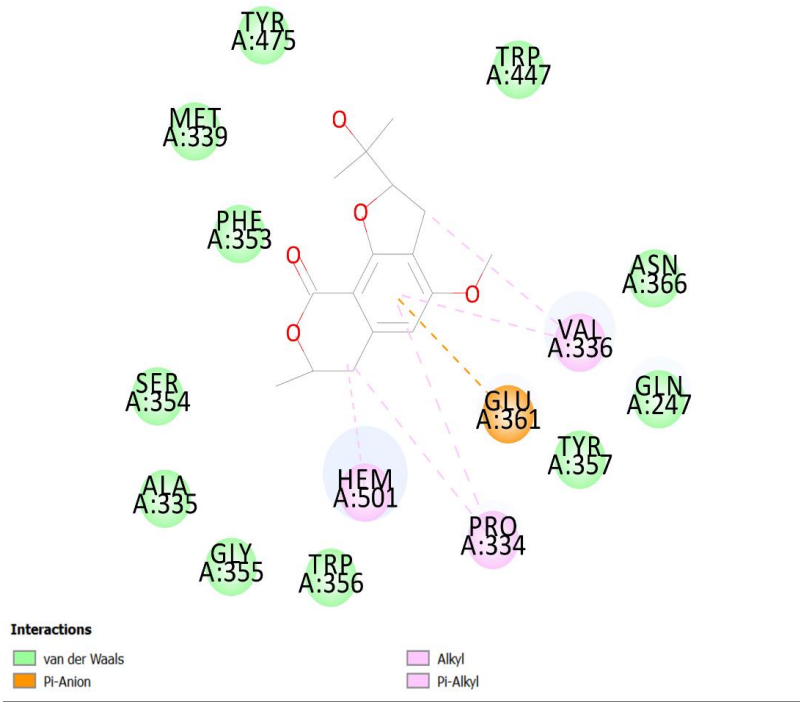

Bisacumol	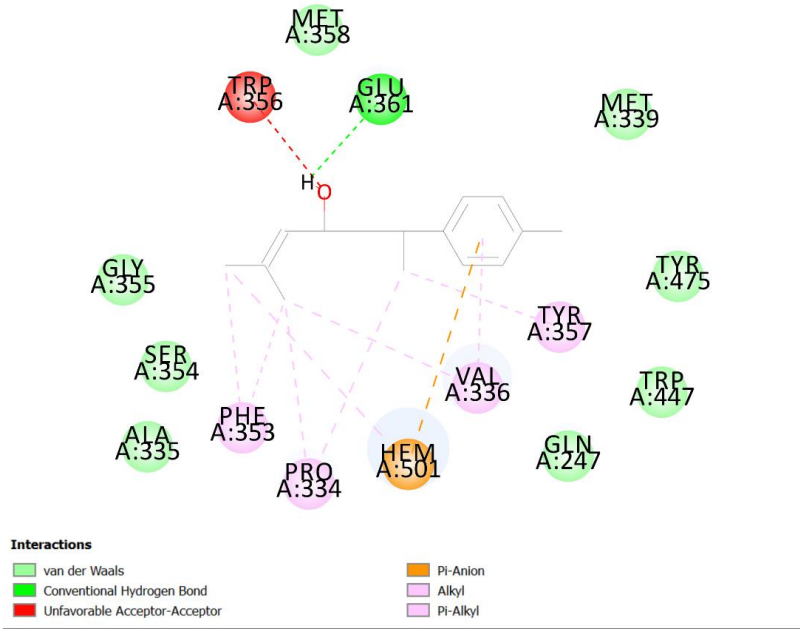
7,Methoxycoumarin	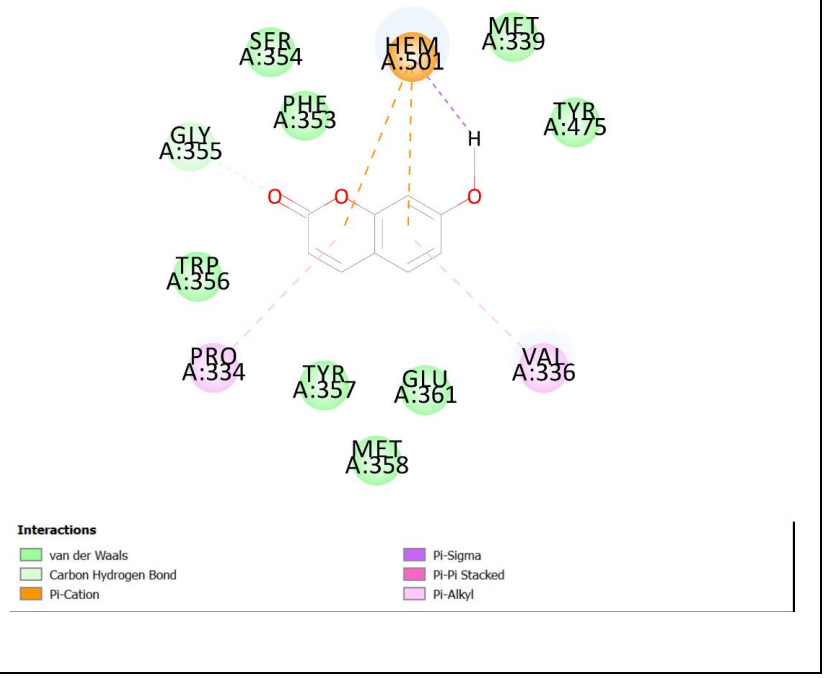

Isorhamnetin 3-O-beta-glucopyranoside-7-O-alpha-rhamnopyranoside	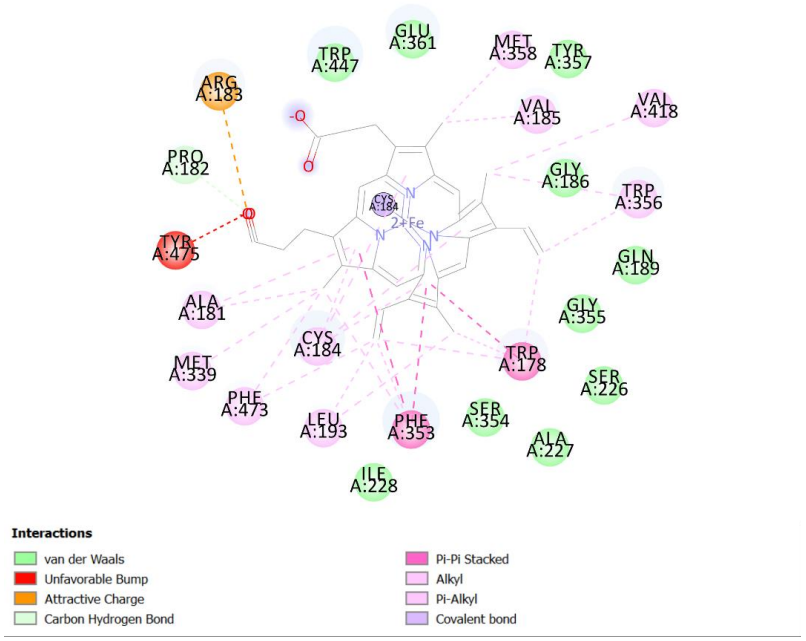
Diethyl phthalate	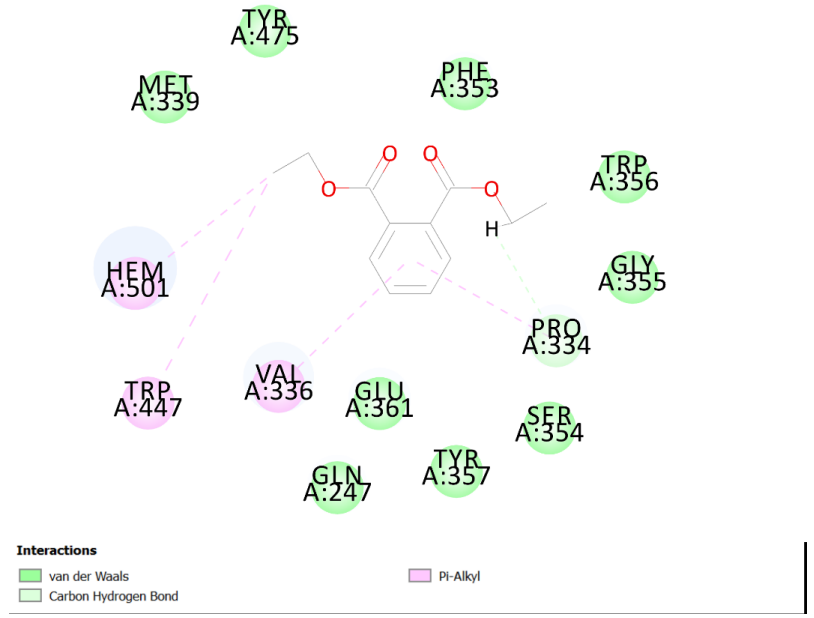

Icariside B2	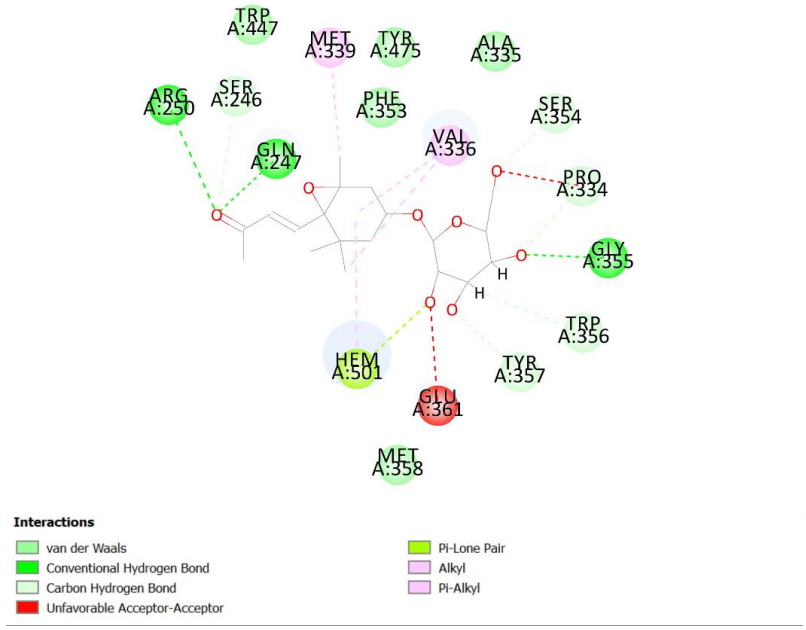
Hispidulin	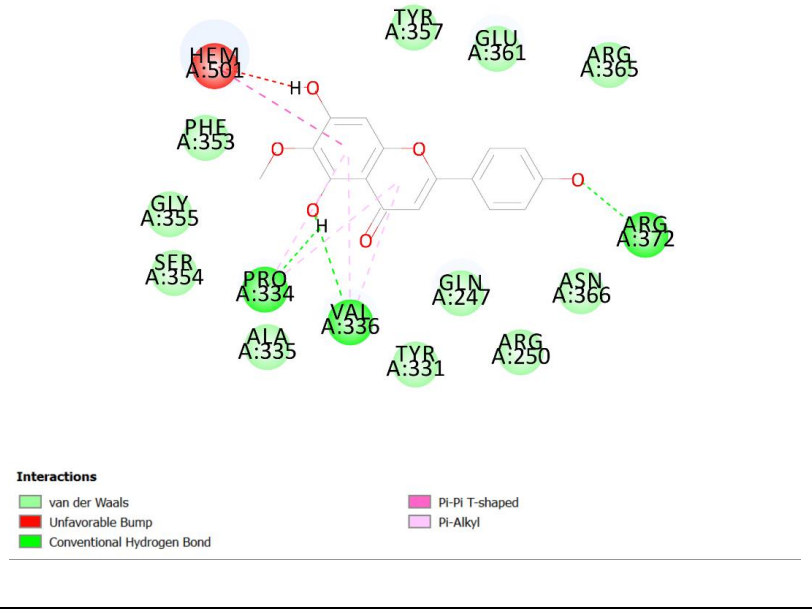

Methyl 2-(methylamino)benzoate	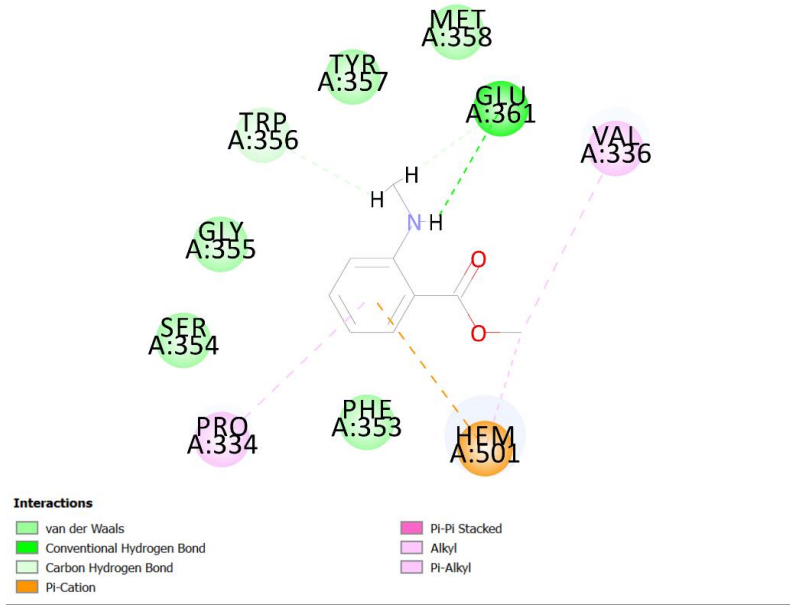

Figure 15: 2D docking representation of β1AR with tentative phytomolecules present in KGS

Phytocomponents	**7VBQ activity**
Vanillic acid	
Trehalose	

Uridine	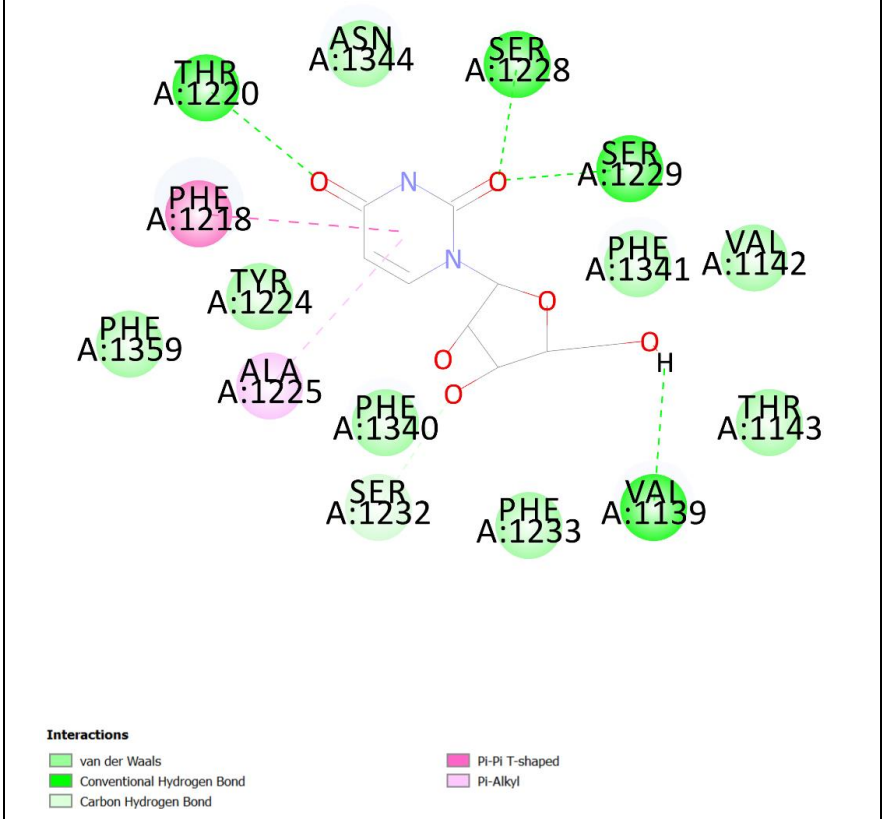
Palmitic acid	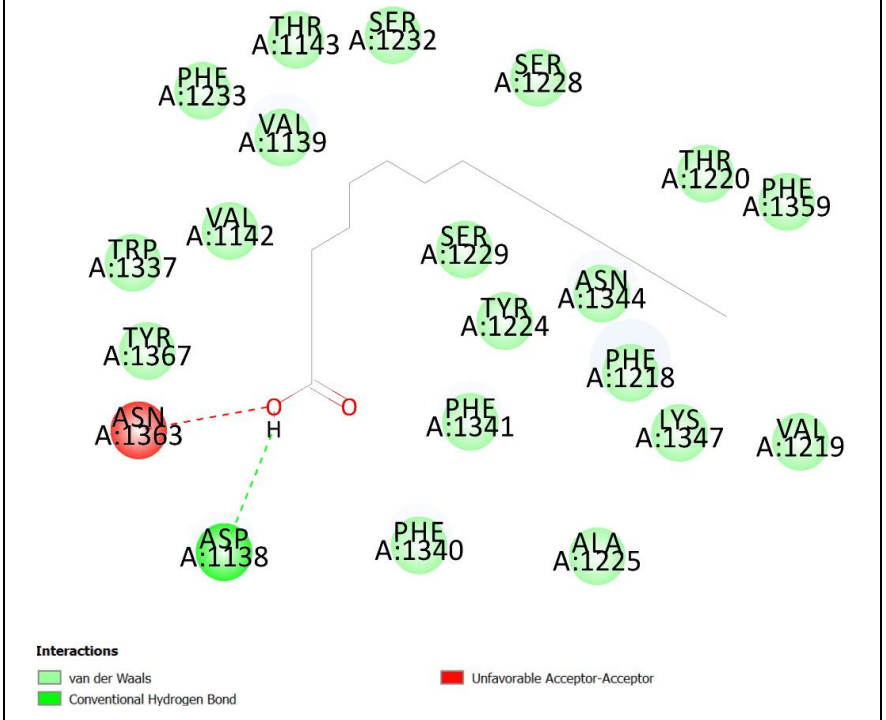

Noneal	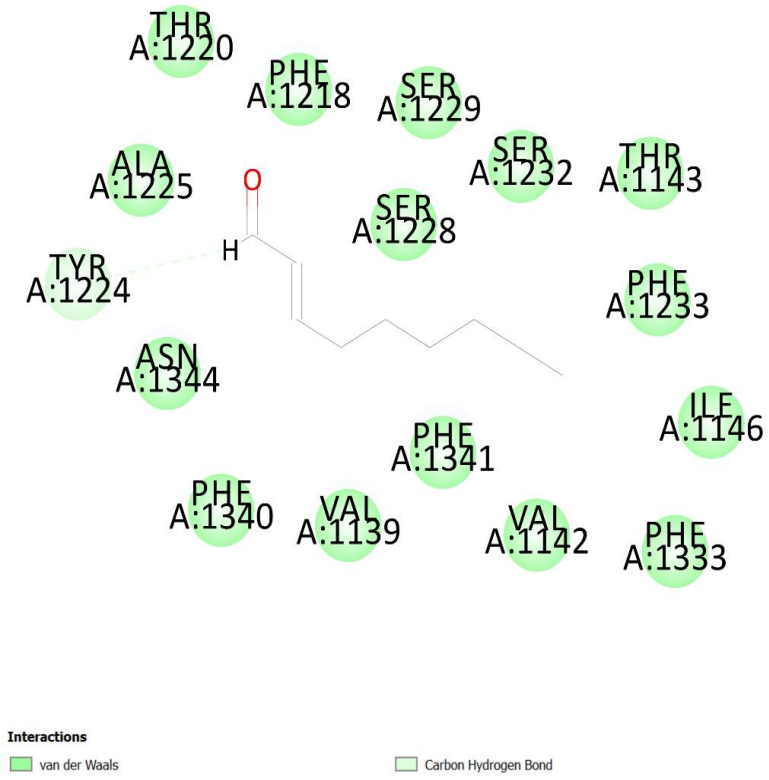
Cinnamic acid	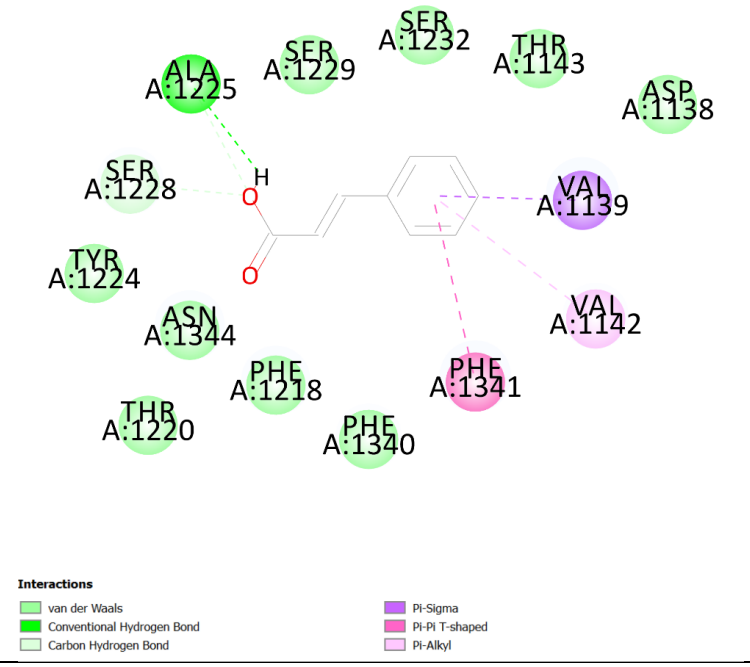

Isoscopoletin	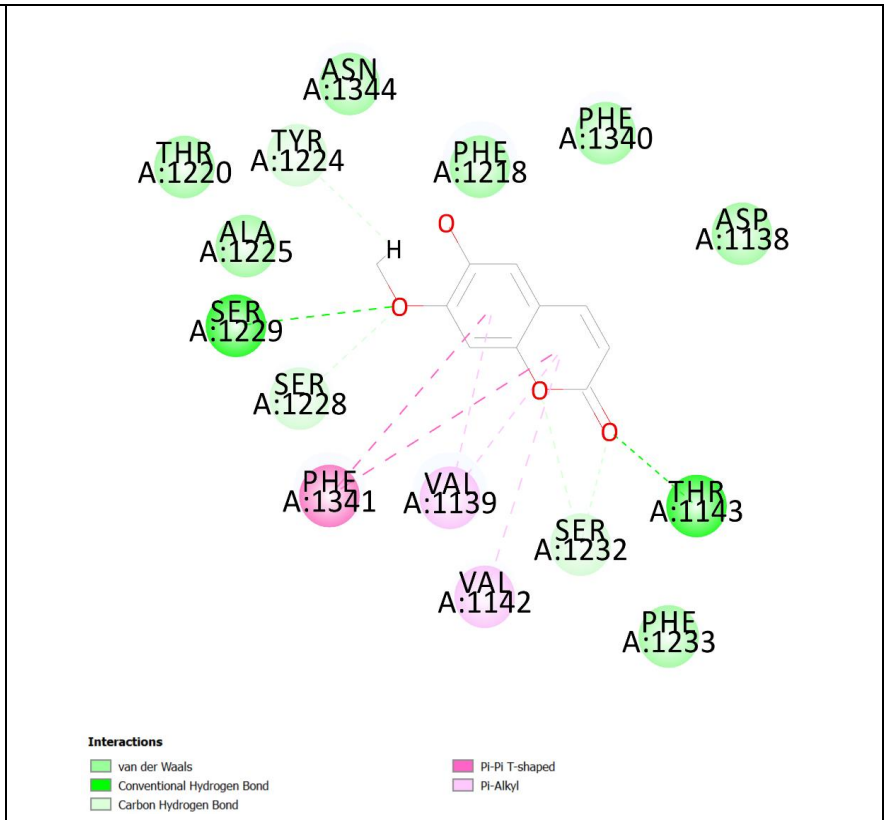
Hexadecanal	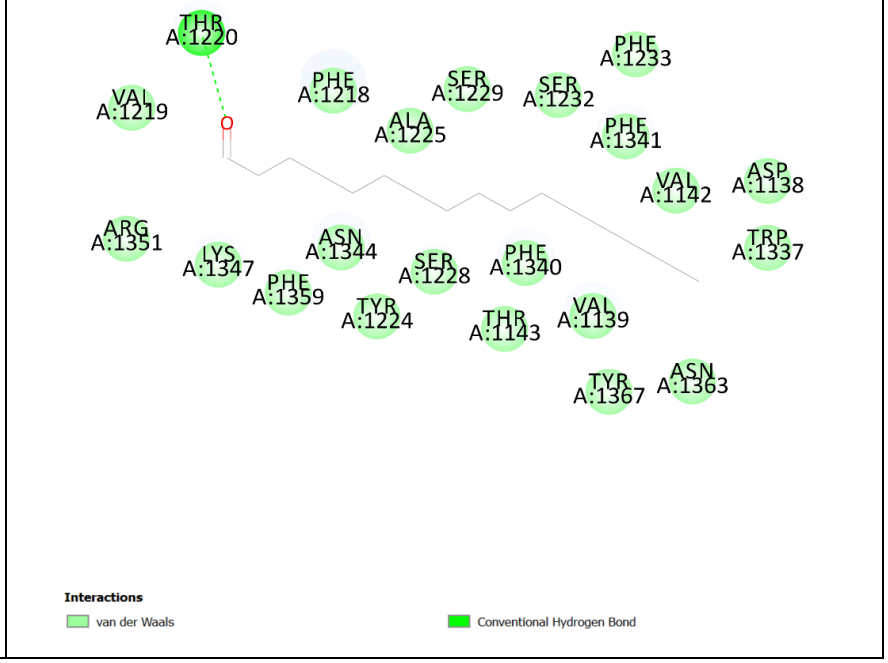

Heptadecanoic acid	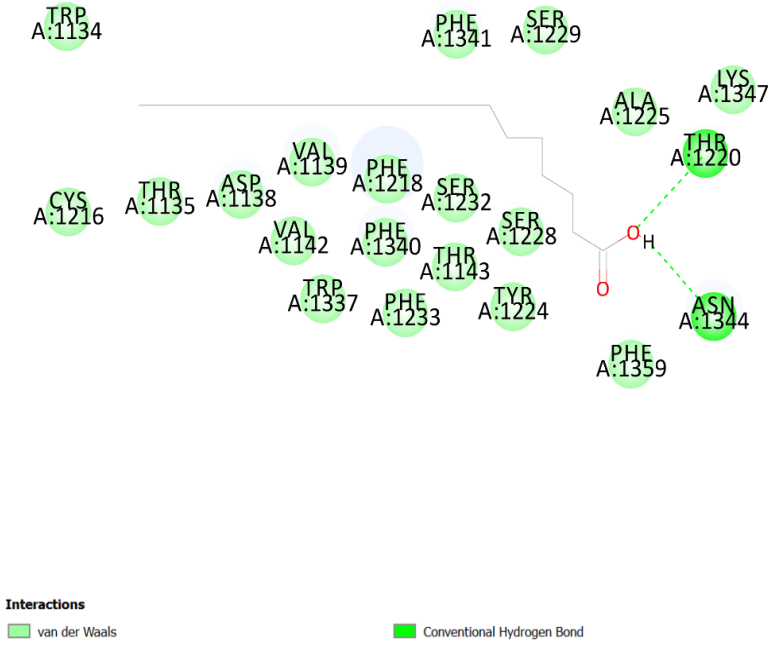
5-Hydroxymaltol	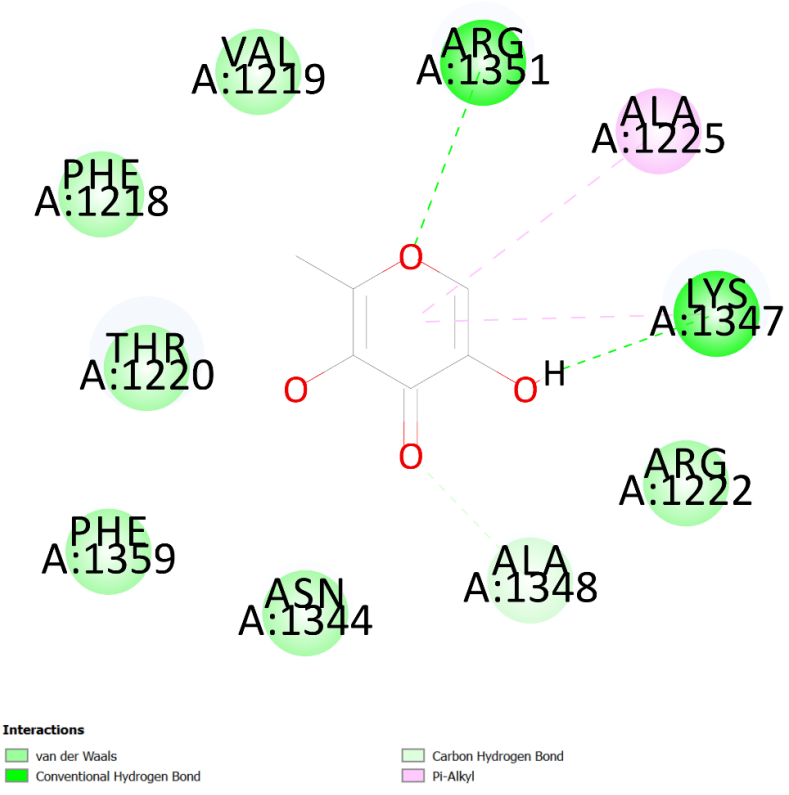

Coriandrone A	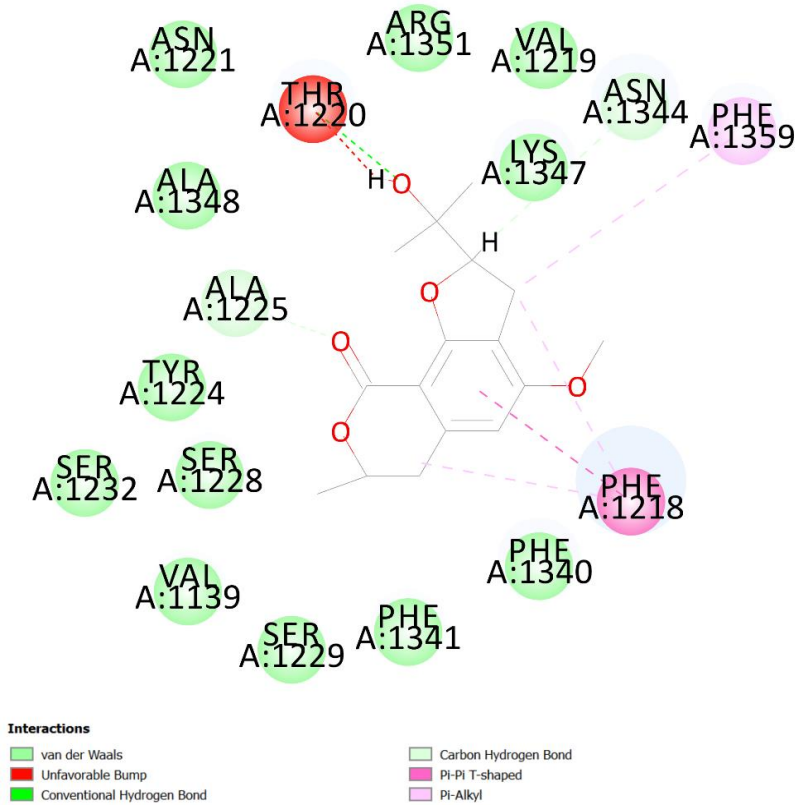
Bisacumol	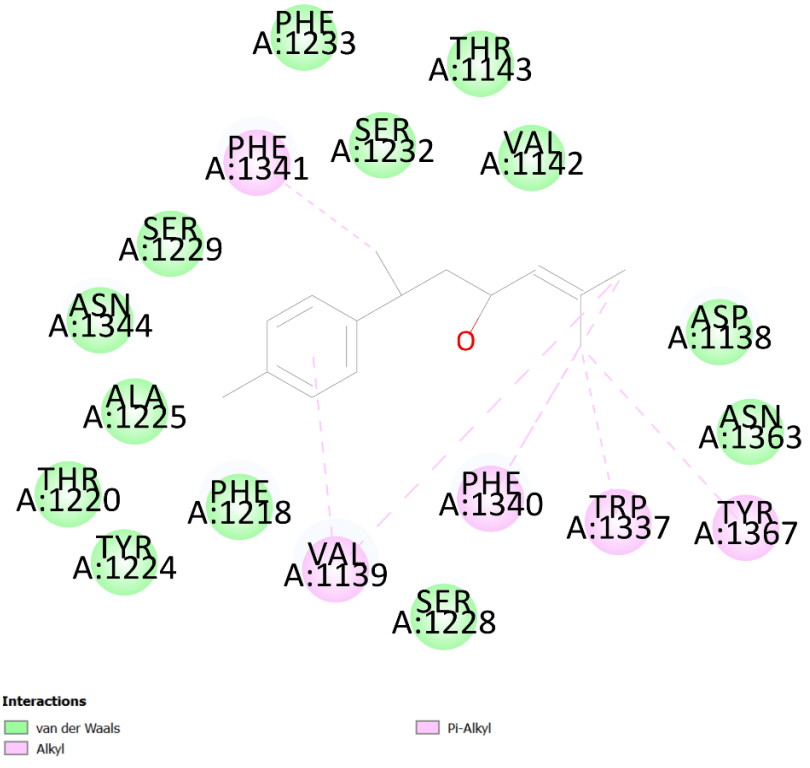

7-Methoxycoumarin	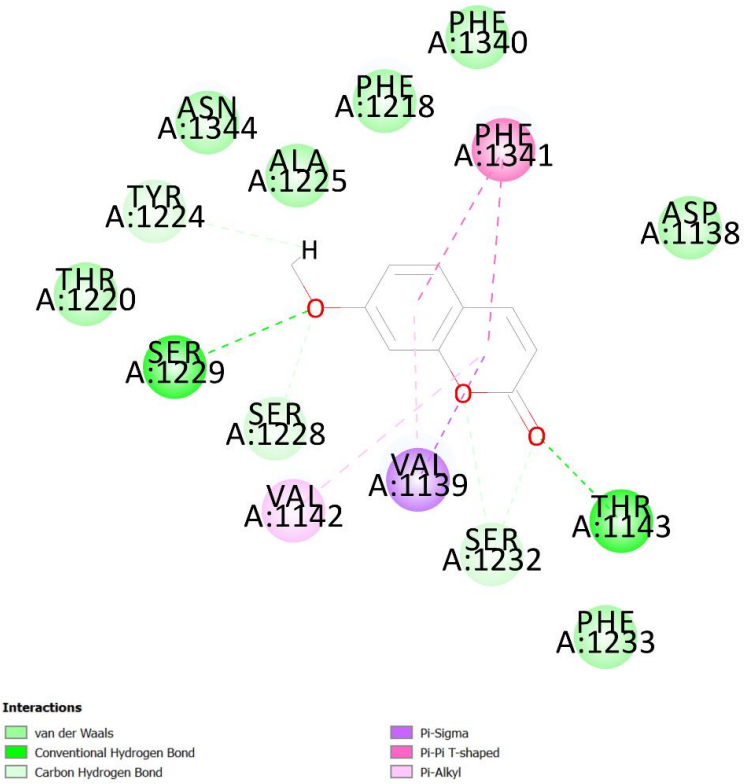
Diethyl phthalate	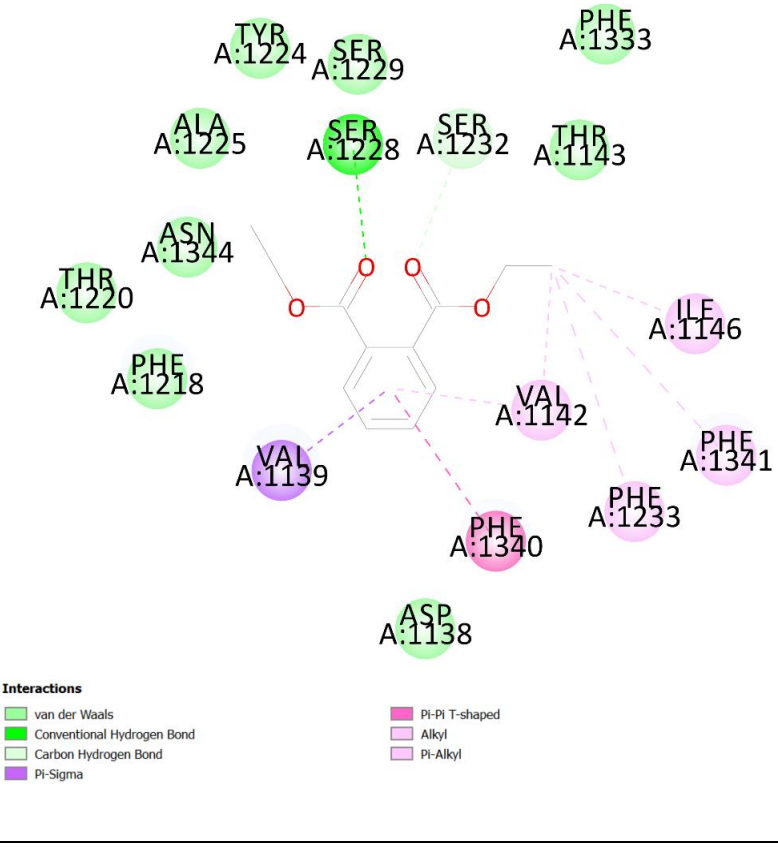

Icariside B2	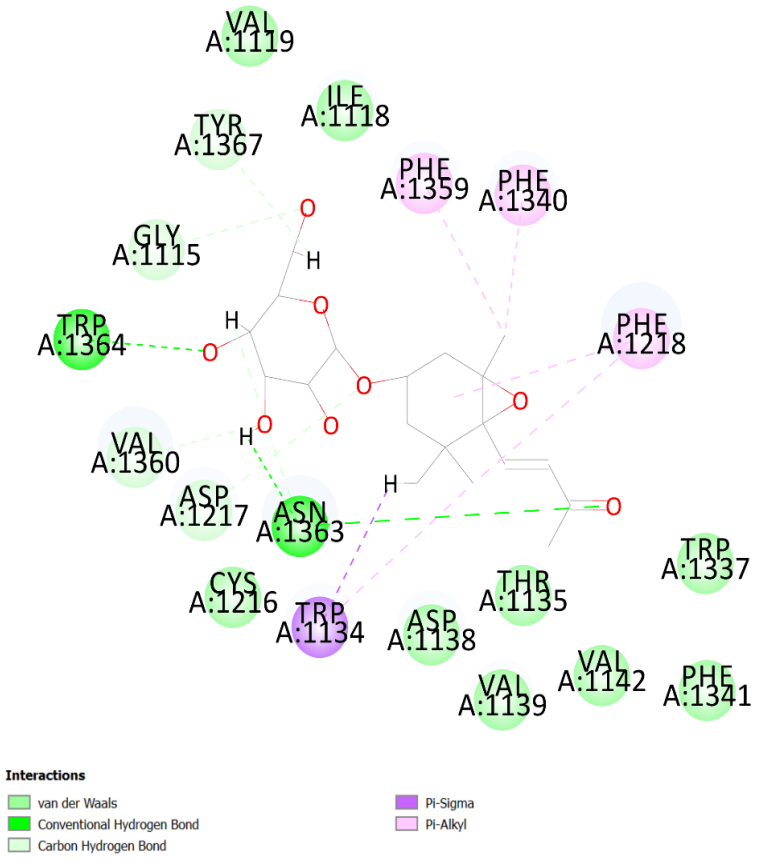
Hispidulin	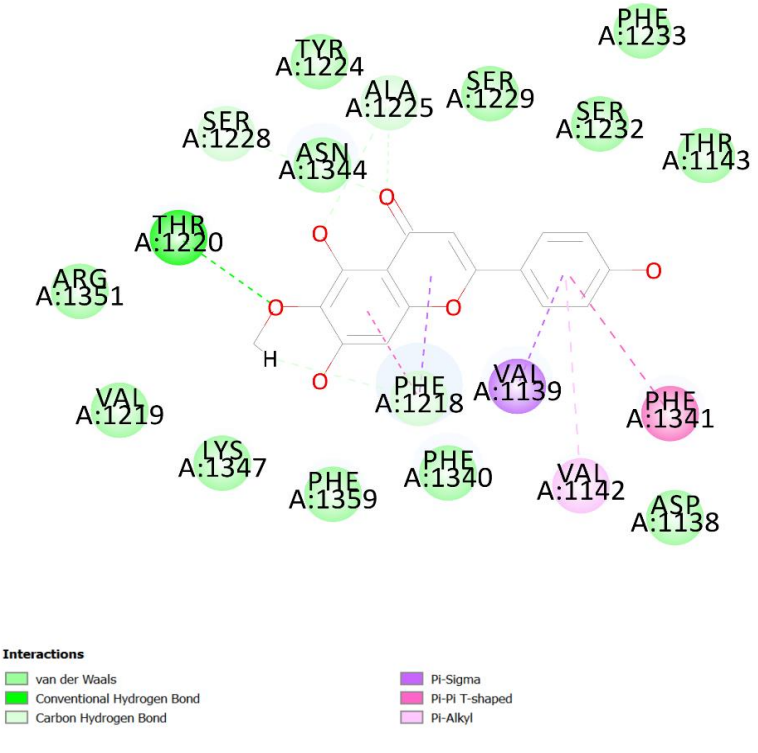

Methyl-2-(methylamino) benzoate	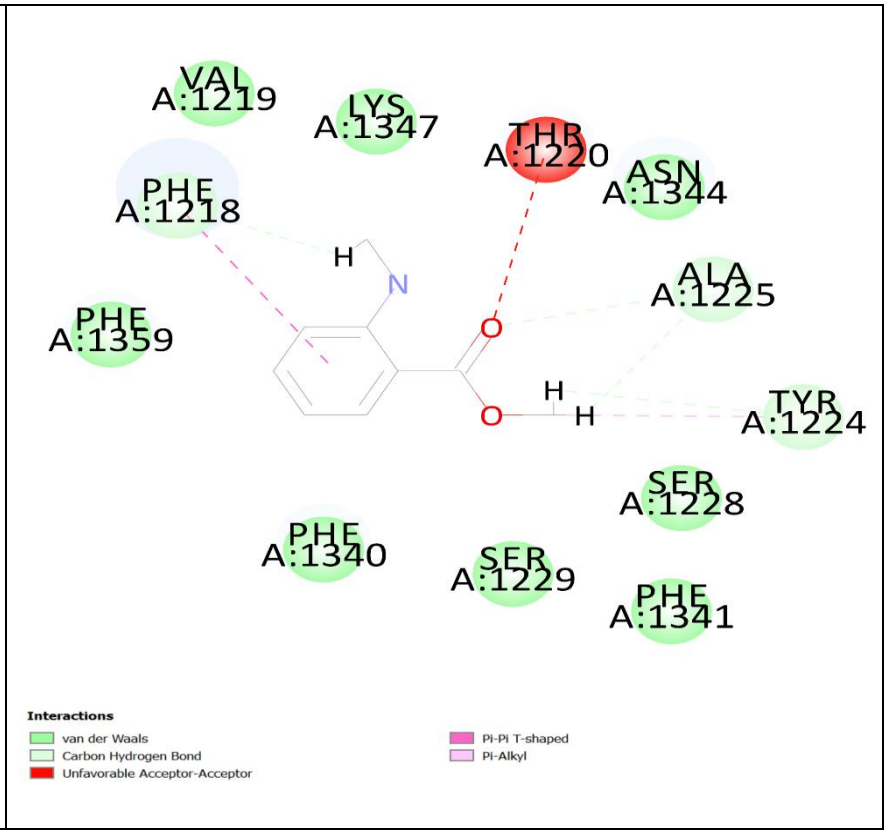

4.0. Discussion

It was demonstrated that KGS at high dose significantly attenuated L-NAME-induced increased SBP and RR interval as well as increased eNOS expression (IHC) in cardiac tissue. According to our literature survey, KGS, for the first time, was tested against ISO-induced cardiac hypertrophy and was able to mitigate ISO induced decreased SBP and other cardiac parameters. KGS in high doses also attenuated ISO-induced prolonged QTc and increased cardiac MDA, CK-MB, Ang-II, Aldosterone, and ANP. KGS High Dose restored the ISO-induced damaged cardiac histopathology and echocardiographic parameters and did not show toxicity in the H9C2 cells up to a dose of 200 µg/ml. KGS, in a dose-dependent manner, attenuated ISO-induced toxicity (H9C2 cells) and decreased intracellular calcium in it at the mentioned dose. Another *in vitro* study involving HLM showed the least inhibition of CYP enzymes. Further analysis of KGS with LC-qTOF in positive mode revealed 19 tentative metabolites, the activity of which was further verified by their interaction with eNOS and β1 receptor molecular docking studies.

In this experiment, KGS high dose attenuated L-NAME induced arterial hypertension (Fig 1A &) 2D), which is also supported by increased RR interval (Fig.1B & 2H) and appears to act through nitric oxide synthase. It is well known that **c**hronic nitric oxide synthesis inhibition in L-NAME-induced arterial hypertension is associated with left ventricular (LV) hypertrophy and re-modelling of the cardiovascular system in rats [27]. KGS appears to increase NO bioavailability and decrease systemic vascular resistance, thus reducing pressure overload on the heart and eventually decreasing cardiac workload, which is evident from decreased SBP and RR interval (Fig.1A & 1B, 2A-2H). KGS might be beneficial in addressing increased cardiac workload-based development of cardiac hypertrophy.

L-NAME increases systolic blood pressure afterload and decreases cardiac eNOS expression (Fig 3) [28]. eNOS has been reported to attenuate the strength and frequency of cardiomyocyte contractility, enhance cardiac myocyte relaxation by increasing its distensibility, inhibit mitochondrial respiration, and improve the efficacy of myocardial oxygen consumption. An enhanced relaxation and increased distensibility of cardiac myocytes can lead to improved ventricular filling and reduce resistance against which the heart must pump, thereby decreasing afterload. Further, eNOS's cardioprotective effects, i.e., reduced oxidative stress, inhibition of fibrosis, and improved myocardial function, prevent maladaptive cardiac remodelling [29].

As per our findings, eNOS expression was found to be elevated in the L-NAME + KGS high dose group (Fig 3), which may be co-related with the beneficial effects of the KGS. KGS, particularly its high dose, appears to reduce cardiac workload probably through preserving cardiac eNOS expression (Fig. 3D), which is also reflected in its ability to reduce SBP (Fig 1A, 2B,2D).

It is well known that ISO stimulates β1 receptors in the sinoatrial node, leading to increased heart rate [30]. This initially increased heart rate can elevate cardiac workload by reducing the diastolic filling time, which affects stroke volume and cardiac output [31]. ISO also increases myocardial contractility in the myocardium, improving cardiac output, but at the same time, it also increases myocardial oxygen consumption [32], contributing to increased cardiac workload [33]. Furthermore, this increased demand on the heart can lead to a state of cardiac exhaustion, where the heart is unable to maintain its increased level of activity**.** ISO is known to possess β2 agonism on the vascular smooth muscle causing vasodilation [34] accompanied by a stiff hypertrophied heart which may be co-related to a significantly decreased SBP (Fig 5F) in our experiment, which also corroborates with previous reports[35] Treatment with KGS high dose significantly improved SBP(5H) indicating improvement in the pumping action of the heart, an essential requirement in heart failure. Previous reports suggest ISO disrupts the repolarisation of ventricular myocytes by inhibiting IKr potassium efflux channels, leading to prolonged QT_c [36]. When the heart rate (HR) of the ISO-induced hypertrophied heart decreases, which was observed in the echocardiography (Fig 9A), the duration of the cardiac cycle increases [37], which can prolong the time available for ventricular repolarisation resulting in prolonged QT_C interval (Fig 4C) [38]. Therefore, a decreased HR in the isoproterenol-induced hypertrophied heart could be associated with an increase in the QTc.

A prolonged QTc (Fig 4C & 5B) is also an indication of a disrupted cardiac electrical system due to ISO-induced increased fibrosis. This may cause cardiac pumping dysfunction, leading to reduced SBP (4B & 5F) as seen in our experiment [39,40]. A significantly short QTc in the KGS high dose group (Fig 4C & 5D) is an indication towards a decreased cardiac hypertrophy (7A & 7C), reduced fibrosis (Fig 7B & 7D). Such changes has been previously claimed to be due to improved electrical conductance throughout the heart leading to enhanced SBP (Fig 4B & 5H). ISO administration increased HW/TL ratio, which conforms with previous reports (Fig. 4D & 4H) and is an indication of cardiac hypertrophy [1]. KGS High Dose alleviated HW/TL ratio, which can be correlated with increased SBP (Fig 4B &

5H). Furthermore, an *in vitro* test utilising a hypotonic solution was performed to induce rupture of goat RBC membrane so as to assess the toxicity and anti-inflammatory potential of KGS on mammalian cell membranes [Fig 4F]. KGS was found to be non-toxic and appears to exert anti-inflammatory activity on mammalian cell membranes, as demonstrated by the goat RBC results [14].

An increased fibrosis in the MT-stained sections of the heart (Fig 7B & 7D) is indicative of collagen deposition and cardiac hypertrophy. ISO-treated rat's cardiac section (Fig 7A & 7C) revealed abnormality of heart muscle cells arrangement, which can disrupt the normal function of the cardiac muscle fibres, eventually leading to impaired heart's ability to contract efficiently [41], which can be co-related with a decreased SBP in the ISO group (Fig 4B & 5F). Increased Myocyte injury can weaken the heart muscle, reduce its contractile strength, and contribute to the development of heart failure [42]. Both KGS low dose and high dose significantly reduced myocyte injury, but only the high dose was able to prevent cardiac hypertrophy, cardiomyocyte damage and fibrosis significantly (Fig 7A-7D). It is well known that ISO induces cardiac fibrosis, which is the deposition of interstitial extracellular matrix protein occurring due to the conversion of cardiac fibroblast to myoblast, an essential step in the formation of fibrosis [43]. Cardiac fibrosis is responsible for ventricular stiffness leading to diastolic dysfunction and cardiac electrical disturbances (QTc prolongation), which are essential requirements for cardiac hypertrophy [44]. In our experiment, KGS high dose attenuated ISO-induced cardiac fibrosis, which can be co-related to decreased QTc.

ISO-induced cardiac hypertrophy involves the generation of ROS, leading to oxidative stress lipid peroxidation of the polyunsaturated acids in the myocardial cell membrane, eventually leading to increased cardiac MDA level, which was also found in our experiment (Fig 4E). ISO-generated oxidative stress disrupts cardiac mitochondria, causing decreased energy generative efficiency, which in turn again increases ROS level, eventually forming a vicious cycle of mitochondrial damage and low efficiency of mitochondrial energy production [45]. A decreased cardiac mitochondrial protein due to ISO administration in our experiment might explain the above fact [Figure 4G]. In this experiment, the KGS High dose attenuated both ISO-induced increased cardiac MDA and decreased mitochondrial protein. KGS High dose, by reducing ISO-induced oxidative stress in the cardiomyocyte, might probably protect cardiac mitochondria. The presence of the KGS High Dose mitigated the increased plasma level of CK-MB, known to be secreted from damaged cardiac cells

because of ISO administration [42]. The significantly decreased plasma CK-MB level in the ISO+ KGS high dose group indicates cardiac protection offered by KGS against ISO, which is also evident from a reduced considerably cardiac myocyte injury (Fig 7C).

Studies have shown that ISO-induced cardiac hypertrophy has been linked to increased plasma angiotensin-II, likely caused by the activation of renal β-receptors and a reduction in SBP [33], which was also observed in our experiment (Fig. 6D & 4B).

Previous reports suggest that Ang-II through the AT_1 receptor promotes cardiomyocyte hypertrophy, cardiac fibroblast hyperplasia, and interstitial cardiac fibrosis. Interstitial fibrosis contributes to ventricular wall stiffness and consequently impairs cardiac compliance by increasing the distance that oxygen must diffuse and, therefore, potentially lowering PaO_2 for the working myocytes [44]. This elevates cardiomyocyte oxygen demand and increases cardiac workload. Ang-II, directly and indirectly, stimulates extracellular matrix protein synthesis by enhancing the expression of the pro-fibrotic factor TGFβ. It can also improve sympathetic activity, leading to increased release of noradrenaline, which further contributes to hypertrophy development [46]. ISO may indirectly induce the release of NA by activating beta-2 adrenoceptors on the chromaffin cells of the adrenal medulla, subsequently leading to the secretion of noradrenaline into the bloodstream.

Furthermore, ISO's effect on beta-2 adrenoceptors at nerve terminals can facilitate noradrenaline release, potentially through cAMP formation [47]. Early studies demonstrated that cultured neonatal rat cardiomyocytes exhibit increased cell size in response to norepinephrine stimulation. [48]. Cardiac hypertrophy development may result from the direct action of norepinephrine on cardiac adrenergic receptors and its indirect effect via stimulation of renal renin release [49]. As per previous studies, catecholamine could cause mitochondrial dysfunction in cardiomyocytes. Some studies have also reported that NA decreases mitochondrial mass and biogenesis [50]. ISO increases plasma aldosterone in Wistar rats [51]. Among other renin-angiotensin–aldosterone systems, aldosterone has been observed to be one of the causes behind the initiation and progression of cardiac hypertrophy, eventually leading to heart failure. Chronic heart failure has been linked to higher levels of aldosterone morbidity and mortality. Aldosterone binds to the cardiac mineralocorticoid receptor (MR), causing myocardial fibrosis and cardiomyocyte apoptosis, leading to cardiac remodelling and compromised cardiac function [52,53]. In our study, the administration of ISO was observed to increase Ang-II, NA and Aldosterone (fig 6A & 6D), which conforms with the reports mentioned earlier. At the same time, the KGS high dose

attenuated their plasma level, thereby decreasing their hypertrophic response and eventually might play a role in reducing cardiomyocyte workload, which can be correlated to decreased fibrosis (Fig 7D) and improved histopathology (Fig 7A-7D) and SBP (Fig 5G & 5H). Previous reports suggest ISO administration is responsible for the release of NA, which in turn causes an increase of atrial stretch (NA via α receptors), thus releasing more ANP from the atria [54].

A decreased plasma ANP in the ISO+KGS High dose is indicative of reduced trial stretch and decreased cardiac workload. The elevated plasma Ang-II, Noradrenaline and Aldosterone might be a compensatory response due to ISO induced decreased SBP.

An increase in Ejection Fraction % (EF) and Fractional Shortening (FS) signifies efficient cardiac pumping, leading to the ejection of a more significant proportion of blood with each contraction. This is often a compensatory response to the increased cardiac workload due to the administration of ISO (Fig 9B & 9C [30]. The hypertrophied heart may have increased contractility, resulting in a more efficient ejection of blood per beat, thus probably requiring a lower heart rate to maintain cardiac output, hence explaining the decreased HR and increased EF [Fig 9A & 9B). However, the presence of KGS (high dose) might have led to a decrease in EF and FS, implying a reduction in the heart's pumping efficiency, i.e. a decreased cardiac workload, thereby mitigating the compensatory increase in EF and FS as observed in cardiac hypertrophy. Increased left ventricular mass, anterior and posterior wall thickness (Fig 9F- 9H & 8) are indicative of left ventricular hypertrophy due to ISO-induced increased cardiac workload [30]. This cardiac muscle thickening may lead to stiffening of the heart walls and result in reduced pumping efficiency over time, which may also be correlated to decreased SBP (Fig 4B & 5F) in our experiment. KGS, particularly the high dose, attenuated the ISO induced above echocardiographic parameters associated with cardiac mascle thickening, indicating a reduction in left ventricular hypertrophy, which can also be correlated to improved HW/TL ratio (Figure 4D) and decreased cardiac fibrosis (figure 7D) in ISO +KGS High dose group.

The ISO induced decreased left ventricular end-systolic volume (LVESV) (Fig. 9D) [55] could be due to the increased contractility of the cardiac muscle in response to ISO administration, which can be co-related to the increased EF. However, KGS increased the (LVESV) indicating reduced contractility of the heart muscle due to decreased cardiac workload. Administration of ISO caused a decreased left ventricle end-systolic diameter (LVESD), which may likely be due to the thickening of the ventricular walls, resulting in a

reduced internal diameter of the ventricle (Fig 9E & 8) [56]. The presence of KGS increased the LVESD, probably protecting from ISO-induced wall thickening and may be correlated to the decreased left ventricular mass (Fig 9F) and decreased HW/TL ratio (Fig 9D & 9H).

I*nvitro* studies (MTT assay) performed using H9C2 cells showed an increase in % cell viability in the presence of KGS in a dose-dependent manner up to 200 µg/ml, indicating no toxicity till the mentioned dose (Fig. 10A). In previous investigations, ISO has been found to be toxic to H9C2 cells [57] which was also observed in our experiment. KGS showed significant cell protection in a dose-dependent manner against ISO-induced cell toxicity, with maximum protection (in terms of % viability) at 200 µg/ml.

Catecholamine autooxidation generates highly cytotoxic free radicals, disrupting the balance between free radical production and the antioxidant system, leading to compromised myocardial membrane integrity. ISO-induced cardiotoxicity is significantly associated with oxidative stress, which has the potential to damage mitochondrial DNA and trigger apoptosis and cell death. Similar findings were noted *invitro* (Fig 10B) in our experiment with decreased % viability of H9C2 cells.

ISO has been reported to cause calcium overload in H9C2 cells. It is well known that Ca^{2+} overload in cells is intricately associated with the induction of oxidative stress and apoptosis. In cardiac hypertrophy, the intracellular Ca^{2+} concentration transiently increases, subsequently leading to ROS generation and the opening of the mitochondrial permeability transition pore (MPTP). The activation of the MPTP results in the release of apoptotic components from the mitochondria into the cytoplasm, ultimately leading to cardiomyocyte death [58]. Increased cardiac intracellular calcium and decreased % viability in ISO-treated cells were also observed in our experiment (Fig 10B, 10C & 10D). Incubation with 200 µg/ml of KGS provided significant protection to H9C2 cells (preventing a decrease in % viability) and decreased intracellular calcium (Fig 10B, 10C & 10D). An increased plasma Ang-II is known to increase intracellular calcium overload (through the AT1 receptor) in the heart, leading to hypertrophy and enhanced cardiac workload [59]. In our experiment, an increase in plasma Ang-II (*invivo*) and intracellular calcium overload (invitro H9C2 cells) due to ISO treatment was observed. KGS at a high dose was able to not only decrease plasma Ang-II, but it also decreased Invitro intracellular calcium in H9C2 cells. KGS may play an essential role in alleviating ISO-induced cardiac hypertrophy through the regulation of intracellular calcium.

In another invitro study, KGS exhibited minimum inhibition of all tested CYP isoforms (CYP1A2, CYP2B6, CYP2C9, CYP2D6, CYP3A4, CYP2C19) with IC50 value >5 µg/mL indicating less interaction with these enzymes. From a drug interaction perspective, KGS is unlikely to cause clinically relevant inhibition of these CYP enzymes, reducing the risk of drug-drug interactions (DDIs). Moreover, the lesser CYP inhibition indicates that KGS does not require significant metabolism through these enzymes for its pharmacological effect. Its efficacy *in vivo/in vitro* is likely mediated by its direct action on the cardiovascular system. The minimum level of CYP interaction also suggests KGS might not have interfered with the metabolism of co-administered test substances, i.e., L-NAME and ISO, in *in vivo* experiments.

LC-qTOF-MS-based analysis of KGS methanolic extract in the positive mode revealed 19 tentative metabolites. KGS is comprised of plant components with individual plants reported with their chemical compounds in them. From the molecular docking of these 19 metabolites, 5 phytochemicals showed best docking score each with eNOS (Tiliroside, Isorhamnetin 3-O-beta-glucopyranoside-7-O-alpha-rhamnopyranoside, Icariside B2, Trehalose, Heptadecanoic acid) and β1AR (Trehalose, Icariside B2, hispidulin, heptadecanoic acid, palmitic acid) (table 3 & 4). Tiliroside [60].

Apart from these best 5 docked metabolites, others might also play a beneficial role in alleviating L-NAME and ISO-induced workload, indicating the holistic approach of KGS, a low-cost medication. The two specific metabolites quantified in KGS i.e. Rosmarinic acid [61] [62] and Trehalose[63], might be responsible for mitigating cardiac workload induced by L-NAME and ISO. However, other bioactive metabolites may also contribute to the cardiovascular activity of KGS. Trehalose has been found to alleviate cardiac hypertrophy induced by transverse aortic constriction (TAC) [64].

5.0.Conclusion: KGS, particularly at high dose, was more effective than the low dose against both L-NAME and ISO-induced animal models of increased cardiac workload. KGS in high doses mitigated the L-NAME-induced reduction in cardiac eNOS expression and reduced arterial systolic blood pressure, thereby decreasing cardiac workload and indicating its potential utility in hypertension through eNOS. However, eNOS expression was not evaluated in the rat vascular endothelium in this experiment, which is one of the limitations of this study. Moreover, KGS also attenuated ISO-induced altered cardiac parameters, as evident from echocardiographic and histopathology reports. It probably mitigates cardiac hypertrophy through RAAS, as observed in our findings. Moreover, its potential role in

mitigating ISO-induced increased intracellular calcium in H9C2 cells is quite evident in our experiment. The reduced plasma Ang-II levels (in vivo) and intracellular calcium (in vitro) by KGS likely indicate the crucial function of calcium modulation via the RAAS in mitigating ISO-induced cardiac hypertrophy. The minimum CYP inhibition by KGS is beneficial from a clinical point of view, suggesting safer use in combination with other conventional drugs.

Although it is too preliminary to mention but considering the metabolite profiling of KGS it can be expected that the observed pharmacological activities of this study might have a relation to two specific metabolites, i.e. Rosmarinic acid (a phenolic compound) and Trehalose (a disaccharide). Overall, KGS might reduce the increased cardiac workload, which is mimicked through invivo/in *vitro* experiments, also reflects its holistic approach, acting through multiple pathways.

References:

[1] D. Chowdhury, A.D. Tangutur, T.N. Khatua, P. Saxena, S.K. Banerjee, M.P. Bhadra, A proteomic view of isoproterenol induced cardiac hypertrophy: prohibitin identified as a potential biomarker in rats, J Transl Med 11 (2013) 130. https://doi.org/10.1186/1479-5876-11-130.

[2] L. Bai, H.J. Kee, X. Han, T. Zhao, S.-J. Kee, M.H. Jeong, Protocatechuic acid attenuates isoproterenol-induced cardiac hypertrophy via downregulation of ROCK1–Sp1–PKCγ axis, Sci Rep 11 (2021) 17343. https://doi.org/10.1038/s41598-021-96761-2.

[3] S. De Moudt, J.O. Hendrickx, C. Neutel, D. De Munck, A. Leloup, G.R.Y. De Meyer, W. Martinet, P. Fransen, Aortic Stiffness in L-NAME Treated C57Bl/6 Mice Displays a Shift From Early Endothelial Dysfunction to Late-Term Vascular Smooth Muscle Cell Dysfunction, Front. Physiol. 13 (2022) 874015. https://doi.org/10.3389/fphys.2022.874015.

[4] H. Dai, N.L. Bragazzi, A. Younis, W. Zhong, X. Liu, J. Wu, E. Grossman, Worldwide Trends in Prevalence, Mortality, and Disability-Adjusted Life Years for Hypertensive Heart Disease From 1990 to 2017, Hypertension 77 (2021) 1223–1233. https://doi.org/10.1161/HYPERTENSIONAHA.120.16483.

[5] T.G. Martin, M.A. Juarros, L.A. Leinwand, Regression of cardiac hypertrophy in health and disease: mechanisms and therapeutic potential, Nat Rev Cardiol 20 (2023) 347–363. https://doi.org/10.1038/s41569-022-00806-6.

[6] I. Bernátová, O. Pecháňová, V. Pelouch, F. Šimko, Regression of Chronic L -NAME-Treatment-induced Left Ventricular Hypertrophy: Effect of Captopril, Journal of Molecular and Cellular Cardiology 32 (2000) 177–185. https://doi.org/10.1006/jmcc.1999.1071.

[7] L. Panthiya, J. Tocharus, A. Onsa-ard, W. Chaichompoo, A. Suksamrarn, C. Tocharus, Hexahydrocurcumin ameliorates hypertensive and vascular remodeling in L-NAME-induced rats, Biochimica et Biophysica Acta (BBA) - Molecular Basis of Disease 1868 (2022) 166317. https://doi.org/10.1016/j.bbadis.2021.166317.

[8] Md.A. Shaharyar, R. Bhowmik, O. Afzal, A.S.A. Altamimi, S.I. Alzarea, W.H. Almalki, S.Z. Ali, P. Mandal, A. Mandal, M. Ayoob, I. Kazmi, S. Karmakar, Anti-Hypertensive Activity of Some Selected Unani Formulations: An Evidence-Based Approach for Verification of Traditional Unani Claims Using LC-MS/MS for the Evaluation of Clinically Relevant Blood Parameters in Laboratory Rats, JCM 11 (2022) 4628. https://doi.org/10.3390/jcm11154628.

[9] S. Kumari, P.B. Katare, R. Elancheran, H.L. Nizami, B. Paramesha, S. Arava, P.P. Sarma, R. Kumar, D. Mahajan, Y. Kumar, R. Devi, S.K. Banerjee, *Musa balbisiana* Fruit Rich in Polyphenols Attenuates Isoproterenol-Induced Cardiac Hypertrophy in Rats via Inhibition of Inflammation and Oxidative Stress, Oxidative Medicine and Cellular Longevity 2020 (2020) 1–14. https://doi.org/10.1155/2020/7147498.

[10] C.R. Taylor, New Revised Clinical and Laboratory Standards Institute Guidelines for Immunohistochemistry and Immunocytochemistry, Applied Immunohistochemistry & Molecular Morphology 19 (2011) 289–290. https://doi.org/10.1097/PAI.0b013e31821b505b.

[11] Diagnostic Immunohistochemistry, 2021. https://shop.elsevier.com/books/diagnostic-immunohistochemistry/dabbs/978-0-323-72172-1 (accessed December 16, 2024).

[12] K.S. Suvarna, C. Layton, J.D. Bancroft, Bancroft's Theory and Practice of Histological Techniques E-Book, Elsevier Health Sciences, 2012.

[13] S. Karmakar, A. Mandal, R. Bhowmik, A. Shaharyar, K. Anand, P. Mandal, A. Sarkar, Natural hepatoprotectives earthworm extract protein & goat milk in-vitro model rat primary hepatocytes exposed to carbon tetrachloride revealed toxicity and oxidative stress, Jrp 28(1) (2024) 258–268. https://doi.org/10.29228/jrp.693.

[14] M. Al Bashera, A. Mosaddik, G. El-Saber Batiha, M. Alqarni, Md.A. Islam, G.D. Zouganelis, A. Alexiou, R. Zahan, In Vivo and In Vitro Evaluation of Preventive Activity of Inflammation and Free Radical Scavenging Potential of Plant Extracts from Oldenlandia corymbosa L., Applied Sciences 11 (2021) 9073. https://doi.org/10.3390/app11199073.

[15] F. Ahmad, W. Alamoudi, S. Haque, M. Salahuddin, K. Alsamman, Simple, reliable, and time-efficient colorimetric method for the assessment of mitochondrial function and toxicity, Bosn J of Basic Med Sci 18 (2018) 367–374. https://doi.org/10.17305/bjbms.2018.3323.

[16] E.A.M. El-Shoura, M.A. Salem, Y.H. Ahmed, L.K. Ahmed, D. Zaafar, Combined β-sitosterol and trimetazidine mitigate potassium dichromate-induced cardiotoxicity in rats through the interplay between NF-κB/AMPK/mTOR/TLR4 and HO-1/NADPH signaling pathways, Environmental Science and Pollution Research 30 (2023) 67771–67787. https://doi.org/10.1007/s11356-023-27021-1.

[17] M.J. Alam, S.K. Uppulapu, V. Tiwari, B. Varghese, S.A. Mohammed, R. Adela, S.K. Arava, S.K. Banerjee, Pregestational diabetes alters cardiac structure and function of neonatal rats through developmental plasticity, Front. Cardiovasc. Med. 9 (2022) 919293. https://doi.org/10.3389/fcvm.2022.919293.

[18] N. Afsheen, Optimization of Cardioprotective Potential of Various Concentrations of Medicinal Plants by Using Response Surface Methodology, PVJ 39 (2019) 13–18. https://doi.org/10.29261/pakvetj/2018.111.

[19] H.P. Osuru, M. Lavallee, R.H. Thiele, Molecular and Cellular Response of the Myocardium (H9C2 Cells) Towards Hypoxia and HIF-1α Inhibition, Front. Cardiovasc. Med. 9 (2022) 711421. https://doi.org/10.3389/fcvm.2022.711421.

[20] High-Throughput In Vitro ADME Analysis with Agilent RapidFire/MS Systems: Cytochrome P450 Inhibition, LabRulez LCMS (n.d.). https://lcms.labrulez.com/paper/9104 (accessed December 16, 2024).

[21] A. Mehmood, S. Javid, M.F. Khan, K.S. Ahmad, A. Mustafa, In vitro total phenolics, total flavonoids, antioxidant and antibacterial activities of selected medicinal plants using different solvent systems, BMC Chemistry 16 (2022) 64. https://doi.org/10.1186/s13065-022-00858-2.

[22] C. Wang, Q. Zhou, S.-T. Wu, Scopolin obtained from Smilax china L. against hepatocellular carcinoma by inhibiting glycolysis: A network pharmacology and experimental study, Journal of Ethnopharmacology 296 (2022) 115469. https://doi.org/10.1016/j.jep.2022.115469.

[23] S.K. Burley, H.M. Berman, G.J. Kleywegt, J.L. Markley, H. Nakamura, S. Velankar, Protein Data Bank (PDB): The Single Global Macromolecular Structure Archive, in: A. Wlodawer, Z. Dauter, M. Jaskolski (Eds.), Protein Crystallography, Springer New York, New York, NY, 2017: pp. 627–641. https://doi.org/10.1007/978-1-4939-7000-1_26.

[24] B. Aksoydan, I. Kantarcioglu, I. Erol, R.E. Salmas, S. Durdagi, Structure-based design of hERG-neutral antihypertensive oxazalone and imidazolone derivatives, J Mol Graph Model 79 (2018) 103–117. https://doi.org/10.1016/j.jmgm.2017.10.011.

[25] Y. Fan, Z. Yu, W. Zhao, L. Ding, F. Zheng, J. Li, J. Liu, Identification and molecular mechanism of angiotensin-converting enzyme inhibitory peptides from Larimichthys crocea titin, Food Science and Human Wellness 9 (2020) 257–263. https://doi.org/10.1016/j.fshw.2020.04.001.

[26] B. Das, P.K. Bhardwaj, N. Sharma, A. Sarkar, P.K. Haldar, P.K. Mukherjee, Evaluation of Mollugo oppositifolia Linn. as cholinesterase and β-secretase enzymes inhibitor, Front. Pharmacol. 13 (2023) 990926. https://doi.org/10.3389/fphar.2022.990926.

[27] O. Pechánová, I. Bernátová, P. Babál, M.C. Martínez, S. Kyselá, S. Stvrtina, R. Andriantsitohaina, Red wine polyphenols prevent cardiovascular alterations in L-NAME-induced hypertension, Journal of Hypertension 22 (2004) 1551–1559. https://doi.org/10.1097/01.hjh.0000133734.32125.c7.

[28] A. Kazakov, R. Hall, P. Jagoda, K. Bachelier, P. Müller-Best, A. Semenov, F. Lammert, M. Böhm, U. Laufs, Inhibition of endothelial nitric oxide synthase induces and enhances myocardial fibrosis, Cardiovascular Research 100 (2013) 211–221. https://doi.org/10.1093/cvr/cvt181.

[29] N. Tran, T. Garcia, M. Aniqa, S. Ali, A. Ally, S.M. Nauli, Endothelial Nitric Oxide Synthase (eNOS) and the Cardiovascular System: in Physiology and in Disease States, Am J Biomed Sci Res 15 (2022) 153–177.

[30] P. Perez-Bonilla, B. LaViolette, B. Bhandary, S. Ullas, X. Chen, D. Hirenallur-Shanthappa, Isoproterenol induced cardiac hypertrophy: A comparison of three doses and two delivery methods in C57BL/6J mice, PLoS ONE 19 (2024) e0307467. https://doi.org/10.1371/journal.pone.0307467.

[31] S. Alhayek, C.V. Preuss, Beta 1 Receptors, in: StatPearls, StatPearls Publishing, Treasure Island (FL), 2024. http://www.ncbi.nlm.nih.gov/books/NBK532904/ (accessed December 16, 2024).

[32] B. Bartelds, J.-W.C. Gratama, K.J. Meuzelaar, M. Dalinghaus, J.H. Koers, W.F. Heikens, W.G. Zijlstra, J.R.G. Kuipers, Comparative Effects of Isoproterenol and Dopamine on Myocardial Oxygen Consumption, Blood Flow Distribution and Total Body Oxygen Consumption in Conscious Lambs With and Without an Aortopulmonary Left to Right Shunt, Journal of the American College of Cardiology 31 (1998) 473–481. https://doi.org/10.1016/S0735-1097(97)00514-7.

[33] F.H.H. Leenen, R. White, B. Yuan, Isoproterenol-induced cardiac hypertrophy: role of circulatory versus cardiac renin-angiotensin system, American Journal of Physiology-Heart and Circulatory Physiology 281 (2001) H2410–H2416. https://doi.org/10.1152/ajpheart.2001.281.6.H2410.

[34] M.G. Matera, C. Page, B. Rinaldi, β2-Adrenoceptor signalling bias in asthma and COPD and the potential impact on the comorbidities associated with these diseases, Current Opinion in Pharmacology 40 (2018) 142–146. https://doi.org/10.1016/j.coph.2018.04.012.

[35] R. Thangaiyan, S. Arjunan, K. Govindasamy, H.A. Khan, A.S. Alhomida, N.R. Prasad, Galangin Attenuates Isoproterenol-Induced Inflammation and Fibrosis in the Cardiac Tissue of Albino Wistar Rats, Front. Pharmacol. 11 (2020) 585163. https://doi.org/10.3389/fphar.2020.585163.

[36] C. Karle, Rapid component IKr of the guinea-pig cardiac delayed rectifier K+ current is inhibited by β1-adrenoreceptor activation, via cAMP/protein kinase A-dependent pathways, Cardiovascular Research 53 (2002) 355–362. https://doi.org/10.1016/S0008-6363(01)00509-0.

[37] G. Heusch, Heart rate in the pathophysiology of coronary blood flow and myocardial ischaemia: benefit from selective bradycardic agents, British J Pharmacology 153 (2008) 1589–1601. https://doi.org/10.1038/sj.bjp.0707673.

[38] A. Tomar, H. Ahluwalia, H.S. Isser, S. Gulati, P. Kumar, I. Yadav, Analysis of ventricular repolarization parameters and heart rate variability in obesity: a comparative study, Sci Rep 14 (2024) 25855. https://doi.org/10.1038/s41598-024-76580-x.

[39] K. Suarez, R. Mack, E.L. Hardegree, C. Chiles, J.E. Banchs, M.D. Gonzalez, Isoproterenol suppresses recurrent torsades de pointes in a patient with long QT syndrome type 2, HeartRhythm Case Reports 4 (2018) 576–579. https://doi.org/10.1016/j.hrcr.2018.08.013.

[40] D. Nanda, P. Pant, P. Machha, D.T. Sowpati, R. Kumarswamy, Transcriptional changes during isoproterenol-induced cardiac fibrosis in mice, Front. Mol. Biosci. 10 (2023) 1263913. https://doi.org/10.3389/fmolb.2023.1263913.

[41] G. Finocchiaro, N. Sheikh, O. Leone, J. Westaby, F. Mazzarotto, A. Pantazis, C. Ferrantini, L. Sacconi, M. Papadakis, S. Sharma, M.N. Sheppard, I. Olivotto, Arrhythmogenic potential of myocardial disarray in hypertrophic cardiomyopathy: genetic basis, functional consequences and relation to sudden cardiac death, EP Europace 23 (2021) 985–995. https://doi.org/10.1093/europace/euaa348.

[42] Y. Sato, T. Kita, Y. Takatsu, T. Kimura, Biochemical markers of myocyte injury in heart failure, Heart 90 (2004) 1110–1113. https://doi.org/10.1136/hrt.2003.023895.

[43] Y. Pan, J. Gao, R. Gu, W. Song, H. Li, J. Wang, Y. Gu, H. Chen, H. Zhang, Effect of injection of different doses of isoproterenol on the hearts of mice, BMC Cardiovasc Disord 22 (2022) 409. https://doi.org/10.1186/s12872-022-02852-x.

[44] J. Schnee, Angiotensin II, adhesion, and cardiac fibrosis, Cardiovascular Research 46 (2000) 264–268. https://doi.org/10.1016/S0008-6363(00)00044-4.

[45] X. Wang, Q. Yu, X. Liao, M. Fan, X. Liu, Q. Liu, M. Wang, X. Wu, C.-K. Huang, R. Tan, J. Yuan, Mitochondrial Dysfunction in Arrhythmia and Cardiac Hypertrophy, Rev. Cardiovasc. Med. 24 (2023) 364. https://doi.org/10.31083/j.rcm2412364.

[46] M.P. Schlaich, D.M. Kaye, E. Lambert, J. Hastings, D.J. Campbell, G. Lambert, M.D. Esler, Angiotensin II and norepinephrine release: interaction and effects on the heart, J Hypertens 23 (2005) 1077–1082. https://doi.org/10.1097/01.hjh.0000166850.80344.cf.

[47] S.-P. Hong, F.C. Leiper, A. Woods, D. Carling, M. Carlson, Activation of yeast Snf1 and mammalian AMP-activated protein kinase by upstream kinases, Proceedings of the National Academy of Sciences 100 (2003) 8839–8843. https://doi.org/10.1073/pnas.1533136100.

[48] P. Simpson, Norepinephrine-stimulated hypertrophy of cultured rat myocardial cells is an alpha 1 adrenergic response., J. Clin. Invest. 72 (1983) 732–738. https://doi.org/10.1172/JCI111023.

[49] A. Rapacciuolo, G. Esposito, K. Caron, L. Mao, S.A. Thomas, H.A. Rockman, Important role of endogenous norepinephrine and epinephrine in the development of in vivo pressure-overload cardiac hypertrophy, J Am Coll Cardiol 38 (2001) 876–882. https://doi.org/10.1016/s0735-1097(01)01433-4.

[50] I.-C. Lin, C.-W. Wu, Y.-J. Lin, M.-H. Lo, K.-S. Hsieh, J.Y.H. Chan, K.L.H. Wu, Milrinone effects on cardiac mitochondria, hemodynamics, and death in catecholamine-infused rats, Pediatr Res 92 (2022) 1309–1315. https://doi.org/10.1038/s41390-022-01964-6.

[51] D. Grimm, Development of heart failure following isoproterenol administration in the rat: role of the renin–angiotensin system, Cardiovascular Research 37 (1998) 91–100. https://doi.org/10.1016/S0008-6363(97)00212-5.

[52] J. Bauersachs, F. Jaisser, R. Toto, Mineralocorticoid Receptor Activation and Mineralocorticoid Receptor Antagonist Treatment in Cardiac and Renal Diseases, Hypertension 65 (2015) 257–263. https://doi.org/10.1161/HYPERTENSIONAHA.114.04488.

[53] J. Grune, N. Beyhoff, E. Smeir, R. Chudek, A. Blumrich, Z. Ban, S. Brix, I.R. Betz, M. Schupp, A. Foryst-Ludwig, R. Klopfleisch, P. Stawowy, R. Houtman, P. Kolkhof, U. Kintscher, Selective Mineralocorticoid Receptor Cofactor Modulation as Molecular Basis for Finerenone's Antifibrotic Activity, Hypertension 71 (2018) 599–608. https://doi.org/10.1161/HYPERTENSIONAHA.117.10360.

[54] L.C. Rump, M.J. Schuster, P. Schollmeyer, Activation of beta 2-adrenoceptors by isoprenaline and adrenaline enhances noradrenaline release in cortical kidney slices of young spontaneously hypertensive rats, Naunyn Schmiedebergs Arch Pharmacol 345 (1992) 25–32. https://doi.org/10.1007/BF00175465.

[55] Y. Kitagawa, D. Yamashita, H. Ito, M. Takaki, Reversible effects of isoproterenol-induced hypertrophy on in situ left ventricular function in rat hearts, American Journal of Physiology-Heart and Circulatory Physiology 287 (2004) H277–H285. https://doi.org/10.1152/ajpheart.00073.2004.

[56] F. Keihanian, M. Moohebati, A. Saeidinia, S.A. Mohajeri, S. Madaeni, Therapeutic effects of medicinal plants on isoproterenol-induced heart failure in rats, Biomedicine & Pharmacotherapy 134 (2021) 111101. https://doi.org/10.1016/j.biopha.2020.111101.

[57] D. Han, C. Wan, F. Liu, X. Xu, L. Jiang, J. Xu, Jujuboside A Protects H9C2 Cells from Isoproterenol-Induced Injury via Activating PI3K/Akt/mTOR Signaling Pathway, Evidence-Based Complementary and Alternative Medicine 2016 (2016) 9593716. https://doi.org/10.1155/2016/9593716.

[58] W. Li, J. Yang, Q. Lyu, G. Wu, S. Lin, Q. Yang, J. Hu, Taurine attenuates isoproterenol-induced H9c2 cardiomyocytes hypertrophy by improving antioxidative

ability and inhibiting calpain-1-mediated apoptosis, Mol Cell Biochem 469 (2020) 119–132. https://doi.org/10.1007/s11010-020-03733-7.

[59] W.C. De Mello, Intracellular angiotensin (1–7) increases the inward calcium current in cardiomyocytes. On the role of PKA activation, Mol Cell Biochem 407 (2015) 9–16. https://doi.org/10.1007/s11010-015-2449-4.

[60] H. Lagunas-Herrera, J. Tortoriello, M. Herrera-Ruiz, G.B. Martínez-Henández, A. Zamilpa, L.A. Santamaría, M.G. Lorenzana, G. Lombardo-Earl, E. Jiménez-Ferrer, Acute and Chronic Antihypertensive Effect of Fractions, Tiliroside and Scopoletin from Malva parviflora, Biol Pharm Bull 42 (2019) 18–25. https://doi.org/10.1248/bpb.b18-00355.

[61] H. Zhou, B. Fu, B. Xu, X. Mi, G. Li, C. Ma, J. Xie, J. Li, Z. Wang, Rosmarinic Acid Alleviates the Endothelial Dysfunction Induced by Hydrogen Peroxide in Rat Aortic Rings via Activation of AMPK, Oxidative Medicine and Cellular Longevity 2017 (2017) 7091904. https://doi.org/10.1155/2017/7091904.

[62] S. Javidanpour, M. Dianat, M. Badavi, S.A. Mard, The cardioprotective effect of rosmarinic acid on acute myocardial infarction and genes involved in Ca^{2+} homeostasis, Free Radical Research 51 (2017) 911–923. https://doi.org/10.1080/10715762.2017.1390227.

[63] K. Suno, Y. Shingu, S. Wakasa, Protective effects of trehalose preconditioning on cardiac and coronary endothelial function through eNOS signaling pathway in a rat model of ischemia–reperfusion injury, Mol Cell Biochem 477 (2022) 2403–2414. https://doi.org/10.1007/s11010-022-04451-y.

[64] Q. Chai, W. Zhang, L. Gao, Y. Yang, M. Miao, D. Liu, L. Chen, M. Zheng, S. Xin, The Action and Mechanism of Trehalose on GATA4 Autophagy Degradation and Ventricular Remodeling, Discovery Medicine 35 (2023) 394. https://doi.org/10.24976/Discov.Med.202335176.40.

CHAPTER-VII

ENHANCING STABILITY AND RELEASE PROFILE OF RA AND TR IN KHAMIRA GAOZABAN SADA (KGS), A TRADITIONAL UNANI PREPARATION USING pH SENSITIVE CHITOSAN-COATED ALGINATE BEADS

Enhancing stability and release profile of RA and TR in Khamira Gaozaban Sada (KGS), a traditional unani preparation using pH-sensitive chitosan-coated alginate beads

1. Introduction

Biopolymers are large molecules composed of numerous repeating units and are classified as single molecules under the IUPAC system. Their biocompatible and biodegradable nature makes them highly valuable for various pharmaceutical applications. Common biopolymers include nucleic acids, proteins, carbohydrates, and lipids, as well as large non-polymeric structures such as macrocycles and lipids. Enhancing the efficacy of bioactive compounds through innovative drug delivery systems remains a pivotal approach for advancing therapeutic strategies for numerous diseases, with significant progress being made in this field.[1]. For certain drugs, the gastrointestinal (GI) tract poses significant challenges as a delivery route, including limitations such as degradation by gastric acids and enzymes, as well as unintended delivery to non-target sites. Therefore, it is essential to develop innovative oral drug delivery systems to overcome these limitations, enabling controlled drug release, maintaining optimal drug concentrations, and enhancing the efficacy of existing formulations [2]. Marine-derived biopolymers represent a diverse group of natural polymers that are increasingly being explored and utilized across various biomedical and pharmaceutical applications. This can be attributed to their characteristics, such as cost-effective production, low toxicity, biocompatibility, biodegradability, and ease of physicochemical modification [3]. Alginate (Alg), a naturally occurring anionic marine biopolymer derived from brown seaweed, consists of (1,4)-linked β-D-mannuronic acid and α-L-guluronic acid monomers. Widely used in printing, medicine, food technology, and water treatment [4], Alginate is also a "smart" drug carrier due to its pH sensitivity. To minimize drug leaching from its porous microcapsules and improve physical stability at higher pH levels, various physical and chemical modifications have been implemented [5]. Chitosan (Cn), a marine biopolymer rich in amino groups, is derived from the deacetylation of chitin, the main component of crustacean exoskeletons like those of lobsters, shrimp, and crabs. It is a linear polymer consisting of randomly distributed (1-4)-linked 2-amino-2-deoxy-β-D-glucopyranose units [6]. Due to its biodegradability, bioactivity, non-toxicity, and excellent biocompatibility, Cn is widely used in wound dressings, artificial tissues, health supplements, and drug delivery systems.[7]. Cn's pH sensitivity, due to its abundant hydrophilic amino groups, makes it ideal for smart drug carriers. Its electrostatic interaction

with negatively charged Alg forms a pH-sensitive polyelectrolyte complex (PEC). This PEC layer (Alg/Cn) not only combines the benefits of individual Alg and Cn microcapsules but also customizes swelling and drug-release profiles in the GI tract. Modifying Alg microcapsules with Cn layers offers a promising strategy for improved control of drug release compared to Alg alone [5]. Khamira KGS) is a highly water-soluble semi-solid honey-based traditional Unani preparation that has been used for centuries in the management of Khafqan (palpitation) and Zoaf-e-Qalb (weak heart as per the Unani terminology)

It is proposed that encapsulating the KGS in sodium alginate beads and subsequently coating it with chitosan would provide a superior controlled release formulation through better encapsulation efficiency and % cumulative drug release, leading to improved bioavailability. The macromolecular chitosan readily adheres to the surface of alginate droplets but is restricted in its diffusion into the inner core [8]

A normal heart derives ATP more from the oxidation of fatty acid than glucose metabolism. However, during cardiac ischaemia and hypertrophy, the heart generates more ATP from glucose metabolism than fatty acid oxidation [9]. It is suspected that the Unani physicians, based on their practice, might have utilized honey and sugar in KGS not only for taste masking but also to achieve better therapeutic outcomes in failing or weak hearts (as per their terminology) while unaware of the above-mentioned pharmacological implications. During the development of KGS-loaded chitosan-sensitive alginate beads (KLCAB), keeping in view of the fact that, as mentioned earlier, the sugar from KGS was not removed. Utilizing response surface methodology, the encapsulation efficiency, was optimized providing a more comprehensive examination of the interactions between experimental variables than a single-factor experimental design. As a result, this could result in an improved comprehension. In addition, it decreases the number of experimental trials needed to produce statistically-validated outcomes [10].

This study aimed to develop statistically optimized KLCAB with improved % efficiency. The pH-sensitive Alg-Cn beads were characterized using Fourier-transform infrared spectroscopy (FT-IR), thermogravimetric analysis (TGA), scanning electron microscopy (SEM), % encapsulation efficiency (%EE), and loading content (LC). The pH-responsive behaviour of the Alg/Cn beads was evaluated by simulating the gastrointestinal (GI) tract environment to assess swelling and in vitro drug release of RA and TR. The goal was to

develop a controlled-release formulation of KGS by determining the % cumulative release of KGS based on RA and TR.

2.0. Materials and Methods

2.1.Material

Medium viscosity Sodium alginate ≥2,000 cP, 2 % (25 °C) (Sigma Aldrich, Cas 9005-38-3), chitosan high Molecular weight (extra pure, deacetylation degree min. 95%, viscosity min 800 mPa.s, (1% aqueous solution) (Cas No-9012-76-4) Khamira Gaozaban Sada (mfg by Hamdard laboratories, India; batch no-24GKD023, expiry 7/2027), acetic acid (99.8%), anhydrous calcium chloride (Anhydrous $CaCl_2$) of analytical grade. Simulated fluids prepared as per USP**.**

2.2 Methods

2.3. Factorial design experiments

The formulation of KGS-loaded chitosan-coated pH-sensitive alginate beads (KLCAB) was carried out using a 2^3 Box-Behnken design facilitated by the Design-Expert® software (version 13.0.5.0, Stat-Ease Inc., Minneapolis, MN). The software generated a total of sixteen experimental runs to optimize the development of KLCAB. The study assessed the effects of three independent variables: sodium alginate concentration (1–5%), calcium chloride concentration (0–10%), and chitosan concentration (5–15%). The percentage encapsulation efficiency (% EE) in terms of rosmarinic acid (RA) and trehalose (TR) served as the dependent variables. The design included all possible combinations of the independent variables, sodium alginate (X1), calcium chloride (X2), and chitosan (X3), tested at various levels, and the experiments were conducted in a randomized order. The % EE for the beads, represented as RA (Y1) and TR (Y2), was analyzed as the response parameters. The Box-Behnken design evaluated the experimental responses using various statistical models, including linear, two-factor interaction (2FI), quadratic, and cubic contributions. The model's significance was determined through statistical parameters, and the equations generated were used to create response surface graphs to visualize the results.

2.4.Development of Sodium Alginate beads

Alginate beads were prepared via a simplified ionic cross-linking method. Alginate was dissolved in 50 mL of hot distilled water (60°C) at varying concentrations and allowed to cool to room temperature (25°C). Using a 5 mL syringe held 10 cm above the surface, the

solution was dropped into 100 mL of CaCl2 solution, where spherical beads instantly formed due to electrostatic interactions between guluronate blocks and Ca^{2+} ions. The beads were stirred in the CaCl2 solution for 30 minutes at 25°C to solidify, rinsed three times with distilled water to remove excess CaCl2, and stored moist at 25°C for further modifications.[5].

2.5.Chitosan (Cn) coating over Alginate beads

Cn was dissolved in an aqueous acetic acid solution (0.5% w/v), and 100 mL of the solution was added to freshly prepared Alg beads. The beads were coated with a Cn layer by gentle stirring for 30 minutes at room temperature, forming a polyelectrolyte complex (PEC) through ionic interactions between the $-COO^-$ groups of Alg and the $-NH_3^+$ groups of Cn. After filtration, the Alg/Cn beads were washed three times with distilled water to remove unreacted Cn. The beads were stored at 25°C for further analysis. [5].

2.6. Loading of KGS

The loading process involved dispersing 0.50 g of KGS into an Alg solution and subjecting it to ultra-sonication for 30 minutes to create a bubble-free and uniformly dispersed mixture of KGS-loaded Alg beads. KLCAB beads were then prepared following the specified procedure. To assess drug loading efficiency and loading content, 100 mg of dried KGS-loaded beads were precisely weighed and ground using a mortar and pestle to facilitate KGS extraction. The powdered sample was added to 50 mL of phosphate buffer solution (pH 7.4) in a 100-mL flask and kept in a shaking water bath at 30°C for 24 hours to ensure complete extraction of KGS from the beads. The mixture was filtered, and the filtrate was collected for further analysis. The KGS content in the chitosan-coated Alg beads was quantified as RA and TR using LC-MS/MS. The loading efficiency and loading content were calculated based on the following equations.

Entrapment efficiency (EE) (%) = (W1/W0) *100---------- eq.(1)

Drug loading content (LC) (%) = (W1/W2) *100----------eq.(2)

Here, W0 represents the initial amount of KGS used in the loading process (0.5 g in this case), W1 denotes the amount of Rosmarinic acid in the weighed beads, and W2 is the mass of the weighed beads [5].

2.7. Bead size measurement:

The size of the prepared beads was measured using Absolute Digimatic Caliper® (Mitutoyo, Kawasaki, Japan)

2.8. FTIR studies

The chemical structures of Alg and Cs, utilized in our formulation and the prepared beads, were analyzed using Attenuated Total Reflectance (ATR) Fourier Transform Infrared Spectroscopy (FT-IR) (Alpha II, Bruker Optik, Germany). This analysis compared the key functional groups in KGS, Alg powder, Cn powder, KGS-loaded Alg beads, and KLCAB. Infrared spectra were recorded over a wavenumber range of 500 to 4000 cm−1.

2.9.Thermogravimetric analysis

The thermal characteristics of the beads were examined using thermogravimetric analysis (TGA) utilizing a Simultaneous Thermal analyser (STA 800), Perkin Elmer (USA), controlled by the software Pyris manager under an atmosphere of nitrogen (N2). A temperature range of 30°C –800°C with a heating rate of 20°C per minute was set for this study.

2.10. Scanning electron microscopy (SEM)

The scanning electron microscope Jeol JSM-6390, Version 1.0 was used to analyze the surface morphology of Alg, KGS-loaded Alg beads, and KLCAB. Prior to analysis, the samples were coated with a fine layer of gold under vacuum conditions and subsequently examined at an accelerating voltage of 5 kV with magnifications of 50X and 500X.

2.11. Beads swelling studies

This method involved immersion of beads so as to quantify the water absorption capacity of the beads and thus examine their swelling characteristics. The dried KLCAB was precisely weighed and then allowed to swell at 37°C in phosphate buffer solutions at pH values of 1.2 and 7.4. At regular intervals i.e. 0,0.25,0.5,1,2,4,6,8,10,12,18,24 hrs, the surplus liquid adhering to the surface of the beads was removed using a filter paper, and the enlarged beads were weighed instantly. Equation 3 was utilized to compute the % swelling degrees of the beads. The swelling degree, expressed as a percentage, is calculated using the formula: (Ws - Wd / Wd) *100. where Ws indicated the swollen beads' weight at a particular period t, while Wd indicated the beginning beads' weight [11].

2.12. Release study of KGS in terms of RA and TR

The in vitro release profile of KGS was assessed by immersing 100 mg of dried, drug-loaded beads into media with pH 1.2 and pH 7.4 at 37°C while gently agitating at 50 rpm. At specified time intervals, 2 mL of the release medium was withdrawn and replenished with an equal volume of fresh medium. The released quantities of RA and TR from KLCAB were quantified using LC-MS/MS (as outlined in Chapter V). The percentage cumulative release of RA and TR in simulated gastric fluid (SGF, pH 1.2) and simulated colonic fluid (SCF, pH 7.4) was determined by incubating bead samples at 37°C with consistent shaking (50 rpm) in the respective solutions for time points of 0, 0.25, 0.5, 1, 2, 4, 6, 8, 10, 12, 18, 24, 48, and 72 hours. These drug release studies were performed in triplicate, and the results were presented as the mean ± standard deviation (mean ± S.D.)

3.0. Results

3.1. Design of Experiment (DOE)

Design of Experiments (DoE) is a comprehensive method used to investigate the critical interactions between dependent and independent variables. In the present work, a 2^3 Box Behnken design was applied to formulate KLCAB. Sixteen formulation batches were prepared and evaluated for % EE in terms of RA(Y1) and % EE in terms of TR (Y2) (Table 3). The influence of various factors on the response was analyzed using polynomial equations generated by the software, incorporating interaction terms. To understand the potential interactions among the variables, 3D response surface plots were generated through response surface mapping. Additionally, model adequacy was confirmed through ANOVA by evaluating the Co-efficient of determination (r^2) and p-value. After analysis, the best-fit model was a Linear model for both the responses. The equation is as follows:

Equation for % EE in terms of RA (Y1):

$$Y1 = 33.87766 + 4.82197 * X1 + 0.859943 * X2 - 3.19092 * X3$$ ------- equation (3)

Equation for % EE in terms of TR (Y2):

$$Y2 = 0.992965 + 3.83874 * X1 + 0.525974 * X2 - 2.43507 * X3$$ -------equation (4)

The best fit model for both responses was the Linear model. Table 1 and Table 2 depicts the model statistics for the two responses Y1 and Y2 respectively

Table 1: Model Fit Statistics for % EE in terms of RA (Y1)

Type of model	Value of p	Lack of Fit for the value of p	Adjusted r^2	Predicted r^2	F Value	
Linear	< 0.0001	0.6959	0.8339	0.7743	26.09	Suggested
2FI	0.1853	0.8184	0.867	0.8151	2.00	
Quadratic	0.3396	0.9429	0.8815	0.8439	1.37	
Cubic	0.9429		0.7882		0.1192	Aliased

Table 2: Model Fit Statistics for % EE in terms of TR (Y2)

Type of model	Value of p	Lack of Fit for the value of p	Adjusted r^2	Predicted r^2	F Value	
Linear	< 0.0001	0.209	0.9388	0.9079	77.70	Suggested
2FI	0.3846	0.1994	0.9409	0.8627	1.14	
Quadratic	0.3137	0.195	0.9489	0.7455	1.47	
Cubic	0.195		0.9745		3.01	Aliased

Table 3: Shows the software generated concentrations for 3 independent factors (X1,X2,X3) and experimentally produced data of 2 responses (Y1) and (Y2)

	Factors			Responses	
	SA (X_1)	$Cacl_2$ (X_2)	Chitosan (X_3)	Encapsulation efficiency of KGS in terms of RA (Y1)	Encapsulation efficiency of KGS in terms of TR (Y2)
F1	3.5	6	0.75	54.5818	14.2727
F2	3.5	10	1	58.5364	16.1688
F3	3.5	6	0.75	52.8454	14.5714
F4	3.5	2	1	49.9	12.3247
F5	5	2	0.75	60.1818	18.987
F6	3.5	2	0.5	53.8546	15.3896
F7	3.5	6	0.75	47.8636	15.8701
F8	2	6	0.5	46.9364	9.64935
F9	2	2	0.75	40.5909	8.35065
F10	5	6	0.5	60.9273	22.961
F11	5	6	1	59.0455	21.1299
F12	2	10	0.75	53.4182	12.7792
F13	5	10	0.75	63.3	25.1039
F14	2	6	1	44.6454	11.3377
F15	3.5	6	0.75	52.9182	15.4026
F16	3.5	10	0.5	56.7909	17.8312

As per the suggested combinations by the software, the % EE in terms of RA was highest in case of F13 with 5% SA, 10% $CaCl_2$ i.e. 63.3% and % EE in terms of TR in the same formulation was found to be 25.10 % % EE and Drug Loading Content (%)

A

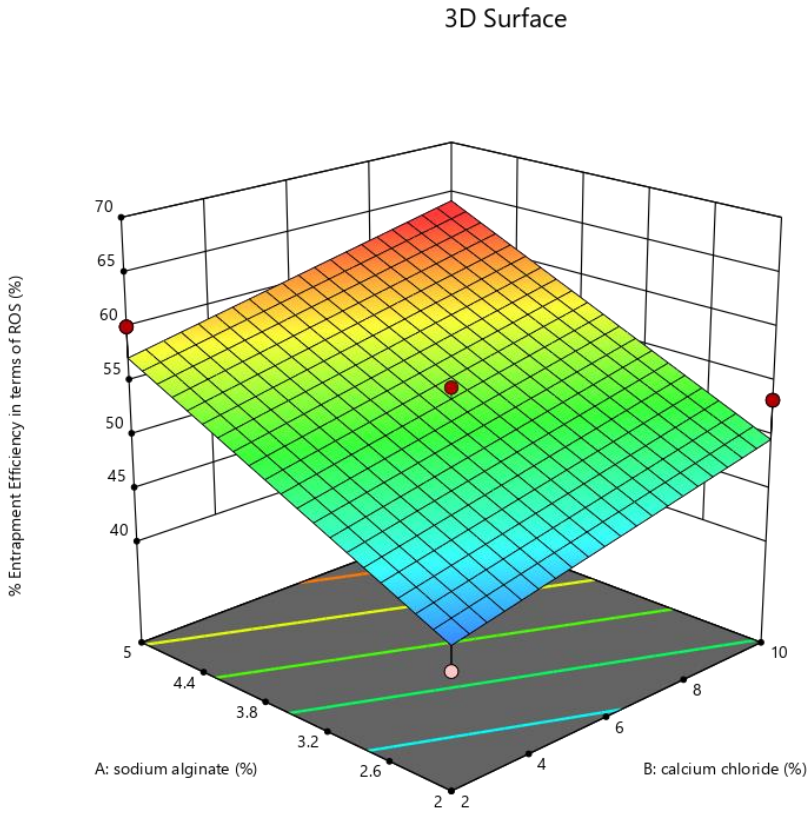

B

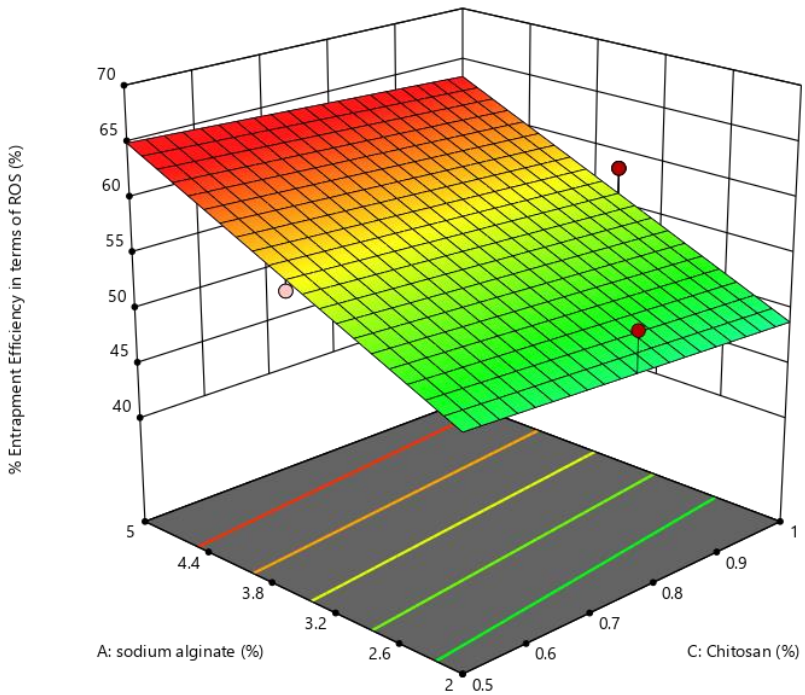

C

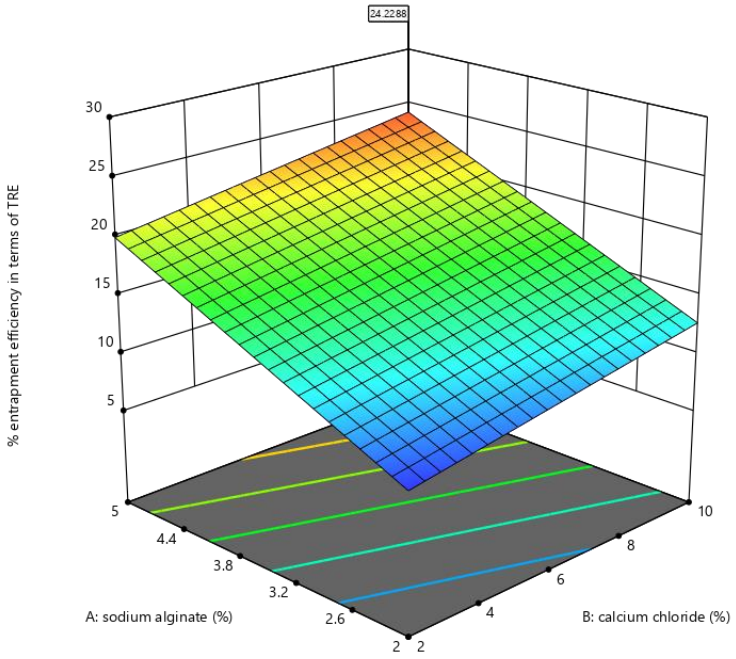

D

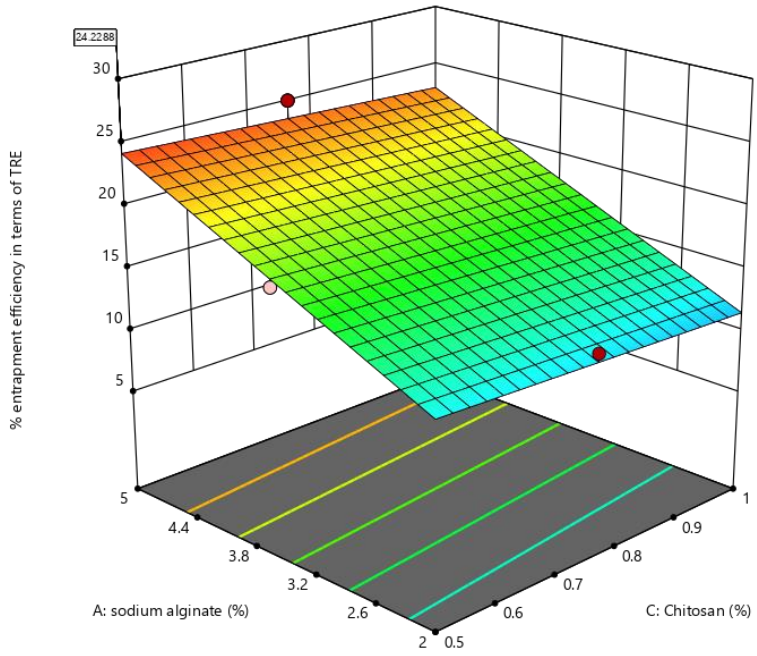

Figure 1: 3D plots illustrating the influence of formulation variables (X1, X2, and X3) on % EE for RA (Y1) and TR (Y2) are depicted as follows:(A) Interaction effect of sodium alginate (X1) and calcium chloride (X2) concentrations on % EE for RA (Y1).(B) Combined influence of sodium alginate (X1) and chitosan (X3) concentrations on % EE for RA (Y1).(C) Interaction effect of sodium alginate (X1) and calcium chloride (X2) concentrations on % EE for TR (Y2).(D) Combined influence of sodium alginate (X1) and chitosan (X3) concentrations on % EE for TR (Y2).

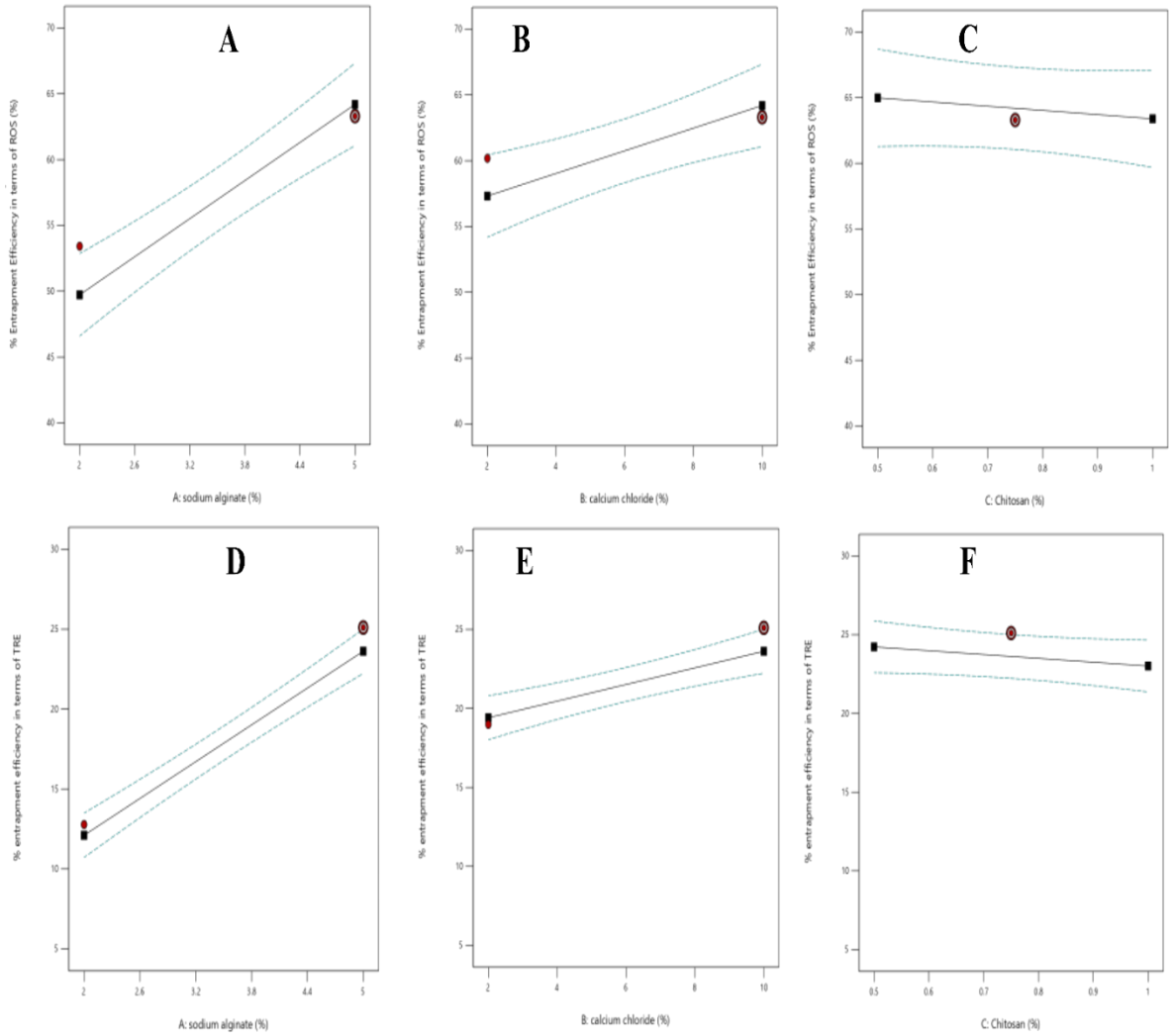

Figure 2: Main-effect plots illustrating the impact of independent formulation parameters (X1, X2, and X3) and their effect on % EE (Y) are presented as follows:(A) Effect of sodium alginate concentration on % EE for RA (Y1),(B) Effect of calcium chloride concentration on % EE for RA (Y1),(C) Effect of chitosan concentration on % EE efficiency for RA (Y1), (D) Effect of sodium alginate concentration on % EE for TR (Y2), (E) Effect of calcium chloride concentration on % EE for TR (Y2), (F) Effect of chitosan concentration on % EE for TR (Y2)

The best polynomial model fit for this design was found to be the linear Model. The independent variables X1, X2, and X3 were evaluated using a linear model. The analysis revealed that the sequential p-value was less than 0.0001, indicating that the linear model is significant. Moreover, the lack of fit p-value was 0.6959, suggesting non-significance of lack of fit, confirming the model's suitability and robustness. An adjusted r^2 value with 0.8339 indicates that 83.39% of the variability in the response is explained by the model.

Furthermore, the predicted R^2 value of 0.7743 demonstrates that the model can predict new data with 77.43% accuracy.

3.2.% EE and % Drug Loading Content of KGS in terms of RA and TR

In Table 4, F13 showed the highest % EE (RA-63.3%; TR-25.1039) and % Drug loading Content (RA-38.76 % ; TR-20.06 %)

Table 4: % EE and % Drug Content in the 16 formulations

Formulation No	% EE in terms of RA and TR		% Drug Loading Content in terms of RA and TR	
	RA	TR	RA	TR
F1	54.58182	14.27273	35.30934	12.4900557
F2	58.53636	16.16883	36.92299	13.9183902
F3	52.84545	14.57143	34.57444	12.7182045
F4	49.9	12.32468	33.28886	10.9723667
F5	60.18182	18.98701	37.57094	15.9572146
F6	53.85455	15.38961	35.00355	13.337085
F7	47.86364	15.87013	32.37012	13.6964806
F8	46.93636	9.649351	31.94333	8.80018951
F9	40.59091	8.350649	28.87165	7.70705981
F10	60.92727	22.96104	37.86013	18.6734263
F11	59.04545	21.12987	37.12489	17.4439798
F12	53.41818	12.77922	34.81868	11.3311838
F13	63.3	25.1039	38.76301	20.0664383
F14	44.64545	11.33766	30.86544	10.1831331
F15	52.91818	15.4026	34.60555	13.3468377
F16	56.79091	17.83117	36.22079	15.1328116

Figure 3: Represents freshly prepared (before drying) (A) Sodium alginate blank beads (B) Sodium alginate loaded with KGS (C) KGS in its traditional form (D) Dried KGS loaded chitosan coated alginate beads.

3.3. Measured beads Size

Table 5: Represents the size of the prepared Alg coated chitosan beads loaded with KGS

Formulation No.	Size of beads (mm)
F1	1.5 ± 0.1014
F2	1.09 ± 0.1401
F3	1.33±0.2573
F4	1.36±0.2426
F5	1.73±0.1814
F6	1.19±0.0600
F7	1.51±0.1757
F8	1.26±0.1769
F9	1.28±0.0757
F10	1.69±0.1153
F11	1.75±0.0264
F12	1.70±0.140
F13	1.59±0.4176
F14	1.21±0.0556
F15	1.35±0.0871
F16	1.56±0.2250

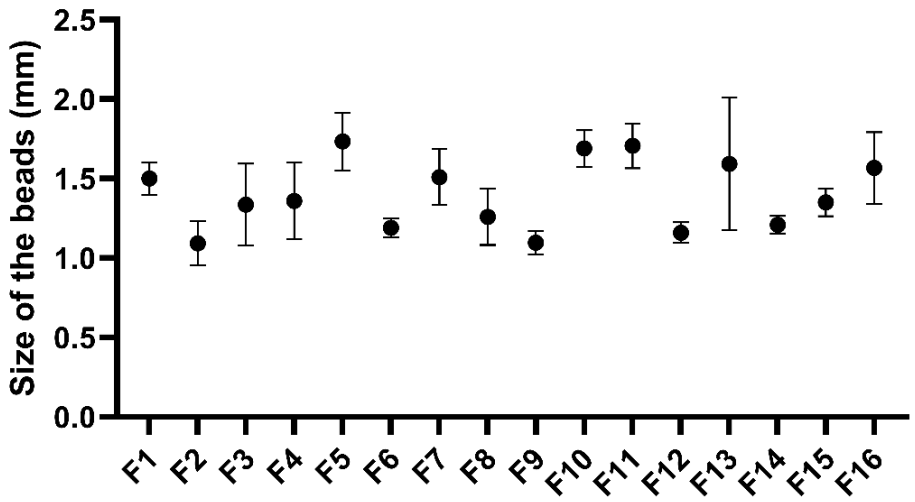

Figure 4: Represents the size of beads recorded in triplicate in the 16 formulations

After drying of the the beads, the KLCAB size (Figure 4 and table 5) was noted and the result showed that the F2 formulation showed the lowest particle size (mm) while F11 showed beads with highest particle size. The particle size was arranged in decreasing order as follows F2 < F6 < F14 < F8 < F9 < F3 < F15 < F4 < F1 < F7 < F16 < F13 < F10 < F12 < F5 < F11.

3.4. FTIR studies of the beads

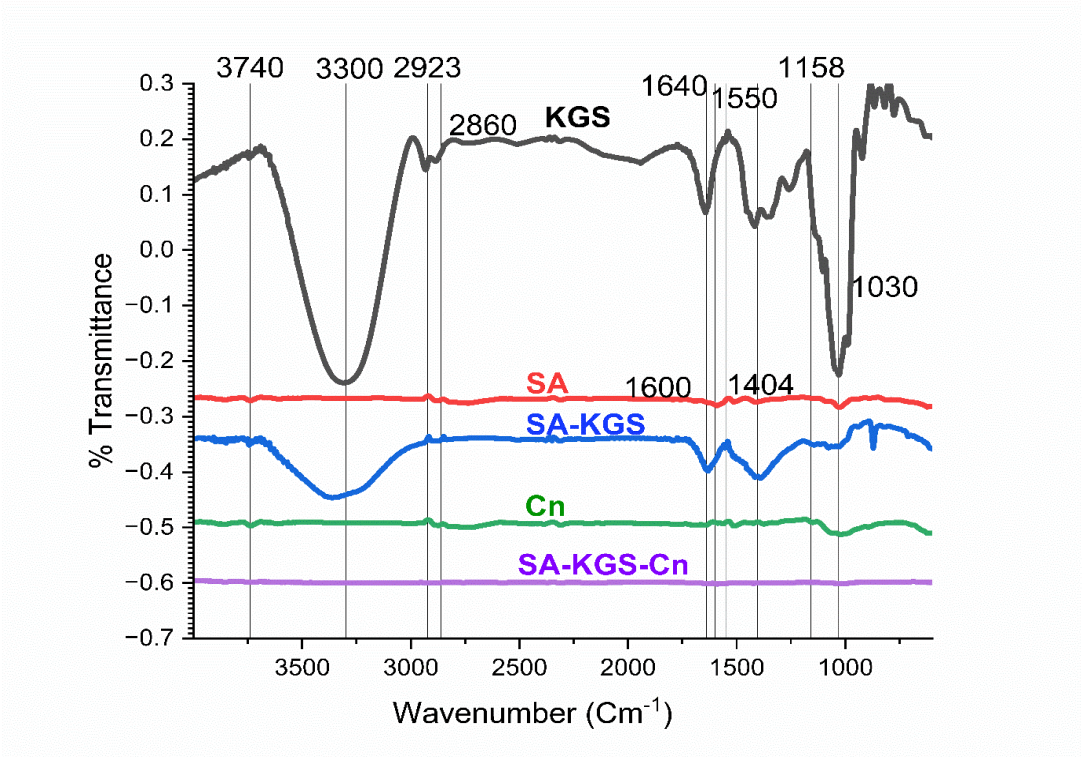

Figure 5: Represents the FTIR spectrum of KGS, native SA powder, native chitosan powder (Cn) powder, SA-KGS (Sodium alginate loaded with KGS), SA-KGS-Cn (KLCAB)

The FTIR spectra (Figure 5) revealed several significant findings. A sharp peak at 3330 cm^{-1} indicates the presence of OH stretching vibrations in KGS, alginate, and chitosan. This intensity decreases in the SA-KGS sample, suggesting the encapsulation of KGS in sodium alginate. In the SA-KGS-Cn coated sample, the signal almost wholly disappears, likely indicating a chitosan coating. The peak at 3740 cm^{-1}, associated with hydroxyl groups not involved in hydrogen bonding, is another key observation. Peaks at 2923 cm^{-1} and 2860 cm^{-1} correspond to C-H stretching vibrations, expected to be present in all samples but disappear in the SA-KGS-Cn group, suggesting interactions due to chitosan coating. A prominent peak around 1640 cm^{-1} is characteristic of the amide I band (C=O stretching) in chitosan, confirming the presence of the chitosan backbone. The peak around 1030 cm^{-1}, attributed to C-O-C stretching vibrations, likely represents the sugar rings of chitosan, while a band at 1550 cm^{-1} may indicate NH-stretching in amide. Additionally, a symmetrical band at 1600 cm^{-1}, indicative of -COO- stretching in alginate, and a narrower symmetrical COO- bond at 1404 cm^{-1} show an increase in intensity in the sodium alginate-loaded KGS sample, indicating interaction with the carboxylate group of alginate. This signal disappears in the SA-KGS-Cn sample, pointing to the interaction between alginate and chitosan.

Furthermore, the peak around 1640 cm^{-1} appears broader and slightly shifts in the SA-KGS-Cn spectrum, indicating an interaction between chitosan's amide groups and alginate's carboxylate groups. The peak at 1030 cm^{-1} shows shifts or broadening, suggesting potential rearrangement of the polymer matrix due to interactions between alginate and chitosan. Lastly, the broadband at 3300 cm^{-1} becomes more pronounced and shifts in the SA-KGS-Cn spectrum, likely due to superimposed O-H and N-H stretching vibrations, hinting at hydrogen bonding between the polymers.

3.5. Thermogravimetric analysis

The thermogravimetric analysis (TGA) showed several (Figure 6) key findings regarding the thermal stability and decomposition patterns of various materials. The Alg powder and chitosan (Cn) showed a loss of 16.90% and 10.57% of the mass, respectively, between 30-200 ^{o}C. At 300 ^{o}C, Alg exhibited a 51.16% decrease in mass. Chitosan powder exhibited a high weight loss of 58.67% between 300-400 ^{o}C. For Khamira Gaozaban Sada (KGS) (Figure 3C), the thermogravimetric analysis showed the following results: an initial weight loss of 1.05% up to 100°C, likely due to moisture evaporation. The decomposition stages ranged from 30°C to 600°C, with only a minimal 2% difference in mass from 600°C to 800°C. At 200°C, there was a decomposition of 15.21%. The TG curve exhibited two

significant mass losses: the first between 200-400°C, accounting for 71.05% of the total weight loss, and the second between 400-600°C, resulting in an additional 80.36% weight loss. The pure Alg powder showed an initial weight loss of 16.90% at 200°C. In the case of chitosan powder, there was an enhanced weight loss of around 250-330°C, with a 48% loss. The thermal degradation study of the beads revealed three significant weight loss stages: (i) 30°C-200°C, with mass losses of 47.48% and 18.42% for alginate (Figure 3A) and KLCAB (Figure 3D), respectively, (ii) 200-300°C, with weight losses of 65.70% and 46.32%; (iii) 300-800°C, with weight decompositions of 83.82% and 81.22%. The temperature required for half of the weight loss (T50) was 283.37°C, 338.58°C, 205.88°C, and 324.17°C for Alg powder, chitosan powder, Alg beads, and Alg/Cn beads, respectively.

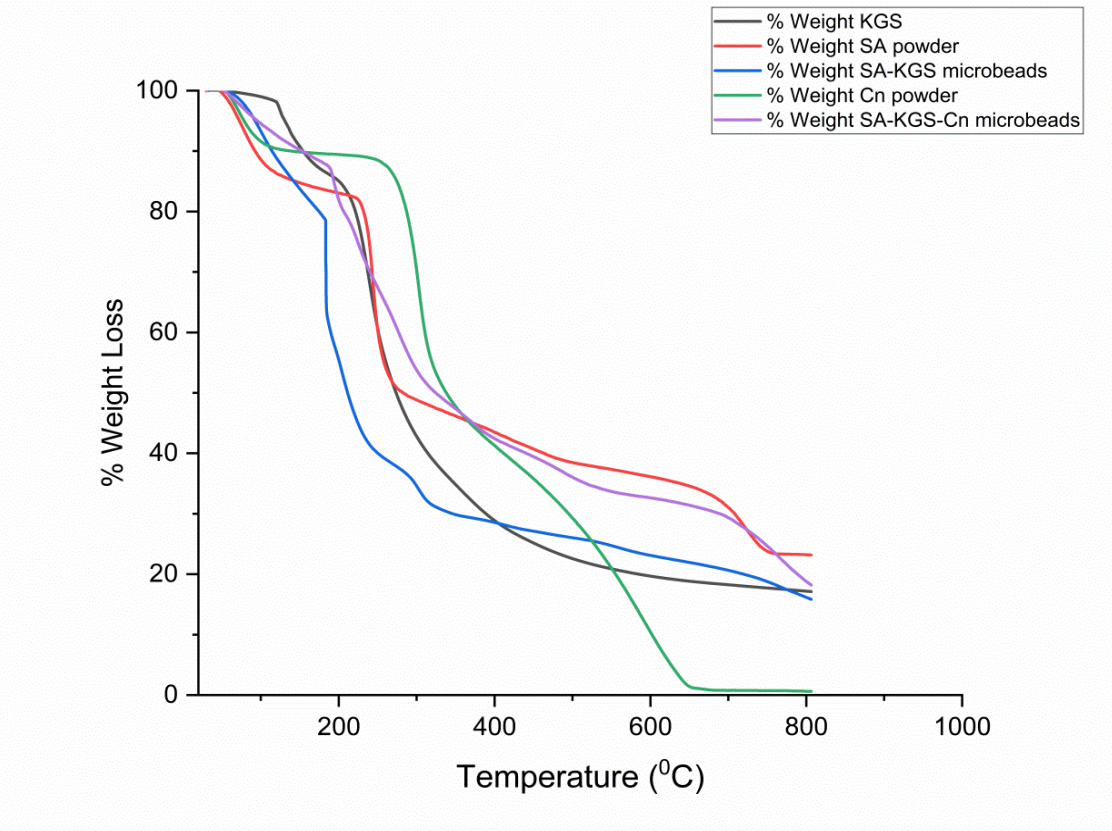

Figure 6: Thermogravimetric analysis showing % weight loss of KGS (black line), native SA (Red line), SA-KGS beads (blue line), native Cn powder (green line), SA-KGS-Cn beads (violet line).

3.6.SEM analysis at 50X and 500X

In Figures 7A and 7D, the blank alginate beads show surface irregularities, including cracks and folds, suggesting a brittle structure. At 500× magnification, deep grooves and roughness are evident, indicating poor cohesion and compactness in the bead structure. The loading of KGS (Figures 7B and 7E) introduces notable changes to the bead surface. At 50× magnification, the surface appears smoother compared to the blank beads, with fewer visible cracks. At 500× magnification, particulate deposits are visible, corresponding to components of the polyherbal extract, with reduced but still present cracks. The chitosan coating (Figures 7C and 7F) changes the beads' surface significantly. At 50× magnification, the coating creates a visibly smoother and more uniform surface, effectively masking the cracks and irregularities observed in uncoated beads. At 500× magnification, cracks are barely visible, indicating improved structural stability due to the chitosan layer.

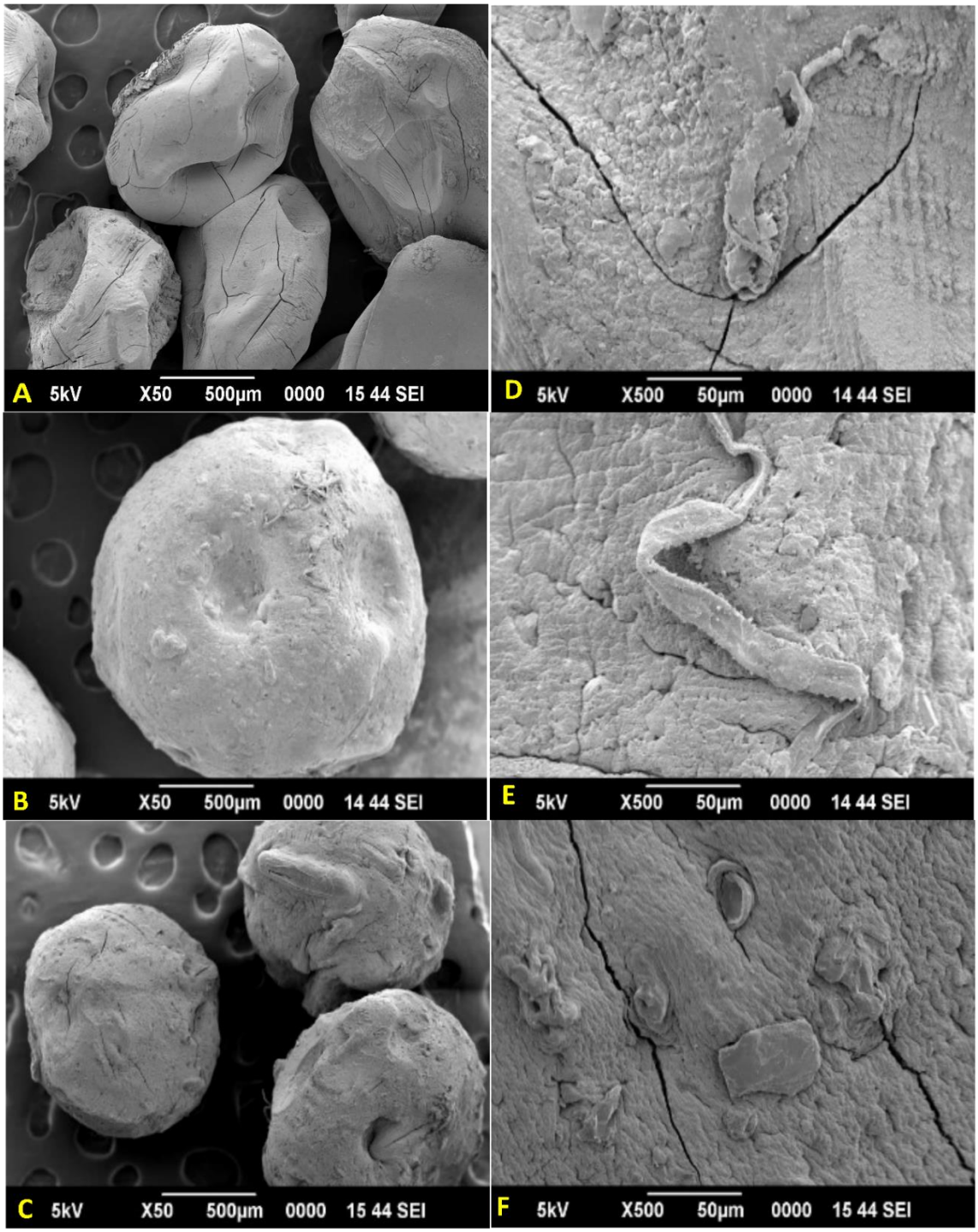

Figure 7: Represents the SEM images of beads captured at 50X magnification for (A) Blank Alg beads (B) Alg loaded with KGS beads (C) Alg loaded with **KGS coated with** Cn. At a magnification of 500 X, for (D) Alg Blank beads (E) Alg loaded with KGS (F) Alg loaded with KGS coated with Cn

3.7.% Swelling

3.7.1.% Swelling at pH 1.2

In Figure 8A at pH 1.2, all 16 formulations of sodium alginate beads coated with chitosan exhibited no swelling initially (0 hrs). Rapid swelling occurred within the first 0.25 hrs, with F9 and F6, which showed the highest swelling at 57% and 50%, respectively. By 1 hr, F9 (118%) and F8 (109%) continued to demonstrate significant swelling. Peak swelling was observed around 2 to 6 hrs, with F14 reaching 343% at 6 hrs. The swelling indices began to stabilize by 8 hrs, with formulations like F14 and F16 maintaining substantial swelling. Long-term swelling data (10 to 24 hrs) showed a gradual decrease in most formulations, but F16 (520%) and F15 (470%) exhibited the highest long-term swelling capacity, indicating variations in formulation composition and sustained hydration. Formulations F9, F8, F14, and F15 showed the most robust and sustained swelling behaviour. At pH 1.2, the F5 formulation exhibits a steady increase in swelling, starting moderately at 56% after 2 hrs and peaking at 255% at 6 hrs. This trend continues, reaching a significant and sustained swelling capacity of 400% by 24 hrs. The F10 formulation shows a gradual increase in swelling, peaking at 250% at 6 hrs and continuing to 520% at 24 hrs, indicating strong and sustained swelling behaviour. The F11 formulation starts with low swelling (44% at 2 hrs), peaks at 61% at 8 hrs, and remains relatively stable, ending at 99.66% at 24 hrs, showing moderate and stable swelling capacity. F5 exhibited a steady increase in swelling, starting moderately at 56% after 2 hrs and peaking at 255% at 6 hrs. This pattern continues, reaching a significant and sustained swelling capacity of 400% by 24 hrs. The F10 formulation shows a gradual increase in swelling, peaking at 250% at 6 hrs and continuing to 520% at 24 hrs, indicating strong and sustained swelling behaviour.

3.7.2.% Swelling at pH 7.4

In Figure 8B at Ph 7.4, In the initial stages, the formulations exhibit rapid swelling within the first 0.25 hrs. F15 achieves the highest swelling index at 358%, while F12 shows the lowest at 28%. As time progresses to 0.5 hrs, the swelling continues to increase significantly across the formulations. F8 and F15, in particular, demonstrate substantial swelling, reaching 413% and 620%, respectively. At the 1st hr, F7 and F9 displayed exceptionally high hydration capacities at 2100% and 1572%, respectively. Swelling increases remarkably for several formulations at 2nd hr, with F7 (2740%) and F9 (3512%). By the 4th hr, F7 and F9 maintained a high swelling nature, along with F8 (2940%) and F15 (3080%). At 6 hrs,

maximum swelling is observed in F8 (3215%) and F15 (3096%). From the 10th to 24 hr, a gradual decrease in swelling is observed in most formulations. F5, F10, F11 and F13 show consistent swelling behaviour within this phase. By 18 to 24 hrs, significant reductions are noted in F1, F2, and F3, while formulations like F5 and F10 still showed relatively consistent swelling

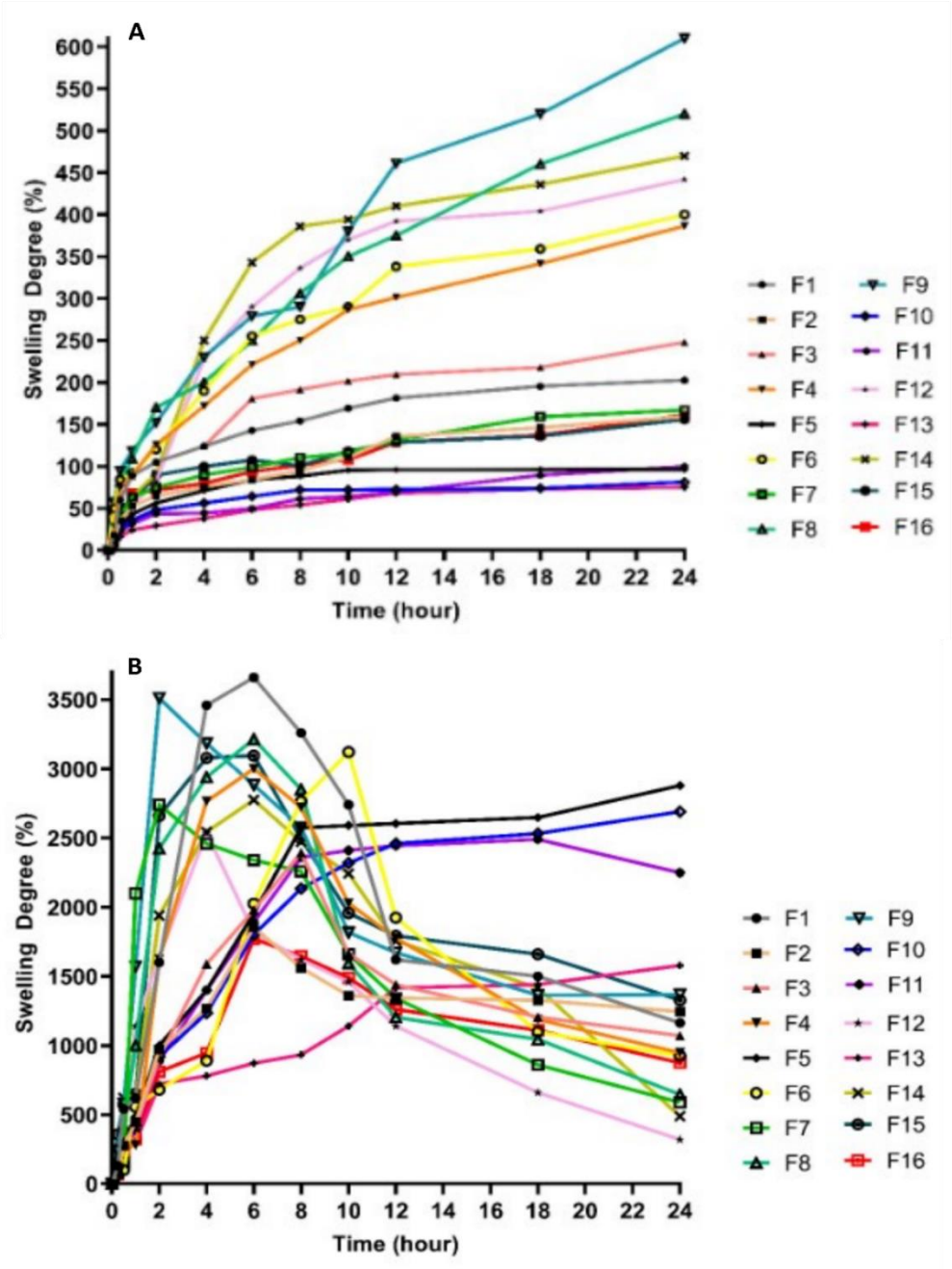

Figure 8: Represents the % swelling of the 16 formulations (F1 to F16) of KGS loaded chitosan coated pH sensitive alginate beads in phosphate buffer of (A) pH 1.2 (B) pH 7.4. for time points 0,0.25,0.5,1,2,4,6,8,10,12,18,24 hrs

3.8.% Cumulative Release of KGS in terms of RA and TR

3.8.1.RA Release at pH 1.2

In Figures 9 and 10, an early burst release was observed at 0.25 hrs in the case of F4 and F9 with an initial burst of 11.04% ±2.06% and 11.41% ±5.37%, respectively. These are significantly higher than most others, which remain near 0–4%. At 1 hr, F1 showed a very high release of 46.81% ±0.057%. The next highest release was observed in F8 at 34.39% ±2.94%. At 1 hr, F1's release (46.8%) is more than 5 times higher than many formulations (e.g., F10, F11, F12), which remain under 10%. At 2-hr, F1, F4, F6, F9 and F14 showed rapid release, i.e. a large portion of ROS within 2 hrs under acidic conditions was released at 48.35%, 46.45%, 43.66%, 39.21%, 42.51% respectively. Release pattern constituting large early bursts was observed, while others remained low initially but increased over time. By the 72 hrs, F5 dramatically showed a release of 41.35% ±1.28%. Many others remained below 10% at 72 hrs (e.g., F2=0%, F7=0%, F8=0%), indicating poor long-term release in acidic conditions for those formulations. F5 released relatively less at early times compared to F1 or F4, but by the end (72 hrs), it surpassed nearly all others, suggesting a more controlled release profile.

3.8.2. RA Release at pH 7.4

In Figures 11 and 12, at pH 7.4, many formulations showed even more pronounced early releases. An early burst release was observed at 1 hr for F6, F9,F8 and F1 at 65.35% ±0.94% (exceptionally high early release), 50.10% ±1.36%, 47.97% ±2.12%, and 28.41% ±1.97% respectively. Compared to pH 1.2, the early release at pH 7.4 is observed to be higher for some formulations, indicating pH sensitivity and possibly weaker matrix integrity at pH 7.4. Within the first 1–2 hrs, multiple formulations exceeded 20–30% release, and some surpassed 50%. By 72 hr, F5 again emerged as the formulation with the highest % cumulative release, i.e. 68.08% ±0.21%, while others showed early burst release, their final %cumulative release either plateaued or remained lower than F5. This pattern of release was similar to ROS release at pH 1.2, where F5 eventually released ROS over an extended period, suggesting its suitability for prolonged release at pH 7.4.

3.8.3.TR Release at pH 1.2

In the case of % cumulative release of TR (Figure 9 and 10) , at 0.5 hrs, several formulations showed considerable release. F3 and F6 showed a release of 14.77% ±4.37% and 14.83% ±1.37 % respectively at 0.5 hr. F1 also showed a strong early response of 13.69% ±2.64%.

At 1 hr, F1 showed 45.74% ±3.95% at 1 hr, which was very high compared to others at the same time. At 2 hrs, % cumulative release of F3 and F9 was found to be 40.41% ±0.89% and 41.09% ±4.36% respectively. So by 2 hrs, F1, F3, and F9 all exceeded 40%, indicating multiple formulations can achieve rapid TR release under acidic conditions. At 4 hrs, F4 was observed at 47.87% ±2.69% while F6 showed at 46.01% ±4.93%. At 72 hrs, F5 reached 39.63% ±2.19%, indicating a more gradual, controlled release profile extending beyond the early hrs.

3.8.4.TR Release at pH 7.4

In Figure 11 and 12, an extremely rapid early release was observed at 1 hr, with F1 showing a release of 51.51% ±2.02%. In contrast, F6 showed 50.57% ±2.36%, implying that these formulations are highly sensitive to pH 7.4, allowing the TR to diffuse out quickly. Other formulations also showed some rapid release at an early time period, but not in comparison to F1 and F6.

By 4 hr and beyond, some formulations achieved high release F14 with % cumulative release of 48.32% ±2.40%, indicating a delayed but still substantial release. By the end of 72 hr, F5 again showed a better release of 42.14% ±5.92% while F4 showed a decent release of 27.17% ±2.83%. Thus, while some revealed high bursts of TR at 1-hr (F1, F6), others such as F5 and F4, continued to release by the end of 72 hr, reflecting a more controlled release pattern at pH 7.4. Among all the formulations, F5 emerged as having more sustained release profiles, achieving a higher % cumulative release over extended periods (24–72 hrs).

Although both RA and TR showed similar trends (burst vs. sustained), the actual percentages differed. RA at pH 7.4 was observed to exhibit highly high early releases in several formulations, while TR at pH 7.4 also showed early bursts but with different sets of formulations.

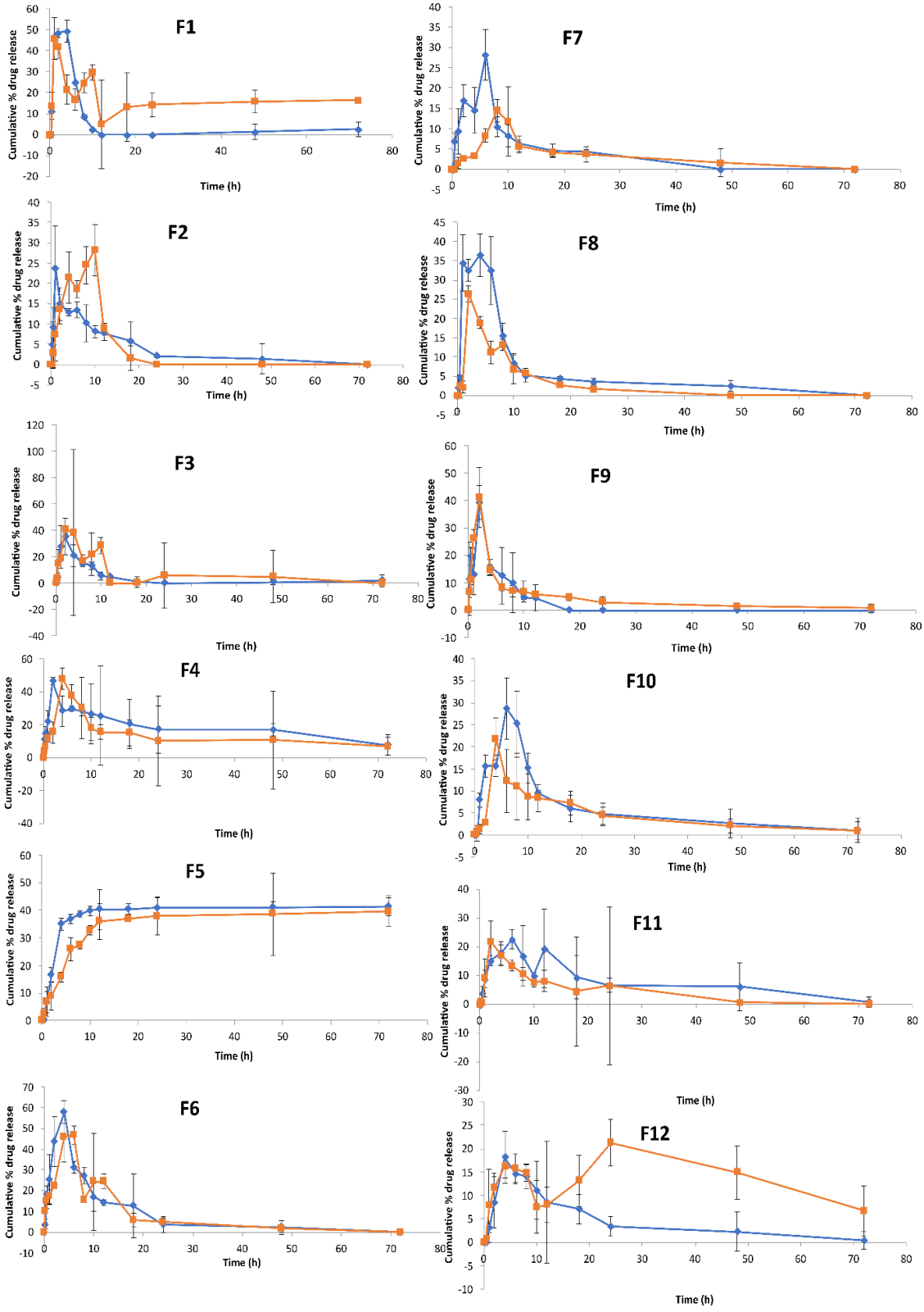

Figure 9: % Cumulative Drug Release of RA and TR in Ph 1.2 at time points 0,0.25,0.5, 1, 2, 4, 6,8,10,12,18,24,48 and 72 hr. The Blue and Red line indicates the % cumulative release of RA and TR respectively. All the Data are represented in Mean ± SD

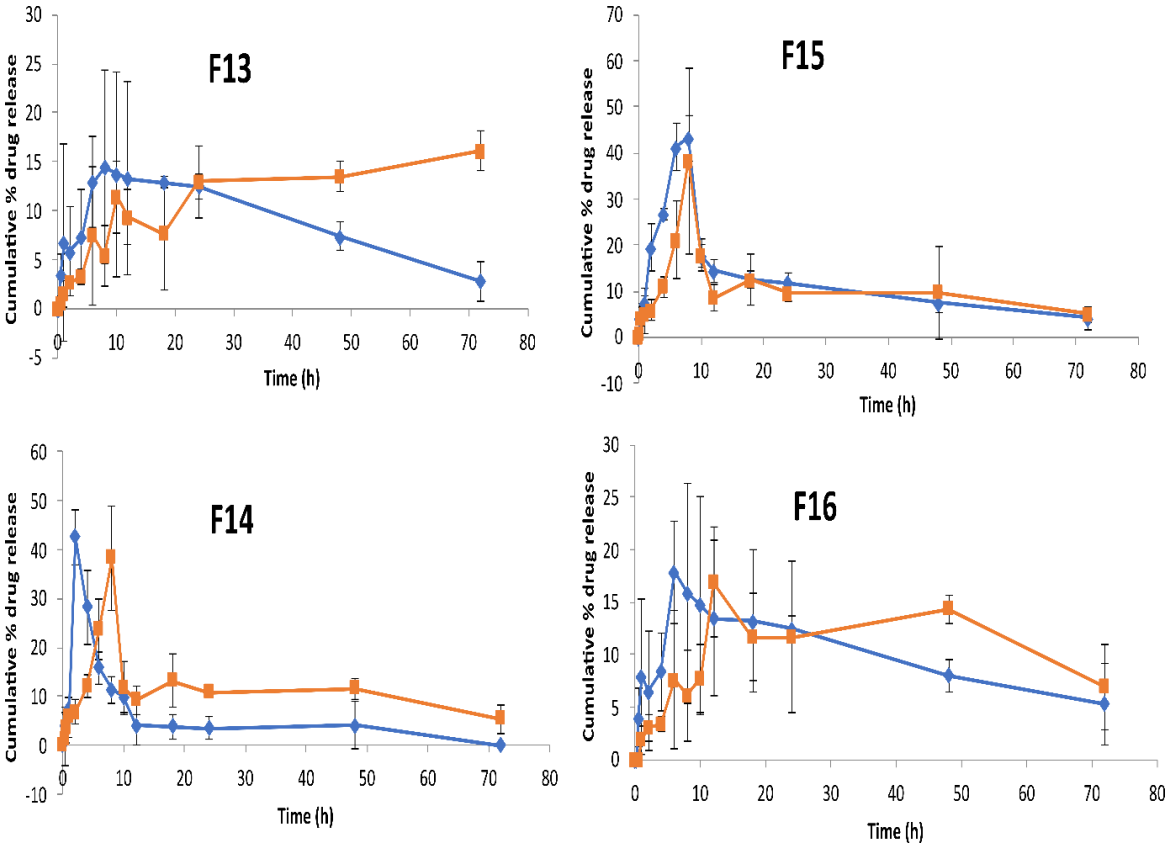

Figure 10: % Cumulative Drug Release of RA and TR in Ph 1.2 at time points 0,0.25,0.5, 1, 2, 4, 6,8,10,12,18,24,48 and 72 hr. The Blue and Red line indicates the % cumulative release of RA and TR respectively. All the Data is represented in Mean ± SD

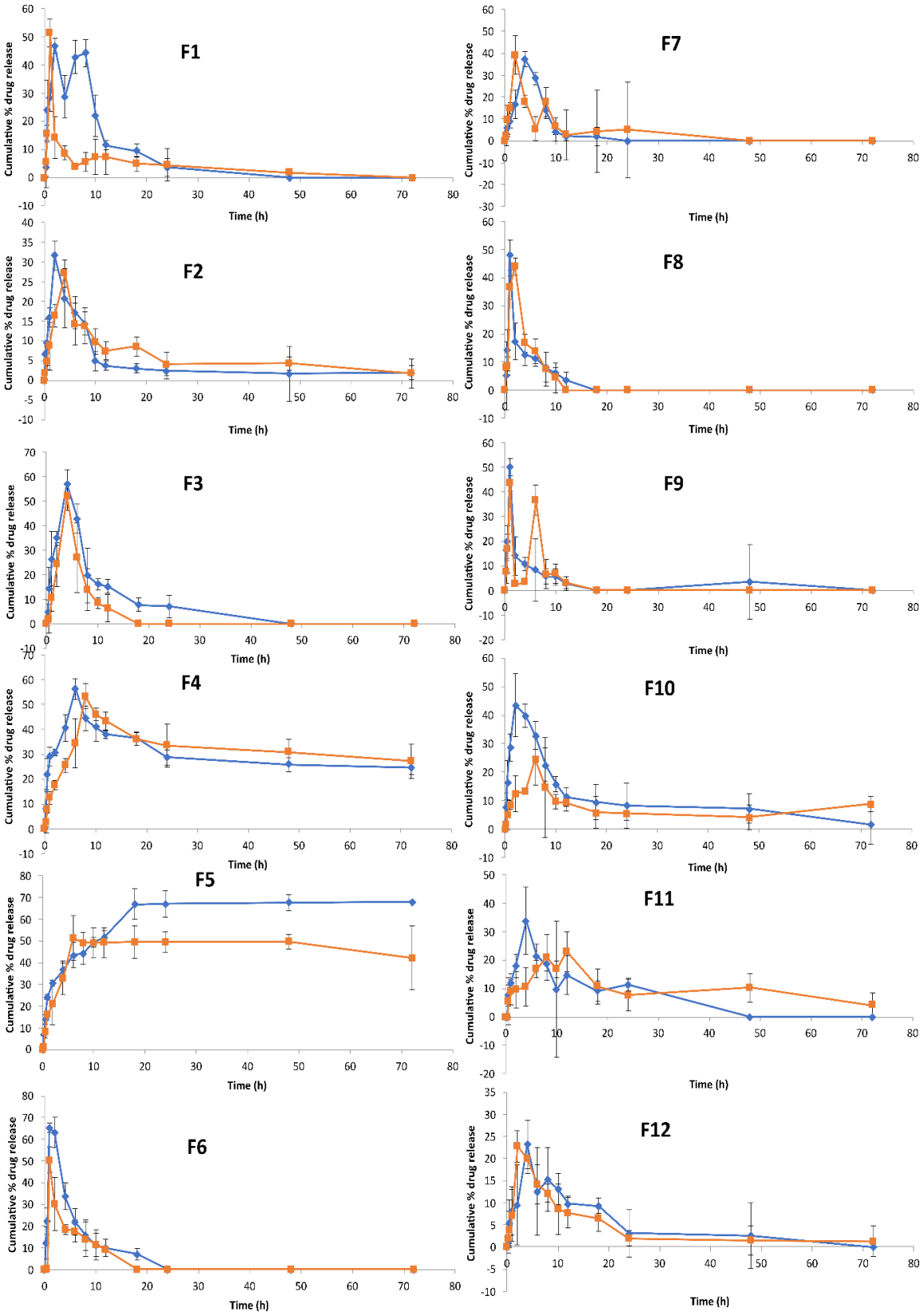

Figure 11: % Cumulative Drug Release of RA and TR in Ph 7.4 at time points 0,0.25,0.5, 1, 2, 4, 6,8,10,12,18,24,48 and 72 hr. The Blue and Red line indicates the % cumulative release of RA and TR respectively. All the Data are represented in Mean ± SD for formulation F13 to F16

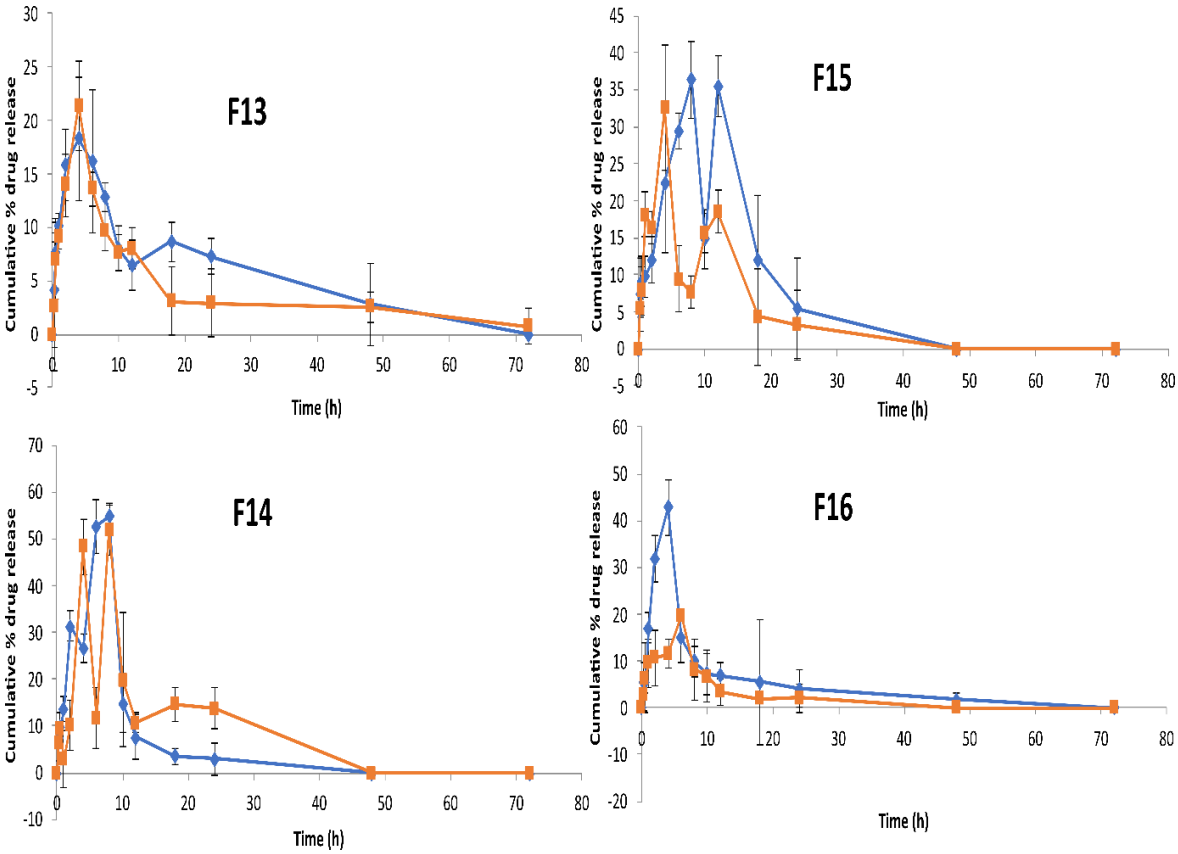

Figure 12: % Cumulative Drug Release of RA and TR in Ph 7.4 at time points 0,0.25,0.5, 1, 2, 4, 6,8,10,12,18,24,48 and 72 hr from KGS loaded in SA coated with chitosan. The Blue and Red line indicates the % cumulative release of RA and TR, respectively. All the Data is represented in Mean ± SD for formulation F13 to F16

3.9. Kinetic Modeling

3.9.1. Model Fit for RA Release at pH 1.2 and 7.4

For RA at pH 1.2, the model fit analysis revealed that the best-fitting formulation for the Zero Order, First Order, Higuchi, Hixson-Crowell, and Weibull models was F5, with an r^2 value of 0.31158, 0.3115, 0.583772, 0.583772, and 0.325167, respectively. The Korsmeyer-Peppas model showed formulation F15 as the best fit with an r^2 value of 0.399228.

For pH 7.4, the analysis indicated that formulation F5 was the best fit across all seven models tested. The best fit for Zero Order, First Order, Higuchi, Hixson-Crowell, Baker-Lonsdale, and Weibull models was F5 among all the formulations, with an r^2 value of 0.516562, 0.516896, 0.79736, 0.516784, 0.91177, and 0.611949, respectively. The Korsmeyer-Peppas model demonstrated the best fit for formulation F5 with an r^2 value of

0.942622. Therefore, formulation F5 showed the highest r^2 values at pH 7.4 across all seven models, particularly in the Korsmeyer-Peppas and Baker-Lonsdale models, for its excellent performance

3.9.2.Model Fit for TR Release at pH 1.2 and 7.4

For pH 1.2, the model fit analysis identified the best formulation for each kinetic model. The best fit was F13 for Zero Order, First Order, Higuchi, Hixson-Crowell and Weibull models with an r^2 of 0.691809924, 0.691893367, 0. 877341113, 0.691865553, 0.708367939 respectively. In the Baker-Lonsdale model, formulation F9 exhibited the best fit with an r^2 value of 0.632170701. Lastly, the Korsmeyer-Peppas model indicated F14 as the best fit with an R^2 value of 0.613109002. Overall, F13 showed the highest r^2 values in five out of seven models, making it the best formulation at this pH. For pH 7.4, the model fit analysis identified the best formulation for each kinetic model. The best fit was F16 for Zero Order, First Order, Higuchi, Hixson-Crowell, Baker-Lonsdale, and Weibull models with an r^2 of 0.244211103, 0.244136615, 0.16250444, 0.244161445, 0.751205116, and 0.229222549 respectively. The Korsmeyer-Peppas model indicated F4 as the best fit with an r^2 value of 0.852230382. Overall, F16 showed the highest r^2 values in six out of seven models, making it the best formulation at this pH.

Table 6: Co-efficient of determination (r^2) of Drug release in terms of RA in different Kinetic Models at pH 1.2 and 7.4

Formulation	**pH**	**Zero Order Model** ($Qt=Q0+k0t$)	**First Order Model** $Qt=Q0e^{-k_1 t}$	**Higuchi Model** $Qt=k_H \sqrt{t}$	**Hixson-Crowell Model** $Qt^{1/3}-Q0^{1/3}=k_H Ct$	**Baker-Lonsdale Model** $3/2[1-(1-Qt/Q0)^{2/3}]-Qt/Q0=k_{BL}t$	**Weibull Model** Log [ln - (1-m)] = b Log (t-Ti)-log a	**Korsmeyer-Peppas Model** $Qt/Q\infty=k_{KP}t^n$
F1	1.2	0.142906	0.142885	0.14566	0.142892	0.1995	0.199499932	
	7.4	0.261708	0.261592	0.168791	0.26163	0.363726	0.233642	0.001138
F2	1.2	0.31158	0.3115	0.244086	0.311527	0.546836	0.294639	0.114672
	7.4	0.210115	0.210052	0.181679	0.210073	0.773051	0.195992	0.211479
F3	1.2	0.223186	0.223053	0.226695	0.223098	0.548056	0.209024	
	7.4	0.218819	0.218559	0.135077	0.218646	0.595817	0.177027	0.001845
F4	1.2	0.096491	0.096537	0.016133	0.096522	0.746041	0.099456	0.160609
	7.4	0.000366	0.000374	0.047551	0.000371	0.720783	0.004409	0.532539
F5	1.2	0.305964	0.306076	0.583772	0.306039	0.03649	0.325167	0.0516
	7.4	0.516562	0.516896	0.79736	0.516784	0.91177	0.611949	0.942622
F6	1.2	0.223759	0.223548	0.141481	0.223618	0.431564	0.813439678	
	7.4	0.240701	0.240478	0.249262	0.240552	0.525039	0.185448	
F7	1.2	0.176139	0.176063	0.088033	0.176088	0.224093	0.160335	
	7.4	0.173986	0.17388	0.098321	0.173915	0.567476	0.129848	
F8	1.2	0.184908	0.18487	0.134295	0.184883	0.171263	0.176907	0.000541
	7.4	0.182159	0.181995	0.211484	0.18205	0.282287	0.145945	
F9	1.2	0.252942	0.252785	0.27608	0.252837	0.584245	0.217537	
	7.4	0.176761	0.176613	0.242583	0.176663	0.475109	0.142707	
F10	1.2	0.094047	0.094034	0.016653	0.094038	0.081609	0.091082	
	7.4	0.23001	0.229938	0.153144	0.229962	0.832485	0.21225	
F11	1.2	0.092236	0.092239	0.007499	0.092238	0.237706	0.092384	
	7.4	0.174352	0.174291	0.061027	0.174311	0.242389	0.160406	0.020283
F12	1.2	0.08466	0.084659	0.007224	0.084659	0.055147	0.085082	

Formulation	**pH**	**Zero Order Model** ($Qt=Q0+k0t$)	**First Order Model** $Qt=Q0e^{-k_1 t}$	**Higuchi Model** $Qt=k_H \sqrt{t}$	**Hixson-Crowell Model** $Qt^{1/3}-Q0^{1/3}=k_H Ct$	**Baker-Lonsdale Model** $3/2[1-(1-Qt/Q0)^{2/3}]-Qt/Q0=k_{BL}t$	**Weibull Model** Log [ln - (1-m)] = b Log (t-Ti)-log a	**Korsmeyer-Peppas Model** $Qt/Q\infty=k_{KP}t^n$
	7.4	0.16077	0.160733	0.045636	0.160745	0.383473	0.152986	0.237036
F13	1.2	0.000712	0.000714	0.069913	0.000713	0.236596	0.000964	
	7.4	0.254514	0.254476	0.116948	0.254488	0.915534	0.246674	0.051177
F14	1.2	0.127888	0.127821	0.086314	0.127843	0.212942	0.113077	0.003081
	7.4	0.154409	0.154257	0.079717	0.154308	0.525217	0.119679	0.018875
F15	1.2	0.058184	0.058181	0.003122	0.058182	0.397557	0.056408	0.399228
	7.4	0.152917	0.152807	0.03906	0.152844	0.571773	0.129916	0.125062
F16	1.2	0.000268	0.000266	0.08246	0.000267	0.229042	3.45E-05	
	7.4	0.16887	0.168759	0.121808	0.168796	0.411983	0.144782	0.020992

Table 7: Co-efficient of determination (r^2) of Drug release in terms of TR in different Kinetic Models at pH 1.2 and 7.4

Formulation	**pH**	**Zero Order Model** ($Qt=Q0+k0t$)	**First Order Model** $Qt=Q0e^{-k_1 t}$	**Higuchi Model** $Qt=k_H \sqrt{t}$	**Hixson-Crowell Model** $Qt^{1/3}-Q0^{1/3}=k_H Ct$	**Baker-Lonsdale Model** $3/2[1-(1-Qt/Q0)^{2/3}]-Qt/Q0=k_{BL}t$	**Weibull Model** Log [ln - (1-m)] = b Log (t-Ti)-log a	**Korsmeyer-Peppas Model** $Qt/Q\infty=k_{KP}t^n$
F1	1.2	0.012066	0.012105	0.002939	0.012092	0.213692	0.022357	
	7.4	0.133688	0.133556	0.151926	0.1336	0.266462	0.105241	0.276491579
F2	1.2	0.130963	0.130919	0.042765	0.130934	0.195641	0.121896	
	7.4	0.120502	0.12048	0.041371	0.120487	0.566861	0.115404	0.136533
F3	1.2	0.182476	0.182388	0.127801	0.182417	0.446734	0.170161	
	7.4	0.124648	0.124555	0.077175	0.124586	0.160451	0.102552	
F4	1.2	0.046507	0.046535	0.002499	0.046526	0.557372	0.049075	0.299409
	7.4	0.072882	0.07278	0.268606	0.072814	0.595794	0.047428	0.85223
F5	1.2	0.477079	0.477258	0.758048	0.477198	0.171725	0.511106	
	7.4	0.105241	0.276492	0.501375	0.225149	0.374601	0.215174	0.815988

Formulation	**pH**	**Zero Order Model** ($Qt=Q0+k0t$)	**First Order Model** $Qt=Q0e^{-k_1 t}$	**Higuchi Model** $Qt=k_H \sqrt{t}$	**Hixson-Crowell Model** $Qt^{1/3}-Q0^{1/3}=k_H Ct$	**Baker-Lonsdale Model** $3/2[1-(1-Qt/Q0)^{2/3}]-Qt/Q0=k_{BL}t$	**Weibull Model** Log [ln - (1-m)] = b Log (t-Ti)-log a	**Korsmeyer-Peppas Model** $Qt/Q\infty=k_{KP}t^n$
F6	1.2	0.218654	0.218451	0.117101	0.218518	0.747002	0.180747	0.014487
	7.4	0.156946	0.156868	0.135641	0.156894	0.047958	0.137024	
F7	1.2	0.033431	0.033429	0.001241	0.03343	0.019544	0.032954	
	7.4	0.173986	0.17388	0.139933	0.173915	0.379275	0.150825	0.02172
F8	1.2	0.133562	0.133529	0.070875	0.13354	0.063134	0.126994	
	7.4	0.18943	0.189322	0.213855	0.189358	0.362578	0.165714	
F9	1.2	0.185579	0.18546	0.18568	0.1855	0.632171	0.159708	0.275336
	7.4	0.13832	0.13824	0.146771	0.138267	0.32507	0.121737	
F10	1.2	0.042607	0.042612	0.000283	0.04261	0.02808	0.04332	
	7.4	0.012177	0.012187	0.000609	0.012184	0.595097	0.014162	0.211202
F11	1.2	0.163934	0.163912	0.070719	0.163919	0.116222	0.159541	0.297606
	7.4	0.007605	0.007612	0.024935	0.00761	0.230325	0.008925	
F12	1.2	0.046371	0.046358	0.19101	0.046363	0.100687	0.043819	
	7.4	0.164868	0.164841	0.08188	0.16485	0.435008	0.159112	0.035188
F13	1.2	0.69181	0.691893	0.877341	0.691866	0.042387	0.708368	
	7.4	0.203997	0.203953	0.114854	0.203967	0.6951	0.194755	0.000257
F14	1.2	0.000603	0.000607	0.027056	0.000606	0.22732	0.001722	0.613109
	7.4	0.085042	0.084967	0.018302	0.084992	0.215323	0.069173	0.261263
F15	1.2	0.002603	0.00261	0.020101	0.002607	0.198306	0.004143	0.606369
	7.4	0.225137	0.225028	0.137994	0.225064	0.578931	0.201747	0.016748
F16	1.2	0.236267	0.23622	0.476657	0.236236	0.000313	0.22917	
	7.4	0.244211	0.244137	0.162504	0.244161	0.751205	0.229223	0.054831

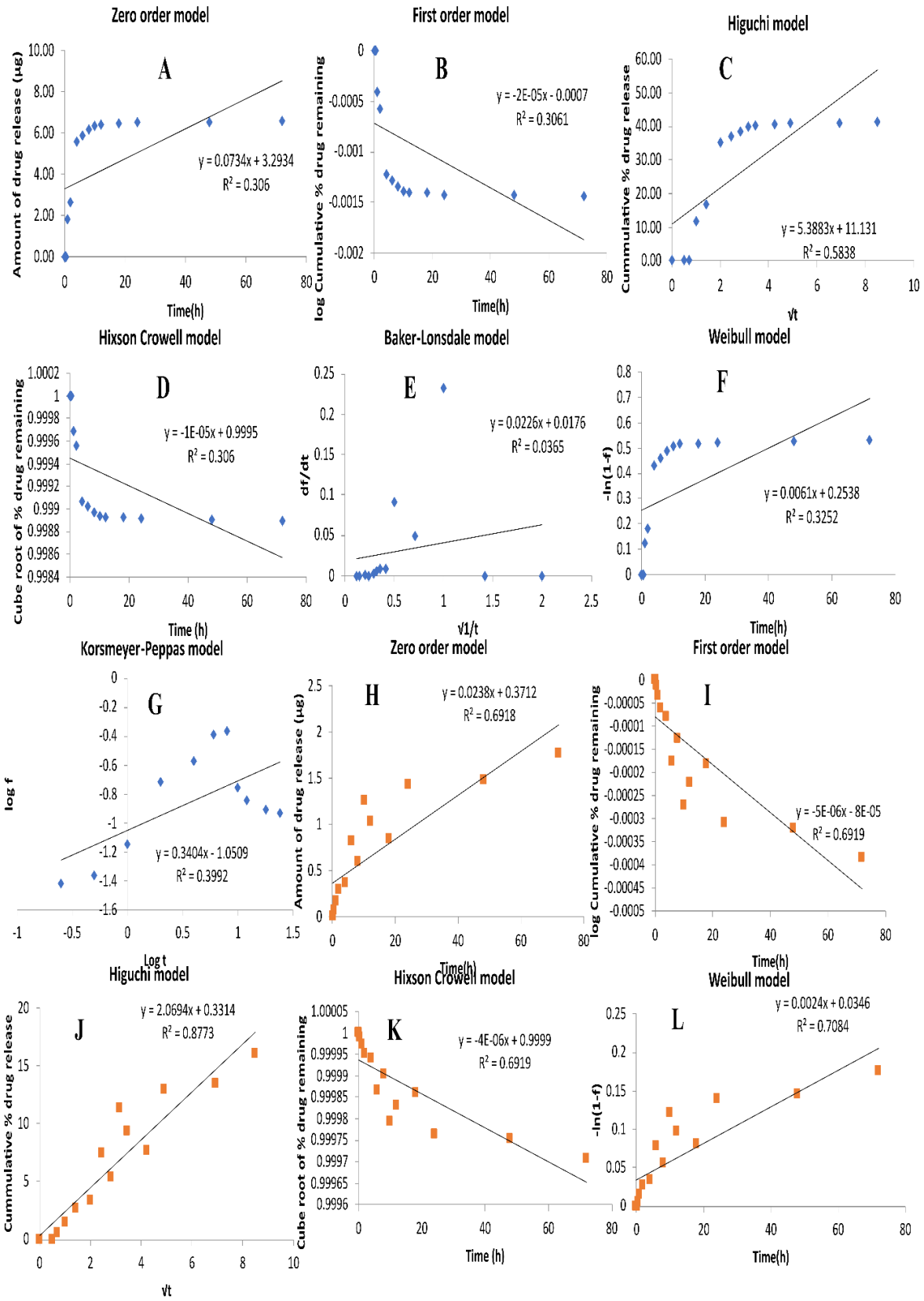

Figure 13: (A) to (F) represents F5 best fit Kinetic models at pH 1.2 while (G) Korsmeyer-peppas for F15 at pH 1.2 (H) to (L) denotes best fit kinetic model for F13. Blue color indicates RA while Red color indicates TR.

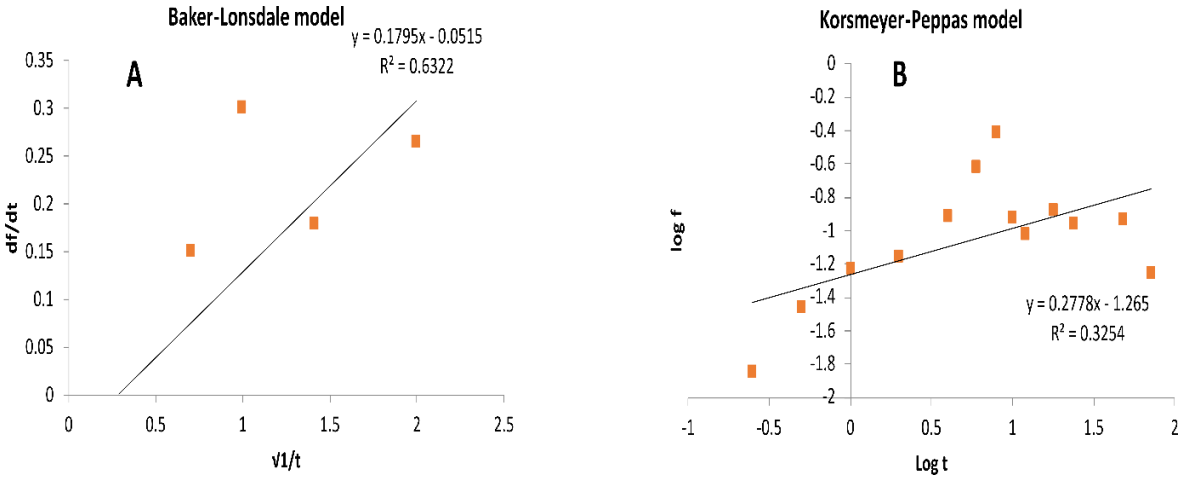

Figure 14: Represents the best kinetic model for (A) F9 and (B) F14 at Ph 1.2 for TR . Blue color indicates RA while Red color indicates TR.

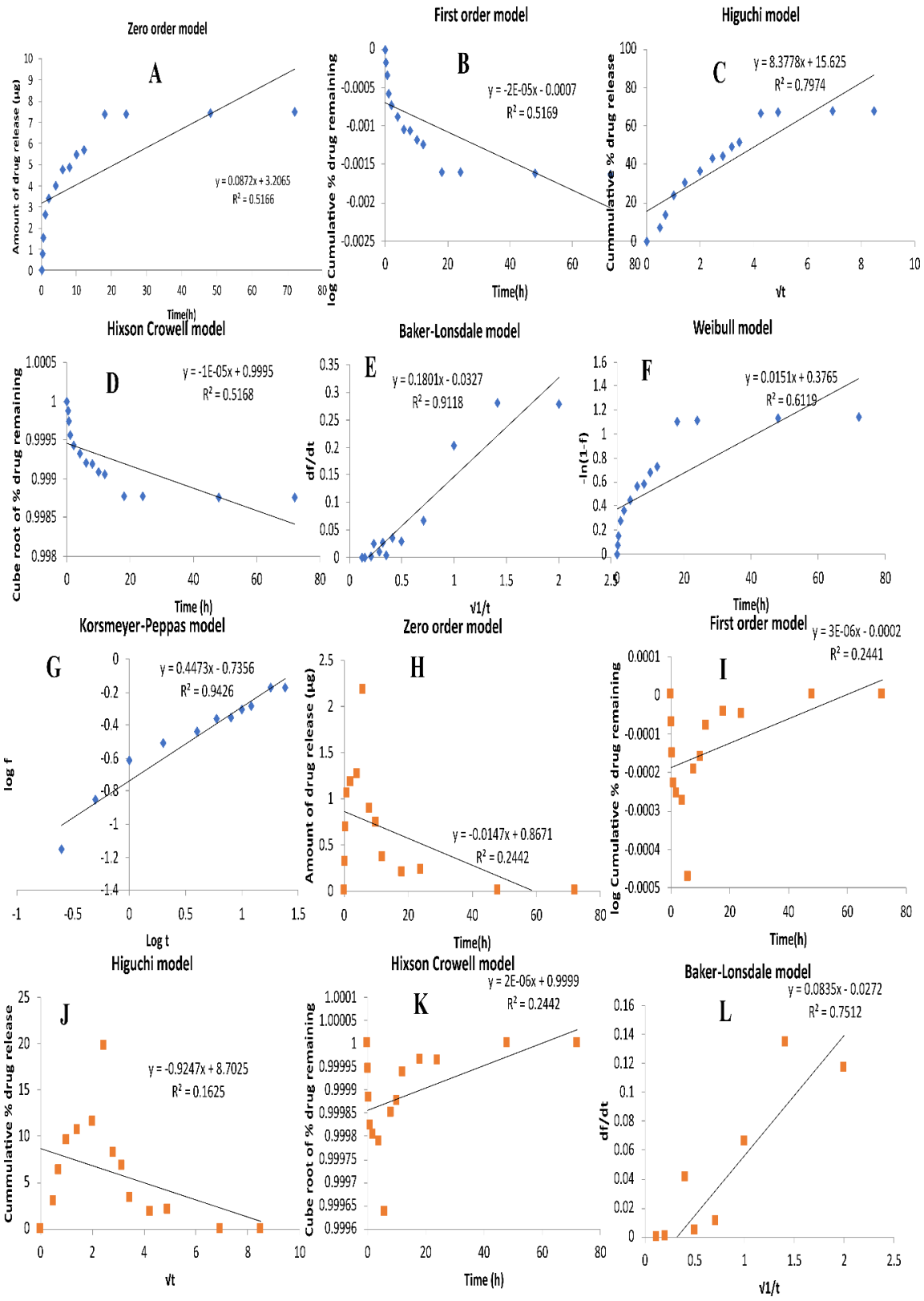

Figure 15: (A) to (G) represents F5 best fit Kinetic models at pH 7.4 while (H) to (L) for F16 at pH 7.4. Blue color indicates RA while Red color indicates TR.

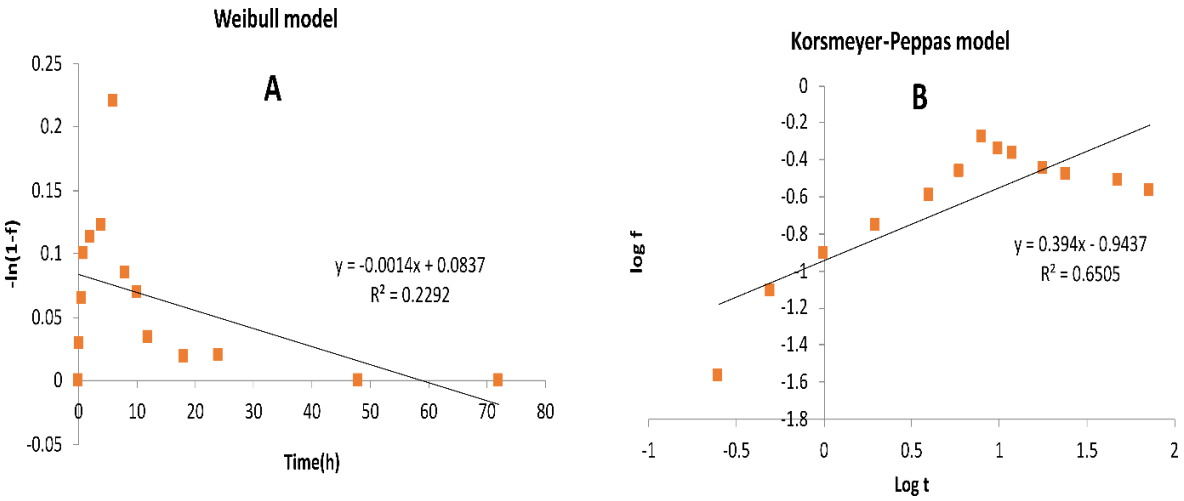

Figure 16: Represents the best kinetic model for (A) F16 and (B) F4 at Ph 7.4 for TR

4.0. Discussion

Drug carriers such as micelles, dendrimers, and microspheres are widely used for oral drug delivery, facilitating drug absorption in the intestinal epithelium through receptor-, paracellular-, carrier-, M cell-, or transcellular-mediated pathways. Conventional biodegradable and biocompatible carrier polymers include chitosan, alginate, PLA, and PGA, which are FDA-approved for human use. Additionally, these polymeric materials offer versatility in size, surface charge, and hydrophobicity, making them suitable for achieving controlled drug release [12,13]

Sodium alginate beads offer numerous pharmaceutical advantages. In this study, chitosan-coated, pH-sensitive alginate beads loaded with KGS was successfully developed,. These beads address therapeutic needs in managing chronic conditions like cardiovascular disorders by reducing plasma drug concentration fluctuations and potentially lowering the total drug dosage needed for clinical efficacy [14]

The chitosan–alginate beads optimized for colon-targeted release of Rosmarinic acid and Trehalose based on the response surface method with Box-Behnken design suggested 16 combinations of formulations where % EE was set as a response. The optimized alginate-chitosan-KGS beads were selected based on maximum % EE, where the equation for ROS and TR obtained by the Design Expert showed that the experiment followed a linear model (Figure/table). Both the equations showed a positive relation between %EE in terms of ROS / TR and X1 (alginate) and X2 (calcium chloride) while negative co-related with chitosan.

For every 1% increase in SA concentration, the % EE of ROS and TR is predicted to increase by 4.82197% and 3.83874%, respectively, when $CaCl_2$ and Chitosan are constant. Similarly, for every 1 % increase in $CaCl_2$ the %EE of ROS and TRE is expected to increase 0.859943% and 0.525974%, keeping SA and Chitosan concentration constant (Figure 2 and Figure 1). Interestingly, from the equation (i) and (ii), it is seen that for every 1% increase in Chitosan concentration, the % EE of ROS and TRE is predicted to decrease by 3.19092% and 2.43507%, respectively, keeping SA and $CaCl_2$ constant. This was also observed in our experiment, where an increase in the concentration of SA and $CaCl_2$ increased %EE i.e. F13 with a composition of SA-5% and $CaCl_2$ – 10%, though the chitosan concentration was moderate (0.75%). In the case of chitosan, the experimental data could not be related to the design expert prediction. The best-fit model predicted by Design expert for both responses was the Linear model (table) (Figure 2).

An optimized formulation of alginate-chitosan-KGS beads was selected using the point prediction method in Design Expert Software, guided by a desirability factor approaching 1. [15]. The formulation that was chosen consisted of 5.0% sodium alginate (X1), 10% $CaCl_2$ (X2), and 0.75% chitosan (X3). The experimentally obtained % EE (EE) in terms of ROS and TRE was 63.3% and 25.10%, respectively, while the predicted % EE for ROS and TRE was 64.99% and 24.22%, respectively. The dependent variables' predicted values were within the desired range. To validate the model, an experimental batch was prepared using the projected independent factors and characterized for the response variables. The close agreement between the predicted and experimentally obtained results confirms the rationality and reliability of the optimized bead formulation. F5, with bead size 1.73 ± 0.1814 mm, has an entrapment efficiency of 60.18%, and F13 (1.59 ± 0.4176 mm) has an entrapment efficiency of 63.30% in terms of ROS. Similarly, higher entrapment efficiency for Trehalose was noted in F13 with bead size 1.59 ± 0.4176 mm (Figure 4), with entrapment efficiency at 25.10% in terms of TR (Table 3). Smaller beads such as F8 (1.26 ± 0.1769 mm) have lower entrapment efficiency for Trehalose (9.65%). This trend is probably due to the fact that smaller beads have a higher surface area-to-volume ratio, which can lead to increased drug release rates and potentially lower entrapment efficiency (Figure 4). Smaller beads may have less polymer available to encapsulate the drug, leading to lower entrapment efficiency i.e., the higher the % SA, the higher the %EE (Table 3) [16].

The sharp peak at 3330 cm^{-1} indicates the presence of OH stretching vibrations in KGS, alginate, and chitosan, which aligns with the LC-qTOF-MS-based TIC data showing a sharp

peak between 1-2 minutes for polar compounds. The decrease in intensity of the OH stretching vibration at 3330 cm^{-1} in the SA-KGS sample suggests effective encapsulation of KGS in sodium alginate. The almost complete disappearance of this signal in the SA-KGS-Cn coated sample likely indicates a successful chitosan coating.

The peak at 3740 cm^{-1}, associated with hydroxyl groups not involved in hydrogen bonding, typically appears sharper at higher wavenumbers compared to hydrogen-bonded hydroxyl groups. This characteristic peak diminishes or shifts in the SA-KGS-Cn spectrum, suggesting the involvement of hydroxyl groups in hydrogen bonding or other intermolecular interactions between alginate and chitosan [17]

C-H stretching vibrations at 2923 cm^{-1} and 2860 cm^{-1}, observed in all samples, correspond to alkyl groups. The disappearance of these signals in the SA-KGS-Cn group can be attributed to the chitosan coating and potential interactions. The prominent peak around 1640 cm^{-1}, characteristic of the amide I band (C=O stretching) in chitosan, confirms the presence of the chitosan backbone. The peak at 1030 cm^{-1}, attributed to C-O-C stretching vibrations, likely represents the sugar rings of chitosan [18]. The band at 1550 cm^{-1} may indicate NH-stretching in amide, supporting the presence of chitosan in the sample [17]. The symmetrical carboxylate functional group stretching at 1600 cm^{-1} in alginate, with a narrower COO- bond at 1404 cm^{-1}, is indicative of its chemical structure. The increased intensity of the 1404 cm^{-1} signal in the sodium alginate-loaded KGS sample suggests interaction with the carboxylate group of alginates. The disappearance of this signal in the SA-KGS-Cn sample points to an interaction between alginate and chitosan. The broader and shifted peak around 1640 cm^{-1} in the SA-KGS-Cn spectrum, compared to individual spectra, suggests an interaction between the amide groups of chitosan and the carboxylate groups of alginates. Similarly, shifts or broadening in the peak around 1030 cm^{-1} indicate potential rearrangement of the polymer matrix due to interactions between alginate and chitosan [19]. The broad band observed at 3300 cm^{-1}, becoming more pronounced and shifting in the SA-KGS-Cn spectrum, is likely due to superimposed O-H and N-H stretching vibrations, indicating hydrogen bonding between the polymers. Overall, the FTIR spectrum suggests ionic interactions between the carboxylate ($-COO^-$) groups of alginates and the amino ($-NH_2$) groups of chitosan, resulting in the formation of a polyelectrolyte complex (PEC) (Figure 5) [20].

The initial weight loss of 16.90% and 10.57% in Alg and chitosan (Cn) powders between 30-200 °C, respectively, indicates moisture loss, which is typical for these biopolymers. At 300 °C, the significant 51.16% decrease in mass of Alg suggests the breakdown of the polymer backbone, which is comprised of mannuronic and glucuronic acids. Chitosan's higher weight loss of 58.67% between 300-400 °C is consistent with its known thermal properties, as previously reported [21]. For KGS, the initial weight loss up to 100°C (1.05%) corresponds to moisture evaporation. The significant mass loss stages from 30°C to 600°C, with only a 2% difference from 600°C to 800°C, and the decomposition of 15.21% at 200°C highlight the loss of physically and chemically bound water and volatile components. This aligns with [22], who reported similar findings in their thermal degradation studies of honey. The observed TG curve indicates two major mass loss stages: oxidative degradation and devolatilization of cellulose, hemicellulose, and lignin between 200-400°C, and char combustion between 400-600°C, corroborating the findings by [21]. The enhanced weight loss in chitosan powder around 250-330°C (48%) is attributed to its inherent thermal properties. For the beads, the three significant weight loss stages indicate different thermal behaviours. The initial stage (30°C-200°C) shows mass losses of 47.48% and 18.42% for alginate and Alg-chitosan beads, respectively, suggesting better encapsulation and moisture barrier properties of the chitosan-coated beads. This higher mass loss in Alg loaded with KGS reflects the joint loss of water from both KGS and alginate [23]. The subsequent stages (200-300°C and 300-800°C) involve the liberation of extra water molecules attached through polar interactions with carboxylate and amine groups of Alg and chitosan, and the decomposition of cyclic products resulting in CO2 release from polysaccharides.

The thermal stability of the beads improved due to the formation of polyelectrolyte complexes (PECs) facilitated by the bonding of alginate with calcium ions (Ca^{2+}) and the favourable interactions between oppositely charged biopolymers. This is reflected in the higher T50 values observed for alginate-chitosan (Alg/Cn) beads compared to plain alginate beads, highlighting the significant contribution of the chitosan coating to enhanced thermal stability. [24,25]

The changes in thermograms between beads and individual polymers provide evidence for ionic interactions leading to the formation of new structures (PECs) with distinct thermal properties. Overall, the produced alginate beads exhibit thermal stability at normal physiological temperatures, highlighting their potential use in drug delivery systems (Figure 6) [22]

The surface irregularities and brittle structure observed in the blank alginate beads, including cracks and folds, likely result from dehydration during preparation or the mechanical weakness of the alginate matrix [26]. These structural issues can impact encapsulation efficiency and the release profile of loaded materials [27]. The smoother surface observed in the KGS-loaded beads, with fewer visible cracks and particulate deposits, suggests that KGS loading improves surface compactness and slightly enhances structural integrity. However, it does not eliminate brittleness [28]. This indicates the need for further coating to achieve a controlled-release formulation [29]. The chitosan coating results in a significantly smoother and more uniform bead surface, effectively masking the cracks and irregularities seen in uncoated beads. This coating acts as a mechanical reinforcement, improving the beads' structural stability and making them suitable for applications requiring controlled release. The chitosan layer likely modulates diffusion and protects the core contents [30,31]. The properties observed in the SEM analysis align with previous studies [32], which highlight the beneficial effects of chitosan coating on structural stability and controlled release capabilities (Figure 7).

The swelling behaviour of sodium alginate beads coated with chitosan displays significant pH-dependent variation, influenced by the ionic interactions between the carboxylic groups of alginate and the amine groups of chitosan, forming a polyelectrolyte complex (PEC) layer. At acidic pH (1.2), minimal initial swelling occurs, probably due to the compactness of the PEC layer, which reduces fluid diffusion into the beads and prevents rapid bead erosion. However, within the first 0.25 hrs, rapid swelling is observed in specific formulations (e.g., F9 and F6), likely due to localized disruption of the compact layer, allowing moderate fluid penetration. Swelling peaks between 2 to 6 hrs (e.g., F14 at 343% by 6 hrs), followed by stabilization and gradual decline, reflecting the beads' ability to maintain structural integrity under acidic conditions while permitting slow hydration. A high swelling in F16 (520%) and F15 (470%) is probably due to protonation of the NH2 group of the chitosan, causing intermolecular repulsion. Further, the hydrophilic nature of chitosan allows it to absorb more water, causing more swelling. F5 showed less and controlled swelling in the acidic medium, probably due to protection offered by the PEC layer and lesser protonation of the amine and carboxylic group [5]. It is well known that higher SA concentration provides more sites for calcium binding, leading to a tighter network and thus less swelling, which can be correlated with higher SA concentration in F5 i.e. 5% (Figure 8A) [33]. In neutral conditions (pH 7.4), the beads exhibit pronounced swelling due to

enhanced penetration of the buffer medium and ion exchange dynamics. The calcium ion presents in the Alg- Ca^{2+} egg box structure has more affinity towards the phosphate ion present in the buffer than the Alg, likely causing its decoupling and also repulsion due to replaced phosphate ions. This may be the reason behind the observed rapid swelling in the early stages (e.g., F15 at 358% within 0.25 hrs). Swelling peaks significantly at 1–6 hrs (e.g., F8 at 3215% and F15 at 3096% by 6 hrs), highlighting the beads' responsiveness to pH changes. Despite this, the chitosan coating slows erosion and ensures controlled swelling over time, as seen in sustained swelling behaviour in formulations like F5 and F10. Except for F5 and F10, most of the formulations swelling decreased, probably due to a higher degree of Ca^{2+} uncoupling, leading to more significant erosion of the polymeric matrix. The compact PEC layer provided by the chitosan-alginate interaction is instrumental in modulating swelling across pH levels, offering a balance between preventing rapid dissolution and allowing pH-responsive swelling (Figure 8B) [5]

The % cumulative Release of RA from F5 at pH 7.4 showed gradual and ultimately high cumulative release over time with Korsmeyer-Peppas (r^2=0.942622) best fit suggesting a simple diffusion (n<0.5) oriented. The strong fit to Korsmeyer-Peppas aligns with the prolonged, controlled release observed, indicating Fickian transport at pH 7.4 (Figure 11). For RA release At pH 1.2, Higuchi model fits the best r^2 (0.585) in F5, indicating Fickian diffusion controlled release. This shift from Higuchi kinetics at pH 1.2 (Figure 9) to Korsmeyer-Peppas at pH 7.4 (Figure 11) for the same formulation indicates pH-dependent changes in the release mechanism. In an acidic environment, the polymer matrix of F5 may swell less, leading to a diffusion-controlled release primarily governed by the concentration gradient (Higuchi model) while in the neutral environment (pH 7.4), the polymer matrix, especially chitosan, tends to swell more due to its pH-sensitive nature. This swelling can facilitate the diffusion of drug molecules but also introduces slight changes in the polymer matrix's physical properties, fitting well with the Korsmeyer-Peppas model (Figure 8B).

For RA in F1 at pH 1.2 and 7.4, (figure 9 and 11) a high % cumulative release showed a very high release (46.81% at 1 hour). Such a quick burst is often poorly fit by standard kinetic models. Indeed, all r^2 values are low (mostly <0.2), indicating none of the classical models describe this immediate release phase well. This suggests that the release mechanism may be accompanied by immediate surface drug dissolution or imperfect matrix formation rather than a controlled diffusion or erosion process.

The % cumulative of TRE from F13 at Ph 1.2 showed Higuchi model ($r^2 = 0.877341$) as the best fit. When swelling is minimal, the polymer matrix remains relatively intact and less porous. This means that the drug molecules have a more consistent and predictable path to diffuse through the matrix without significant changes in the polymer's structure. In this case, the Higuchi model, which describes drug release from F13 as a diffusion-controlled process (proportional to the square root of time), fits well in conditions where the polymer matrix does not undergo extensive swelling or erosion. For TRE release at pH 7.4, F16 showed the best fit for Baker Lonsdale model (r^2=0.751205), which indicates that the release from F16 is primarily diffusion-controlled through a spherical matrix. TRE released from F4 at pH 7.4 showed Korsmeyer-Peppas (r^2 0.8522) is observed to be higher than other models showing a Fickian diffusion (n<0.5). Interestingly, both the release of TRE from F4 at pH 7.4 (r^2=0.85223) and RA from F15 at pH 1.2 (r^2=0.399228) showed Korsmeyer Peppas as the best-fit model, indicating Fickian diffusion, facilitated by significant swelling enhancing matrix porosity (Figure 9-16).

5.0. Conclusion: This study successfully developed and optimized chitosan-coated, pH-sensitive alginate beads encapsulating Khamira Gaozaban Sada (KGS), a traditional Unani polyherbal preparation, to enhance the % Encapsulation efficiency. A stable and controlled release formulation was developed, releasing KGS in terms of RA and TRE. Using a Box-Behnken design, 16 formulations were analyzed, and F13 (5% sodium alginate, 10% $CaCl_2$, and 0.75% chitosan) emerged as the optimal formulation with high entrapment efficiencies of 63.3% (RA) and 25.1% (TRE). The linear model predicted by the design software was validated, demonstrating close agreement between predicted and experimental values and confirming the reliability of the optimization process. Further, with an increase in Sodium alginate % EE increased. FTIR and TGA analyses confirmed successful encapsulation and chitosan coating, showing strong ionic interactions between alginate and chitosan, which enhanced thermal stability and structural integrity. SEM studies revealed that the chitosan coating effectively reduced surface irregularities and improved bead uniformity, resulting in enhanced mechanical stability and controlled release profiles. Swelling studies demonstrated significant pH sensitivity, with limited swelling under acidic conditions (pH 1.2) due to the compact polyelectrolyte complex (PEC) layer. The pronounced swelling under neutral conditions (pH 7.4), attributed to ion exchange and matrix erosion dynamics. These behaviours highlight the beads' suitability for colon-targeted drug delivery. The release profiles exhibited controlled and prolonged drug release, with F5 and F13 showing

optimal performance across pH conditions. The release mechanisms were predominantly diffusion-controlled, with Korsmeyer-Peppas and Higuchi models providing the best fits at pH 7.4 and pH 1.2, respectively, depending on the formulation. F5 demonstrated exceptional release characteristics, achieving high cumulative release percentages for both RA and TRE, emphasizing its potential for Controlled drug delivery. The optimized alginate-chitosan beads successfully addressed the challenges of pH sensitivity and controlled release, showcasing their potential as a robust delivery system for bioactive compounds in the treatment of cardiovascular disorders.

References:

[1] Baranwal, J.; Barse, B.; Fais, A.; Delogu, G.L.; Kumar, A. Biopolymer: A Sustainable Material for Food and Medical Applications. **Polymers 2022**, *14*, 983. https://doi.org/10.3390/polym14050983

[2] Hua, S. Advances in Oral Drug Delivery for Regional Targeting in the Gastrointestinal Tract—Influence of Physiological, Pathophysiological and Pharmaceutical Factors. **Front. Pharmacol. 2020**, *11*, 524. https://doi.org/10.3389/fphar.2020.00524.

[3] Tennakoon, P.; Chandika, P.; Yi, M.; Jung, W.K. Marine-Derived Biopolymers as Potential Bioplastics, an Eco-Friendly Alternative. **iScience 2023**, *26*, 106404. https://doi.org/10.1016/j.isci.2023.106404.

[4] Abourehab, M.A.S.; Rajendran, R.R.; Singh, A.; Pramanik, S.; Shrivastav, P.; Ansari, M.J.; Manne, R.; Amaral, L.S.; Deepak, A. Alginate as a Promising Biopolymer in Drug Delivery and Wound Healing: A Review of the State-of-the-Art. **Int. J. Mol. Sci. 2022**, *23*, 9035. https://doi.org/10.3390/ijms23169035.

[5] Sun, X.; Liu, C.; Omer, A.M.; Yang, L.Y.; Ouyang, X.K. Dual-Layered pH-Sensitive Alginate/Chitosan/Kappa-Carrageenan Microbeads for Colon-Targeted Release of 5-Fluorouracil. **Int. J. Biol. Macromol. 2019**, *132*, 487–494. https://doi.org/10.1016/j.ijbiomac.2019.03.225.

[6] Jiménez-Gómez, C.P.; Cecilia, J.A. Chitosan: A Natural Biopolymer with a Wide and Varied Range of Applications. **Molecules 2020**, *25*(17), 3981. https://doi.org/10.3390/molecules25173981.

[7] Rajinikanth, B.S.; Rajkumar, D.S.R.; K., K.; Vijayaragavan, V. Chitosan-Based Biomaterial in Wound Healing: A Review. **Cureus 2024**, *16*(2), e55193. https://doi.org/10.7759/cureus.55193.

[8] Gåserød, O.; Smidsrød, O.; Skjåk-Braek, G. Microcapsules of Alginate–Chitosan. I. A Quantitative Study of the Interaction Between Alginate and Chitosan. **Biomaterials 1998**, *19*, 1815–1825. https://doi.org/10.1016/S0142-9612(98)00060-X.

[9] Tran, D.H.; Wang, Z.V. Glucose Metabolism in Cardiac Hypertrophy and Heart Failure. **J. Am. Heart Assoc. 2019**, *8*, e012673. https://doi.org/10.1161/JAHA.119.012673.

[10] Deshmukh, R.K.; Naik, J.B. Diclofenac Sodium-Loaded Eudragit® Microspheres: Optimization Using Statistical Experimental Design. **J. Pharm. Innov. 2013**, *8*, 276–287.

[11] Lertsarawut, P.; Laksee, S.; Rattanawongwiboon, T.; Hemvichian, K. Eco-Friendly Alginate-Starch-Based Water Super-Absorbent Beads Spherically Shaped and Uniformly Fabricated via Spherification and Radiation-Assisted Polymerization. **Carbohydr. Polym. Technol. Appl. 2024**, *7*, 100456. https://doi.org/10.1016/j.carpta.2024.100456.

[12] Agrawal, U.; Sharma, R.; Gupta, M.; Vyas, S. P. Is Nanotechnology a Boon for Oral Drug Delivery? **Drug Discov. Today 2014**, *19*, 1530–1546.

[13] Pridgen, E. M.; Alexis, F.; Farokhzad, O. C. Polymeric Nanoparticle Technologies for Oral Drug Delivery. **Clin. Gastroenterol. Hepatol. 2014**, *12*, 1605–1610.

[14] Katz, B.; Rosenberg, A.; Frishman, W. H. Controlled-Release Drug Delivery Systems in Cardiovascular Medicine. **Am. Heart J. 1995**, *129*, 359–368. https://doi.org/10.1016/0002-8703(95)90019-5.

[15] Verma, A.; Sharma, G.; Jain, A.; Tiwari, A.; Saraf, S.; Panda, P. K.; Katare, O. P.; Jain, S. K. Systematic Optimization of Cationic Surface Engineered Mucoadhesive Vesicles Employing Design of Experiment (DoE): A Preclinical Investigation. **Int. J. Biol. Macromol. 2019**, *133*, 1142–1155. https://doi.org/10.1016/j.ijbiomac.2019.04.118.

[16] Bansal, A. K.; Pande, V. Development and Evaluation of Dual Cross-Linked Pulsatile Beads for Chronotherapy of Rheumatoid Arthritis. **J. Pharm. (Cairo) 2013**, *2013*, 906178. https://doi.org/10.1155/2013/906178. Epub 2012 Dec 9. PMID: 26556001; PMCID: PMC4595973.

[17] Cheng, J.; Zhu, H.; Huang, J.; Zhao, J.; Yan, B.; Ma, S.; Zhang, H.; Fan, D. The Physicochemical Properties of Chitosan Prepared by Microwave Heating. *Foods* **2020**, *8*, 1486. https://doi.org/10.1002/fsn3.1486.

[18] Sakugawa, K.; Ikeda, A.; Takemura, A.; Ono, H. Simplified Method for Estimation of Composition of Alginates by FTIR. *J. Appl. Polym. Sci.* **2004**, *93*, 1372–1377. https://doi.org/10.1002/app.20785.

[19] Maniar, V.; Kalsara, K.; Upadhyay, U. A Review of FTIR: An Useful Instrument. *Sigma Inst. Pharm.*, **2023**.

[20] Bhokare, S. S.; Biradar, V. R.; Chakole, R. D.; Charde, M. S. Applications of FTIR Spectroscopy: Review. *Int. J. Sci. Dev. Res.* **2022**, *7*, 213-219.

[21] Wongsiriamnuay, T.; Tippayawong, N. Thermogravimetric Analysis of Giant Sensitive Plants under Air Atmosphere. *Bioresour. Technol.* **2010**, *101*, 9314-9320. https://doi.org/10.1016/j.biortech.2010.06.141

[22] Silva, I. A. A.; Souza, A. L.; Cordeiro, A. M. T. M.; Soledade, L. E. B.; Queiroz, N.; Souza, A. G. Thermal Degradation of Honeys and Evaluation of Physicochemical Properties. *J. Therm. Anal. Calorim.* **2013**, *114*, 353–358. https://doi.org/10.1007/s10973-012-2926-x.

[23] Yu, C.Y.; Zhang, X.C.; Zhou, F.Z.; Zhang, X.Z.; Cheng, S.X.; Zhuo, R.X. Sustained Release of Antineoplastic Drugs from Chitosan-Reinforced Alginate Microparticle Drug Delivery Systems. *Int. J. Pharm.* **2008**, *357*, 15-21.

[24] Mohy Eldin, M.S.; Omer, A.M.; Wassel, M.A.; Tamer, T.M.; Ibrahim, S.A. Novel Smart pH-Sensitive Chitosan Grafted Alginate Hydrogel Microcapsules for Oral Protein Delivery: I. Preparation and Characterization. *Int. J. Pharm. Pharm. Sci.* **2015**, *7*, 320-326.

[25] Č, B.; Milić, J.; Cekić, N.; Krajišnik, D.; Daniels, R.; Savić, S. Chitosan Oligosaccharide as Prospective Cross-Linking Agent for Naproxen-Loaded Ca-Alginate Microparticles with Improved pH Sensitivity. *Drug Dev. Ind. Pharm.* **2013**, *39*, 77-87.

[26] Chan, E.S.; Lim, T.K.; Voo, W.P.; Pogaku, R.; Tey, B.T.; Zhang, Z. Effect of Formulation of Alginate Beads on Their Mechanical Behavior and Stiffness. *Particuology* **2011**, *9*, 228-234. https://doi.org/10.1016/j.partic.2010.12.002.

[27] Yang, L.; Kong, M.; Chao, F.; Liu, W. F.; Liu, Y.; Cheng, X. J.; Chen, X. G. Preparation and Property of Layer-by-Layer Alginate Hydrogel Beads Based on Multi-Phase Emulsion Technique. *J. Sol-Gel Sci. Technol.* **2012**, *62*, 217–226. https://doi.org/10.1007/s10971-012-2712-z.

[28] Ismail, F.; El Fadl, A.; Abou Taleb, M.F. Effect of Structurally Different Magnetic Alginate Nanocomposite Beads on Fenton-Like Oxidation of Direct Dyes. *J. Inorg. Organomet. Polym.* **2024**, https://doi.org/10.1007/s10904-024-03445-1.

[29] Bedade, D.K.; Sutar, Y.B.; Singhal, R.S. Chitosan Coated Calcium Alginate Beads for Covalent Immobilization of Acrylamidase: Process Parameters and Removal of Acrylamide from Coffee. *Food Chem.* **2019**, *275*, 95-104. https://doi.org/10.1016/j.foodchem.2018.09.090.

[30] Mansfield, J.; Eiselt, P.; Yeh, J.; Mooney, D.J. Environmental SEM Study of Sodium Alginate Beads. *Microsc. Microanal.* **1999**, *5*(S2), 300-301. https://doi.org/10.1017/S1431927600014823.

[31] Bhia, M.; Motallebi, M.; Abadi, B.; Zarepour, A.; Pereira-Silva, M.; Saremnejad, F.; Santos, A.C.; Zarrabi, A.; Melero, A.; Jafari, S.M.; Shakibaei, M. Naringenin Nano-Delivery Systems and Their Therapeutic Applications. *Pharmaceutics* **2021**, *13*(2), 291. https://doi.org/10.3390/pharmaceutics13020291.

[32] Moura-Alves, M.; Souza, V.G.L.; Silva, J.A.; Esteves, A.; Pastrana, L.M.; Saraiva, C.; Cerqueira, M.A. Characterization of Sodium Alginate-Based Films Blended with Olive Leaf and Laurel Leaf Extracts Obtained by Ultrasound-Assisted Technology. *Foods* **2023**, *12*(22), 4076. https://doi.org/10.3390/foods12224076.

[33] Kowalski, G.; Witczak, M.; Kuterasiński, Ł. Structure Effects on Swelling Properties of Hydrogels Based on Sodium Alginate and Acrylic Polymers. *Molecules* **2024**, *29*, 1937. https://doi.org/10.3390/molecules29091937.

CONCLUSION

Conclusion:

In the initial studies, several polyherbal Unani preparations were screened for their antihypertensive potential in an L-NAME-induced hypertension model. Among these, Dawa-ul-Motadil Misk showed significant blood pressure-lowering effects, while KGS yielded non-significantly increased SBP suggestive of a central sympathomimetic activity. Moreover, sensitive LC-MS/MS methods were successfully developed and validated to quantify adrenaline, noradrenaline, aldosterone, and ANP, in rat plasma. The robust analytical techniques were instrumental in accurately assessing plasma biomarker levels across various experimental animal groups.

Further, KGS's exhibited cardioprotective action, in mitigating doxorubicin-induced cardiac hypertrophy. KGS significantly improved systolic blood pressure, ECG parameters mitochondrial protein and oxidative stress marker in vivo. KGS, particularly the high-dose exhibited enhanced efficacy, indicating a dose-dependent therapeutic benefit. Metabolite profiling using LC-qTOF-MS revealed important 30 tentative bioactive metabolites, including Rosmarinic acid, Trehalose in negative mode. RA and TR were quantified at 0.110 ± 0.017 and 0.077 ± 0.005 mg/g of KGS, respectively using LC-MS/MS. The ACE activity was further supported by molecular docking against ACE that highlighted potential ACE inhibition and antioxidant mechanisms. However, lowering of systolic blood pressure and increased plasma ACE could not be co-related. Probably, KGS increased the SBP through other pathways independent of ACE.

Furthermore, KGS effectively reduced cardiac workload in both L-NAME-induced hypertension and isoproterenol-induced cardiac hypertrophy animal models. Improved cardiac parameters measured through ECHO studies and histopathological findings, reduced oxidative stress, and decreased cardiac fibrosis together pointed toward KGS's holistic therapeutic potential. Moreover, in vitro studies on H9C2 cells confirmed its cytoprotective effects against isoproterenol as well as its role in reducing intracellular calcium indicating it may alleviate isoproterenol induced cardiac hypertrophy through Ang-II (in vivo) and modulation of intracellular calcium (in vitro/ H9C2 cells). Its CYP450 enzyme inhibition assay indicated its low potential to cause drug-drug interactions. LC-qTOF-MS analysis revealed 19 tentative metabolites in positive mode which were docked against eNOS and β1 adrenergic receptor where Tiliroside and Trehalose respectively showed the best docking score.

Finally, to overcome challenges related to the gastrointestinal stability and bioavailability of KGS, a chitosan-coated alginate bead formulation was successfully optimized via a Box-Behnken design. This approach significantly enhanced the encapsulation efficiency, stability, and controlled release profile of Rosmarinic acid and Trehalose, making it promising for colonic delivery. This research paves the way for translational studies and evidence based clinical use of these traditional, cost-effective medication for managing hypertension and cardiac hypertrophy.

Animal Ethics Committee Approval Letters

TAAB BIOSTUDY SERVICES
69, IBRAHIMPUR ROAD, FLAT NO. 1A, JADAVPUR, KOLKATA-700 032, INDIA
Mobile : 098300 36297 / 9836434884 / 8918165004, E-mail : taab_bio@yahoo.com
Website : www.taabbiostudyservices.com

Institutional Animal Ethics Committee
TAAB BIOSTUDY SERVICES
69, IBRAHIMPUR ROAD, FLAT 1A,
JADAVPUR, KOLKATA – 700032

INSTITUTIONAL ANIMAL ETHICS COMMITTEE
TAAB Biostudy Services, 69 Ibrahimpur Road, Jadavpur, Kolkata – 700 032

The members of the **Institutional Animal Ethics Committee (IAEC)** held on 28.09.2020,have scrutinized the various aspects of the protocols for carrying out the Research Project Submitted by the Principal Investigator, Prof Sanmoy Karmakar, In-charge Bioequivalence Study Center, Jadavpur University Kolkata-32, which has been received and recommended by the **Central Council for Research in Unani Medicine, Ministry of AYUSH, Govt of India** under "Expression of Interest Scheme for Study in collaborative mode" for carrying out the following study on Wister **Rats & Swiss albino Mice** and have approved the same to be performed at the Animal House of TAAB Biostudy Services, Kolkata – 700 032.

Study Title: **"Pharmacological studies on the probable mechanism of action of Khamira Gaozaban Sada (KGS) in the management of Hypertension, Involving Quality Control and Formulation optimization Studies for this age old Unani Preparation"**

28/09/2020
Prof Dr. T. K. Pal
Chairperson, Institutional Animal Ethics Committee
Registration No. 1938/PO/Re/S/17/CPCSEA

TAAB BIOSTUDY SERVICES Kolkata-700032

যাদবপুর বিশ্ববিদ্যালয়
কলকাতা-৭০০০৩২, ভারত

*JADAVPUR UNIVERSITY
KOLKATA-700 032, INDIA

FACULTY OF ENGINEERING & TECHNOLOGY
DEPARTMENT OF PHARMACEUTICAL TECHNOLOGY

Certificate

This is to certify that the project proposal no. **JU/IAEC-22/20** entitled **"Evaluation of cardioprotective effect of 2 Unani formulations"**, submitted by **Md. Adil Shaharyar** has been approved/recommended by the IAEC of Department of Pharmaceutical Technology, Jadavpur University, in its meeting held on 01.06.2022 and 30 Wistar Rats. (Number and Species of animals) have been sanctioned under this proposal for a duration of next .....12..... months.

Authorized by	Name	Signature	Date
Chairman	Prof. Sanmoy Karmakar	Sanmoy Karmakar	01/6/22
Member Secretary	Prof. Pallab Kanti Haldar	P. Haldar	01/6/2022
Main nominee of CPCSEA	Dr. Sankar Maiti	Sankar Maiti	01-06-2022

* Established on and from 24th December, 1955 vide Notification No.10986-Edn/IU-42/55 dated 6th December, 1955 under JadavpurUniversity Act, 1955 (West Bengal Act XXIII of 1955) followed by Jadavpur University Act,1981 (West Bengal Act XXIV of 1981)

Website :www.jadavpur.edu
Telephone :+91-33-2457-2274
E-mail :hodpharmacy@jadavpuruniversity.in

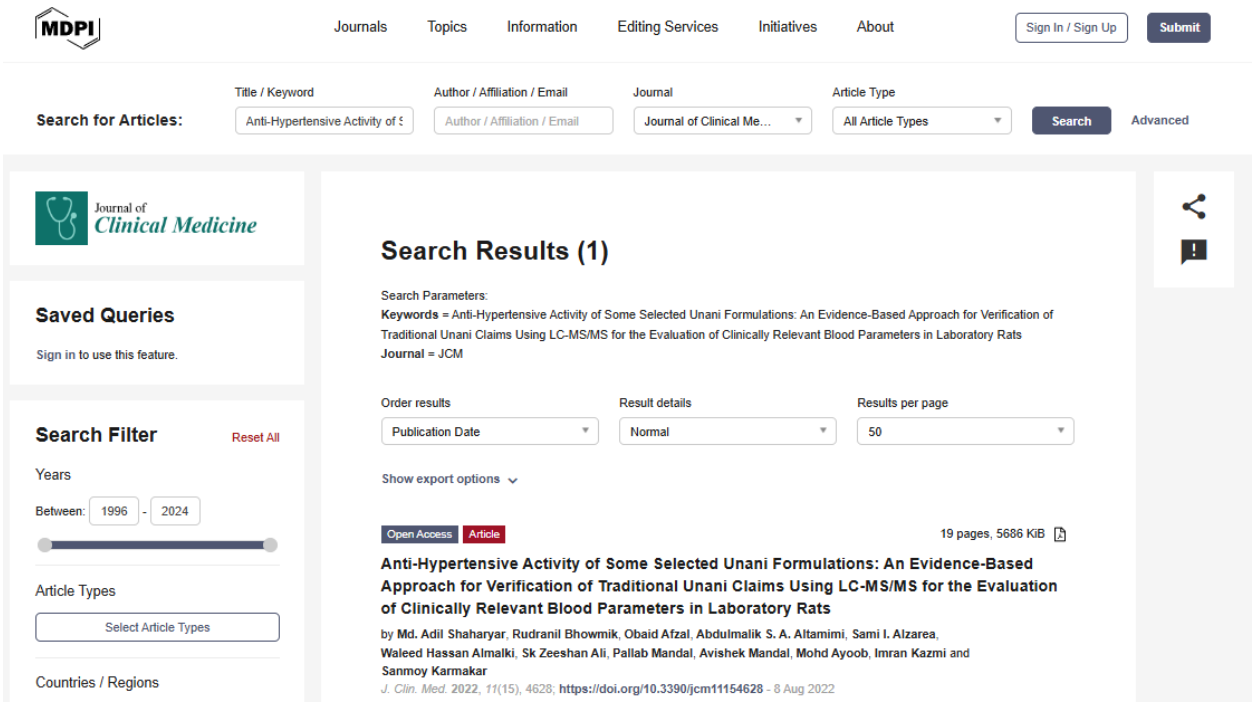
MDPI
Journals
Topics
Information
Editing Services
Initiatives
About
Sign In / Sign Up
Submit
Search for Articles:
Title / Keyword
Anti-Hypertensive Activity of S
Author / Affiliation / Email
Author / Affiliation / Email
Journal
Journal of Clinical Me...
Article Type
All Article Types
Search
Advanced
Journal of Clinical Medicine
Saved Queries
Sign in to use this feature.
Search Filter
Reset All
Years
Between: 1996 - 2024
Article Types
Select Article Types
Countries / Regions
Search Results (1)
Search Parameters:
Keywords = Anti-Hypertensive Activity of Some Selected Unani Formulations: An Evidence-Based Approach for Verification of Traditional Unani Claims Using LC-MS/MS for the Evaluation of Clinically Relevant Blood Parameters in Laboratory Rats
Journal = JCM
Order results
Publication Date
Result details
Normal
Results per page
50
Show export options
Open Access
Article
19 pages, 5686 KiB
Anti-Hypertensive Activity of Some Selected Unani Formulations: An Evidence-Based Approach for Verification of Traditional Unani Claims Using LC-MS/MS for the Evaluation of Clinically Relevant Blood Parameters in Laboratory Rats
by Md. Adil Shaharyar, Rudranil Bhowmik, Obaid Afzal, Abdulmalik S. A. Altamimi, Sami I. Alzarea, Waleed Hassan Almalki, Sk Zeeshan Ali, Pallab Mandal, Avishek Mandal, Mohd Ayoob, Imran Kazmi and Sanmoy Karmakar
J. Clin. Med. 2022, 11(15), 4628; https://doi.org/10.3390/jcm11154628 - 8 Aug 2022

Journal of
Clinical Medicine

MDPI

Article

Anti-Hypertensive Activity of Some Selected Unani Formulations: An Evidence-Based Approach for Verification of Traditional Unani Claims Using LC-MS/MS for the Evaluation of Clinically Relevant Blood Parameters in Laboratory Rats

Md. Adil Shaharyar [1], Rudranil Bhowmik [1], Obaid Afzal [2], Abdulmalik S. A. Altamimi [2], Sami I. Alzarea [3], Waleed Hassan Almalki [4], Sk Zeeshan Ali [1], Pallab Mandal [1], Avishek Mandal [1], Mohd Ayoob [5], Imran Kazmi [6,*] and Sanmoy Karmakar [1,*]

[1] Bioequivalence Study Centre, Department of Pharmaceutical Technology, Jadavpur University, Kolkata 700032, West Bengal, India
[2] Department of Pharmaceutical Chemistry, College of Pharmacy, Prince Sattam Bin Abdulaziz University, Al-Kharj 11942, Riyadh, Saudi Arabia
[3] Department of Pharmacology, College of Pharmacy, Jouf University, Sakaka 72341, Al-Jouf, Saudi Arabia
[4] Department of Pharmacology, College of Pharmacy, Umm Al-Qura University, Makkah 21955, Makkah, Saudi Arabia
[5] The Calcutta Unani Medical College and Hospital, 8/1, Abdul Halim Lane, Kolkata 700016, West Bengal, India
[6] Department of Biochemistry, Faculty of Science, King Abdulaziz University, Jeddah 21589, Makkah, Saudi Arabia
* Correspondence: ikazmi@kau.edu.sa (I.K.); sanmoykarmakar@gmail.com (S.K.); Tel.: +966-543970731 (I.K.); +91-8017136385 (S.K.)

check for updates

Citation: Shaharyar, M.A.; Bhowmik, R.; Afzal, O.; Altamimi, A.S.A.; Alzarea, S.I.; Almalki, W.H.; Ali, S.Z.; Mandal, P.; Mandal, A.; Ayoob, M.; et al. Anti-Hypertensive Activity of Some Selected Unani Formulations: An Evidence-Based Approach for Verification of Traditional Unani Claims Using LC-MS/MS for the Evaluation of Clinically Relevant Blood Parameters in Laboratory Rats. *J. Clin. Med.* **2022**, *11*, 4628. https://doi.org/10.3390/jcm11154628

Academic Editors: Nandu Goswami and Graziamaria Corbi

Received: 6 July 2022
Accepted: 4 August 2022
Published: 8 August 2022

Publisher's Note: MDPI stays neutral with regard to jurisdictional claims in published maps and institutional affiliations.

Abstract: Background: Systemic arterial hypertension, which is associated with an increased risk of cardiovascular disease(CVD), is the most significant modifiable risk factor for mortality and morbidity worldwide. WHO has recognized Unanipathy as an alternate system of medicine. The aim of the present study is to investigate the anti-hypertensive activity of some selected unani formulations using L-NAME model. **Method:** Group I or hypertensive control group: L-NAME administered for 7 days and left for the next 7 days; Group II or KASgroup: L-NAME administered (i.p) for 7 days and L-NAME + KAS (1000 mg/kg b.w) for the next 7 days; Group III or DMM group: L-NAME administered (i.p) for 7 days and L-NAME + DMM (2000 mg/kg b.w) for the next 7 days; Group IV or MSR group: L-NAME administered (i.p) for 7 days and L-NAME + MSR (300 mg/kg b.w) for the next 7 days; Group V or HJ group: L-NAME administered (i.p) for 7 days and L-NAME + HJ (113 mg/kg b.w) for the next 7 days; Group VI or KGS group: L-NAME administered (i.p) for 7 days and L-NAME +KGS (2000 mg/kg b.w) for the next 7 days. Non-invasive systolic blood pressure and RR-interval (ECG) was measured. Plasma was investigated forsodium, potassium, nitrite, ANP, adrenaline, noradrenaline and aldosterone on day 0, 7 and 14 using LC-MS/MS. **Result:** Treatment showed a non-significant lowreduction in SBP (systolic blood pressure) of KAS, MSR and HJ while that of DMM was quite significant ($p < 0.05$), but in the case of KGS, SBP increased. DMM on day 14 significantly ($p < 0.05$) reduced plasma nitrite while no significant plasma Na+ was noted. In the case of both DMM and KGS, potassium increased significantly ($p < 0.05$) on day 14. No significant changes in plasma ANP and aldosterone was observed against DMM and KGS while blood levels of adrenaline and noradrenaline significantly ($p < 0.05$) changed. No significant change in body weight was found. **Conclusions:** L-NAME KAS, MSR and HJ showed no change in SBP while DMM showed a significant reduction in SBP with decreased plasma nitrite. Probably, DMM may have anti-hypertensive activity mediated through NO inhibition while KGS may involve central sympathomimetic action.

Keywords: systolic blood pressure; unani system; adrenaline; ECG; noradrenaline

International Conferences attended

PPM

SFEC 2020 7th International Congress of Society for Ethnopharmacology, India

Theme: Ethnopharmacology in development of Scientifically Validated Quality Products from Medicinal Plants & Regulatory Aspects

Organized by : Bioactive Natural Product Laboratory (BNPL), School of Pharmaceutical Education and Research, Jamia Hamdard

In Association with : Society for Ethnopharmacology, India

Certificate of Presentation

presented to

Md. Shaharyar

For Contribution in the Scientific programme (POSTER) of SFEC 2020 held at Convention Centre, Jamia Hamdard, New Delhi, India on 15-17th February, 2020

Title: Pharmacological studies on mechanism of action of Khamira Gaozaban Sada (KGS) in the management of Hypertension, involving Quality Control and formulation optimization studies for this age old Unani preparation

Prof. Pulok K. Mukherjee
Secretary, Society for Ethnopharmacology

Prof. Ahmed Kamal
Organizing Chairman

Dr. Sayeed Ahmad
Organizing Secretary

JSS ACADEMY OF HIGHER EDUCATION & RESEARCH (DEEMED TO BE UNIVERSITY) MYSURU

International Society for Ethnopharmacology

Azadi Ka Amrit Mahotsav

9th SFEC 2022

22nd to 24th April 2022

International Congress of SOCIETY FOR ETHNOPHARMACOLOGY, INDIA

(Globalizing Local Knowledge and Localizing Global Technologies)

Theme : Redefining Ethnopharmacology for the Global Health and Wellbeing

Certificate of Participation

This is to certify that Prof./Dr./Mr./Ms. MD Adil Shaharyar

has Presented a PAPER in ORAL/POSTER SESSION in the 9th International Congress of the Society for Ethnopharmacology, India (SFEC-2022) held at JSS College of Pharmacy, JSS Academy of Higher Education & Research, Mysuru, Karnataka, India from 22nd to 24th, April 2022.

Title of presentation: Khamira Gaozaban Sada (KGS), whether anti-hypertensive or else - A critical analysis involving dissonance between plasma biomarker and blood pressure in rats.

Dr. T.M. Pramod Kumar	Dr. K. Mruthunjaya	Mr. Birendra K. Sarkar
Organizing Chairman, SFEC - 2022	Organizing Secretary, SFEC - 2022	President - SFE - India

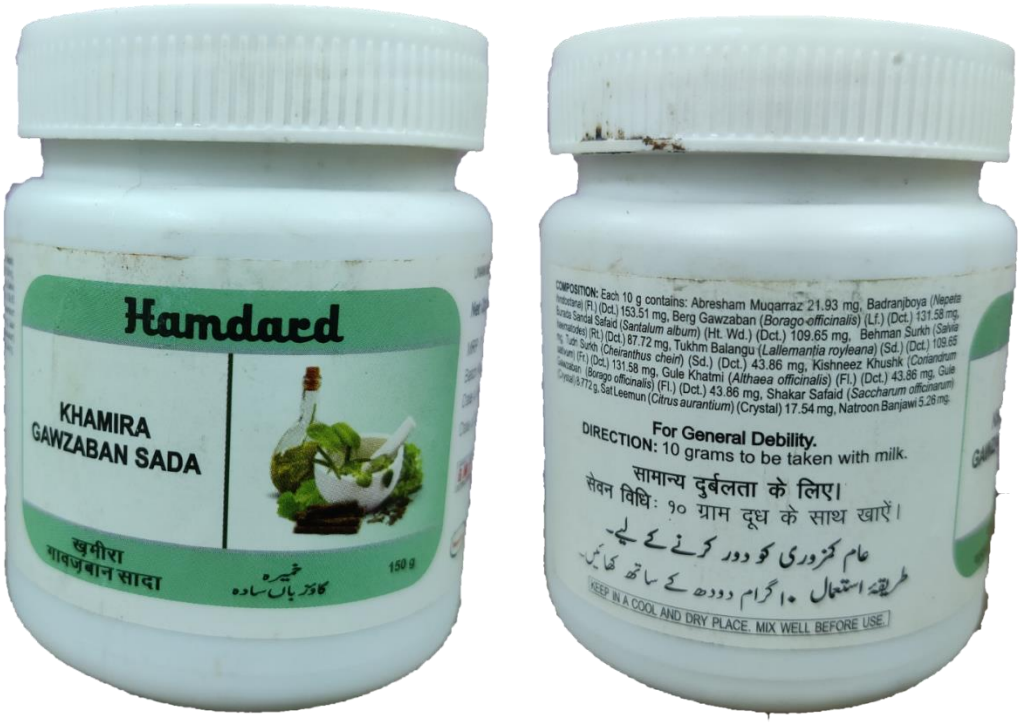

Sanmoy Karmakar
07/07/2025

Sanmoy Karmakar, M.Pharm, PhD
Professor & Former Head
In-charge Bioequivalence Study Center
Dept. of Pharmaceutical Technology
JADAVPUR UNIVERSITY, KOL - 32,INDIA